The Dissertation Committee for Sean Craig Jenkins
certifies that this is the approved version of the following dissertation:

The Attenuation and Reduction of a Simulated Hot Streak Due to Mainstream Turbulence, Hot Streak Pitch Position and Film Cooling

Committee:

_____

David G. Bogard, Supervisor

_____

Michael E. Crawford

_____

Ofodike A Ezekoye

_____

Janet L Ellzey

_____

Philip L Varghese

The Attenuation and Reduction of a Simulated Hot Streak Due to Mainstream Turbulence, Hot Streak Pitch Position and Film Cooling

by

Sean Craig Jenkins, MSE, BFA

Dissertation

Presented to the Faculty of the Graduate School of

the University of Texas at Austin

in Partial Fulfillment

of the Requirements

for the Degree of

Doctor of Philosophy

The University of Texas at Austin

December 2004

Dedicated to Beth

Acknowledgements

First, I would like to thank my supervisor, Dr. David Bogard, for supporting this project and guiding me through my graduate engineering career. He was a large factor in my growth as a researcher and engineer. His critical eye and countless hours have helped my work and personal development more than I can express.

I must also thank my wife, Elizabeth Jenkins, for all of her help and patience, especially while writing my dissertation. I could not have done it without her. She has always been there to pick up the slack when I was too busy working. I also want to thank my son Tad for nearly continuous entertainment while writing at home since his birth nearly one year ago. I also appreciated the forced work breaks that little ones always create. I also want to thank my parents and my wife's parents for all their assistance and support.

To Jay Rutledge and Dave Robertson, my fellow lab coworkers, I appreciate all the work and assistance you gave me in rebuilding the facility and running experiments. We really did function like a team. Thanks also to Krishna Varadarajan, who was essential at the beginning of this project. I also need to thank Jay Hyatt for helping with the first parts of the tunnel modifications. I would like to recognize all the "small tunnel" guys, Jason Albert, Elon Terrell, and Brian Mouzon; I appreciate your help and companionship in the lab. To the new "big tunnel" guys, Tricia Demling and Dan Warren, I wish you luck with your experiments and thank you for your help with mine.

Finally, I would like to thank my committee members, Dr. Crawford, Dr. Ezekoye, Dr. Ellzey, and Dr. Varghese for their patience, understanding, and guidance. I appreciate the effort you put forth as members of my committee.

The Attenuation and Reduction of a Simulated Hot Streak Due to Mainstream Turbulence, Hot Streak Pitch Position and Film Cooling

Publication No._____

Sean Craig Jenkins, Ph.D.
The University of Texas at Austin, 2004

Supervisor: David G. Bogard

This study investigated the effects of the vane and mainstream turbulence level on a simulated hot streak in a simulated three vane cascade. The effect of film cooling on the reduction of the hot streak was investigated for a fully film-cooled vane. To determine how the showerhead, suction side and pressure side coolant regions contributed to hot streak reduction, these regions were tested individually with and without the hot streak activated. The effect of mainstream turbulence level and coolant density ratio on coolant profiles and hot streak reduction was also investigated. Finally, superposition of coolant profiles and hot streak profiles was compared with measured data to evaluate the capability of additive superposition in predicting hot streak reduction due to film cooling.

The effects of mainstream turbulence on the attenuation of a hot streak were found to be significant, with changes in the shape and size of the hot streak. Comparisons between the hot streak impacting the vane at the stagnation line and passing through the mid-passage showed that the peak hot streak temperature was the same for an impinging and non-impinging hot streak. Interaction with the adiabatic vane caused very sharp temperature gradients in the hot streak at the trailing edge of the vane, resulting in

an increase or decrease in hot streak peak strength depending on pitch position. Additional attenuation of the hot streak occurred in the stator/rotor axial gap.

Results with film cooling indicated that, while full-coverage film cooling had a substantial effect on the hot streak, this effect was primarily due to the showerhead and suction side coolant with a much lesser effect due to the pressure side. It was discovered that coolant profiles at the trailing edge could be scaled by the coolant hole exit temperature, while reduction of the hot streak was less for film cooling at low density ratio. Measurements also showed a much higher degree of coolant spreading under conditions of high mainstream turbulence. Overall, downstream of the vane using high blowing ratios, the hot streak peak was reduced by 83% compared with the peak value upstream of the vane.

Table of Contents

Chapter 1: Introduction

1.1 Introduction 1

1.2 Parameters 5

1.3 Literature Review 8

1.4 Objectives of the Current Study 14

Chapter 2: Facility and Procedures

2.1 Facility 15

2.2 Experimental Procedures 26

2.3 Repeatability 42

2.4 Uncertainty Analysis 44

Chapter 3: Effects of the Vane and Turbulence Level with No Film Cooling

3.1 Introduction 48

3.2 Initial/Reference Conditions 49

3.3 Effect of Turbulence Level 51

3.4 Effects of the Vane at Low Mainstream Turbulence 54

3.5 Effects of the Vane at High Mainstream Turbulence 64

3.6 Effect of Vane Roughness on Hot Streak Attenuation 71

3.7 Evolution of the Temperature Profile 74

3.8 Turbulence Effects in the Stator/Rotor Axial Gap at High Mainstream Turbulence 85

3.9 Turbulence Effects in the Stator/Rotor Axial Gap at Low Mainstream Turbulence 91

Chapter 4: Effects of Showerhead Film Cooling on Hot Streak Reduction

4.1 Introduction 97

4.2 Showerhead Coolant Profiles at the Trailing Edge 97

4.3 Effects of Showerhead Film Cooling on Hot Streak Reduction 100
4.4 Effect of Varying Showerhead Blowing Ratio 102
4.5 Evolution of the Showerhead Coolant Profile 106
4.6 Turbulence Effects in the Stator/Rotor Axial Gap with Showerhead Film Cooling 107

Chapter 5: Effects of Suction Side Film Cooling on Hot Streak Reduction
5.1 Introduction 113
5.2 Suction Side Coolant Profiles at the Trailing Edge 114
5.3 Effect of Suction Side Film Cooling on Hot Streak Reduction 117
5.4 Effect of Varying Suction Side Blowing Ratio 119
5.5 Evolution of the Suction Side Coolant Profile 121
5.6 Turbulence Effects in the Stator/Rotor Axial Gap with Suction Side Film Cooling 125

Chapter 6: Effects of Pressure Side Film Cooling on Hot Streak Reduction
6.1 Introduction 132
6.2 Pressure Side Coolant Profiles at the Trailing Edge 133
6.3 Effect of Pressure Side Film Cooling on Hot Streak Reduction 136
6.4 Effect of Varying Pressure Side Blowing Ratio 137
6.5 Evolution of the Pressure Side Coolant Profile 138
6.6 Turbulence Effects in the Stator/Rotor Axial Gap with Pressure Side Film Cooling 141

Chapter 7: Effects of Full Coverage Film Cooling on Hot Streak Reduction
7.1 Introduction 144
7.2 Full Coverage Coolant Profiles at the Trailing Edge 144
7.3 Effect of Full Coverage Film Cooling on Hot Streak Reduction 148
7.4 Effect of Varying Full Coverage Blowing Ratios 151

7.5 Evolution of the Full Coverage Coolant Profile 156
7.6 Turbulence Effects in the Stator/Rotor Axial Gap with Full Coverage Film Cooling 162
7.7 Effect of Full Coverage Film Cooling on a Passage Hot Streak 167

Chapter 8: Effects of Turbulence Level
8.1 Introduction 171
8.2 Effect of Turbulence Level on Showerhead Coolant Dispersion 171
8.3 Effect of Turbulence Level on Suction Side Coolant Dispersion 178
8.4 Effect of Turbulence Level on Pressure Side Coolant Dispersion 183
8.5 Effect of Turbulence Level on Full Coverage Coolant Dispersion 184

Chapter 9: Effects of Density Ratio on Hot Streak Reduction/Aero-Engine Scaling
9.1 Introduction 189
9.2 Aero-Engine Scaled Hot Streak Reduction 189
9.3 Effect of Density Ratio on Coolant Profiles 190
9.4 Effect of Density Ratio on Hot Streak Reduction 199

Chapter 10: Superposition Analysis and Predictions
10.1 Introduction 206
10.2 Superposition of Midspan Profiles at the Trailing Edge 206
10.3 Superposition of Midspan Profiles Downstream of the Vane at Position B 217
10.4 Superposition of Midspan Profiles at Low Mainstream Turbulence 219
10.5 Superposition of Full Field Measurements 222
10.6 Prediction of the Ideal Hot Streak Pitch Position with Film Cooling 225
10.7 Predictions of Aero-Engine Scaled Hot Streak Reduction 237

Chapter 11: Conclusions

11.1 Summary of Work 242

11.2 Recommendations for Future Work 247

Bibliography 249

Vita 253

Nomenclature

C = vane chord length, 594 mm

d = film cooling hole diameter, 4.11 mm

DR = density ratio of coolant to mainstream, $\frac{\rho_c}{\rho_\infty}$

k = thermal conductivity

L_P = length measured along pressure side of vane from the stagnation point to the trailing edge

L_S = length measured along suction side of vane from the stagnation point to the trailing edge

M = blowing ratio for the suction and pressure side, where U_∞ is the local freestream velocity at the hole location, $\frac{\rho_c U_c}{\rho_\infty U_\infty}$

M^* = blowing ratio for the showerhead region, where U_0 is the approach velocity to the vane, $\frac{\rho_c U_c}{\rho_0 U_0}$

p = film cooling hole pitch in the spanwise direction

P = pitch between vanes, 460 mm

S = span length of vane, 550 mm

T_{ij} = hot streak or coolant temperature at a point in the flow

$T_{0,HS}$ = upstream peak hot streak temperature at the reference location

T_∞ = mainstream temperature

Tu = turbulence intensity, $\frac{u_{rms}}{U}$ x 100%

U_0 = approach velocity to the vane

U_∞ = local freestream velocity

y = flow normal coordinate originating at the trailing edge or vane wall (positive towards suction side of test vane, negative towards pressure side of test vane)

z = spanwise coordinate

Greek Symbols

ϕ = injection angle with respect to the surface plane

θ = streamwise injection angle

ρ = density

Λ_f = turbulence integral length scale

Θ_R = normalized coolant temperature ratio, $\dfrac{T_{ij} - T_\infty}{T_\infty - T_{0,C}}$

Θ_R = normalized hot streak temperature ratio, $\dfrac{T_{ij} - T_\infty}{T_{0,HS} - T_\infty}$

Subscripts

C = coolant

HS = hot streak value

P = along pressure side

R = normalized

rms = root-mean-square

S = along suction side

∞ = mainstream

0 = approach condition

Superscripts

* = showerhead (blowing ratio)

Chapter 1: Introduction and Literature Review

1.1 Introduction

The gas turbine engine is idealized by the Brayton cycle, consisting of four stages: adiabatic compression; idealized heat transfer into the working fluid; adiabatic expansion; and idealized heat transfer out of the working fluid. Analysis of the cold air standard ideal cycle reveals that thermal efficiency is a function of pressure ratio only. However, the pressure ratio is limited by the maximum allowable turbine inlet temperature, currently constrained by cooling and metallurgical limitations to about 2000 K [1]. Since the turbine inlet temperature field is non-uniform and component durability is dependent on temperature, the highest value must be considered. In Figure 1.1, a cut-away view of a gas turbine engine shows the low and high pressure compressor, the combustor, and the high and low pressure turbines. In a gas turbine engine, heat transfer into the working fluid is accomplished by combustion of fuel and air, resulting in a rapid rise in

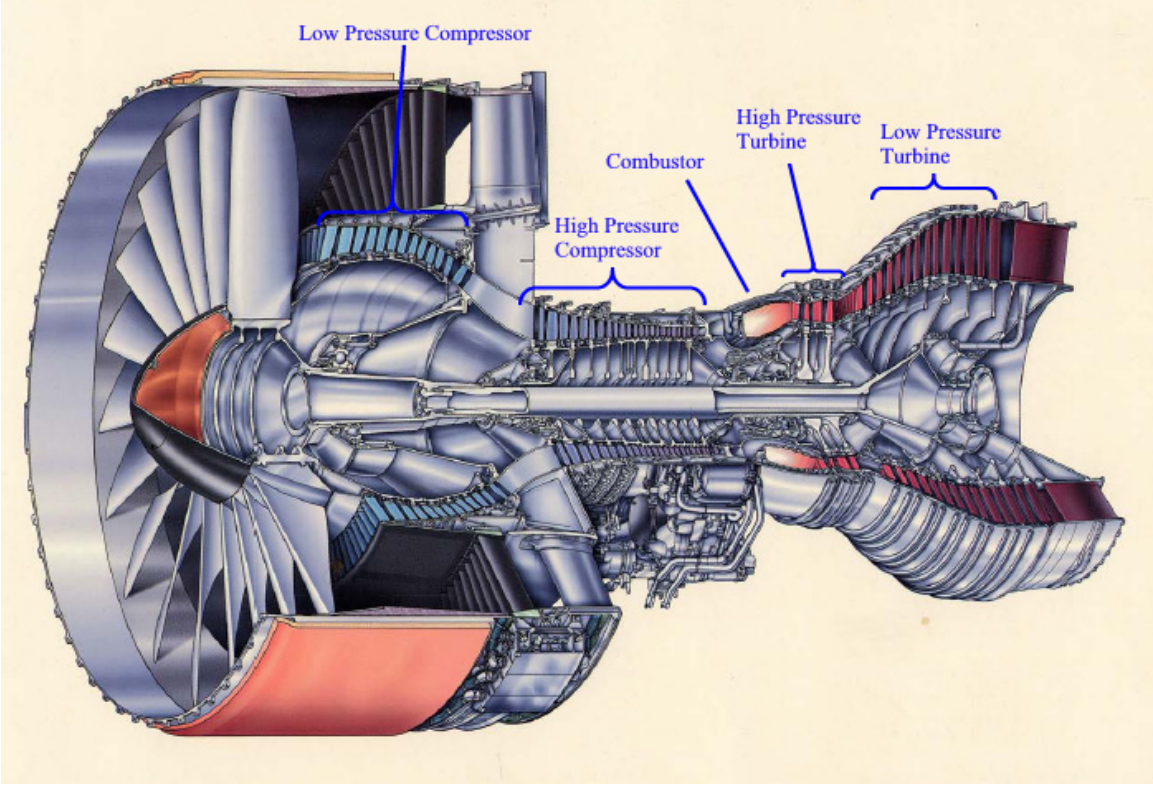

Figure 1.1: Cut-away view of Pratt & Whitney PW4000 engine showing low and high pressure compressor, combustor, and high and low pressure turbine.

From http://www.pw.utc.com/presskit/images/pw4000112_cutaway_high.jpg

temperature. Although this process is tightly controlled, non-uniformities in the temperature profiles exiting a modern combustor are severe enough to cause high, localized heating of components in the high-pressure turbine downstream. The temperature non-uniformities have been appropriately named "hot streaks," and have been studied within a range of T/T_∞ = 1.1 to 2.5, where T_∞ is the mainstream temperature. The hot streak exiting the combustor may impact the 1st stage nozzle guide vane leading edge, pass between vanes through the mid-passage, or pass at any position between these two extremes depending on the relative positioning of discrete combustors and vanes. In Figure 1.2, a close up view of the combustor and the 1st stage nozzle guide vane shows the relative orientation of the components. Dilution jets in the combustor along with the combustion process itself create high levels of turbulence at the combustor exit. According to several researchers this turbulence intensity level may range from as low as Tu = 1.5% for a catalytic combustor to about 20% for an aero-engine combustor [2]. Hot streaks exiting the combustor are of significant importance to engine designers since the engine designer must consider the highest temperatures affecting the turbine section. Hot

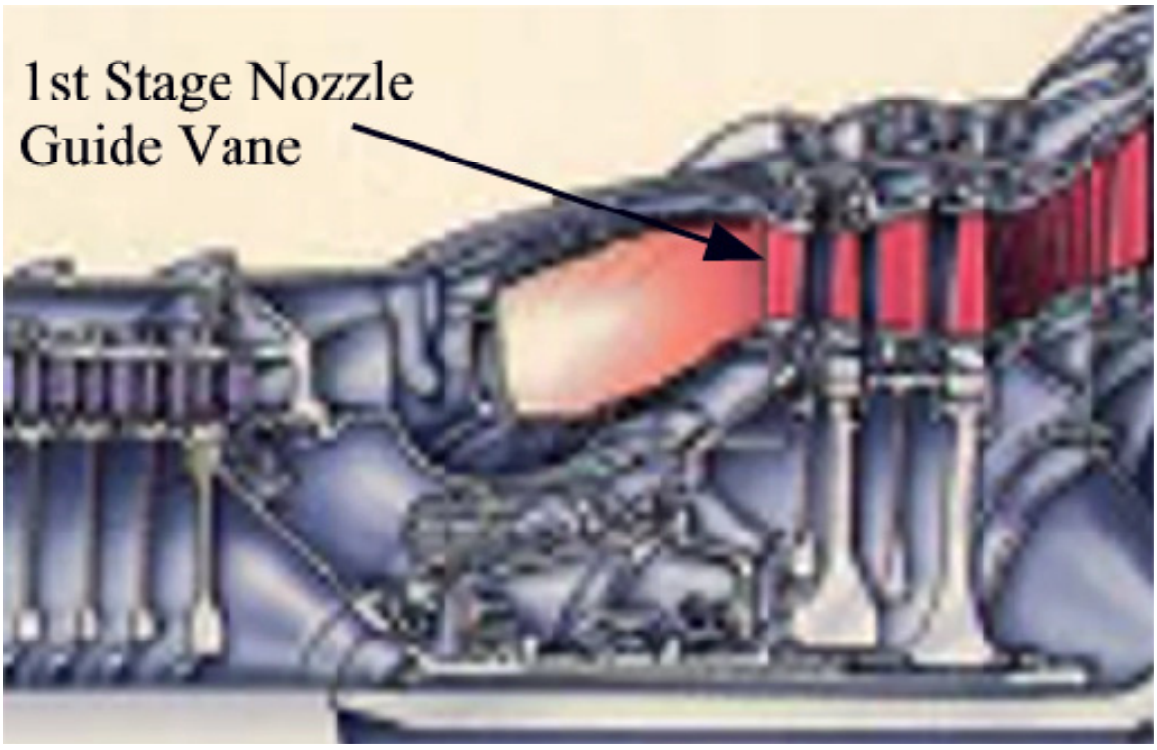

Figure 1.2: Close up view of combustor and 1st stage nozzle guide vane of high pressure turbine. From http://www.pw.utc.com/presskit/images/pw4000112_cutaway_high.jpg

streaks play a large role in failures of the first stage nozzle guide vanes and rotor blades due to thermal loading and since the engine designer must account for the highest temperature levels in any portion of the turbine section, a greater level of effort is required when hot streaks exist in the flow. Researchers have noted that lowering the surface temperature of a turbine blade by as little as 25° C could double the life of the component (Han et al [1]). Depending on the position of the hot streak relative to the first stage nozzle guide vane, a greater amount of cooling may be required to maintain vane surface temperatures at acceptable levels. Appropriate positioning of the temperature non-uniformities, or "hot streaks," exiting the combustor relative to the first stage nozzle guide vane has been a concern for engine designers for some time. At this point, modern gas turbine engines have been refined such that appropriate positioning of the exit of the combustor with respect to the vanes or passages between vanes is possible. "Clocking" of the hot streak involves aligning the hot streaks with respect to the guide vanes in a repeatable fashion in engines where an integer multiple of combustors to first stage nozzle guide vanes makes this possible. Previous researchers have studied the effects of "clocking," but the results are limited and the literature is somewhat contradictory. Effects of the vane on the hot streak are complex and depend not only upon the hot streak position, but also on the turbulence field parameters. In general, realistic turbulence conditions of both intensity and length scale have not been simulated experimentally or computationally, and in particular, a range of pitch positions have not been investigated. Furthermore, those studies that investigated the effect of vane impingement versus non-impingement focused on surface measurements of the downstream rotor, and therefore do not directly address the attenuation of the hot streak itself. Likewise, interactions of the hot streak with the vane and external coolant flow that may change the resultant surface temperature distribution on the rotor have been largely ignored. These interactions may have a large effect on the cooling requirements of the first stage rotor blades immediately downstream.

A diagram describing how internal and film cooling may be used in a turbine airfoil is shown in Figure 1.3. Internal coolant is supplied by drawing bleed air from the compressor upstream. Since this bleed air supply is at a significantly cooler temperature than the combustion gases exiting the combustor, it is well suited for cooling the turbine

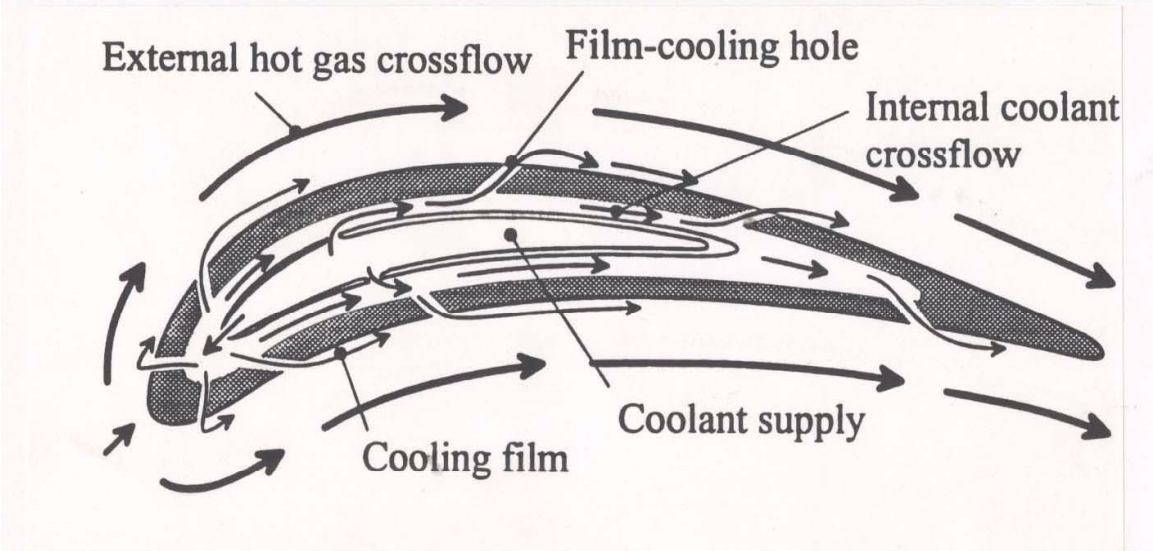

Figure 1.3: Schematic of film cooling supply and internal and external cooling.
From Gritsch, Schulz, and Wittig (1997)

vane both internally and externally. In the figure, a centrally located coolant supply provides internal coolant flow, which is permitted to escape through small film-cooling holes in the vane surface as shown in Figure 1.4. These film-cooling holes provide a coolant film or layer, which ideally lies against the surface of the vane, providing cooling and protection from the external hot gas flow. Since coolant is bled from the compressor of the engine, the resultant loss of efficiency must be made up by a higher allowable combustor exit temperature to give a net benefit.

In the gas turbine industry, a wide range of blowing ratios and density ratios are used in practice, dependent on a large number of constraints. Since the use of compressor bleed reduces cycle efficiency, engine designers must compromise between cooling demands and cycle efficiency to meet durability needs. It is of critical importance to understand how film cooling of the first stage nozzle guide vane may help to alleviate cooling needs of the first stage rotor through dispersion of the hot streak since rotating stages are much more difficult to cool. A clear understanding of how blowing ratio and density ratio affect the hot streak would further allow engine designers to improve engine designs.

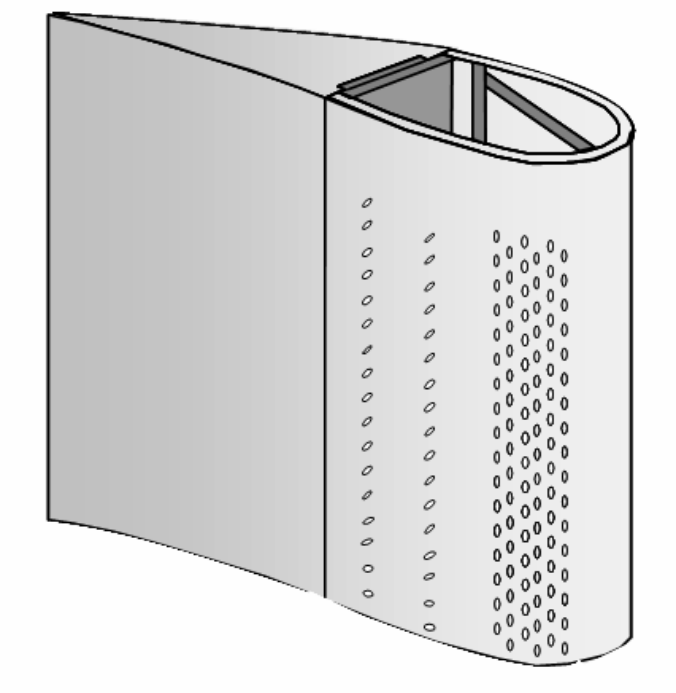

Figure 1.4: Schematic of film cooling holes for showerhead and pressure side.

1.2 Parameters

Two parameters are used in this study to define the "strength" of the hot streak. For some results, the temperature data were normalized by the mainstream temperature to produce the hot streak temperature ratio, T/T_{∞}.

For other results, the use of a normalized temperature ratio, Θ_R, was found to be more appropriate. The normalized temperature ratio, Θ_R, was defined based on the peak hot streak temperature, $T_{0,HS}$, measured at a standard reference position upstream of the vane leading edge. Since the local temperature is scaled by the peak value upstream, Θ_R, may be thought of as the hot streak reduction, or as a percentage of the original hot streak. It is shown in Equation 1.1 as follows:

$$\Theta_{R,ij} = \frac{T_{ij} - T_{\infty}}{T_{0,HS} - T_{\infty}} \tag{1.1}$$

where Θ_R, is computed at a point (ij) based on the temperature at that point, T_{ij}, and the mainstream temperature at the measurement plane, T_{∞}. The normalized temperature ratio, Θ_R, varies from 0 to 1 for hot streak fluid, with a value of 1 signifying no reduction

of the hot streak peak and 0 signifying the fluid is at mainstream temperature. Coolant fluid (below the mainstream temperature) resulted in negative values.

It should be noted that the hot streak temperature ratio, T/T_∞ , is dependent on a consistent mainstream temperature for comparison purposes. A large variation in the mainstream temperature, T_∞, affects the hot streak temperature ratio since the hot streak power is fixed resulting in a fixed temperature increase. The use of this ratio is appropriate in most cases as the effect of the variation in the mainstream temperature was negligible. On the other hand, the normalized temperature ratio, Θ_R, has no such vulnerability since it is related only to temperature differences.

For comparisons between coolant profiles under different mainstream conditions, such as low and high mainstream turbulence, it is inappropriate to use the normalized temperature ratio since the hot streak at the reference position may not be the same for both mainstream conditions. In these situations, the normalized coolant temperature, Θ_C, was more appropriate. The normalized coolant temperature relates the temperature at a point in the flow to the coolant temperature at the coolant hole exit, $T_{0,C}$, as shown in Equation 1.2:

$$\Theta_{C,ij} = \frac{T_{ij} - T_\infty}{T_\infty - T_{0,C}} \tag{1.2}$$

where the value of Θ_C, is calculated at a point (ij) based on the fluid temperature at that point, T_{ij}. This ratio is similar to the adiabatic effectiveness used in studying the performance of film cooling on the vane surface, which is defined in the same way except that the fluid temperature, T_{ij}, is replaced by the adiabatic wall temperature, T_{AW}. The normalized coolant temperature Θ_C, varies from -1 to 0, with a value of -1 referring to fluid at the coolant hole exit temperature and a value of 0 corresponding to the mainstream temperature. The ratio was set up in this way so that coolant would be represented in the same way as the normalized temperature ratio, Θ_R, which was also negative for temperatures below the mainstream, i.e. coolant temperatures.

The mass flux ratio, or "blowing ratio," M (or M^*), is defined as the ratio of coolant to external mass fluxes. For the suction and pressure side film cooling holes, it is

defined as shown in Equation 1.3, where the velocity, U_∞ is the local velocity at that row of holes.

$$M = \frac{\rho_c U_c}{\rho_\infty U_\infty} \tag{1.3}$$

For the showerhead, since the velocity is zero at the stagnation point, it makes sense to define the blowing ratio in terms of the approach condition as shown in Equation 1.4, where the velocity, U_0, is the approach velocity.

$$M^* = \frac{\rho_c U_c}{\rho_0 U_0} \tag{1.4}$$

Other film cooling parameters used to scale adiabatic effectiveness include the momentum flux ratio, I, defined as follows:

$$I = \frac{\rho_c U_c^2}{\rho_\infty U_\infty^2} \tag{1.5}$$

and the velocity ratio, shown in Equation 1.6:

$$VR = \frac{U_c}{U_\infty} \tag{1.6}$$

In both Equations 1.5 and 1.6, the denominator would be modified to refer to the approach condition for the showerhead region as previously described above for the blowing ratio.

Finally, the density ratio is of significant importance to both film cooling and hot streak reduction. The density ratio, DR, is defined as shown:

$$DR = \frac{\rho_c}{\rho_\infty} \tag{1.7}$$

Invoking the ideal gas law, it can be shown that the density ratio is equivalent to the ratio of mainstream to coolant temperature, i.e. $DR = (T_\infty/T_c)$. This has importance for hot streak reduction since the result of the mixing process of coolant and hot streak fluid is a function of the difference between coolant and mainstream temperature, $\Delta T_C = T_\infty - T_c$, and the difference between the hot streak and mainstream temperature, $\Delta T_{HS} = T_{HS} - T_\infty$, Additionally it is important since the hot streak temperature difference, ΔT_{HS}, is fixed while the coolant temperature may be adjusted over a fairly large range, thereby

allowing the simulation of other hot streak temperature ratios by scaling the ratio $\Delta T_{HS}/\Delta T_C$ by a multiplicative factor. This would allow a lower density ratio, i.e. coolant temperature nearer to the mainstream, to simulate the effect of a higher hot streak peak temperature.

An important parameter in turbulent mixing of scalar quantities, such as temperature, is the full or half-width of the scalar profile. In this study, the full-width at 20% of the maximum was used to describe the relative sizes of hot streaks under different conditions or at different positions in the flow, and is commonly used in the literature to describe the mixing of jets in turbulent flows. The 20% width, $\delta_{20\%}$, is defined as the full profile width at 20% of the maximum of the difference between peak and base as shown schematically in Figure 1.5 (or minimum for negative profiles such as coolant profiles).

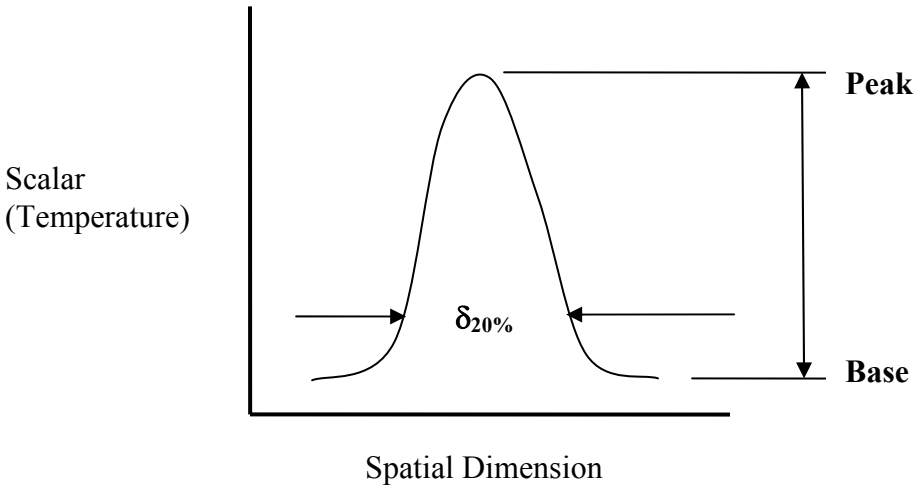

Figure 1.5: Schematic of full-width at 20%, $\delta_{20\%}$.

1.3 Literature Review

Several researchers have studied the effects of hot streaks in simulated vane cascades consisting of one or more stages. Additional research has been done using computer simulations, which have generally used experimental data as a benchmark or starting point. As described in the review paper by Dorney, et al [3] experimental hot

streak simulations have been conducted by NASA Glenn Research Center (Schwab, et al. [4]; and Stabe, et al. [5]), the United Technologies Research Center (Butler, et al. [6]), and Massachusetts Institute of Technology (Shang, et al. [7] and Shang and Epstein [8]). Among these, a variety of hot streak configurations have been investigated with a range of relevance to the actual engine.

Among these, the NASA CERTS experiments [4-5] were the only ones to consider somewhat realistic inlet conditions by using a circumferential slot with mass injection giving radially varying temperature and total pressure profiles. Their hot streak temperature ratio was 1.2 at a measurement location of about one chord length upstream of the vane, and the shape of the hot streak was roughly parabolic in the spanwise, or radial, direction, but circumferentially uniform. However, since measurements were only taken downstream of the rotor, it was not possible to determine the shape or the strength of the hot streak in the stator/rotor axial gap. No turbulence levels were given and the description of the facility was only sufficient to infer that these levels were well below those found in an actual engine.

The United Technologies Research Center tests performed by Butler, et al. [6] were conducted in a low speed, rotating rig comprising one stage with components that were not cooled, in which the approach flow to the first vane passed through a contraction. The hot streak consisted of heated air at a temperature ratio of 2.0, which was seeded with CO_2, and was introduced through a pipe in the middle of the vane passage at a radial location 40% above the hub. At the inlet of the stator passage, the hot streak was reported as a mostly flat profile, with high gradients at the edges. Carbon dioxide was used for concentration measurements to track the migration of the hot streak and for wall concentration measurements such that surface heat transfer could be inferred. The major findings from this study were that the rotor flow field was significantly affected by the hot streak resulting in hotter gas migrating to the pressure side of the rotor. Increases in spanwise flow were observed on the pressure side of the rotor as well. Again, the facility description suggested that turbulence levels were low, but no such levels were reported in the paper.

A comprehensive study of the aerodynamics and secondary flows in the same facility were performed by Joslyn and Dring [7] and included measurements of the

redistribution of a simulated hot streak profile set to impinge on the first stage vane leading edge. The simulated profile was produced by using CO_2 as a trace gas, which was measured by drawing gas through standard static pressure taps, a rotating 19-element rake or a transverse probe. Measurements of the radial (spanwise) profile showed a reduction of the peak value of about 20% from the inlet measurements at 0.97 chord upstream of the first stage vane leading edge to the rotor leading edge (0.50 chord downstream of the first stage vane). Mainstream turbulence levels were listed as 0.5%, so the redistribution of the inlet profile was attributed mainly to secondary flows and the radial flow in the first stator wake. While these measurements documented the effects of aerodynamics and secondary flows on the temperature profile, mainstream turbulence levels were not realistic.

Later experiments using the United Technologies Large-Scale Rotating Rig were performed by Roback and Dring [8], where hot, neutral and cold streaks were generated. The streak was again introduced through a pipe in the middle of the vane passage. Their hot streak temperature ratio was 1.5 and had a similar inlet shape to that of Butler, et al. [6]. Similar to their predecessors working at the same facility, turbulence levels were not provided, however the description of the facility strongly suggests that turbulence levels were very low since a number of measures were taken to ensure this condition. Carbon dioxide was used as a trace gas and the results were presented as normalized trace gas concentrations on the surface of the first stage rotor. Results accounted for density ratio, variation in the spanwise position, and position relative to the vane. The bulk of the data were taken on the surface of the first stage rotor, but no information was available to allow one to ascertain the strength of the hot (or cold) streak immediately downstream of the first stage vane. Attenuation levels as the hot streak passed around the vane were also not possible to determine since profiles upstream of the vane were not given. However, concentration profiles taken across the span in the plane of the rotor leading edge showed both the shape and peak levels were roughly the same for an impinging and non-impinging hot streak. A simulation of trailing edge cooling was performed by coolant ejection at several coolant-to-freestream velocity ratios. However, results were not given for the combination of a hot streak and trailing edge coolant at the rotor leading edge as were given for the impinging and non-impinging hot streak.

The experiments conducted by Shang et al. [10] at MIT used two different hot streak configurations. Their facility consisted of a one and a half stage vane cascade oriented radially in the same manner as the actual engine. One hot streak was a discrete circular hot streak with a diameter length scale of one vane pitch (and roughly the span height) with a temperature ratio of 1.1. The other was a radially varying, but circumferentially uniform hot streak with a temperature ratio of 1.1, and both were used to evaluate the effect of the hot streak on the rotor surface. Their measurements include a gas temperature profile at the entrance to the rotor section (downstream of the vane), but unfortunately do not reference this profile to the upstream condition. In addition, these researchers chose two distinct turbulence levels generated by a turbulence grid at 3% and 8%, measured just upstream of the vane. The turbulence grid had a spacing of 2.5 cm with a nozzle guide vane true chord of 5.9 cm. One important observation of this study was that rotor heat transfer was not affected by the differing turbulence level, however it is plausible that a much larger difference in turbulence level would have some effect. Although the turbulence levels used were much closer to those found in an actual engine, current combustor designs result in much higher turbulence intensity levels.

The computational studies that have been conducted on hot streaks range from two-dimensional, steady, inviscid simulations to three-dimensional, viscous, unsteady simulations. Most numerical simulations, along with the previously described experiments, have primarily introduced the hot streak so that it passed through the middle of the vane passage and have been focused on the effect of the hot streak on the heat load on the rotor downstream of the first vane. Although ultimately rotor heat load is an important consideration, attenuation of the hot streak due to turbulence effects is best described by a direct comparison of fluid temperatures.

In contrast to the Roback and Dring [9] study, the numerical simulations done by Gundy-Burlet and Dorney [11] showed that “clocking” the hot streak so that it is positioned at the leading edge of the vane results in a diminishing of the effect of the hot streak on the downstream rotor as evidenced by decreased pressure side rotor surface temperature ratios on the order of about 40%. This was attributed to the deceleration and increased mixing of the hot streak as it interacted with wake of the vane. However, fluid temperatures in the wake region were not documented, so an attenuation of the hot streak

by impact on the vane was not confirmed. Inlet mainstream turbulence levels were not mentioned so presumably these levels were nominally zero.

A more recent computational study by Gundy-Burlet and Dorney [12] presented time-averaged surface temperature profiles for the first-stage stator, first-stage rotor, and second-stage stator with hot streaks positioned radially at 20%, 40%, and 60% span. Their primary observation was that impingement of the first-stage stator resulted in a significant increase in heat load compared to the hot streak positioned to pass through the mid-passage. Impinging the hot streak on the more easily cooled first-stage stator also reduced the heat load on the first-stage rotor. They also demonstrated the migration of the hot streak away from the hub on the suction side of the first-stage stator for the 20% span position, as well as the migration of the hot streak toward the hub for the 40% span position and even more so for the 60% span position. Results for the pressure side illustrated the spreading of the hot streak in the spanwise direction for all spanwise positions with the greatest spreading for the 60% span position. The computational results most relevant to the present study were spanwise profiles "aft" of the first-stage stator. These results were time and circumferentially averaged, so a direct comparison with upstream peak values is not appropriate, however, comparisons between impinging and mid-passage hot streaks showed a range of results. The largest difference between impinging and mid-passage hot streaks was observed for the hot streak positioned at 60% span, where the impinging hot streak peak was much hotter than the mid-passage hot streak peak, however temperature ratio peaks were nearly the same for 40% span. In contrast to 60% span, the impinging hot streak peak was cooler than the mid-passage hot streak peak for the hot streak positioned at 20% span. Their conclusion was to recommend impinging the first-stage stator in the lower portion of the span, since other positions involved greater heating of more sensitive areas and predicted the first-stage stator would be easier to cool given that the heat loads were shown to not vary strongly with time. They also noted that temperature ratios of 1.1 to 1.6 were typical of actual engine operating environments according to a private conversation with Pratt & Whitney's R. K. Takahashi, confirming their choice of an appropriate hot streak temperature ratio. Since inlet mainstream turbulence levels were not indicated, they are presumed to be nominally zero, especially since the primary cause of hot streak reduction

aft of the first-stage stator was attributed to interaction with "trailing-edge shedding from stator 1."

The ratios of the hot streak temperature to mainstream temperature that have been used in previous studies have ranged from T/T_∞ = 1.1 to 2.5. Using numerical simulation, Dorney et al. [13] investigated the effect of the hot streak temperature ratio for a range of T/T_∞ = 1.5 to 2.5. Increasing the temperature ratio from T/T_∞ = 1.5 to 2.0 was found to have very little effect on the predicted kinematics of the hot streak, while higher temperature ratios would be affected more strongly. Gundy-Burlet and Dorney [12] noted that T/T_∞ = 1.1 to 1.6 was typical of engine operating environments. However, since ground-based power generation engines are generally designed to have more uniform temperatures at the combustor exit, it is reasonable to expect that characteristic temperature ratios for the hot streak would be at the low end of this range.

For the experimental studies previously described, a number of deficiencies may be noted, making further investigation crucial to the understanding of hot streak attenuation. Turbulence effects have been largely ignored as well as the possible combined effects of high mainstream turbulence and vane impingement. Additionally, there have been no previous experimental studies that addressed the effects of the interaction of a hot streak with a fully film-cooled nozzle guide vane.

For the MIT study, which was the only study to consider turbulence levels as a relevant parameter, the direct comparison between upstream and downstream conditions was missing. For this reason, it is unclear if the hot streak profile entering the vane cascade was affected by mainstream turbulence existing in the flow.

There have been no previous studies investigating the effects of high mainstream turbulence on the attenuation of a hot streak. It is clear that the hot streak, a co-flowing heated jet, will attenuate much more under high turbulence than under low to moderate turbulence conditions, however, no previous attempts have been made to quantify this effect for actual engine operating conditions. Furthermore, the interaction of a hot streak with a film cooled first stage guide vane has not been previously investigated. Therefore, establishing how much attenuation of a hot streak is possible in a rigorous and quantitative fashion by impacting a highly film cooled vane under conditions of high mainstream turbulence has obvious importance for turbine designs.

A companion study investigating the effects of the hot streak on film cooling performance of the showerhead and first row of suction side holes was performed by Varadarajan [14].

1.4 Objectives of the Current Study

In the present study, experiments were conducted with a simulated hot streak to determine how mainstream turbulence, impact on the vane, and film cooling diminished the strength of the hot streak. The goal of the study was to determine how much the hot streak strength could be reduced by appropriate positioning of the hot streak and use of film cooling. Experiments were conducted to determine the ideal position of the hot streak relative to an uncooled first stage nozzle guide vane, and the effects of hot streak positions between the stagnation line and the mid-passage. To determine the effects of film cooling, a range of blowing ratios were used for individual film-cooling regions as well as for full coverage film-cooling at two different density ratios. Measurements were taken at several positions along the vane, at the trailing edge of the vane, and downstream of the trailing edge to determine how the coolant from these regions mixed with the hot streak. Armed with a wide array of measurements of coolant and hot streak temperature fields, superposition analysis of the coolant and hot streak was performed to determine if the mixing process of the hot streak and coolant could be simulated by a numerical prediction using superposition of temperature profiles for the coolant alone and the hot streak alone. Finally, with the use of scaled density ratios, the simulation of aero-engine conditions was performed to evaluate the effect of film cooling on the hot streak in an aero-engine environment where hot streak temperature ratios tend to be higher than those for ground-based engines.

Chapter 2: Facility and Experimental Procedures

2.1 Facility

2.1.1 Test Facility

The test facility was a closed-loop, low-speed wind tunnel, driven by a 50 hp variable pitch, variable speed fan. The test section, shown in Figure 2.1, was a simulated three vane, two passage cascade with adjustable bleed and adjustable walls to maintain the proper flow around the test airfoil. A full description of the facility is given in Polanka [15].

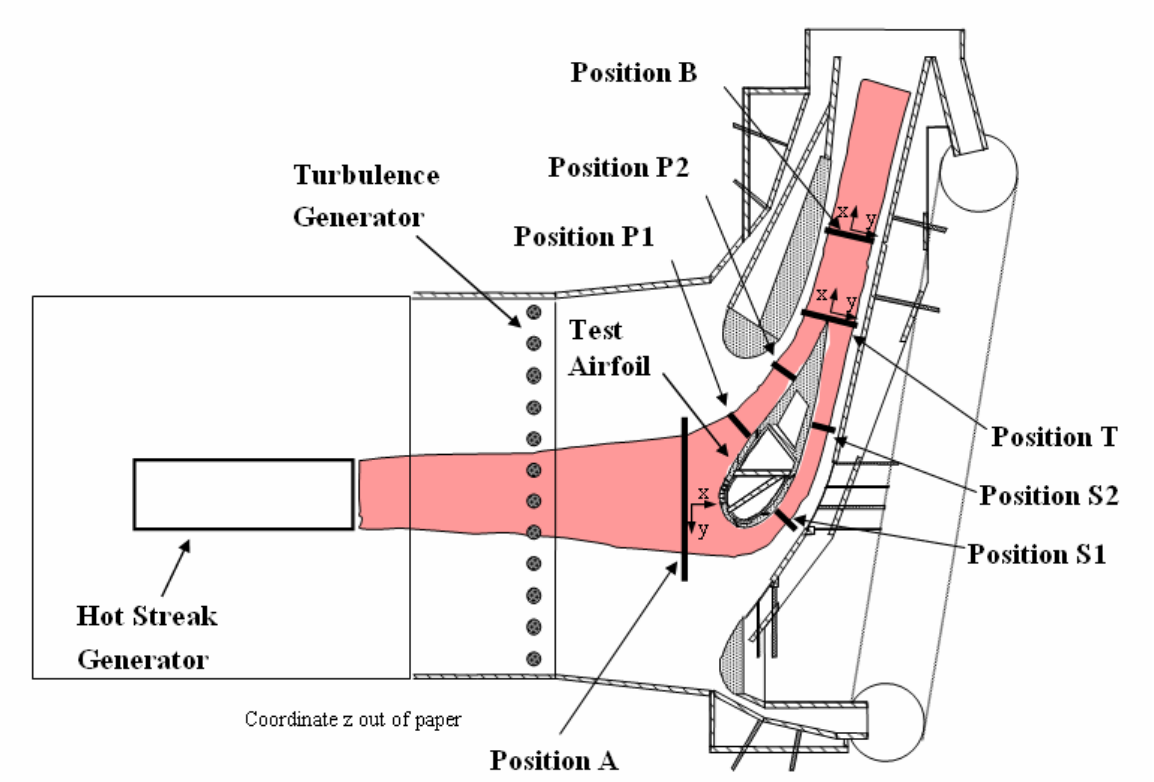

Figure 2.1: Simulated vane cascade with hot streak generator.

The test airfoil was a scaled up model of a first stage turbine guide vane with the Reynolds number matched to actual engine operating conditions. The vane had a chord length of C = 594 mm, a span of S = 550 mm, and the pitch between airfoils was P = 460 mm. The mainstream approach velocity was U_0 = 5.8 m/s for all experiments, matching the inviscid pressure distribution for the actual airfoil, resulting in a Reynolds number of

Re = 1.06 x 10^6 based on chord length and cascade exit velocity of 28.6 m/s. Additioinal details of the documentation of the test facility are also available in Polanka [15]. The test vane was constructed of polyurethane foam selected for strength and low thermal conductivity, with a value of k = 0.048 W/m·K. For all coolant regions, the coolant hole diameter was d = 4.11 mm and the pitch in the vertical, or spanwise, direction between coolant hole centerlines was 5.55d.

Three separate regions of coolant holes were available for performing experiments using film-cooling. The showerhead region, shown in Figure 2.2, had six rows of coolant holes with a row spacing of 3.33d. These holes were oriented laterally, i.e. 90° to the streamwise direction, and have an injection angle of 25° relative to the surface. The pressure side film cooling holes are also shown in Figure 2.2, consisting of two rows of coolant holes. These rows were located at s/d = -25 and s/d = -45, where s/d = 0 was located at the stagnation line at the leading edge of the airfoil, and s was the distance along the airfoil. The pressure side coolant holes had an injection angle of ϕ = 30° and a streamwise angle of θ = 45°. In addition to the showerhead and pressure side

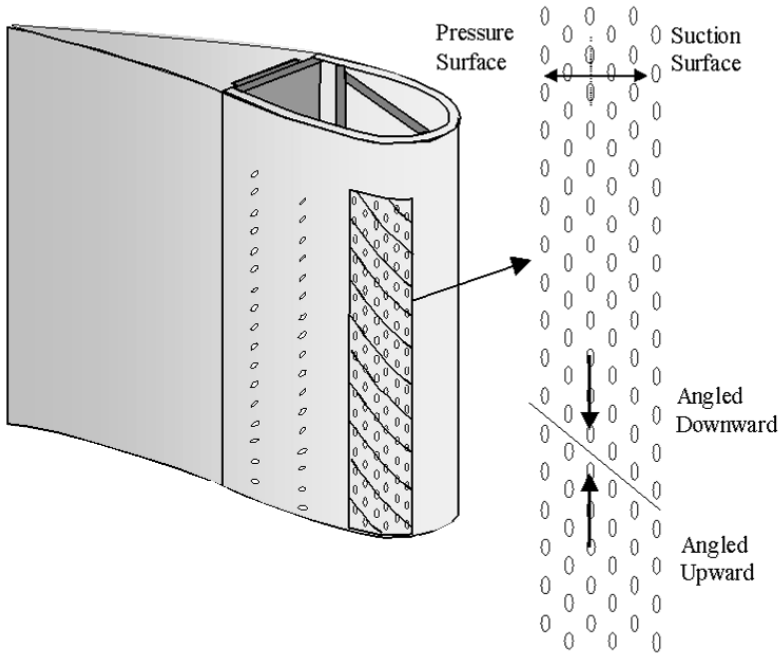

Figure 2.2: Showerhead and pressure side cooling holes.

coolant holes, the film cooling schematic in Figure 2.3 shows the three rows of suction side coolant holes. Their locations with respect to the stagnation line were x/d = 30, x/d = 53, and x/d = 84. The injection angles were ϕ = 50°, 45°, and 35° respectively and the streamwise angles were θ = 0°, 45°, and 45° respectively. The positions and injection angles for the showerhead, pressure side, and suction side are tabulated in Table 2.1. The nominal mainstream temperature was 300 K and for most experiments coolant consisting of cryogenically cooled air supplied at 187.5 K resulted in a density ratio of 1.6. Each coolant region had a separate pressure plenum providing coolant supply as shown in Figure 2.3. Additional details of the film cooling supply and of the construction of the film cooling holes are given in Cutbirth and Bogard [16].

Region	s/d	Injection Angle [ϕ]	Streamwise Angle [θ]
Pressure Side	-25	30	45
	-45	30	45
Showerhead	-7	25	90
	-3	25	90
	0	25	90
	3	25	90
	7	25	90
	10	25	90
Suction Side	30	50	0
	53	45	45
	84	35	45

Table 2.1: Coolant hole locations and angles.

High mainstream turbulence was generated using an array of 38 mm diameter vertical rods, spaced 85 mm apart, and located 0.88C upstream of the stagnation point as shown in Figure 2.1. The turbulence generator nominally produced a turbulence intensity of Tu = 20% with an integral length scale of Λ_f = 33 mm at Position A. This level of turbulence intensity was shown to be representative of actual engine operating conditions [2]. The turbulence generation rods were constructed of a material with very low thermal conductivity to avoid interference with the hot streak. Additional details of the turbulence generator, the downstream mean velocity, and turbulent fluctuating velocity profiles are available in Cutbirth [17].

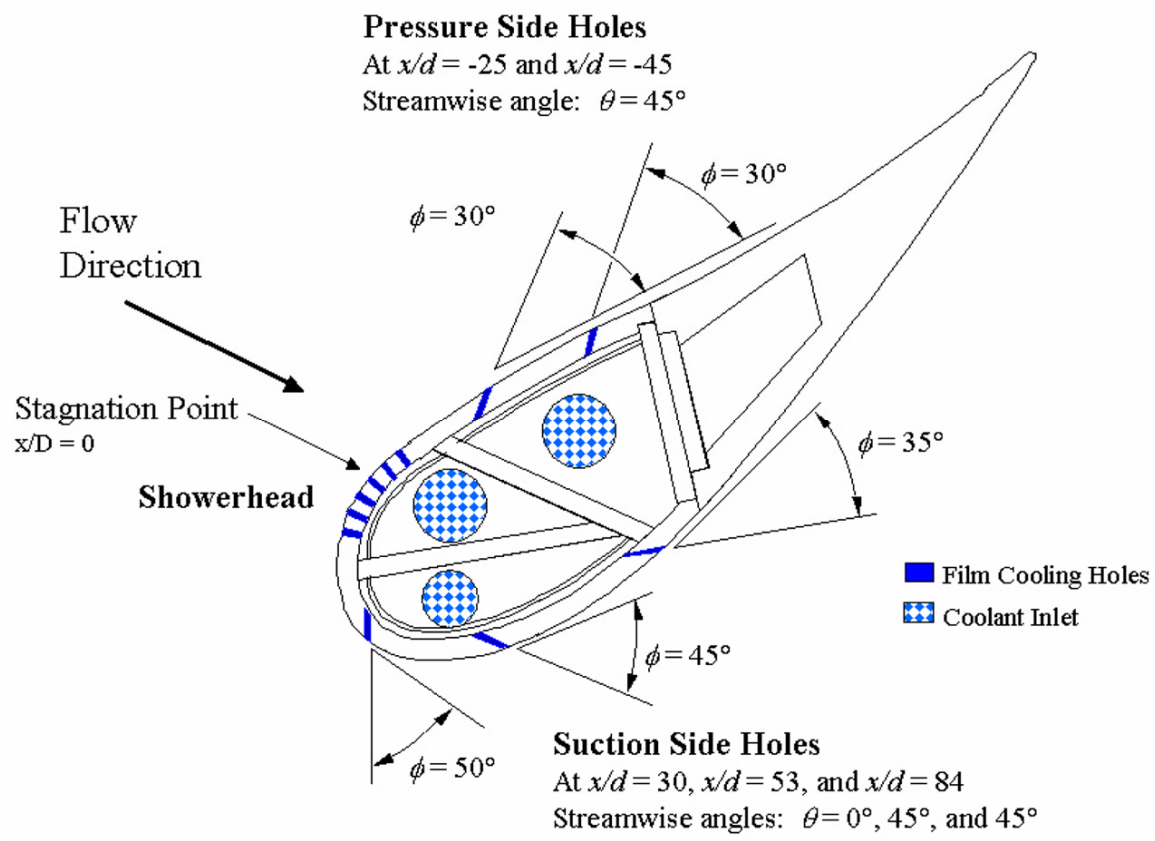

Figure 2.3: Schematic of film cooling hole configuration.

2.1.2 Hot Streak Installation

As part of this project the wind tunnel facility was modified to incorporate a hot streak generator upstream of the test section. As shown in Figure 2.4, the inlet nozzle for the test section was moved upstream and new constant area section was installed to house the hot streak generator. The tunnel section constructed to contain the hot streak generator had the same dimensions as the entrance to test section with a height of 55 cm and width of 102 cm. The hot streak generator section was 117 cm long in the streamwise direction and was situated immediately downstream of the nozzle section of the wind tunnel.

The hot streak generator consisted of a metal duct which housed 80/20 nichrome heating elements spaced to heat the flow evenly. It was supported by six metal rods on each side, and provided 7 kW of heating which could be run at full and half power. The

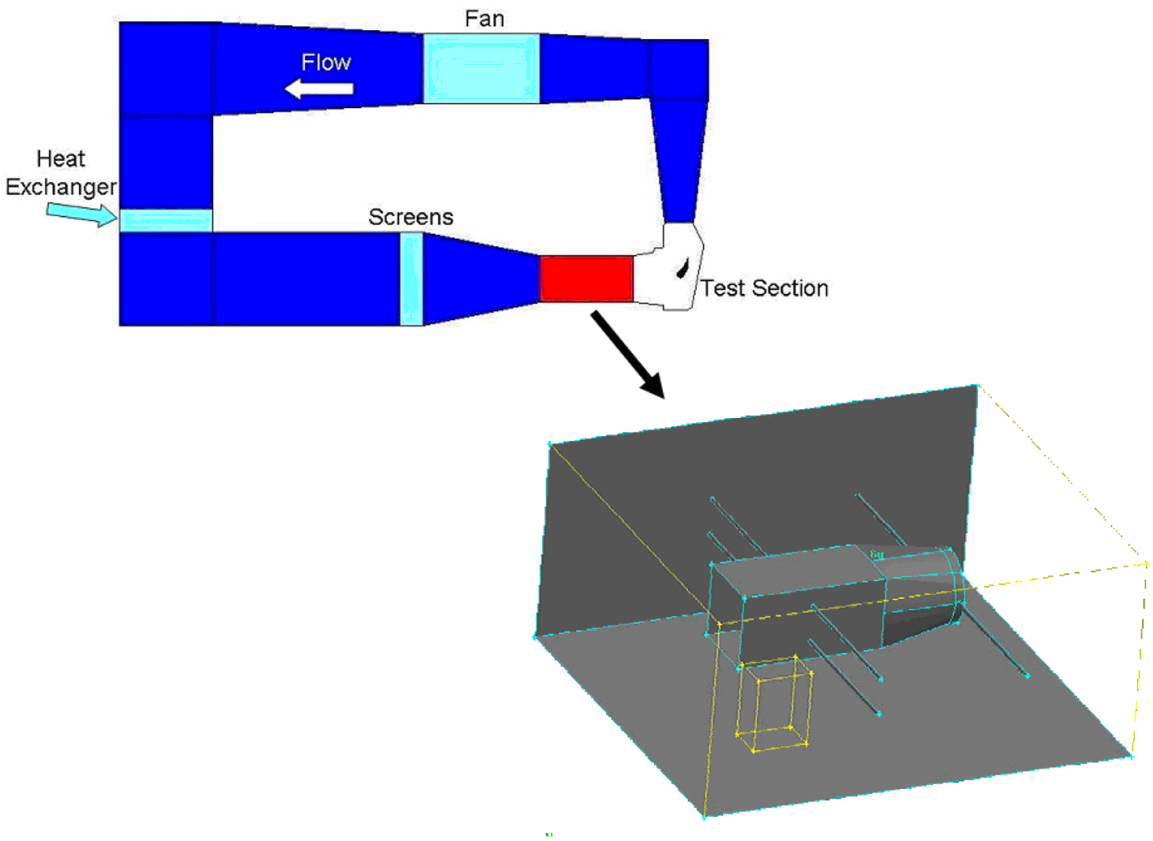

Figure 2.4: Wind tunnel schematic showing detail of the hot streak generator.

heating elements were enclosed in a square metal duct, 200 mm by 200 mm in cross section and 406 mm in length, followed by a transition section leading to a 200 mm diameter exit (0.43*P*). The transition section was 200 mm in length and its exit was located 1.7*C* upstream of the vane leading edge. The hot streak generator was positioned vertically, or spanwise, in the center of the tunnel and was fully adjustable across the pitch so that the hot streak could be positioned to impact various positions on the vane or pass through the center of the passage between vanes. The hot streak generator was designed to give a nominal temperature ratio of $T/T_\infty = 1.1$ upstream of the vane under high turbulence conditions. As mentioned in Chapter 1, this temperature ratio was a good representation of ground-based engines.

2.1.3 Secondary Flow Loop (Coolant Loop)

Fluid from the main tunnel was extracted from just upstream of the main tunnel fan. As shown in the schematic in Figure 2.5, the flow was driven by a constant speed,

constant pitch, 7.5 hp centrifugal blower and sent towards the coolant heat exchanger. A diverter valve was used to permit excess secondary loop flow to be dumped back into the main tunnel at approximately the same location as it was extracted. Secondary loop flow then passed through the coolant heat exchanger and at the exit the flow was split into three loops, one for each coolant region. Each loop was equipped with its own orifice meter and valves as appropriate for the typical range of flow rates. The valves were positioned for use by one operator just outside the corner of the test section as shown in Figure 2.5. The suction side and pressure side loops were each fitted with a 1 ½ inch globe valve, and the showerhead was controlled with at 1 ½ inch gate valve. The suction side loop had a secondary 1 inch needle valve in parallel with the globe valve to permit fine control of low flow rates necessary for adiabatic film cooling tests. Additionally, each loop was insulated based on the relative mass flow rate of coolant to that region such that all three loops produced roughly the same density ratio. For this reason, the suction side had the most insulation while the showerhead had the least. Downstream of the flow control valves, the loops entered the base of the tunnel below the test vane, allowing flow to enter separate plenums for each coolant region. An impingement plate, or baffle, was positioned 5.5 mm from the inside wall of the test vane for the suction and pressure side cooling plenums to equalize coolant flow through the coolant holes and to better simulate the actual turbine vane internal geometry. See the preceding section

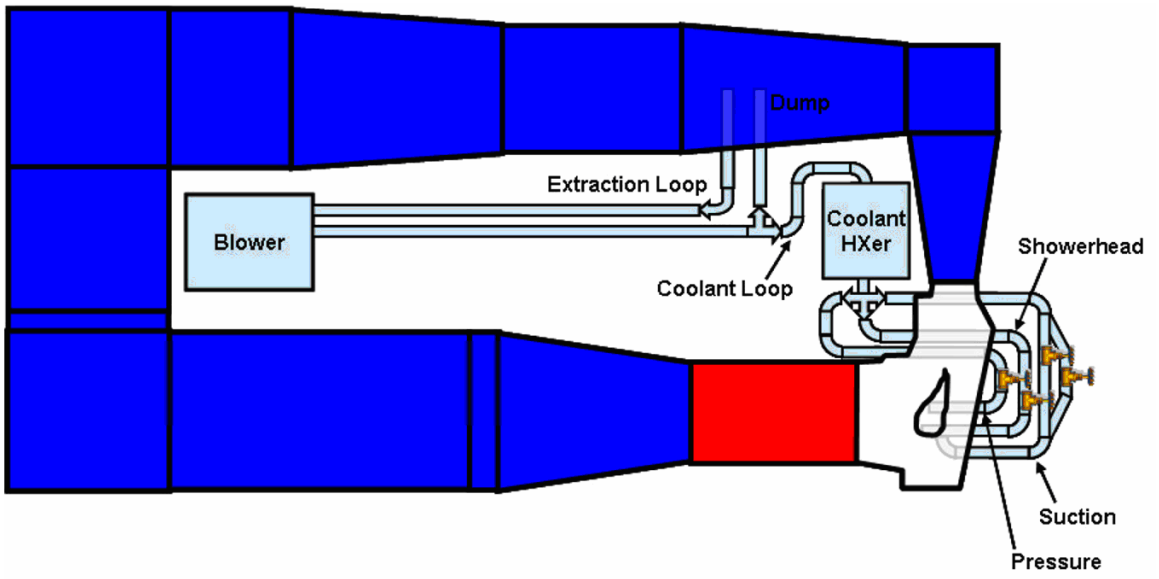

Figure 2.5: Schematic of secondary loop with coolant piping.

(§2.1.1) for details of the geometry of the coolant holes for individual regions. Liquid nitrogen was used to cool secondary loop flow by passing through the tubing of several multiple pass fin-tube heat exchangers encased in a large airtight and insulated box, labeled "Coolant HXer" in Figure 2.5. The secondary flow loop fluid was cooled by passing through the fins of these heat exchangers. The nitrogen flow was then dumped into the secondary flow loop to further assist with cooling of the secondary loop flow to be used as coolant in the vane. In general, the positive pressure created by adding mass to the secondary flow loop (and thereby the main tunnel as well) helped to reduce humidity levels by preventing ingestion of room air into the tunnel.

2.1.4 Velocity and Turbulence Conditions at the Cascade Inlet

Adjustments to the hot streak generator section of the wind tunnel were made upon installation to ensure a uniform velocity distribution. As mentioned previously, the hot streak generator was fully adjustable across the pitch using the support bars which slide through holes in the sides of the hot streak generator section. Additional resistance rods (external to the hot streak generator) were used to equalize the flow resistance across the duct and create a uniform velocity distribution exiting the hot streak generator section. Various numbers of rods, rod diameters, and locations were tested until a final configuration was obtained. The final positions and sizes of the resistance rods are shown in Figure 2.6.

Since the resistance rods located in the hot streak generator section produced a moderate level of turbulence, a fine mesh screen was positioned between the hot streak generator section and the test section to reduce turbulence levels as the flow approached the vane. Turbulence intensity and integral length scales were established using hot-wire anemometer measurements at Position A shown in Figure 2.1.

Mean velocity profiles were measured at Position A, both downstream of the hot streak generator and downstream of the resistance rods to the side of the hot streak generator. A pitot-static probe was used for velocity measurements at low mainstream turbulence and a hot wire anemometer was used for velocity measurements at high mainstream turbulence. Profiles were measured with and without the high turbulence generation rods. These profiles are shown in Figures 2.7a and 2.7b for the position

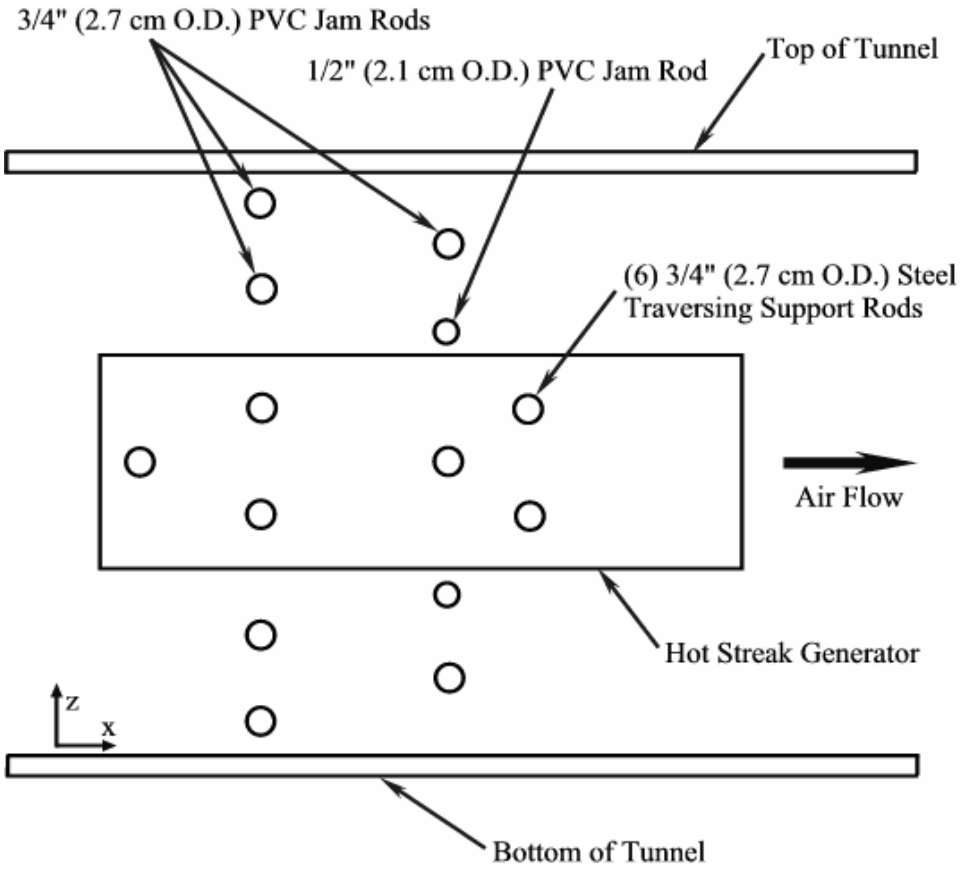

Figure 2.6: Final positions and sizes of resistance rods, horizontal view of hot streak generator section.

downstream of the hot streak generator and resistance rods, respectively. The profiles between 0.16*S* and 0.84*S* showed that for the low turbulence case the mean velocity profile was uniform within ± 4%, and within ± 1% for the high turbulence case.

The velocity profile with the hot streak generator activated indicated an increase in velocity proportional to the rise in temperature. This increase in velocity is shown in Figure 2.8, and followed the relation $V_{hs} = V_{\infty}*(T_{hs}/T_{\infty})^{1/2}$, consistent with a conserved total pressure. The profile comparing the velocity over only the resistance rods is provided for comparison.

Turbulence measurements including turbulence intensity (*Tu*) and the integral length scale (Λ_f) were made with a hot-wire anemometer at Position A with and without the turbulence generator. The turbulence length scale was computed by multiplying the

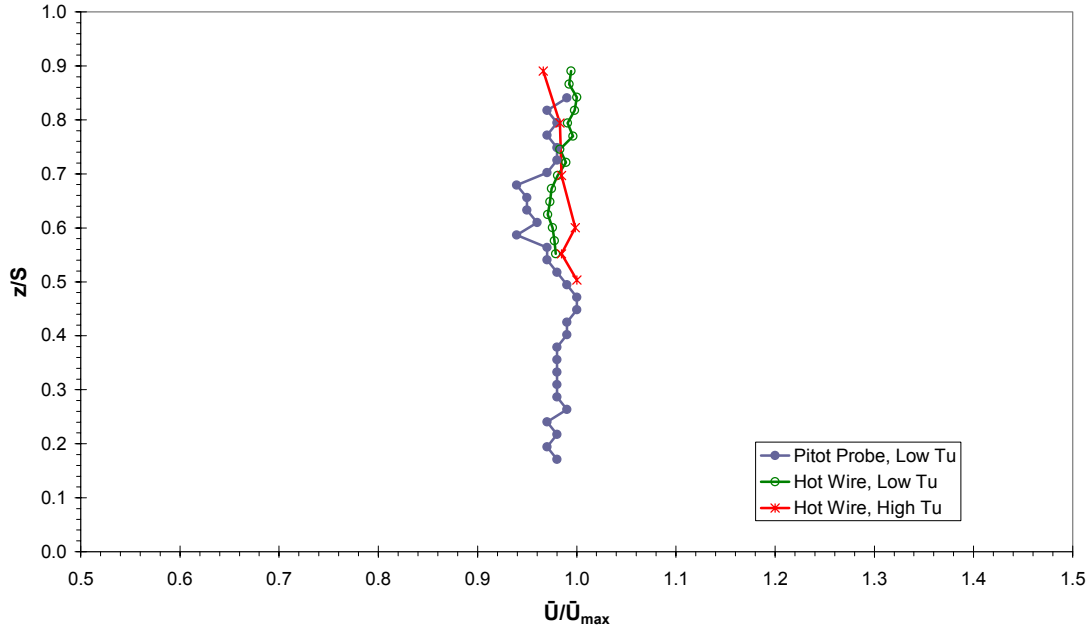

Figure 2.7a: Normalized mean velocity distribution over the hot streak centerline measured at Position A, low and high *Tu*.

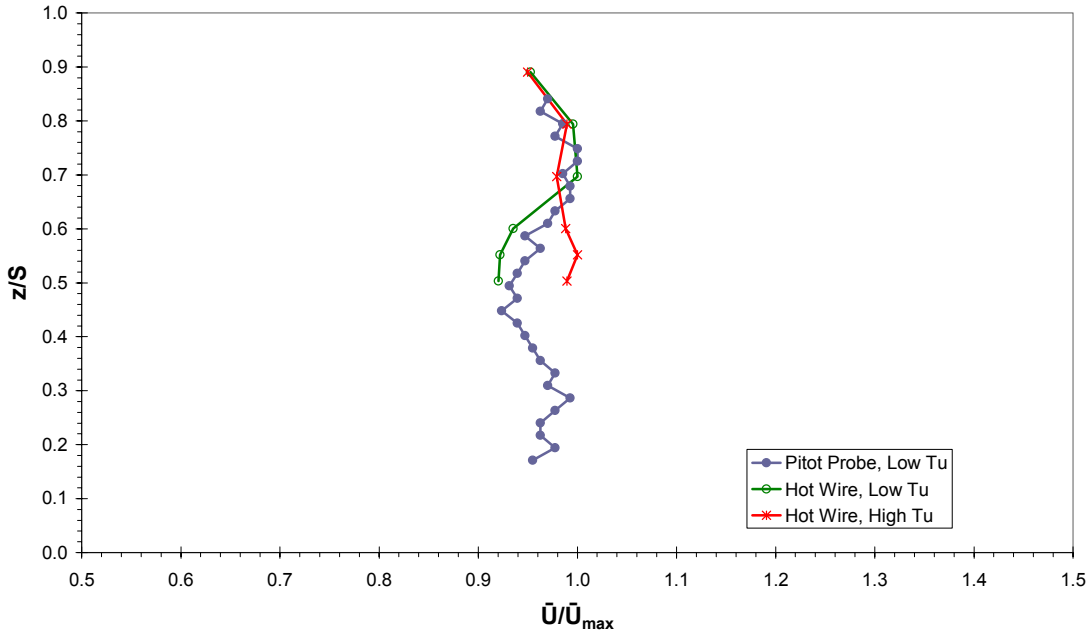

Figure 2.7b: Normalized mean velocity distribution downstream the resistance rods measured at Position A, low and high *Tu*.

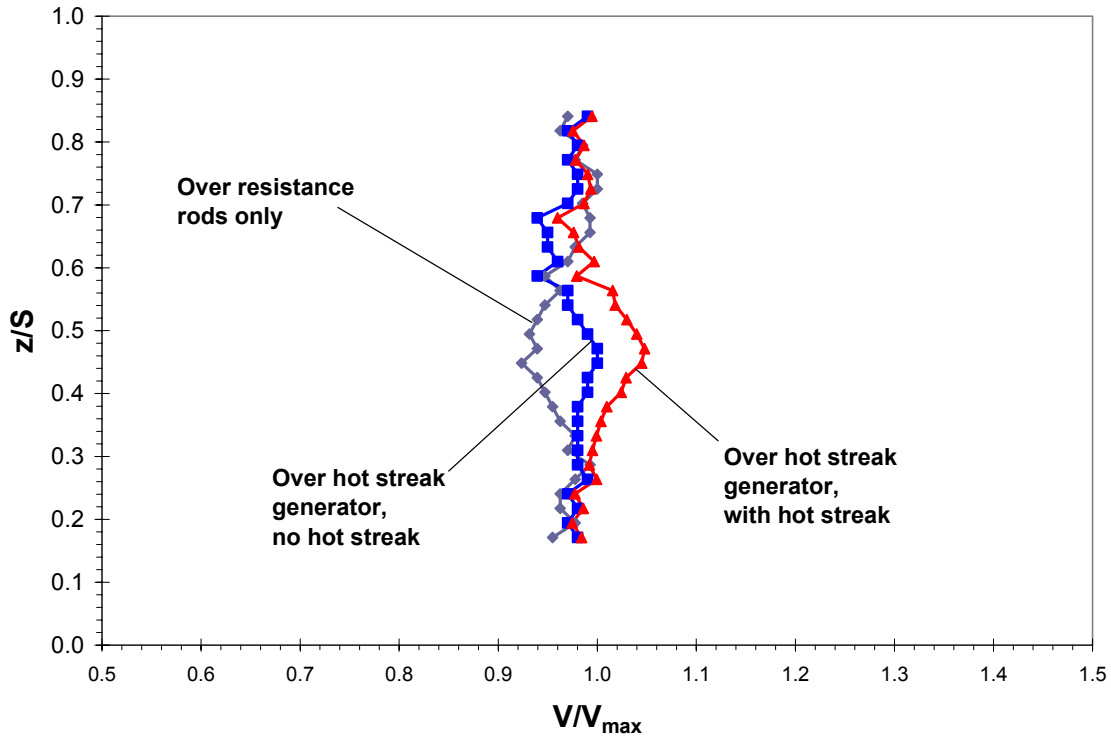

Figure 2.8: Normalized velocity distribution for vertical traverse over the resistance rods and over the hot streak generator measured at Position A, *Tu* = 3.5%.

turbulence time scale by the mean velocity. Turbulence time scales were found by autocorrelation of the velocity data. The hot-wire system consisted of a TSI Thermo Systems Inc Model 1050 Constant Temperature Anemometer, a Model 1057 Signal Conditioner unit, a Model 1056 Variable Decade Probe Resistance unit, and a Model 1051-6 monitor and power supply. The hot-wire anemometer was calibrated using a Dwyer Series 471 Thermo-Anemometer to make velocity measurements. These measurements were made at Position A (see Figure 2.1) downstream of the resistance rods and downstream of the hot streak generator centerline. Measured turbulence intensity and integral length scale profiles are shown in Figures 2.9a and 2.9b, respectively. For the low turbulence condition, i.e. no turbulence generator rods, the values of the turbulence intensity and integral length scale depended on the position in the flow. The turbulence intensity downstream of the resistance rods was nominally Tu = 5% with an integral length scale of Λ_f = 32 mm, with a slight variation in the spanwise direction. Similar turbulence intensity and length scales were found above the hot streak

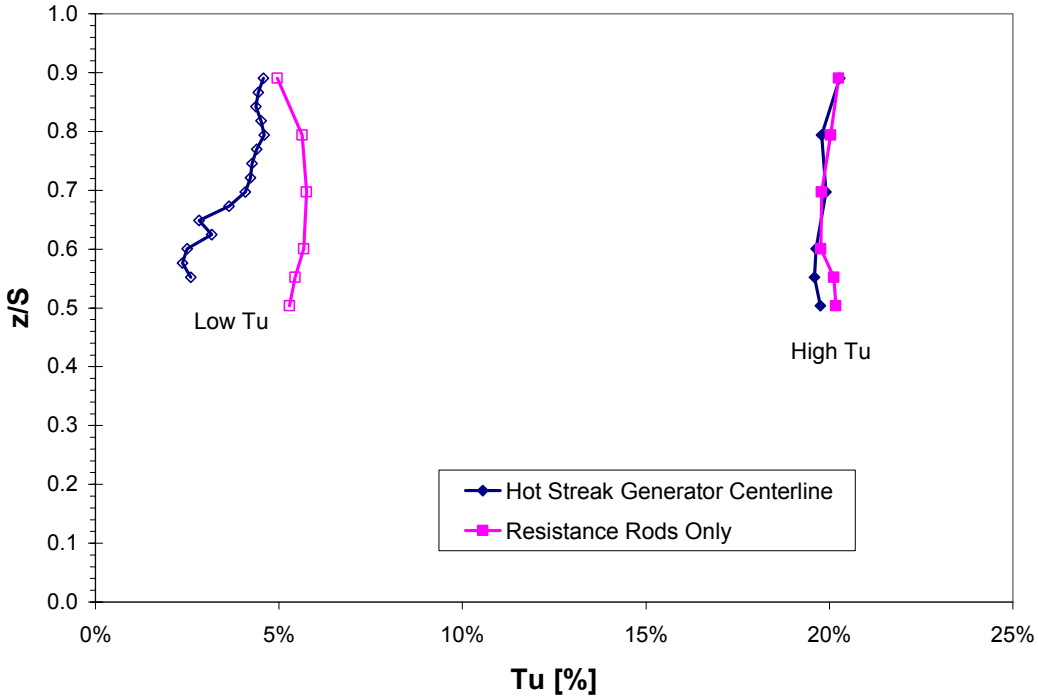

Figure 2.9a: Turbulence intensity for low and high turbulence conditions across the hot streak generator centerline and resistance rods.

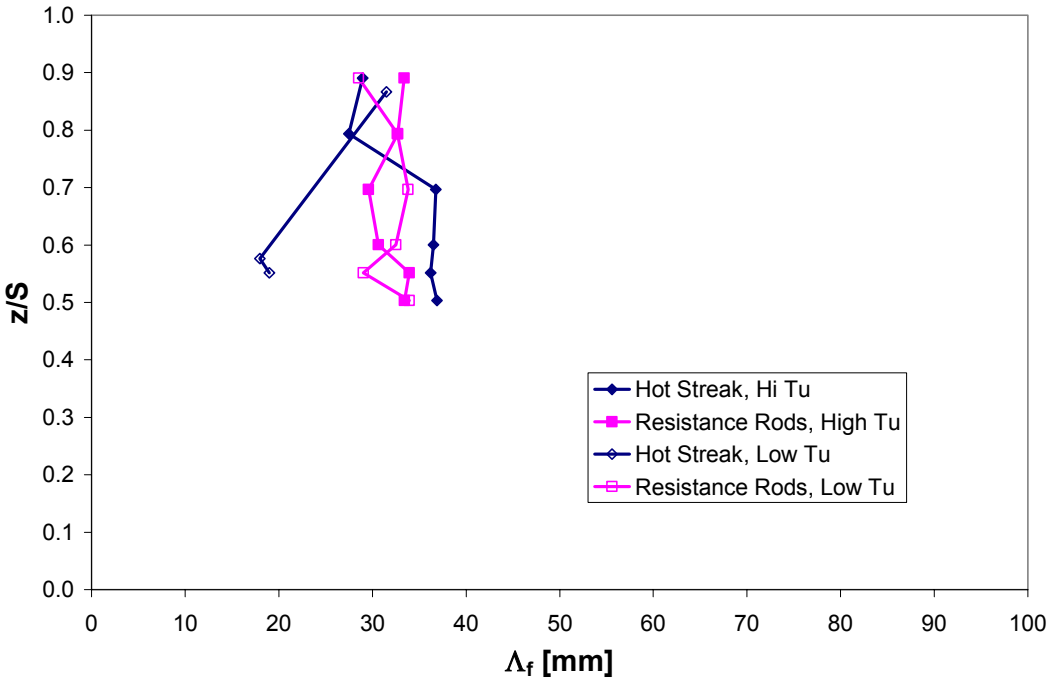

Figure 2.9b: Integral length scale for low and high turbulence over resistance rods and hot streak centerline.

generator. However, at a position coincident with the center of the hot streak the turbulence intensity was Tu = 2.5% with an integral length scale of Λ_f = 18 mm. Although these were significant variations between the core of the hot streak and the surrounding flow, the primary focus of this study was the high mainstream turbulence condition that simulates actual turbine conditions. With the turbulence generator in place, the turbulence intensity was nominally Tu = 20% and integral length scale was nominally Λ_f = 33 mm as shown in Figures 2.9a and 2.9b. These matched the turbulence intensity and integral length scales measured previously in the facility before the hot streak generator was installed (Cutbirth [17]). For the high mainstream turbulence condition, i.e. with the turbulence generation bars installed as shown in Figure 2.1, there was good uniformity for the turbulence intensity and length scale. Evidently, the high level of turbulence produced by the turbulence generation rods overwhelmed the low turbulence generated by the hot streak generator section.

2.2 Experimental Procedures

For hot streak tests without film cooling, drying out the main tunnel and secondary flow loop was not necessary. However, with film cooling, it was necessary to reduce the humidity level substantially to prevent frost accumulation within the coolant plenums and at the entrances and exits of coolant holes. Even at very low humidity levels, on the order of RH = 8%, enough frost accumulated to completely block coolant holes over a long testing period.

2.2.1 Desiccant Packs and Rack

The desiccant rack, situated downstream of the wind tunnel fan as shown in Figure 2.4, held 7 desiccant packs at approximately a 30° angle to the horizontal to increase air flow through the desiccant material. The desiccant packs were roughly 44.5 cm x 74 cm x 3 cm and were constructed of a metal frame with a layer of window screening and a layer of metal grill to protect against tearing, shown schematically in Figure 2.10. These were the same desiccant packs used by previous researchers. They contained a desiccant material designed to absorb carbon dioxide and water vapor since the cryogenic temperatures reached in the coolant supply were low enough to condense

CO_2 as well as "normal" humidity. The desiccant was regenerated by baking at high temperatures for several hours, thus driving off absorbed CO_2 and water vapor.

2.2.2 Desiccant Preparation

A test involving film cooling at a high density ratio required a great deal of preplanning. The desiccant packs were baked in a furnace for no less than 4 hours at approximately 550 K (530° F) or higher. Since the furnace cooled slowly, the furnace was turned down to approximately 400 K (260° F) about 12 hours prior to the test day to facilitate the removal of the packs from the furnace and the placement of the packs in the desiccant rack in the wind tunnel.. This procedure was found to provide equivalent drying to removing the packs at high temperature, but obviously resulted in much more manageable desiccant packs.

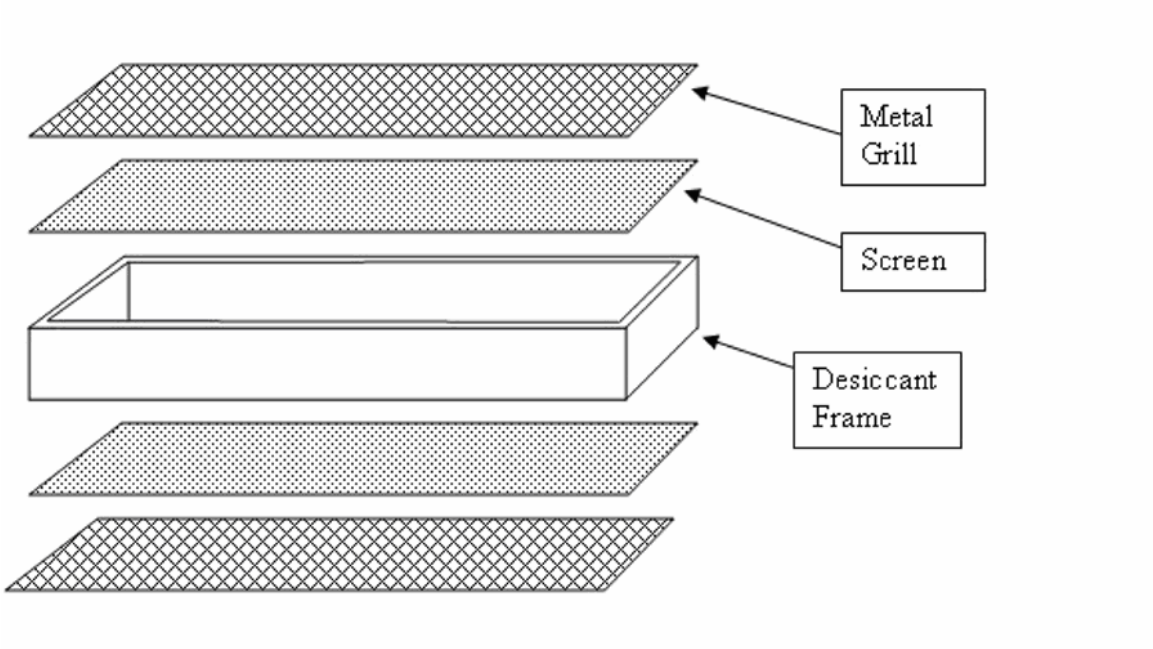

Figure 2.10: Schematic of desiccant frame.

2.2.3 Drying Procedure

Since the tunnel needed to be dried to less than RH = 8% to prevent frost build-up, additional measures were developed to supplement the desiccant packs. The tunnel was purged with a full tank of liquid nitrogen, utilizing the LN_2 heating loop designed for the small wind tunnel in the same lab. This heating loop was controlled by two high

voltage Variacs and utilized a convection loop with a blower to further heat the nitrogen flow. The warmed nitrogen gas entered the tunnel just downstream of the test section. It was important to allow air to escape from the tunnel during this procedure since a large amount of mass was added. Two inspection holes located on the top of the screens (the screen location is shown in Figure 2.4) were uncovered during nitrogen purging to accomplish this need. It was also important that lab personnel were not exposed to the oxygen-poor environment inside the tunnel once purging commenced. Oxygen levels well below 10% (21% being normal levels) were measured using an oxygen meter near open ports and the desiccant hatch during one purging session to establish the safety procedures necessary during the nitrogen purging process. Thus, the nitrogen flow was turned off before opening any hatches or ports to prevent positive pressure inside the tunnel from venting oxygen poor tunnel air to the room where personnel would have been exposed. During the nitrogen purge, the blower for the secondary loop was employed, along with opening all of the coolant valves to allow simultaneous drying of the main tunnel and secondary loop. Once the tunnel humidity reached about 20% RH, the tunnel was shut off to allow the desiccant packs to be placed in the desiccant rack. It was also advisable to keep the hallway door next to the desiccant rack hatch closed to prevent excessive ingestion of room air in the tunnel. The nitrogen purging was also turned off at this time for safety reasons mentioned above. Desiccant packs were brought from the furnace in a specially designed cart, partially constructed of fire brick. The cart was fully enclosed to prevent excessive absorption of CO_2 and water vapor as the packs were transported. Heavyweight fiberglass and leather gloves were used to move the desiccant packs due to their high temperature and rough exterior. The placement of the desiccant packs into the desiccant rack was accomplished as quickly as possible (ideally by two persons) to prevent the tunnel air from mixing with room air with the hatch open. After the packs were inserted, the tunnel was turned on along with the nitrogen purge. Nitrogen purging was usually continued until the tank was empty (approximately 1 hour total). The tunnel humidity level was monitored about every 15 minutes until a minimum humidity level of $RH = 8\%$, was reached, at which point cool-down of the secondary loop commenced.

2.2.4 Cool-down procedure

The coolant heat exchanger and secondary loop system was designed to provide stable cryogenic temperatures over a long period of time. As a result, it was a highly over-damped system, responding to changes in LN_2 supply very slowly. The LN_2 flow rate was monitored so that the heat exchanger exit temperature trendline showed a slow decrease. As indicated in the secondary loop description, the heat exchanger exit plenum was a three-way connector supplying coolant to separate coolant loops for the individual coolant regions. Generally for hot streak film cooling tests, all three regions were utilized individually or in combination at some point in the experiment. For this reason, all valves were opened fully at the beginning of the cool-down process to permit cooling of the vane interior coolant plenums. After the coolant temperature reached about 250 K (DR = 1.2), the valves were adjusted to balance the cooling of the individual regions, since with all valves fully open, they cooled at substantially different rates. As indicated before, the individual coolant loops were insulated according to the coolant supply needs for that individual region, while the valves would permit a much higher flow rate. Cool-down generally required approximately 1-2 hours, and it was found that a slow gradual cool-down would permit more stable operating conditions. Once the density ratio reached about DR = 1.5 ($T_{coolant}$ = 200 K), the coolant valves were adjusted to approximately the desired blowing ratios. This allowed the cool-down process to reach a more stable condition as excess coolant flow tended to promote too rapid of a cool-down process. If the valves were left open, subsequent closing of the valves to their desired settings when at the required density ratio often resulted in severe system instabilities which were very time consuming to correct. When using all coolant regions simultaneously it was necessary to heat the showerhead loop to prevent the showerhead density ratio from increasing well above its desired value. A heat gun was used to heat the brass showerhead coolant valve while the showerhead coolant flow was reduced to roughly ¼ its desired value. As a rule of thumb, the showerhead density ratio was heated to about DR = 1.55 before increasing the coolant flow to the desired value. While increasing the flow rate during the experiment, heating of the coolant valve was often required, but care was taken to avoid melting the PVC connectors during this procedure. During an experiment, fine tuning of the density ratio was accomplished by adjusting the

nitrogen flow rate and sometimes required some heating of the appropriate coolant loop. For individual coolant region experiments, once stability was reached by proper adjustment of the nitrogen flow rate, only minor adjustments of the coolant valve and nitrogen flow rate were required over fairly long periods of time.

2.2.5 Uniformity of Mainstream Temperatures

Since the hot streak measurements depend upon a uniform mainstream, measurements were made to determine if inlet temperature non-uniformity was an issue. For previous studies using the facility, small mainstream temperature non-uniformities were not a concern since measurements were made over a relatively small span or pitch. Measurements of the mainstream temperature approaching the vane showed that the heat exchanger caused a considerable temperature non-uniformity due to complete blockage of 18 of the 20 coolant tubes. The coolant tubes made 4 passes through the tunnel in a spanwise direction and connected to common inlet and outlet plenums, which equalized pressure through the tube array. Since the heat exchanger used the domestic water supply, which is much colder in winter months, the temperature non-uniformity was much more noticeable during these times. Measurements at Position A made prior to any repairs showed a variation of as much as 2.5° C in the mainstream in the pitchwise direction. This was due to the positions of the two open cooling tubes, which were the 7^{th} and 13^{th} counting from the outside tunnel wall, thus cooling portions of the flow significantly while leaving the remainder unaffected. Although temperature non-uniformities were likely much higher immediately downstream of the heat exchanger, mixing downstream between the heat exchanger and Position A reduced the effect somewhat giving the total variation of about 2.5° C (see schematics in Figures 2.1 and 2.4). Extensive rebuilding and repair of the tunnel heat exchanger (shown in the schematic in Figure 2.4) was done to eliminate clogged tubes. Since a common inlet plenum supplied water to the cooling tubes and the water was supplied at about 60 psi (typical of domestic water supply pressures), sufficient pressure during normal operation could not be produced to keep all the tubes clear. Due to the high mineral content of the water supply and lack of sufficient driving pressure, calcification of the tubes was more pronounced than would normally be expected. Clearing of the tubes consisted of

recirculation of commercial radiator cleaners, drain cleaners, and ultimately a dilute hydrochloric acid solution through the heat exchanger utilizing a large tank and swimming pool pump to drive the flow. Between cleanings, fresh water was used to remove any residual chemical to prevent damage to the tube array. The heat exchanger plenums were removed from the coolant tubes during this time and water was driven through each tube pass individually to finally clear all remaining contaminants. Once the tubes were completely cleared, to facilitate future repairs and to allow adjustment of the flow through the heat exchanger, the plenums supplying the tube array were removed and refitted with a valving system which allowed independent cleaning of each tube pass. A photograph of the current valve system is shown in Figure 2.11. The pressure and flow rate through the heat exchanger using the domestic water supply was substantially less than the design point for the heat exchanger. Subsequently, it is expected that cleaning may be necessary on a fairly frequent basis to ensure an even distribution of cold water

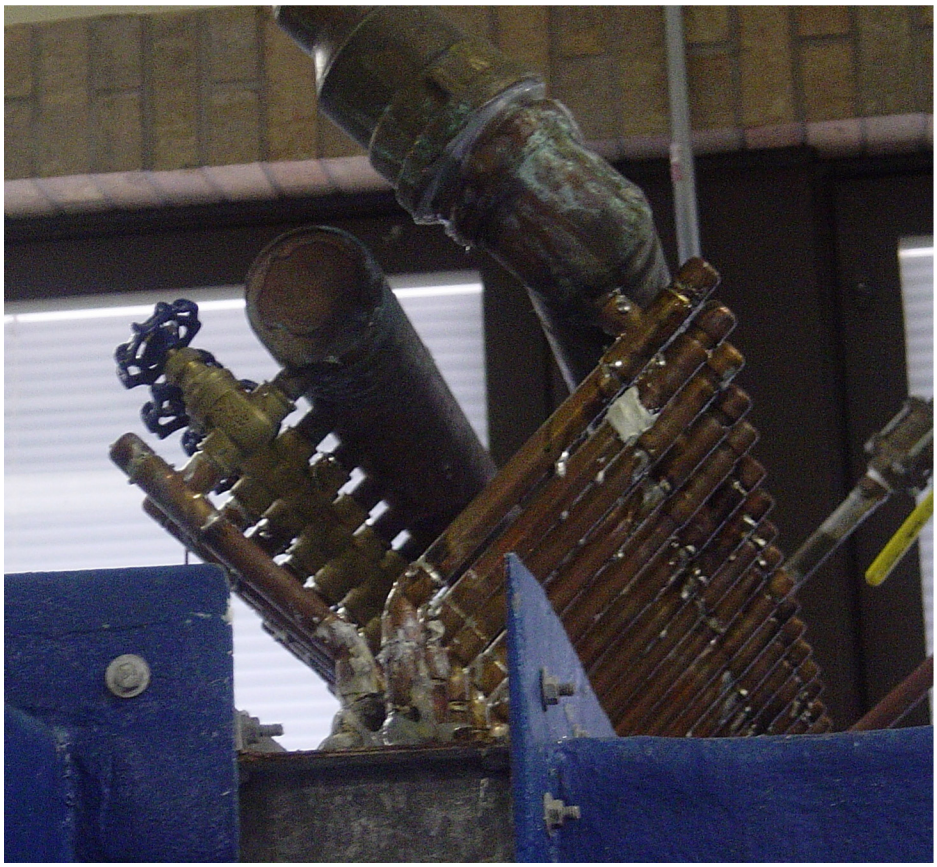

Figure 2.11: Retrofitted heat exchanger with tubing and valving to plenums.

flow through all of the tubes. Figure 2.12a and 2.12b show the temperature profiles in the horizontal (pitchwise) and vertical (spanwise) directions after the repairs were made. For the horizontal measurements, $y/P = 0.0$ was upstream of the stagnation line of the test vane, and other measurements showed that the profile was roughly symmetric about this line ($y/P > 0.0$). As shown in the figures, temperature profiles were uniform within 0.5° C after the repairs were completed.

2.2.6 Hot Streak Generator Operation

Although some experiments in this study involved film cooling only, the hot streak generator was employed for most of the tests and some additional considerations were taken into account during its operation. The hot streak generator contained two sets of heating elements at nominally 3.5 kW each, situated in the streamwise direction. For the low turbulence condition (no turbulence generator rods), the hot streak generator was run at ½ power only to reduce the possibility of damaging the test vane leading edge by exposing it to very high temperatures. It was also found that a slightly more concentric hot streak was produced by using the upstream heater. For the high turbulence condition, both heaters are be used to produce a nominal temperature ratio of $T/T_\infty = 1.1$ at the standard upstream reference location, Position A. The hot streak generator was activated by a start-stop switch, one for each heater. The switches were located on the wall opposite the hot streak generator section and had lights to indicate operation. The indicator lights were oriented in the same fashion as the heating elements, with a red light for the downstream heater and a yellow light for the upstream heater. A special safety feature was incorporated into the wiring which prevented operation of the hot streak generator without adequate tunnel velocity. Despite this precaution, the hot streak generator should not be activated without a mainstream velocity of at least $U_{inf} = 5.5$ m/s. Since the hot streak generator heated up several components in the main tunnel loop, it was necessary to allow a short period of time for the hot streak to become steady. Generally, this time period was about 5 minutes. Conversely, when deactivating the hot streak generator, a similar period of time was permitted to elapse before the temperature non-uniformity was observed to die away.

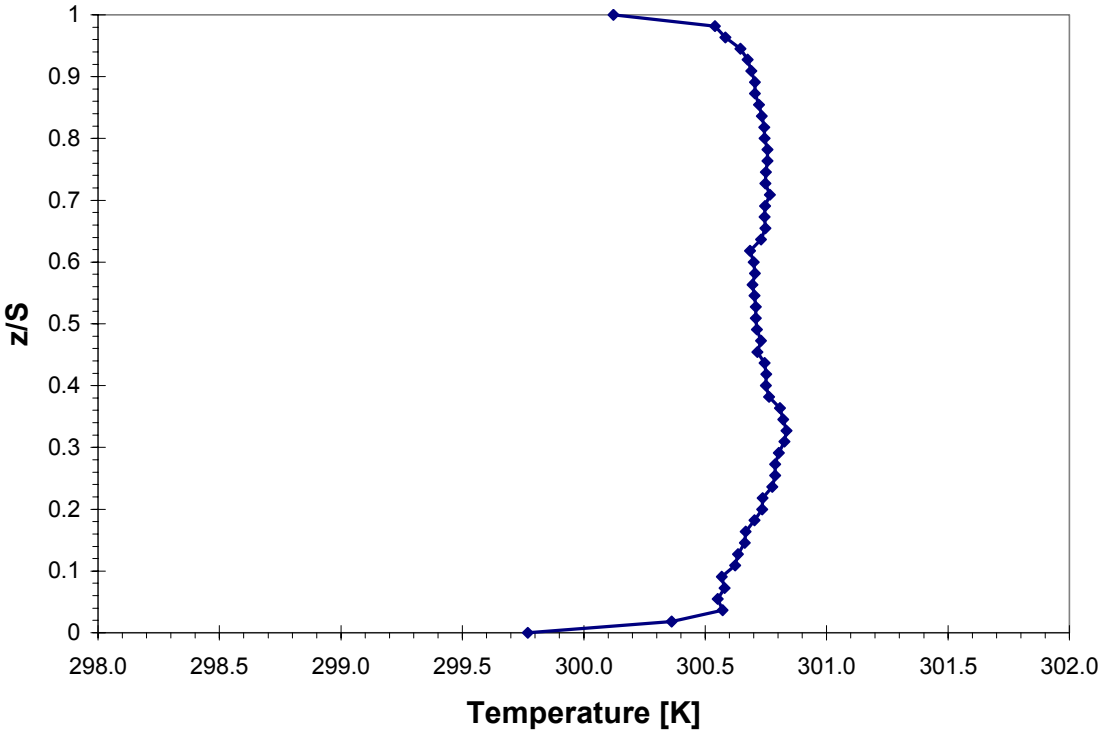

Figure 2.12a: Vertical (spanwise) measurements of the mainstream approach temperature at Position A, no hot streak.

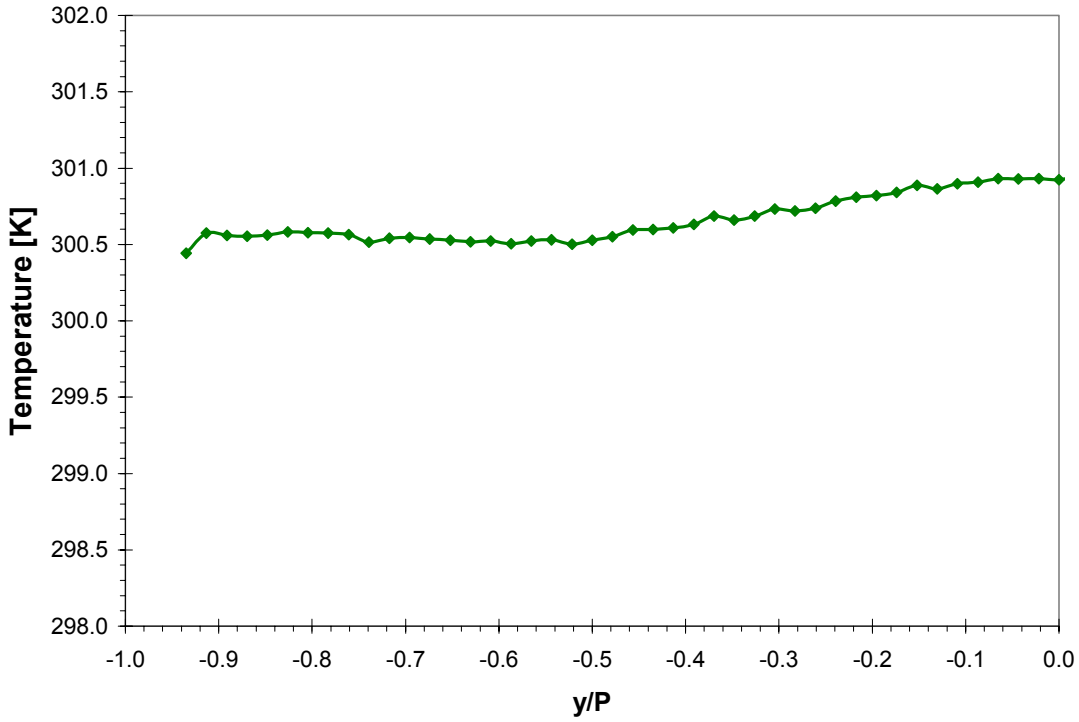

Figure 2.12b: Horizontal (pitchwise) measurements of the mainstream approach temperature at Position A, no hot streak.

2.2.7 LabVIEW Set-up, Monitoring, and Data Collection

In Figure 2.13, a snapshot of the tunnel monitor in LabVIEW is shown. This program was written by Robertson [18] specifically for hot streak measurements in the facility and is available in that reference. This front panel provided the user with blowing ratios and density ratios for each region along with the coolant heat exchanger outlet temperature and two mainstream temperature measurements, one at the vane leading edge and one at the thermocouple rake location. Up to four thermocouple channels could be monitored in Chart 1 on the front panel, while Chart 3 was used to monitor the instantaneous temperature profile read by the thermocouple rake. A sample setup file for LabVEW is shown in Figure 2.14 demonstrating the format and required parameters. Due to the complexity of the coding required for any given experiment, a separate user guide by Robertson [18] was written to explain the various parameters and is available in that reference. Since the front panel for the tunnel monitor was designed to plot variables in order, it is important to plan the order of the thermocouples to plot them appropriately. More details of the design and implementation of the LabVIEW system are available in Robertson [18].

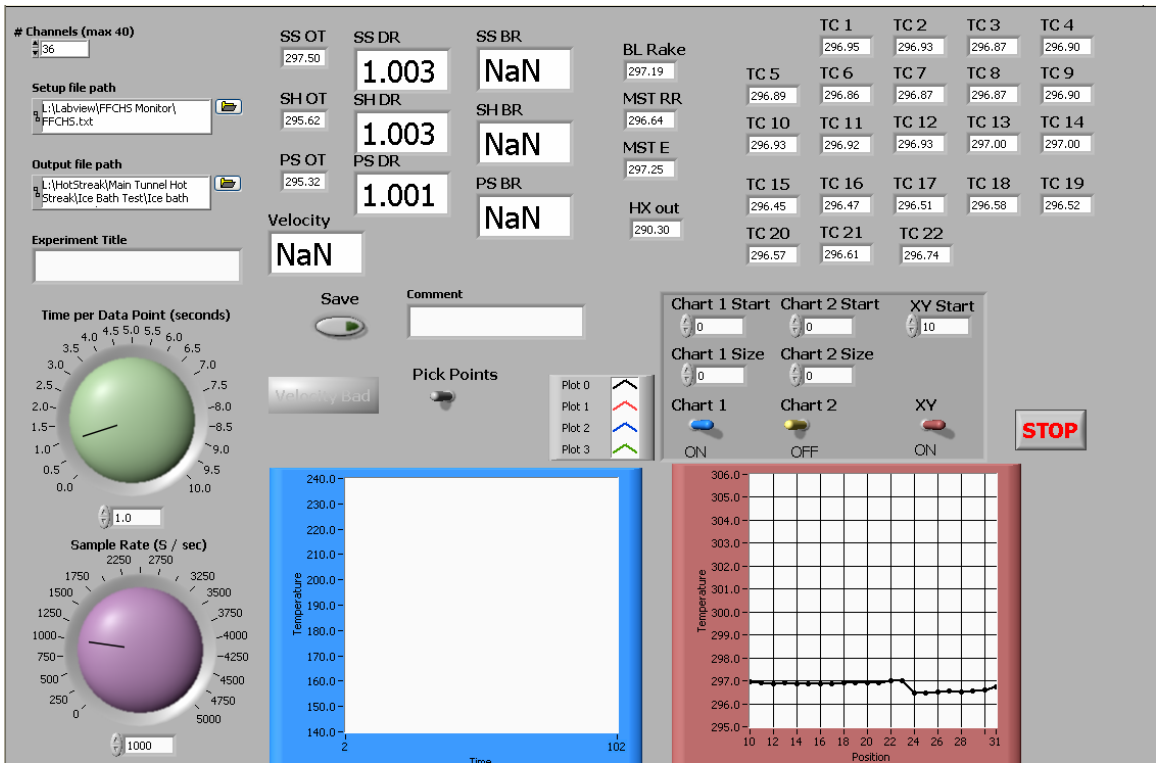

Figure 2.13: Tunnel monitor front panel in LabVIEW.

```
order   flag    CS      HL      LL      Title
01      12      200     +0.12   -8.85   SS OT
02      13      201     +0.12   -8.85   SH OT
03      14      202     +0.12   -8.85   PS OT
04      11      203     +0.74   -0.48   MST E
05      10      204     +0.74   -0.48   MST RR
06      15      205     +0.12   -6.37   SS DR
07      15      206     +0.12   -6.37   SH DR |
08      15      207     +0.12   -6.37   PS DR
09      20      210     +1.31   -1.12   TC 1
10      20      211     +1.31   -1.12   TC 2
11      20      212     +1.31   -1.12   TC 3
12      20      213     +1.31   -1.12   TC 4
13      20      214     +1.31   -1.12   TC 5
14      20      215     +1.31   -1.12   TC 6
15      20      216     +1.31   -1.12   TC 7
16      20      217     +1.31   -1.12   TC 8
17      20      218     +1.31   -1.12   TC 9
18      20      219     +1.31   -1.12   TC 10
19      20      220     +1.31   -1.12   TC 11
20      20      221     +1.31   -1.12   TC 12
21      20      222     +1.31   -1.12   TC 13
22      20      223     +1.31   -1.12   TC 14
23      20      224     +1.31   -1.12   TC 15
24      20      225     +1.31   -1.12   TC 16
25      20      226     +1.31   -1.12   TC 17
26      20      227     +1.31   -1.12   TC 18
27      20      228     +1.31   -1.12   TC 19
28      20      229     +1.31   -1.12   TC 20
29      20      230     +1.31   -1.12   TC 21
30      20      231     +1.31   -1.12   TC 22
31      10      108     +0.12   -8.85   HX out
32      66      120     +5.50   +0.00   Velocity
33      37      121     +6.50   +0.00   SS BR
34      58      122     +6.50   +0.00   SH BR
35      49      123     +6.50   +0.00   PS BR

24 25
```

Figure 2.14: Example input file for LabVIEW tunnel monitor.

For these experiments, two different thermocouple rakes were used. One consisted of 22 K-type thermocouples with a spacing of 7.8 mm. This thermocouple rake was used to acquire temperature data at Position T and Position B as shown in Figure 2.1. The second thermocouple rake consisted of 6 E-type thermocouples with a spacing of 14.2 mm and was used in preliminary measurements as well as measurements at the standard reference Position A and at Positions S1, S2, P1, and P2.

Additional data was acquired using a single thermocouple probe which was positioned at midspan and rotated about its axis to take fine scale measurements near the vane wall. A traverse with a 1/5° resolution using a Vernier scale was utilized for this purpose, providing Δy = 0.1 mm with a probe length of 6.5 cm. Detailed measurements

conducted with the single thermocouple probe were made at approximately the same vane surface locations as Positions S1, S2, P1, and P2. Due to the size of the thermocouple probe and the position of the access port in the top of the tunnel beside the vane, the nominal positions of the traverses were slightly downstream of those shown in Figure 2.1. A schematic of the vane and single thermocouple probe is shown in Figure 2.15 describing the relative location of the measurement planes and arc made by the probe. To differentiate the positions S1, S2, P1, and P2 from those pertaining to the fine scale measurements, the downstream positions for the single thermocouple probe are referred to as S1', S2', P1', and P2', with nominal positions of $0.36L_S$, $0.70L_S$, $0.38L_P$, and $0.71L_P$ respectively. Since the thermocouple probe was traversed in an arc, the position closest to the vane was slightly farther downstream than the position parallel to the vane wall as shown in the schematic in Figure 2.15. However, the maximum range of streamwise displacement for the traverses was $\pm 0.015L_S$ and $\pm 0.02L_P$ for the suction side and pressure side respectively. Since the hot streak attenuation occurred over much larger distances, this range of streamwise displacement was not expected to cause errors in the reported findings.

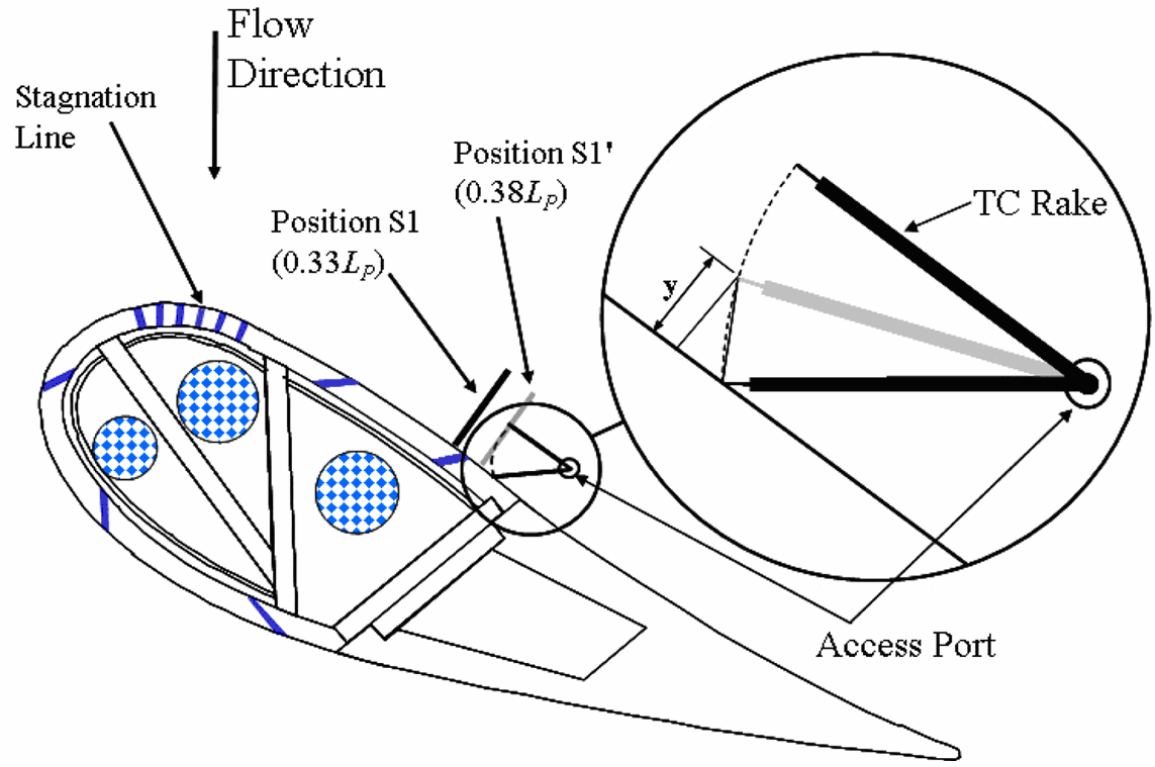

Figure 2.15: Schematic of the single thermocouple probe and its traversing arc.

2.2.8 Computation of Individual Row Blowing Ratios

Since the suction side rows of coolant holes had a common plenum as shown in Figure 2.3, blowing ratios for each row of holes had to be computed independently. The LabVIEW tunnel monitor used a user-defined average external velocity to compute an average blowing ratio for the 3 rows of coolant holes, thereby giving an overall mass flow rate for the suction side. More details of the LabVIEW computation are available in Robertson [18]. Since the external velocity differed between rows, at 23.4 m/s, 29.3 m/s, and 31.1 m/s for the 1st, 2nd, and 3rd row of coolant holes respectively for an inlet velocity of 5.8 m/s, the pressure difference between the common plenum and the coolant hole exits for each row also differed. As a result, mass flow rates differed somewhat between the coolant rows, but blowing ratios differed even more. To find the actual blowing ratios for each row of holes, based on an average blowing ratio, a formula was derived from the mass flow balance. The mass flow rate was calculated using an iterative method detailed in Goldstein [19], which first computed the orifice meter discharge coefficient using the Reynolds number through the orifice plate for the suction side (see §2.1 for a description of the secondary flow loop). The mass flow rate through the orifice plate was then computed and since mass is conserved, this was also the total mass flow rate through the film cooling holes. The total coolant mass flow rate was used to find the average blowing ratio using the average external velocity.

Since the total mass flow rate was known, this may be written as:

$$\dot{m}_{Tot} = \dot{m}_1 + \dot{m}_2 + \dot{m}_3 \qquad (2.1)$$

where the subscripts 1, 2, and 3 refer to the coolant rows 1, 2, and 3. Using the modified Bernoulli's equation including losses, the mass flow rate for a given row can be written as:

$$\dot{m}_1 = C \cdot A\sqrt{2 \cdot \rho \cdot (p_{plenum} - p_{\infty,local})} \qquad (2.2)$$

where C is a multiplicative factor, A is the total area of the coolant holes in the row, ρ is the coolant density, $p_{\infty,local}$ was the local external static pressure, and p_{plenum} was the plenum pressure (unknown). Since the area of the plenum was much larger than the area of the holes, the discharge coefficient, K, may be substituted for C. Thus, given the discharge coefficient the equation may be written as:

$$\dot{m}_{Tot} = \sum_{n=1}^{3} K \cdot A\sqrt{2 \cdot \rho \cdot (p_{plenum} - p_{n,\infty,local})} \qquad (2.3)$$

where the subscripts refer to coolant rows and the only unknown is the plenum pressure, p_{plenum}. The discharge coefficient was given by Burd et al. [20], who found that discharge coefficients for coolant holes ranged from $K = 0.4$ to 0.75, with a value between $K = 0.6$ to 0.7 the most likely for the suction side hole configuration used in this study. Adiabatic effectiveness data was available only for the 1st row on the suction side and since this was used as a basis for the choice of blowing ratios for hot streak reduction, its predicted discharge coefficient of $K = 0.6$ was used for all rows on the suction side. Equation 2.3 was solved for p_{plenum} using the iterative equation solver in an HP 48GX calculator, and the results converted to blowing ratio by calculating the jet velocity for each row and by using the definition of blowing ratio:

$$M = \frac{\rho_c U_c}{\rho_\infty U_\infty} \qquad (2.4)$$

reproduced here for convenience. Mass flow rates increased downstream due to the increase in the local external velocity, as shown in Figure 2.16a. At an average blowing ratio of $M_{avg} = 0.7$, and for a discharge coefficient of $K = 0.6$, the 2nd row mass flow rate was about 35% greater than the 1st row mass flow rate and the 3rd row mass flow rate was about 45% greater than the 1st row mass flow rate. The variation of mass flow rate distribution with discharge coefficient showed that there was a small effect. As expected, the mass flow rate was always greater for a downstream row. However, the relation between blowing ratios was affected differently as shown in Figure 2.16b. As shown in this figure, the blowing ratio relation between rows was inverted within the range of discharge coefficient shown, and the 1st row blowing ratio was estimated to be between $M_{local} = 0.70$ and 0.54 for a discharge coefficient of $K = 0.50$ to 0.75. It should be pointed out that even with a good estimate of the discharge coefficient based on empirical data, the sensitivity of the individual row blowing ratio to the discharge coefficient was so great that without specific knowledge of the discharge coefficient of the suction side coolant holes, some uncertainty remained. Pressure side local row blowing ratios were calculated using the method above, where calculations only required consideration of two

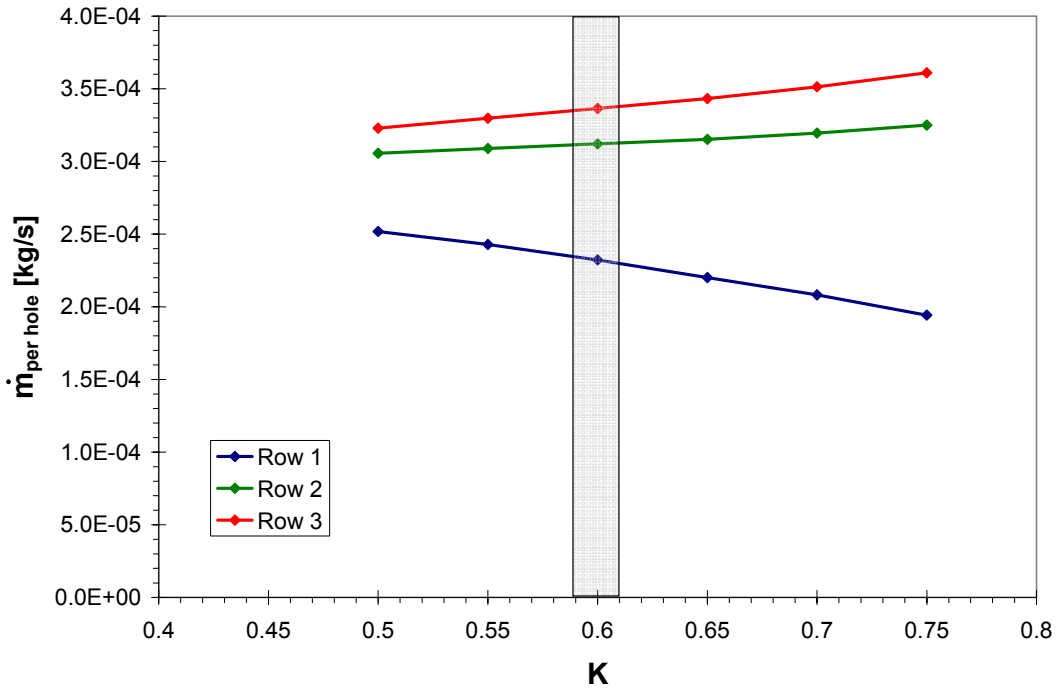

Figure 2.16a: Local single hole mass flow rates for suction side rows 1, 2, and 3 (SS4, SS5, and SS6) based on discharge coefficient, *K*, for an average blowing ratio of M_{avg} = 0.7.

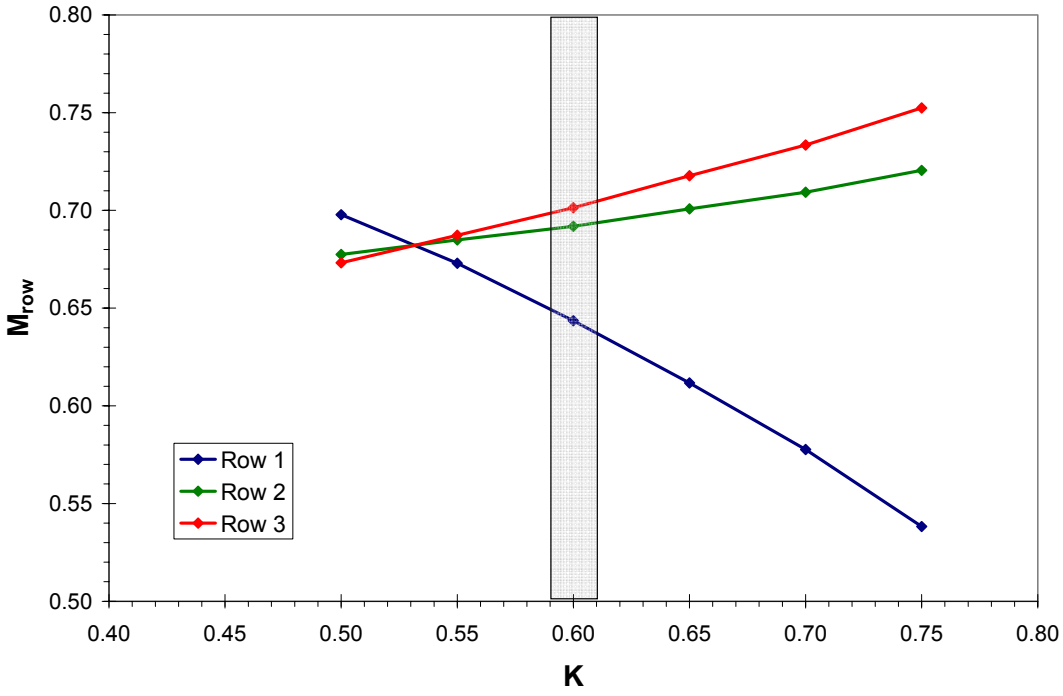

Figure 2.16b: Local blowing ratios for suction side rows 1, 2, and 3 (SS4, SS5, and SS6) based on discharge coefficient, *K*, for an average blowing ratio of M_{avg} = 0.7.

rows of coolant holes. For the pressure side, at an average blowing ratio of M_{avg} = 0.6, and for a discharge coefficient of K = 0.6, the 2nd row mass flow rate was about 50% greater than the 1st row mass flow rate. Local row blowing ratios for this condition were M = 0.55 and M = 0.64 for the 1st row and 2nd row respectively.

2.2.9 Hot Streak Profiles for Superposition Calculations

Coolant and hot streak profiles were used to estimate the combined effect of the film-cooled hot streak using additive superposition. The pitchwise positions of the thermocouples were very difficult to duplicate if the rake was removed from the tunnel facility between tests. Since the computation was carried out on a point-by-point basis, some interpolation of hot streak values was necessary in order to match positions of points in the coolant data. Fortunately, the vertical, or spanwise, position of the thermocouple rake was easy to duplicate between experiments, so no interpolation was required in the spanwise direction. To validate the interpolation of hot streak values, a comparison is made in Figure 2.17 between the experimentally measured values and

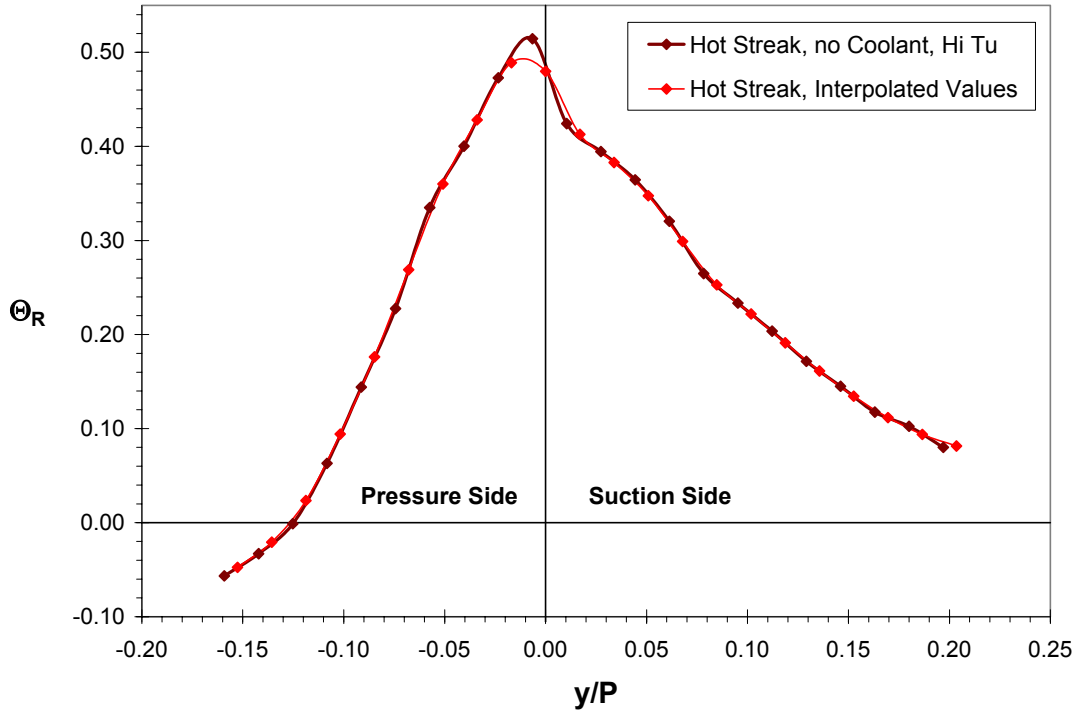

Figure 2.17: Comparison of measured and interpolated normalized temperature ratio (Θ_R) profiles at Position T at midspan (z/S = 0.50), for the hot streak at the stagnation line without coolant, high mainstream turbulence (Tu = 20%).

interpolated values which match coolant profile thermocouple pitch positions. Obviously, the peak of the hot streak could not be captured given the interpolated positions, but did not pose a problem since coolant measurements were also obviously not made at that location. A similar procedure was used for hot streak profiles at Position B, and for full field (y-z contours) for use in superposition computations.

2.2.10 Derivation of Superposition Equations

An energy balance at a point in the flow shows that the energy contained at that point is a function of the mass flow rate, specific heat and temperature difference with respect to a reference temperature, in this case the mainstream temperature. The variation of the density in the mass flow rate may be considered negligible, and since the specific heat varied only slightly for the full range of temperatures during the experiments, this may also be considered as a constant. At a point in the flow, the velocity field is relatively unaffected by the presence of the hot streak as shown by Dorney [13]. As such, the energy at a point in the flow may be expressed as a superposition of energy levels at that point for the coolant profile and hot streak profile separately as in Equation 2.5:

$$(\rho UdA)\cdot c_p\left(T_f - T_\infty\right)_{SP} = (\rho UdA)\cdot c_p\left(T_f - T_\infty\right)_C + (\rho UdA)\cdot c_p\left(T_f - T_\infty\right)_{HS} \quad (2.5)$$

where the subscript *SP* refers to the superposition result, and the subscripts *C* and *HS* refer to measurements of the coolant and hot streak temperatures respectively. Here the velocity is invariant with a given position and the specific heat may be considered nearly constant. For the range of temperatures observed, the density varied by no more than about 5%, so it too may be considered nearly constant. Therefore, this equation may be written as the superposition of fluid temperatures differences from the mainstream as Equation 2.6,

$$\left(T_f - T_\infty\right)_{SP} = \left(T_f - T_\infty\right)_C + \left(T_f - T_\infty\right)_{HS} \quad (2.6)$$

Dividing both sides by the peak hot streak-to-mainstream temperature difference results in Equation 2.7,

$$\frac{\left(T_f - T_\infty\right)_{SP}}{\left(T_{0,HS} - T_\infty\right)} = \frac{\left(T_f - T_\infty\right)_C}{\left(T_{0,HS} - T_\infty\right)} + \frac{\left(T_f - T_\infty\right)_{HS}}{\left(T_{0,HS} - T_\infty\right)} \quad (2.7)$$

which can be quickly related to the normalized temperature ratio, Θ_R, using its definition, repeated in Equation 2.8,

$$\Theta_{R,ij} = \frac{T_{ij} - T_\infty}{T_{0,HS} - T_\infty} \tag{2.8}$$

to obtain the superposition equation,

$$\Theta_{R,SP} = \Theta_{R,C,\exp} + \Theta_{R,HS,\exp} \tag{2.9}$$

where the subscripts *HS* and *C* refer to coolant only and hot streak only experimental results and the subscript *SP* refers to the superposition result. This equation is used in Chapter 10 to predict hot streak reduction due to coolant flow under various conditions.

2.3 Repeatability

Repeatability was evaluated both within an experiment and between tests for hot streak and coolant measurements. For all thermocouple rake traverses, a measurement at the midspan was taken first. The rake was then traversed to the top of its range and measurements were taken through the midspan point. Some examples of hot streak and coolant repeatability are shown in Figures 2.18a and 2.18b respectively. The repeatability within a test was generally very good and was closely monitored throughout the experiments.

Repeatability of the hot streak temperature ratios was not possible over long periods of use due to aging of the hot streak generator nichrome heating elements. Over a period of two years, the peak temperature dropped by 15%, however this was partially due to misuse of the hot streak generator by leaving it activated with the wind tunnel off, thus overheating the elements. Over a period of six months, during which a majority of the experiments were completed, no change was observed in the hot streak peak at Position A. When normalized by the upstream temperature difference as in Θ_R, the hot streak was repeatable over a period of more than a year. Figure 2.19 shows the normalized temperature ratio at Position A for two tests separated by 14 months. Due to the aging effect, results to be evaluated using the temperature ratio were taken over a short period of time, although this could be avoided by normalizing the measured fluid temperatures using Θ_R if necessary.

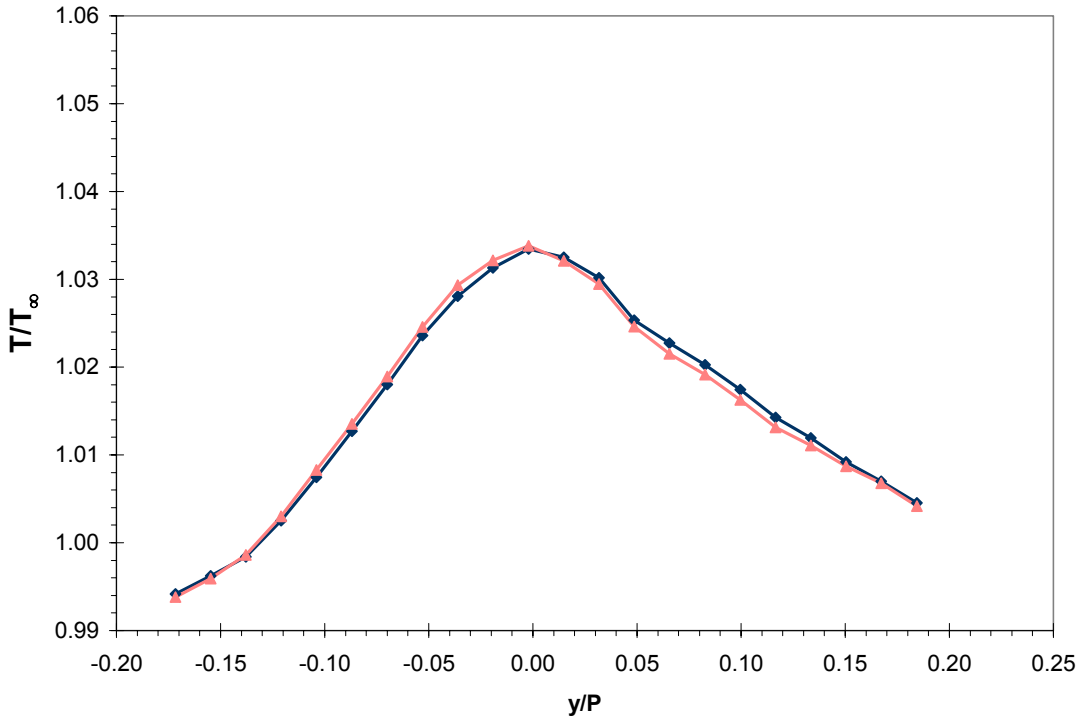

Figure 2.18a: Within-a-test repeatability for the hot streak (Position B, Hi Tu, Stagnation Line).

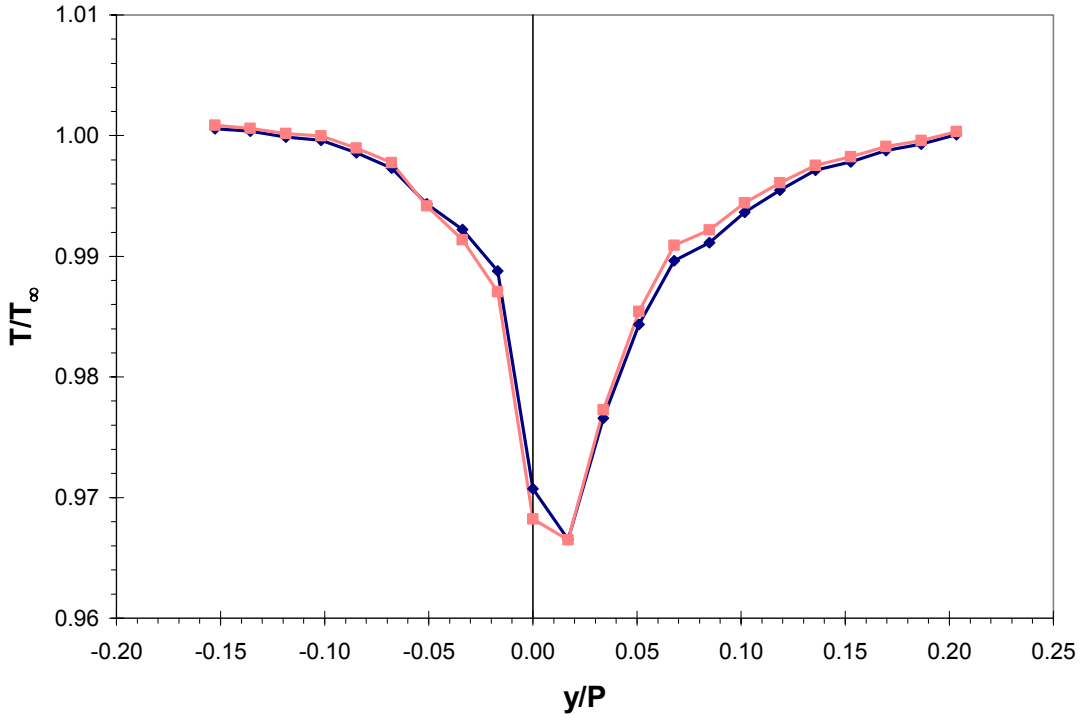

Figure 2.18b: Within-a-test repeatability for coolant only (Full Coverage, Su = 1.0, Sh = 2.0, Pr = 1.0, Hi Tu).

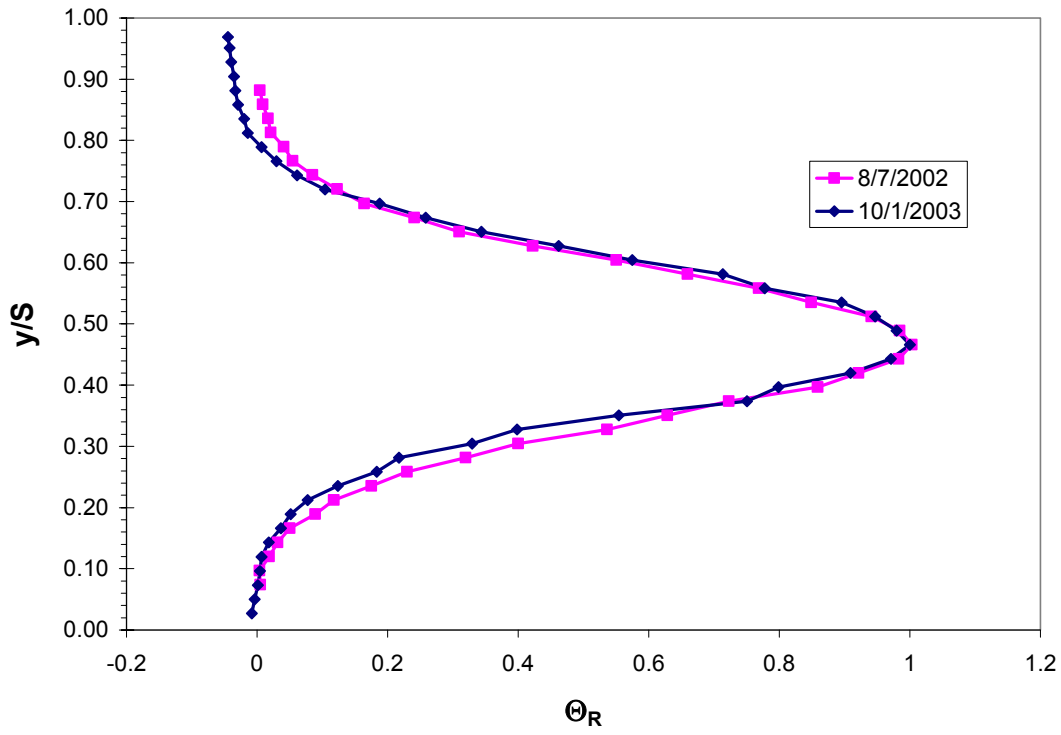

Figure 2.19: Test-to-test repeatability for the hot streak over 14 months (Position A, Hi Tu).

2.4 Uncertainty Analysis

To eliminate bias uncertainty of the measurements for the thermocouple rake, the equipment was tested against a known standard, i.e. an ice bath. An additional set of data was acquired at room temperature and compared against a thermocouple probe with a known bias error. The results of these two tests are shown in Figures 2.20a and 2.20b. These figures show that the bias error was constant across a wide range of temperatures, thus a correction could be used within the range of values observed during testing. The thermocouple bias was monitored at several occasions, usually before or after a group of experiments to ensure that an appropriate bias correction was made for that data set. Over time the bias errors did change, and a more sophisticated correction was required. Since the thermocouple rake was difficult and time consuming to remove from the tunnel facility, ice bath tests were only used when the rake was moved from one location to another. For later experiments, the thermocouple rake was compared with a single thermocouple which was traversed across the rake positions. To ensure that an adequate range of temperatures was observed, and since the bias did not remain constant with

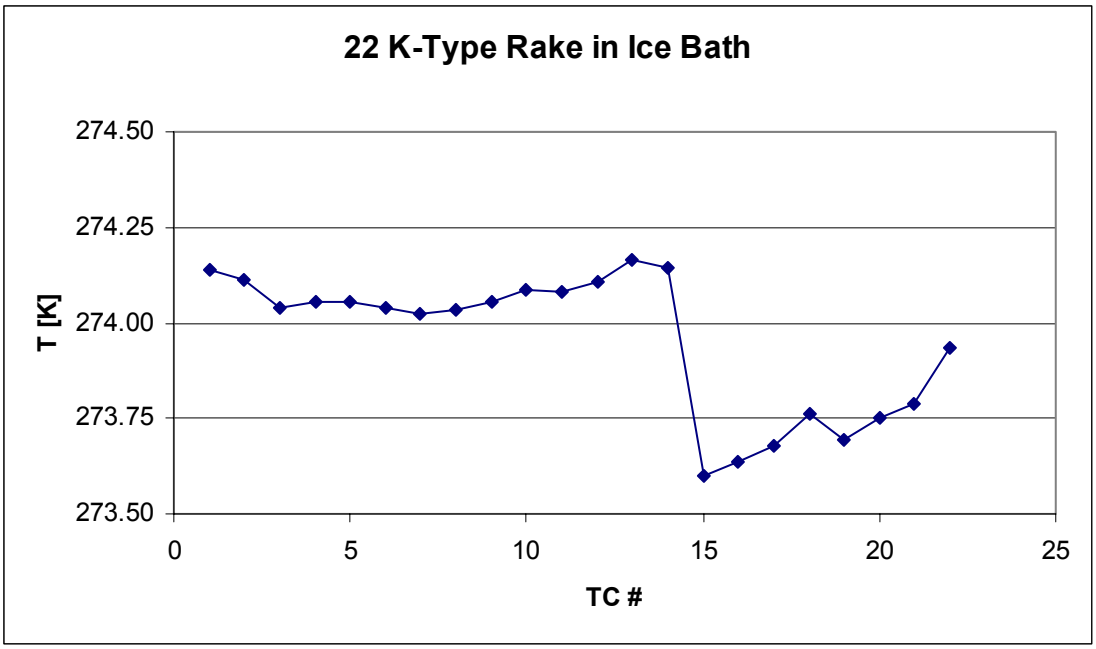

Figure 2.20a: Measurements for determining thermocouple bias errors using an ice bath.

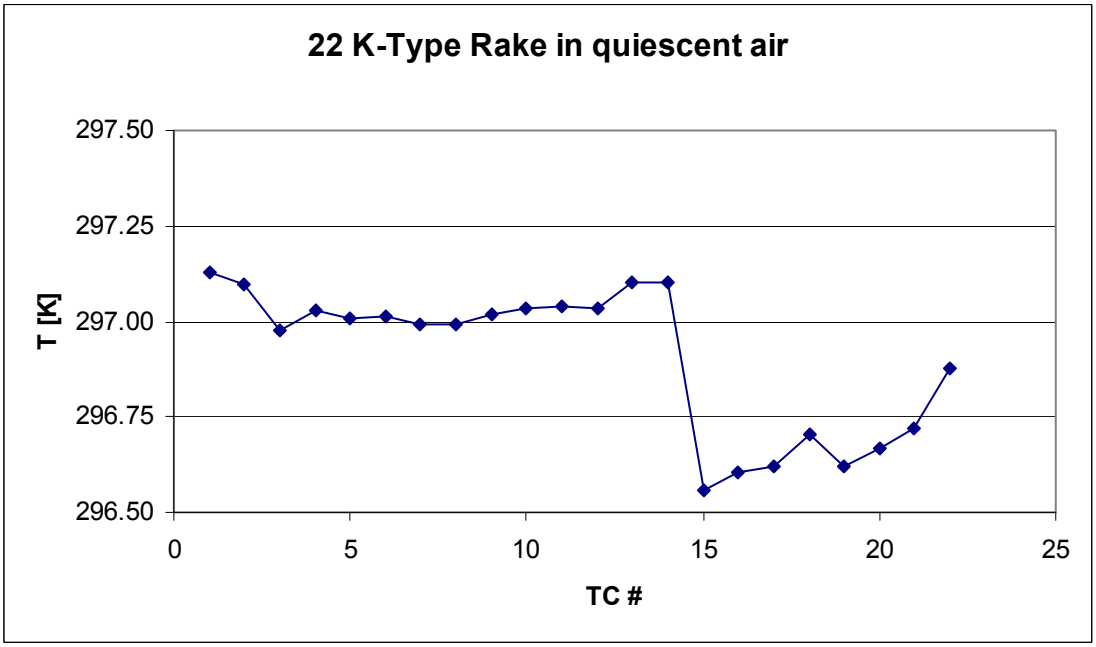

Figure 2.20b: Measurements for determining thermocouple bias errors at mainstream temperature.

temperature, these single thermocouple traverses were performed with showerhead film cooling, with the mainstream only, and with the hot streak activated. As such, the thermocouple rake was exposed to the range of temperatures that were encountered while taking data for experiments. Since the bias error of the single thermocouple probe was

known from ice point and boiling point measurements, it was used as the basis for determining the bias offset. It was found that a linear fit could be used for the bias across the range of temperatures encountered, and this linear fit was used to correct the bias error in the later tests. In this way, biases between thermocouples and thermocouple channels could be removed leaving only random or precision error.

Based on statistical analysis of the temperature measurements, the precision uncertainty (95% confidence interval) of the time averaged temperature values ranged between ±0.1 K at the mainstream temperature to ±0.4 K at the peak hot streak temperature. This error was random error resulting from the data acquisition system. Based on the temperature uncertainties, the uncertainty in the temperature ratio, T/T_∞, was calculated to be ±0.001 and the uncertainty in the normalized temperature ratio, Θ_R, was calculated to be ±0.02.

The uncertainty of the velocity was computed using the standard error of fit. Since the PX 2650 transducer was used in conjunction with a pitot-static probe in the mainstream for all velocity measurements, bias uncertainty was calculated during calibration and was found to be ±0.008 in H_2O, resulting in a velocity bias of ±0.3 m/s. Precision uncertainty was computed (95% confidence interval) from data taken under uniform conditions and was found to be ±0.01 m/s. Since the bias remains constant over time, the experiments were self consistent if the velocity was set at the same reported velocity.

For the thermocouples used to compute the density ratio, the bias uncertainty was ±0.5 K and the precision uncertainty was ±0.15 K. The partial derivatives method (Kline and McKlintoch [21]) was used to compute the bias and precision uncertainty of the density ratio which were ±0.005 and ±0.0015 respectively. In general, the variation in the reported density ratio for a particular test was much larger than this amount, usually on the order of ±0.05. For this reason, both bias and precision uncertainty of the density ratio were negligible and the focus was shifted to variations in the reported density ratio for a given experiment.

Computation of the blowing ratio was accomplished by an iterative method given by Goldstein [19]. The discharge coefficient was calculated using the Reynolds number at the orifice plate, requiring an iterative method. The mass flow rate through the orifice

plate was then computed giving the flow rate through the coolant holes. The sequential perturbation method (Moffat [22]) was used to compute bias and precision uncertainties in the blowing ratios. The transducer and associated uncertainties are presented in Table 2.2. A range of uncertainties were computed with the highest level of bias uncertainty at the lowest blowing ratio and the lowest level of bias uncertainty at the highest blowing ratio.

		Pressure [in H_2O]		Blowing Ratio	
	Transducer	Bias	Precision	Bias	Precision
Showerhead	PX 138	±0.0061	±0.0004	±0.0019	±0.0003
Suction Side	PX 164	±0.0087	±0.0001	±0.036 to ±0.071	±0.0018
Pressure Side	PX 142	±0.055	±0.0005	±0.009 to ±0.188	±0.0004

Table 2.2: Uncertainties in the blowing ratios.

Finally, an order of magnitude conduction analysis was conducted to determine the possible effect of conduction of the hot streak into the vane. The objective of experiments impacting the vane with the hot streak was to measure the hydrodynamic effect of the vane on the hot streak, as opposed to thermal effects. Since measurements were made along the vane and downstream, heat loss into the vane wall would diminish the strength of the hot streak, causing erroneous results. The vane was constructed of a very low conductivity material in order to reduce the possibility of conduction error and was designed to simulate an adiabatic wall. For the largest temperature differential across the vane surface, i.e. the hot streak at the stagnation line (0.0*P*), a maximum decrease in the near wall temperature of ΔT = 0.2 K was estimated. Clearly this temperature reduction applied only for the portion of the hot streak in close proximity to the vane, and in this region could have had the effect of reducing the hot streak by no more than T/T_∞ = 0.001, or Θ_R = 0.007. For the results presented, differences in hot streak peak temperature ratio differed by much more than this amount. It should also be noted that the total attenuation of the hot streak from Position A to Position T was about ΔT = 12.5 K, so compared to this significant decrease in temperature due to turbulence effects, the conduction error was diminishingly small.

Chapter 3: Effects of the Vane and Turbulence Level with No Film Cooling

3.1 Introduction

Measurements of the hot streak were made under conditions of low and high turbulence to quantify the added effects of high turbulence on the attenuation of the hot streak. First, measurements were made at a standard reference position 0.21C upstream of the vane, Position A in Figure 3.1, for both the low and high turbulence condition. Subsequently, the effect of the vane on the hot streak was investigated under low and high mainstream turbulence conditions by comparing an impinging hot streak to the hot streak passing through the mid-passage. A range of pitch positions between the pressure side and suction side mid-passage were tested to determine if the vane served to increase or decrease the attenuation rate of the hot streak. Simulated vane roughness was also tested for an impinging hot streak at both turbulence conditions to quantify this effect on hot streak attenuation. Measurements along the vane at several positions were made to further clarify how the hot streak evolved from Position A upstream of the vane to Position T at the trailing edge. Finally, turbulence effects in the stator/rotor axial gap, i.e.

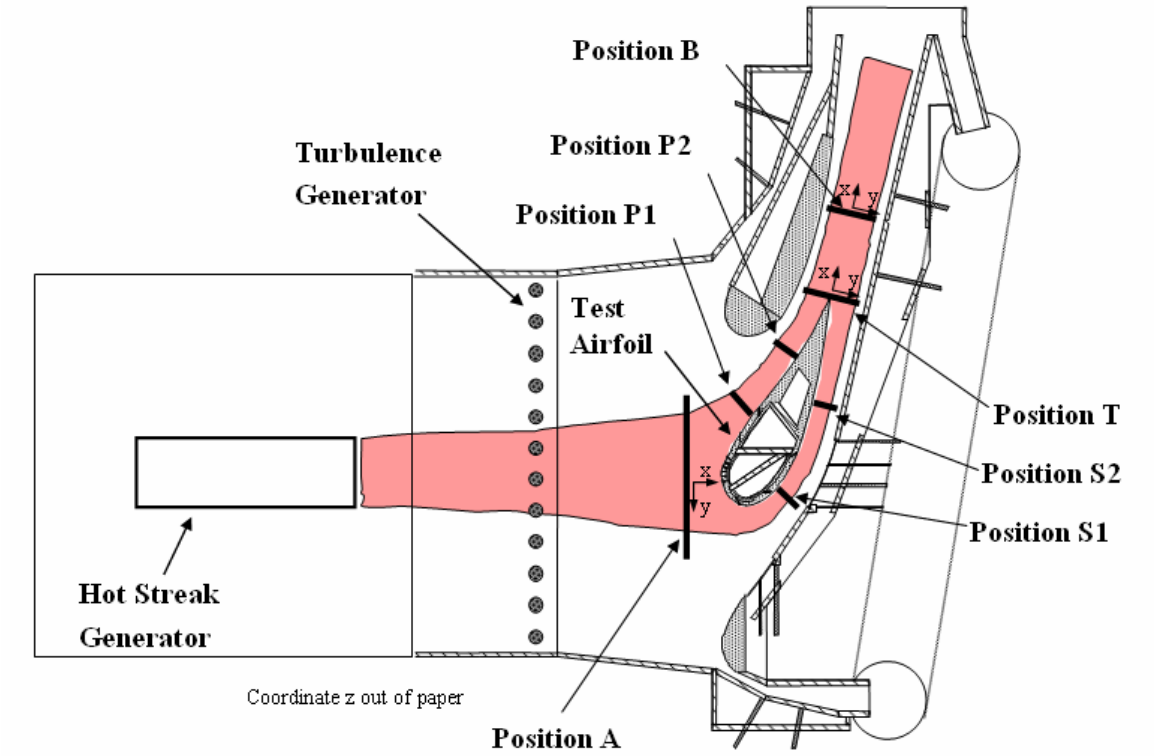

Figure 3.1: Simulated vane cascade with hot streak generator.

the independent effect of the vane wake and the additional downstream distance, were investigated by comparing profiles taken at Position T, at the trailing edge, with those observed 0.32C downstream at Position B.

3.2 Initial/Reference Conditions

To ascertain the level of attenuation of the hot streak as it interacted with the vane or passed through the vane passage, the hot streak temperature profiles were first measured at Position A as shown in Figure 3.1, 0.21*C* upstream of the stagnation line. This was approximately the location of the combustor exit plane, so it served as the reference location for all measurements in the simulated turbine vane cascade. Time-averaged temperature ratio contours for the low mainstream turbulence conditions are shown in Figure 3.2. These measurements were made using a 6 E-type thermocouple rake with 14.2 mm spacing, positioned at several pitchwise locations to capture the entire hot streak. As described in Chapter 2, the hot streak generator was operated at half power for the low turbulence condition and at full power for the high turbulence condition to obtain a nominal peak hot streak temperature ratio of $T/T_\infty = 1.1$ at Position A. Since the

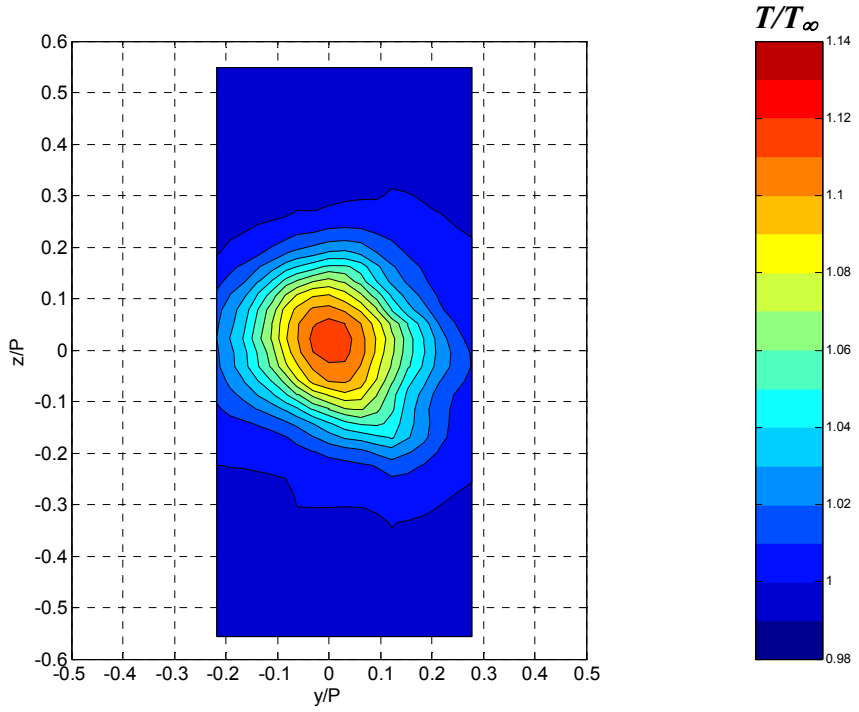

Figure 3.2: Normalized temperature ratio (T/T_∞) plot at Position A, 0.21*C* upstream of the stagnation line, with hot streak at low turbulence (Tu = 3.5%).

pitch between airfoils was P = 460 mm and the span was S = 550 mm, both the spanwise and pitchwise directions were normalized by the pitch, P, to maintain a constant proportionality for shape comparisons. The spanwise coordinate, z/P, was centered at midspan, while the pitch was centered on the stagnation streamline, i.e. on the streamline stagnating at the stagnation line of the vane. Since the stagnation streamline curved slightly toward the suction side as it approached the vane, it was not geometrically upstream of the stagnation line on the vane. The hot streak under low turbulence conditions had a peak temperature ratio of T/T_∞ = 1.11, and was nominally circular. Here it was helpful to use the 20% width as defined in Chapter 1, which, for the hot streak at low mainstream turbulence was nearly the same in the pitchwise and spanwise directions at $\delta_{20\%}$ = 0.40P. Recall that the 20% width, $\delta_{20\%}$, is defined as the full profile width at 20% of the maximum of the difference between peak and base as shown previously in the schematic in Figure 1.5. As shown in Figure 3.2, the hot streak peak was centered at midspan and on the stagnation streamline ($z/P = y/P$ = 0.0).

For the high turbulence condition, the hot streak passed through the turbulence generator located 0.88C upstream of the vane stagnation line as shown in Figure 3.1. The hot streak generator was operated at full power to obtain the desired nominal hot streak peak temperature ratio of T/T_∞ = 1.1, and presumably the decreased hot streak peak temperature ratio despite double the heater power was primarily due to the increased dispersion. The wider hot streak under high turbulence conditions, shown in Figure 3.3, had a peak value of T/T_∞ = 1.090, and was wider in the pitchwise direction than the spanwise direction. The 20% width in the pitchwise direction was $\delta_{20\%}$ = 0.79P, while the 20% width in the spanwise direction was $\delta_{20\%}$ = 0.51P, about 35% smaller. Note that the level for the 20% width was T/T_∞ = 1.018 since a value of T/T_∞ = 1.00 was the base and T/T_∞ = 1.09 was the peak. The spreading of the hot streak in the pitchwise direction was attributed to the action of the turbulence generator which consisted of narrowly spaced, large diameter rods oriented spanwise. Due to the interaction of the wakes of these rods, the hot streak initially spread more in the pitchwise direction than in the spanwise direction. However, as documented by Polanka [15] for this facility, the anisotropy in the turbulence field disappeared by Position A. As seen in the figure, the

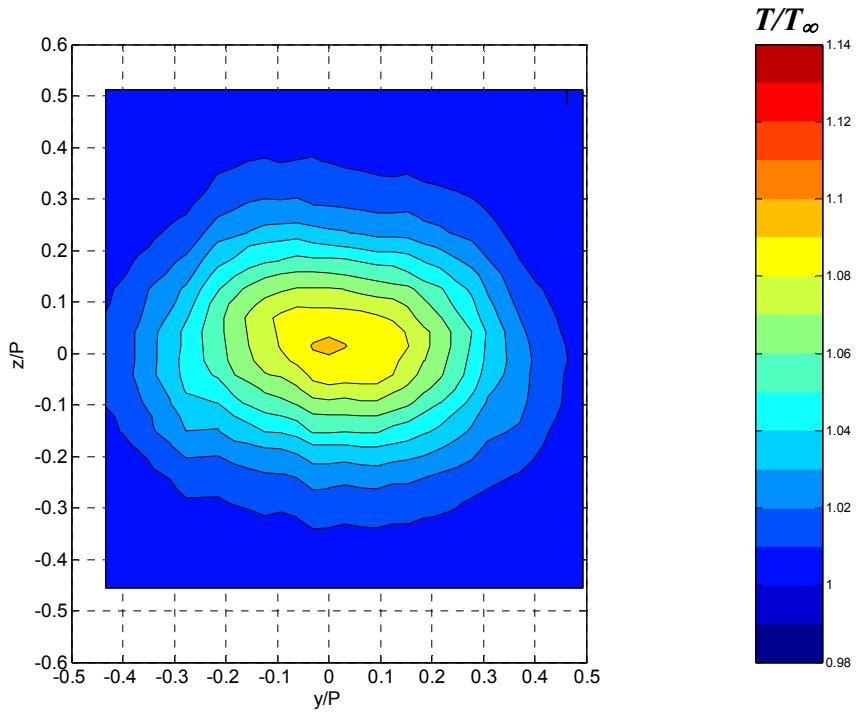

Figure 3.3: Normalized temperature ratio (T/T_∞) plot at Position A, 0.21C upstream of the stagnation line, with hot streak at high turbulence (Tu = 20%).

center of the hot streak was nominally centered at midspan and on the stagnation streamline. The results of a numerical integration of the hot streak temperature field confirmed that the hot streak contained twice the thermal energy under full power operation (high turbulence case) versus half power (low turbulence case).

For reference, the hot streak peak temperature ratio measured 1.03C upstream of the stagnation line (slightly upstream of the turbulence generator) was T/T_∞ = 1.29 at full power (both heaters) and T/T_∞ = 1.13 at half power using the upstream heater. Under low turbulence, the hot streak temperature ratio decreased from T/T_∞ = 1.13 at 1.03C upstream of the stagnation line to T/T_∞ = 1.11 at Position A. Under high turbulence, the temperature ratio dropped from T/T_∞ = 1.29 at 1.03C upstream of the stagnation line to T/T_∞ = 1.09 in the same distance, but passing over the turbulence generator.

3.3 Effect of Turbulence Level

Since the maximum temperature difference between the hot streak and the mainstream for the hot streak at Position A varied between the low and high mainstream

turbulence conditions, the normalized temperature ratio, Θ_R, was used. This parameter scaled the temperature values relative to the peak temperature at the reference position (Position A) and the mainstream temperature as described in §1.2. Therefore, by definition, the non-dimensional temperature ratio was unity (Θ_R = 1.0) at Position A for the hot streak peak. The mean temperature profiles in terms of Θ_R are shown in Figure 3.4. Downstream measurements at Position T were made with a 22 K-type thermocouple rake with 7.8 mm spacing. Also shown in Figure 3.4 are the Θ_R profiles at Position T, located at the trailing edge (see Figure 3.1) for the hot streak passing through the mid-passage at -0.5*P* (the pressure side mid-passage). Both low and high mainstream turbulence caused a significant decrease in the peak temperature of the hot streak, although the spreading of the high mainstream turbulence profile may have been limited by the walls of the airfoils, thereby limiting the decay of the peak. These profiles showed the greater decrease in the peak Θ_R value for the high mainstream turbulence case, where Θ_R = 0.59 at Position T, relative to the low mainstream turbulence case, where Θ_R = 0.77

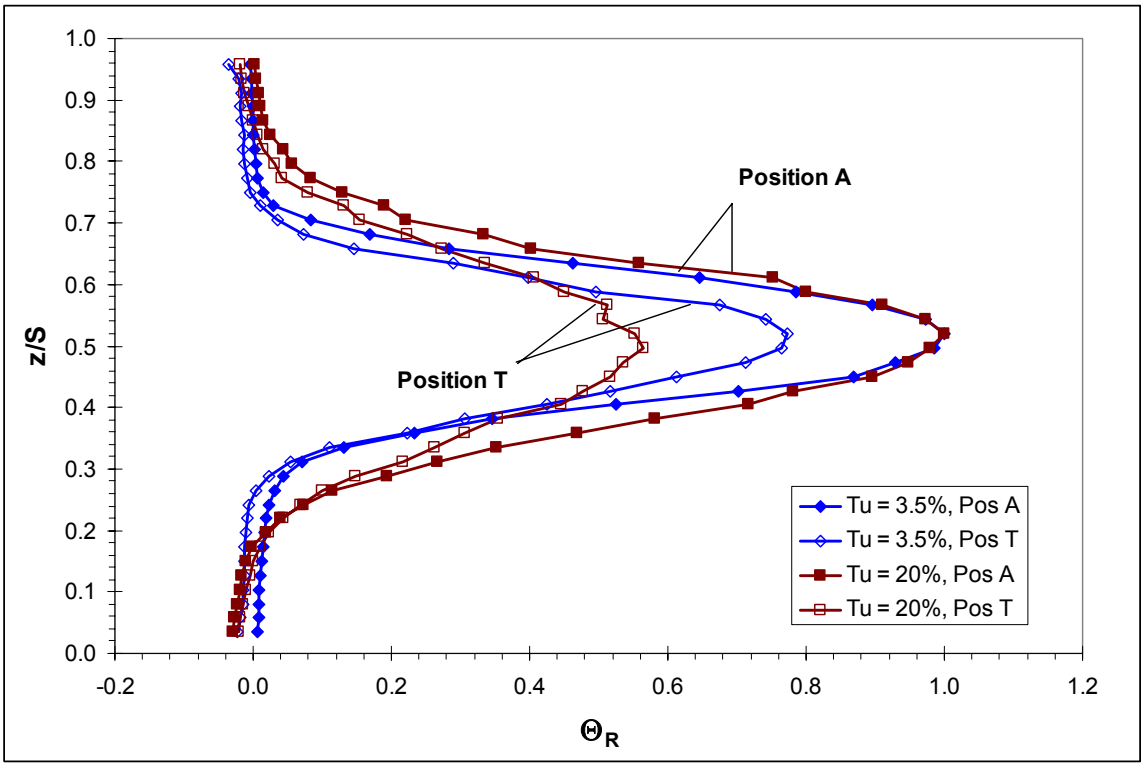

Figure 3.4: Peak normalized temperature ratio (Θ_R) profiles at Position A and T for *Tu* = 3.5% and 20% for the hot streak through the pressure side mid-passage.

at Position T. Temperature ratios below $\Theta_R = 0.00$ can be attributed to slight variations in the mainstream temperature across the pitch and span as described in Chapter 2.

At Position A, the hot streak at low turbulence had an estimated width of $\delta_{20\%} = 0.33S$ in the spanwise direction (equivalent to $0.40P$) while the hot streak under high turbulence had an estimated spanwise width of $\delta_{20\%} = 0.43S$ (equivalent to $0.51P$), about 40% wider. Here the 20% width was taken at $\Theta_R = 0.20$ since the peak was defined as $\Theta_R = 1.00$. As expected, the hot streak became wider (i.e. taller) in the spanwise direction for the high turbulence case, from $\delta_{20\%} = 0.43S$ at Position A to $\delta_{20\%} = 0.47S$ at Position T, an increase of about 10%. However, $\delta_{20\%}$ for the low turbulence case was essentially unchanged.

The extent of the spreading of the hot streak is shown by normalized temperature contours in the *y-z* plane. The Θ_R contours for the low and high mainstream turbulence cases at Position T (at the trailing edge) are shown in Figure 3.5. In this figure $y/P = 0$ corresponds to a streamline originating from the trailing edge of the vane, with negative and positive y/P values corresponding to the pressure side and suction side of the test vane, respectively. Furthermore, $y/P = \pm 0.2$ correspond to the wall and vane on either side of the test vane (see Figure 3.1). Naturally, at Position T, the hot streak was contracted in the pitch-wise direction due to the factor of five narrowing of the passage in that direction. Immediately apparent in comparing the hot streaks for the low and high mainstream turbulence cases was the much greater spread of the hot streak for the high turbulence case. The greater spread of the hot streak resulted in much lower temperature gradients for the high turbulence case. For high mainstream turbulence, the hot streak was constrained between airfoils, resulting in high gradients at $y/P = 0.0$.

To confirm that results were consistent with conservation of energy, i.e. no heat lost through walls or the vane, the full field data was analyzed for both turbulence conditions at Positions A and B. This analysis was performed by Jason Dees, and accounted for the variations in velocity and density both at Positions A and B. A numerical integration of the total energy flux for low mainstream turbulence, showed a difference of 3% between Position A and the hot streak passing through the mid-passage to the pressure side of the test vane at Position B. For the high mainstream turbulence

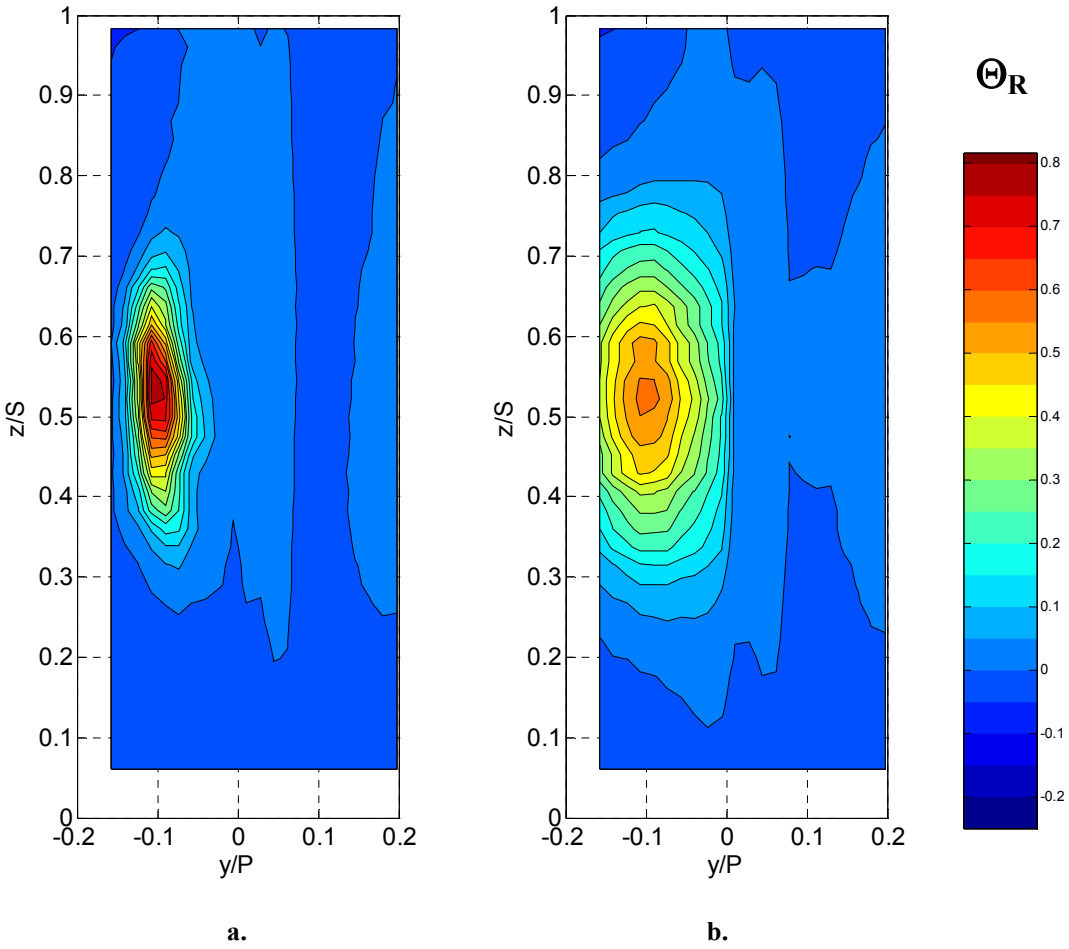

Figure 3.5: Normalized temperature ratio (Θ_R) plot at Position T with hot streak through the pressure side mid-passage at 0.5*P*.

a. Low turbulence (*Tu* = 3.5%)

b. High turbulence (*Tu* = 20%)

condition, comparisons were made between Position A and Position B for hot streaks impinging on the vane and passing through the mid-passage. These comparisons showed less than a 10% difference between the Position A and Position B results with equally good agreement between the impinging and non-impinging hot streak.

3.4 Effects of the Vane at Low Mainstream Turbulence

Experiments to determine the effect of the pitch position of the hot streak on the attenuation of the hot streak were performed by positioning the hot streak generator in varying pitch increments to both the pressure and suction sides of the test vane. The

baseline position of the hot streak was a position such that the center of the hot streak impacted the stagnation line of the vane, i.e. 0.0*P*. Positions of ±10 mm, ±20 mm, ±30 mm, ±40 mm, and ±46 mm, representing pitch changes of ±0.022*P*, ±0.043*P*, ±0.065*P*, ±0.087*P*, and ±0.1*P*, were chosen to determine the effect of fine scale pitch position changes. To determine the effect of larger pitch position changes, the hot streak generator was adjusted between the stagnation line (0.0*P*) and ±0.5*P* to both sides of the test vane in increments of 0.1*P*. For pitch position comparisons, the rake was positioned at midspan, where the hot streak peak occurred.

Under conditions of low turbulence, a sharp temperature gradient was produced for pitch positions on either side of the stagnation line. This is demonstrated in Figure 3.6a for the hot streak positioned at ±0.1*P* where it is evident that a very sharp temperature gradient existed at Position T (at the trailing edge) between the two parts of the hot streak that passed on either side of the vane. These sharp temperature gradients can be attributed to the interruption of the hot streak dispersion by the wall of the vane. The schematic in Figure 3.6b indicates the splitting line and how the two regions of the hot streak attenuate differently. The "tail" region of the hot streak, i.e. the part that does not include the peak, attenuated more quickly because it was isolated from the peak region of the hot streak that would normally transport high temperature hot streak fluid towards the outer "tail" region. On the other hand, the "peak" region of the hot streak attenuated less because hot fluid from the core of the hot streak towards the right side was blocked by the vane. Consequently the difference in hot streak temperature between the two sides of the hot streak split by the vane was accentuated resulting in a sharp temperature gradient in the hot streak at the trailing edge of the vane. The peak temperature ratio was higher for the hot streak on the pressure side than the suction side due to several factors including the longer distance traveled along the suction side. This difference in streamline lengths is shown in Figure 3.7. Measurements were made directly around the test vane in the tunnel facility, giving the pressure side streamline length of 660 mm, or 1.11*C*, and the suction side streamline length of 895 mm, or 1.51*C*, more than 35% longer. Presumably this difference in streamline length was one factor causing the "tail" (or "peak") region passing around the suction side to attenuate more

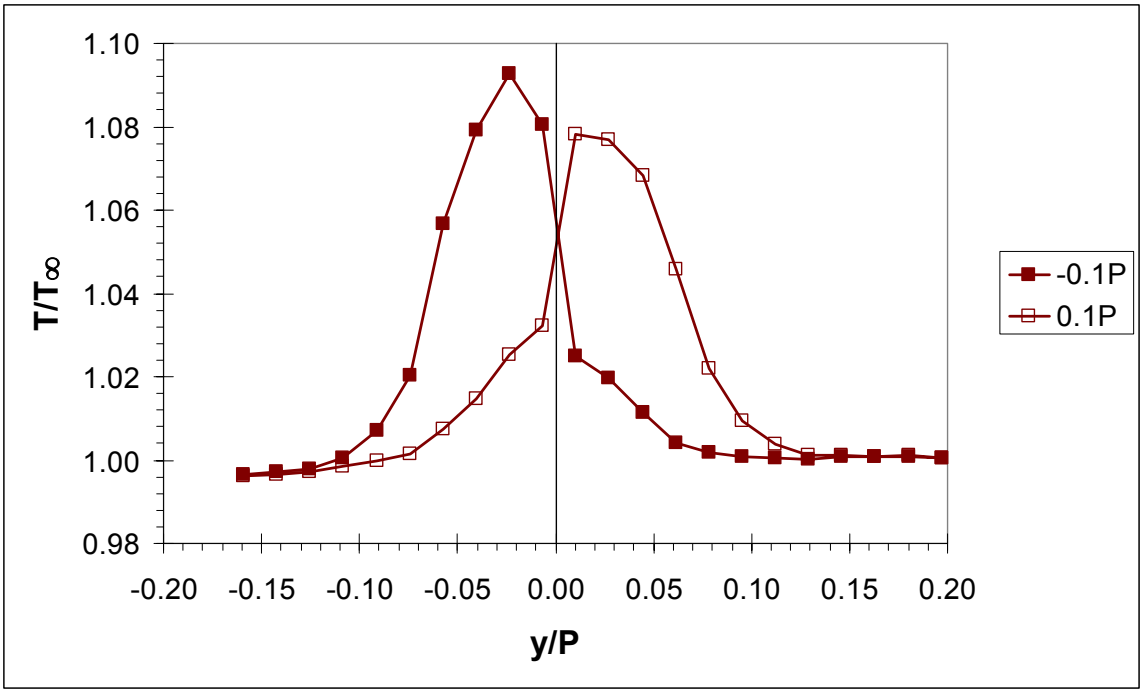

Figure 3.6a: Temperature profiles of the hot streak at Position T with hot streak position at -0.1*P* and +0.1*P*, *Tu* = 3.5%.

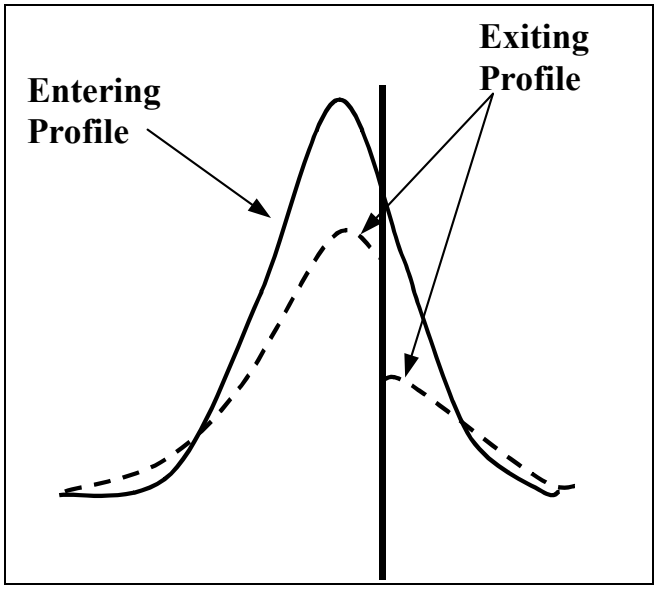

Figure 3.6b: Schematic of entering (stagnation line) and exiting (trailing edge) temperature profiles.

than the corresponding "tail" (or "peak") region passing around the pressure side, as shown in Figure 3.6a. Despite the longer distance around the suction side, the velocity distribution around the vane surface resulted in a longer transit time around the pressure

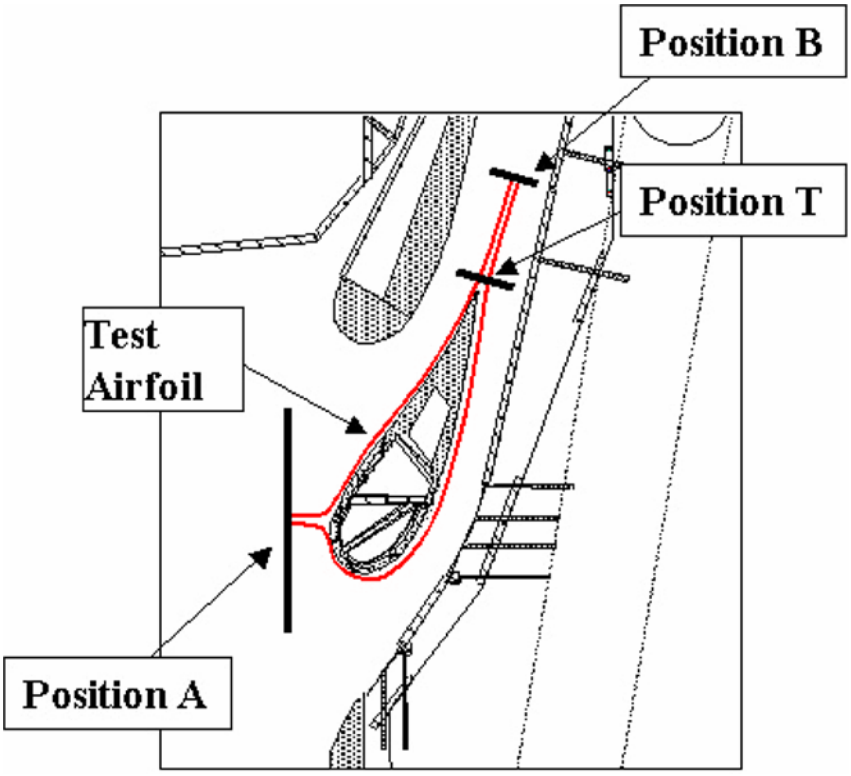

Figure 3.7: Comparison of the length of streamlines from Position A to Position T passing along the suction and pressure sides of the vane.

side. The transit time was estimated to be about 40% greater for fluid passing around the pressure side than the suction side by integrating the velocity distribution for this vane geometry. Differences in the compression of streamlines on the suction and pressure sides, shown in Figure 3.8 (obtained from Thole [23]), also contributed to differences in the attenuation rates between the suction and pressure sides of the hot streak. These differences also resulted in a lower peak region for the hot streak positioned toward the suction side versus positioned to the pressure side.

In Figure 3.9, comparing the hot streak positioned to impact the stagnation line to intermediate positions between those shown in Figure 3.6a (±0.1*P*), it is evident that the greatest attenuation level occurred at the stagnation line position (0.0*P*). Temperature ratio profiles for pitch positions between -0.1*P* and +0.1*P* indicated that splitting of the hot streak resulted in a higher hot streak peak temperature ratio for all pitch positions to either side of the stagnation line. In general, as indicated above, pitch positions to the suction side resulted in lower peaks than those to the pressure side. Since the hot streak

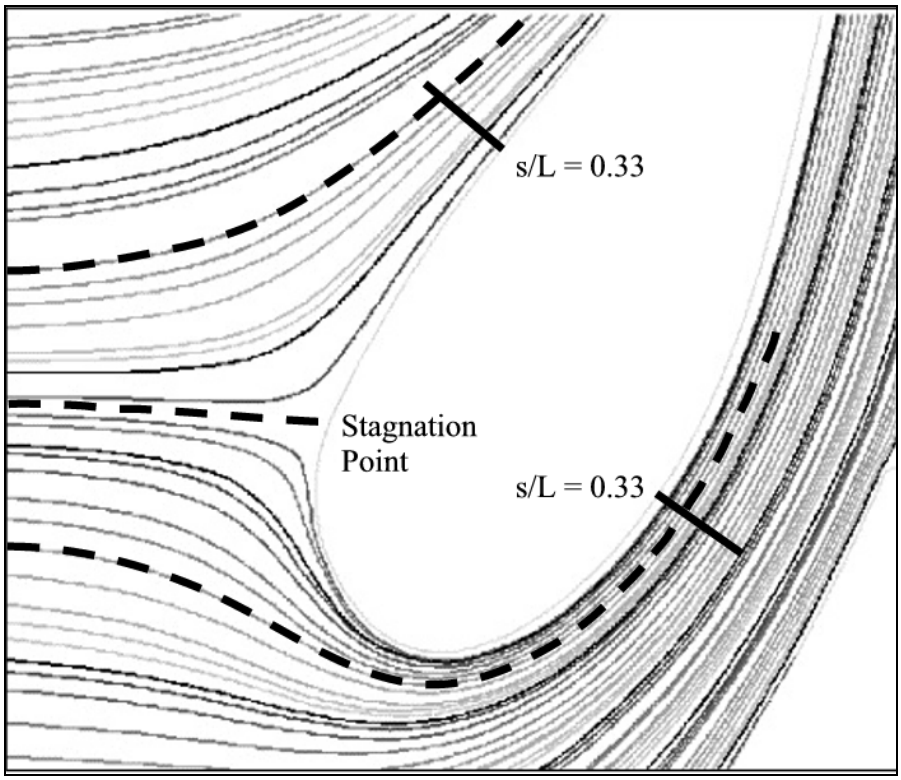

Figure 3.8: Streamlines passing around the vane on the suction and pressure side to a position of s/L = 0.33. From Thole [23].

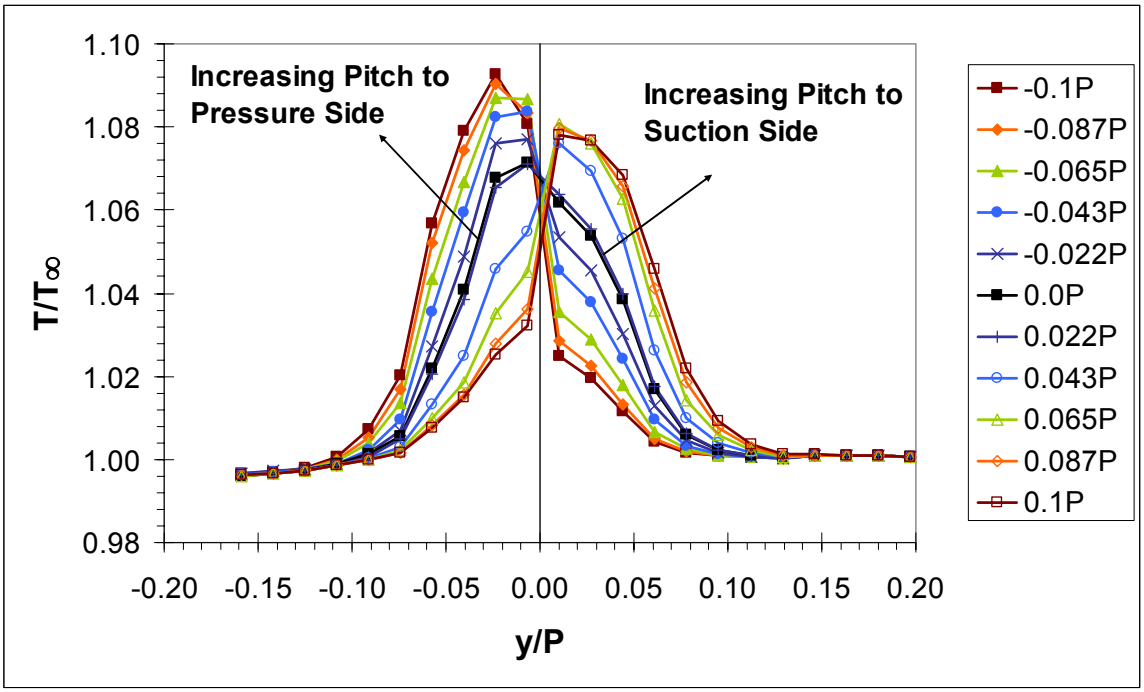

Figure 3.9: Temperature profiles of the hot streak at Position T with hot streak position varying from -0.1*P* to +0.1*P*, *Tu* = 3.5%.

positioned to impact the stagnation line was split equally to either side, heat loss was maximized from the core towards the "tail" region on both sides, and the hot streak peak was minimized. In particular, for hot streak pitch positions of 0.1*P* from the stagnation line, the peak hot streak temperature was 15% lower on the suction side than on the pressure side. The lowest peak, for the hot streak positioned on the stagnation line, was nearly 25% lower than on the pressure side at 0.1*P*.

The variations of the hot streak temperature profiles downstream of the vane for hot streaks positioned laterally from –0.5*P* to +0.5*P* are shown in Figure 3.10. Immediately apparent was a lower level of peak temperatures for the hot streak positioned on the suction side of the vane, i.e. y > 0.0*P*, compared to the pressure side of the vane, y < 0.0*P*. This distinct difference in the strength of the hot streak, especially for ±0.5*P*, can be attributed to the longer length of streamlines in the mid-passage passingaround the suction side relative to the pressure side up to the measurement plane at Position T, which was normal to the flow direction. The difference in streamline length is illustrated in Figure 3.11. The streamlines at the mid-passage positions of -0.5*P*

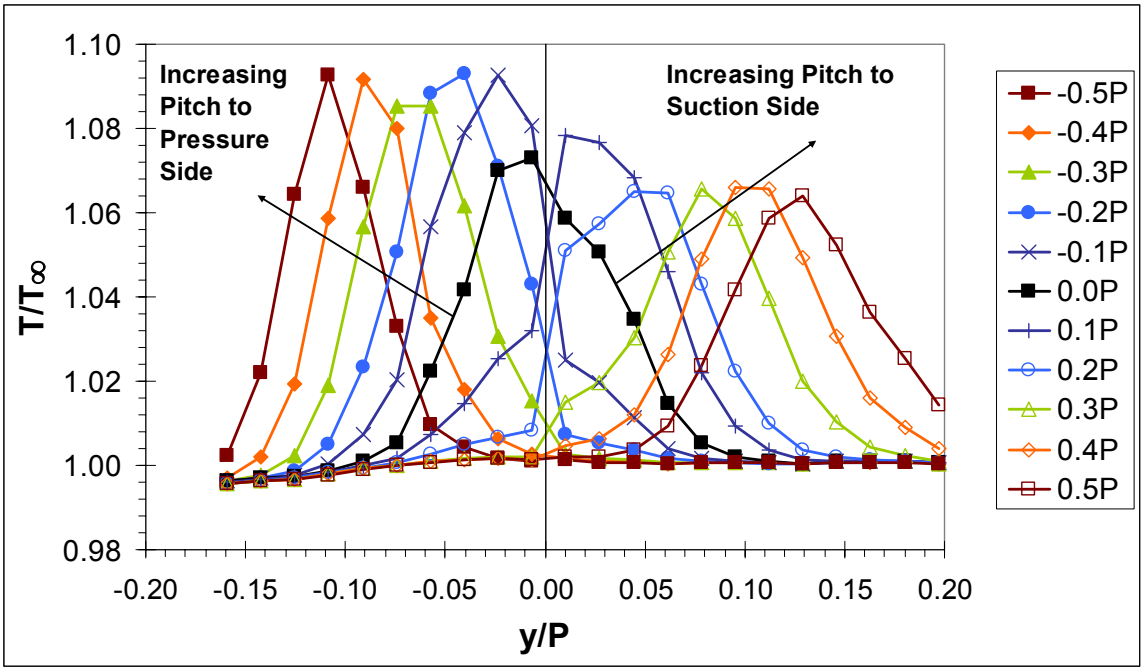

Figure 3.10: Temperature profiles of the hot streak at Position T with hot streak position varying from -0.5*P* to +0.5*P*, *Tu* = 3.5%.

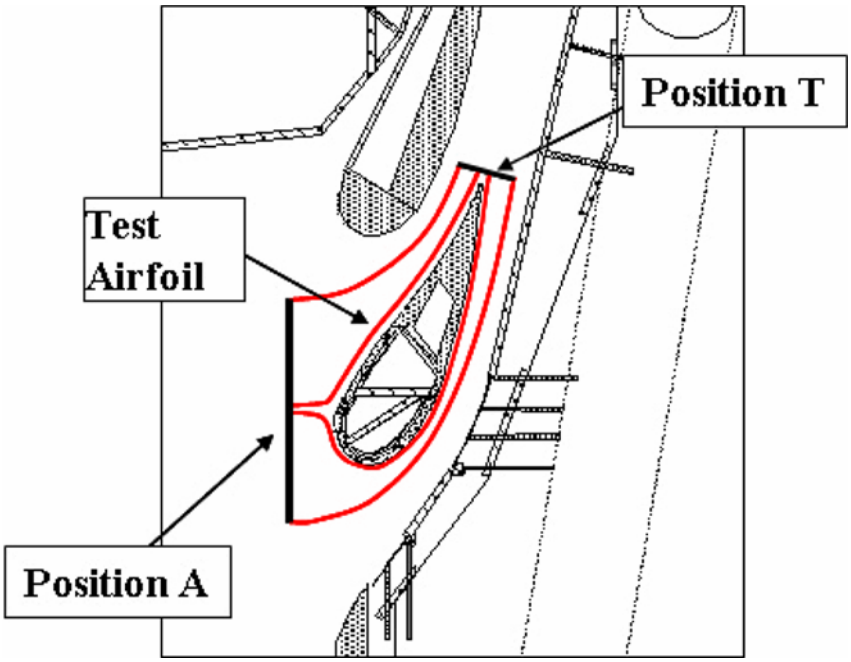

Figure 3.11: Comparison of the length of streamlines from Position A to Position T passing through the mid-passage on the suction and pressure sides of the vane.

and +0.5*P* had different streamline path lengths because of the orientation of the downstream measurement plane and were 465 mm (0.78*C*) and 915 mm (1.54*C*) for the pressure and suction sides respectively. Since the facility was designed to simulate periodic cascade, streamlines at mid-passage were equivalent. This also meant that streamlines at the mid-passage positions of -0.5*P* and +0.5*P* had significantly different transit times. To confirm that equivalent hot streak strengths would be obtained at mid-passage under conditions of low turbulence if measurements were made at equivalent streamline lengths, measurements of the hot streak were made at the upstream position on the suction side as indicated on Figure 3.12. It should be noted that the positions indicated in Figure 3.12 are along a constant axial plane, i.e. parallel to the inlet plane at the vane leading edge. The transit time to these two locations were also the same due to the periodic nature of the facility. Results from these measurements, shown in Figure 3.13, confirmed that the hot streak peak temperature ratio was the same at mid-passage through both passages if measured at equivalent distances. However, as seen in the figure, the hot streak was slightly wider passing through the suction side passage. This may be attributed to the boundary condition present for the suction side, where, as seen in

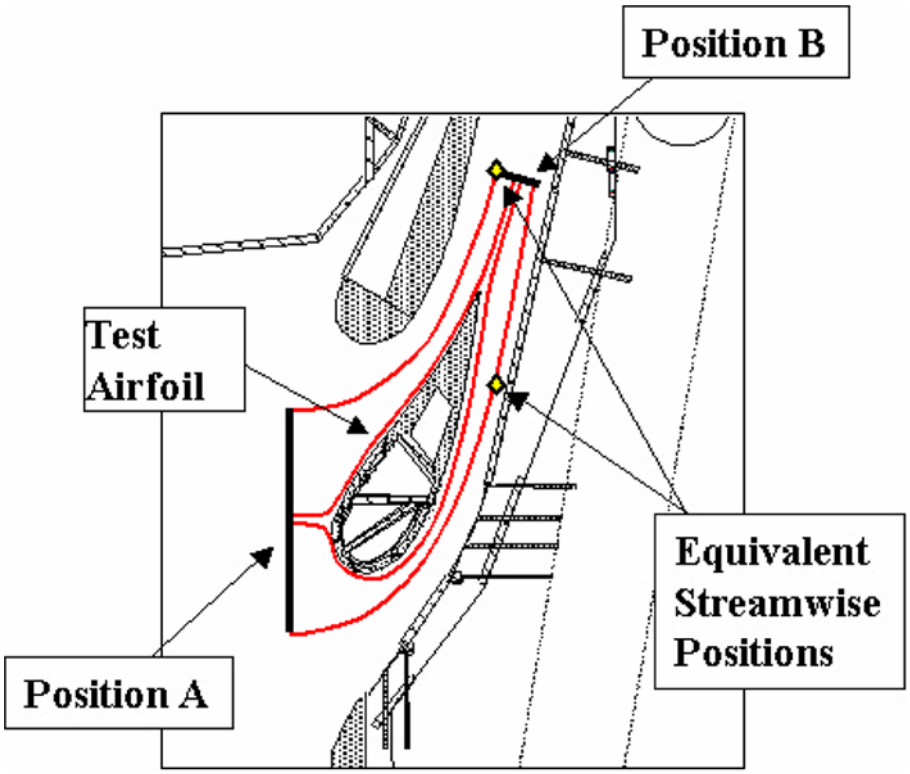

Figure 3.12: Illustration of equal streamwise positions for streamlines from Position A passing through the mid-passage on the suction and pressure sides of the vane.

Figure 3.12, the hot streak was bounded by the test vane and artificially by the outer wall as compared to the pressure side passage which was bounded by the vane wall and the wake.

Comparing the peak hot streak temperature at Position T for the hot streak impacting at various positions on the suction side of the vane as shown in Figure 3.10, the peak temperature for the hot streak positioned at +0.1*P* was clearly greater than for the hot streak positioned from +0.2*P* to +0.5*P*. This may be attributed to the decrease in attenuation of the peak hot streak temperature because of the splitting of the hot streak by the vane as discussed previously. Another factor that may be involved is the possible reduction of the large scale mainstream turbulence by the close proximity of the vane. This would also lead to a decreased attenuation of the hot streak peak temperature.

In order to address the issue of impinging vs. non-impinging hot streak strength, measurements were taken at equal axial positions, i.e. positions coincident with a plane

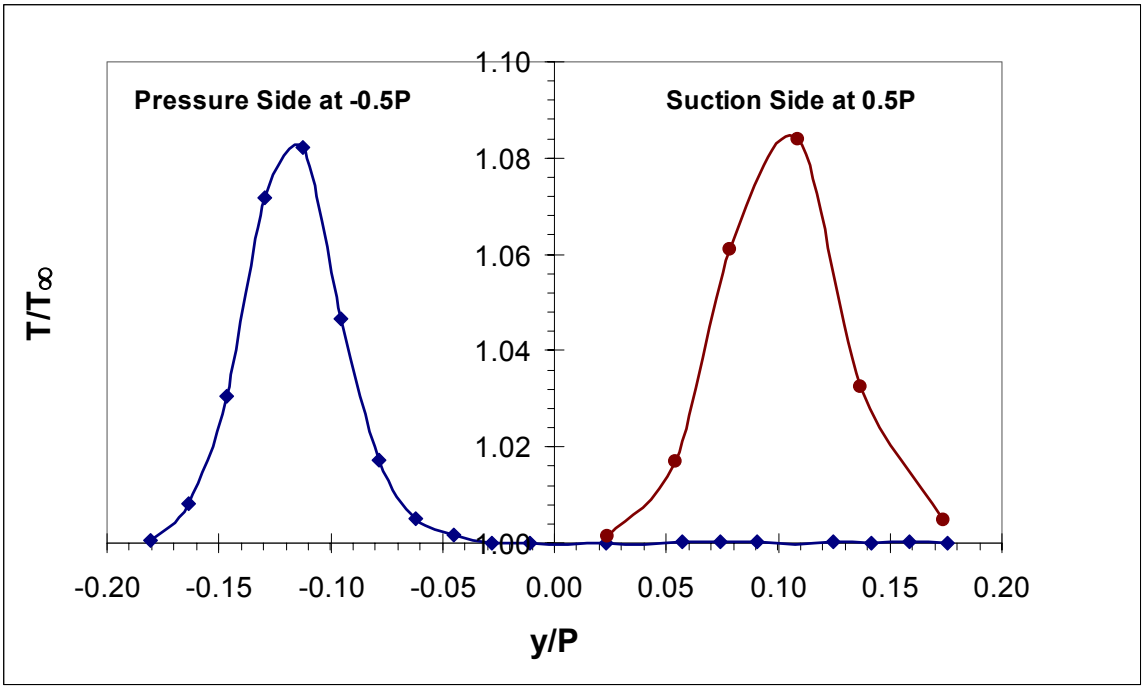

Figure 3.13: Comparison of hot streak profiles at equivalent streamwise distances shown on Figure **6.**

cut at a constant axial location through the engine. These positions are shown in a schematic of the vane cascade in Figure 3.14 for the hot streak impacting the stagnation line and passing through the suction side mid-passage at +0.5P. This axial position was roughly the location of the inlet plane to the first stage rotors. Position B, for the impinging hot streak, was 0.32*C* downstream of the trailing edge, and is a particularly relevant position for engine designers since the leading edge of the first stage rotors is usually between about 0.3*C* to 0.5*C* downstream of the first-stage stator. Thus, measurements made at this axial plane may be considered as measurements at the rotor inlet plane.

The comparison, shown in Figure 3.15, indicates that the hot streak had the same peak temperature ratio, although the hot streak passing over the vane was slightly wider. This may have been due to the finite width of the trailing edge, and/or the boundary layer thickness. It is clear that under conditions of low turbulence, the hot streak was not diminished more greatly due to interaction with an adiabatic vane.

As a supplementary illustration of the equivalency of the hot streak at equal axial positions for impinging and non-impinging hot streaks, contour plots in the y-z plane are

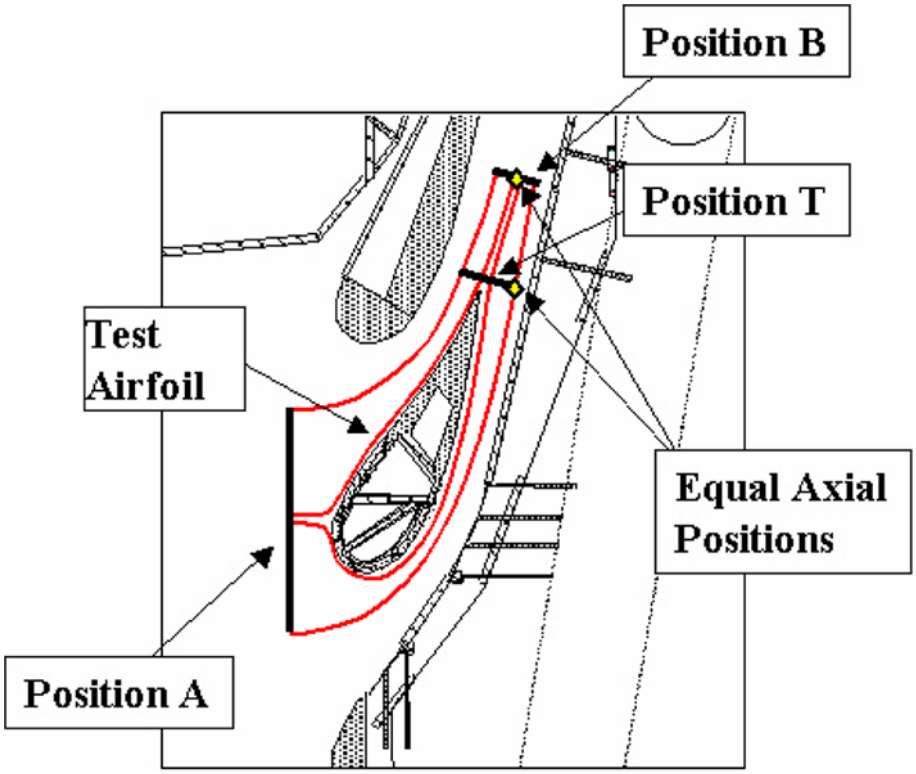

Figure 3.14: Tunnel schematic showing positions along an axial plane for hot streak positions of 0.0*P* and +0.5*P* (axial plane shown with blue dashed line).

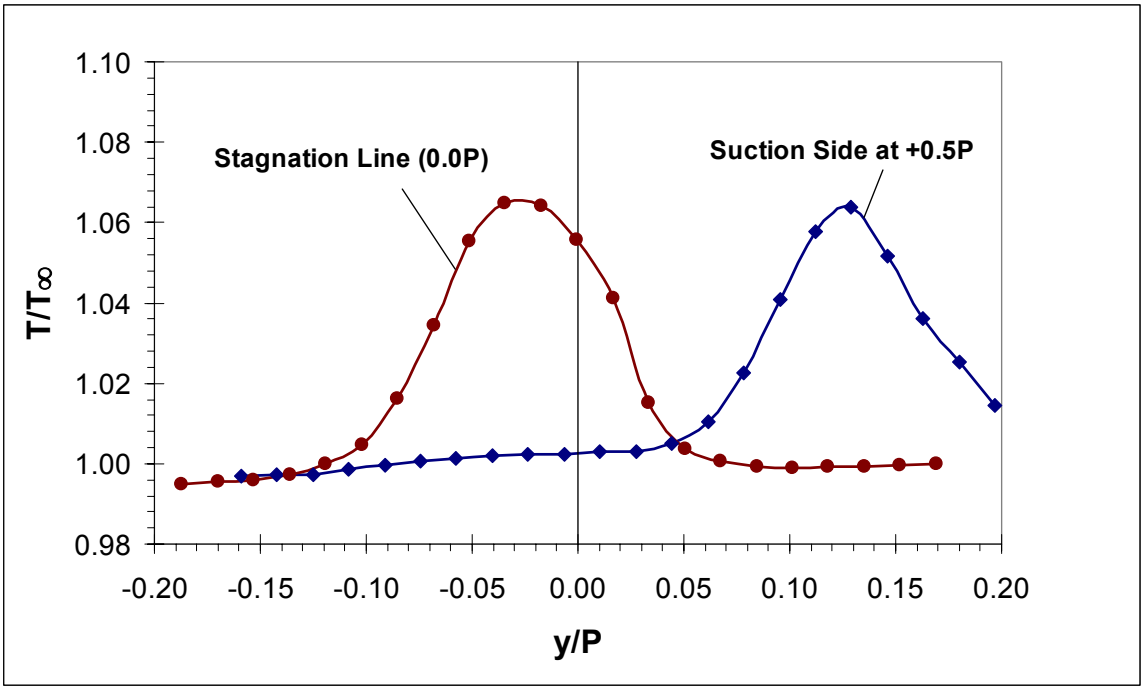

Figure 3.15: Comparison of hot streak profiles impacting the vane at 0.0*P*, and passing through the mid-passage at +0.5*P* at equal axial positions, *Tu* = 3.5%.

shown in Figure 3.16 for the hot streak positioned at 0.0*P* and +0.5*P*. Although the hot streak had a slightly different shape passing through the mid-passage versus impacting the stagnation line, the size of the hot streak in the spanwise direction was nearly the same. Additionally, the areas of the hottest regions, i.e. $\Theta_R > 0.45$, were very similar as well.

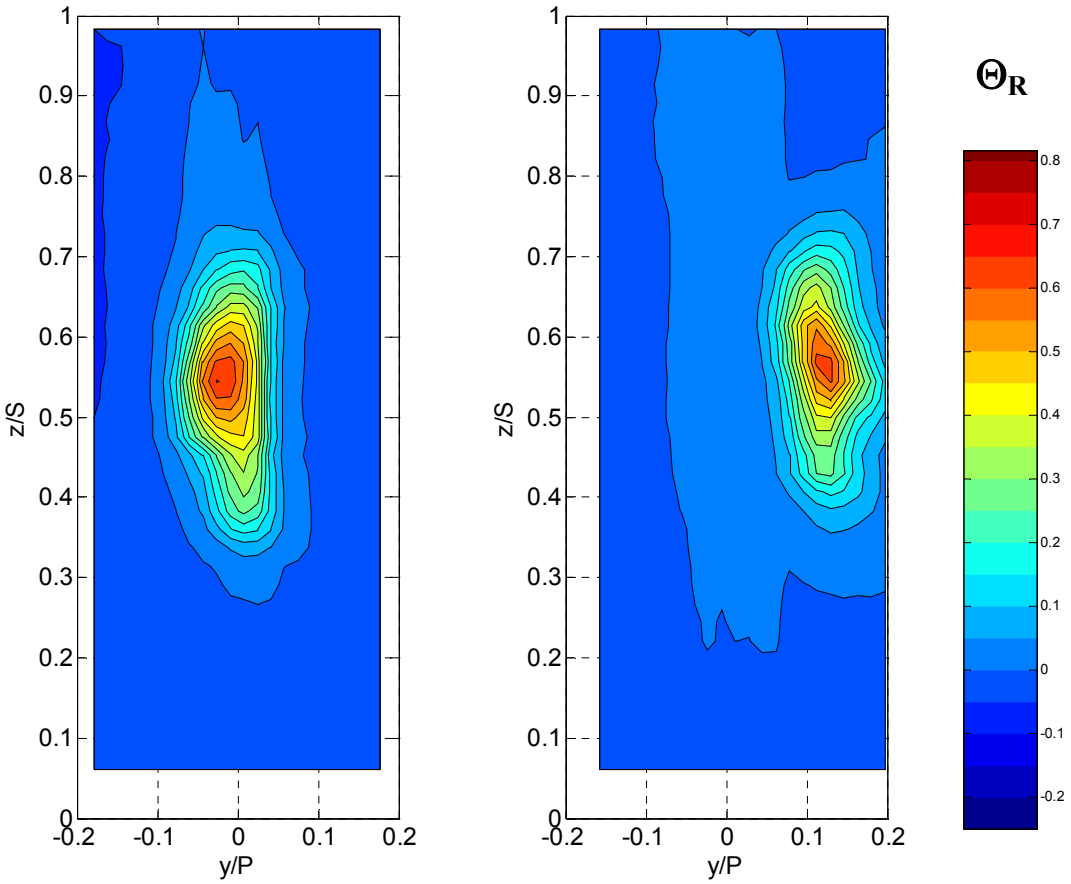

Figure 3.16: Normalized temperature ratio (Θ_R) plot at equal axial positions, low turbulence (*Tu* = 3.5%), with hot streak:

a. Impacting the stagnation point

b. Through the mid-passage at +0.5*P*

3.5 Effects of the Vane at High Mainstream Turbulence

Hot streak temperature profiles measured at Position T for conditions of high mainstream turbulence (*Tu* = 20%) are shown in Figures 3.17a and 3.17b for hot streaks

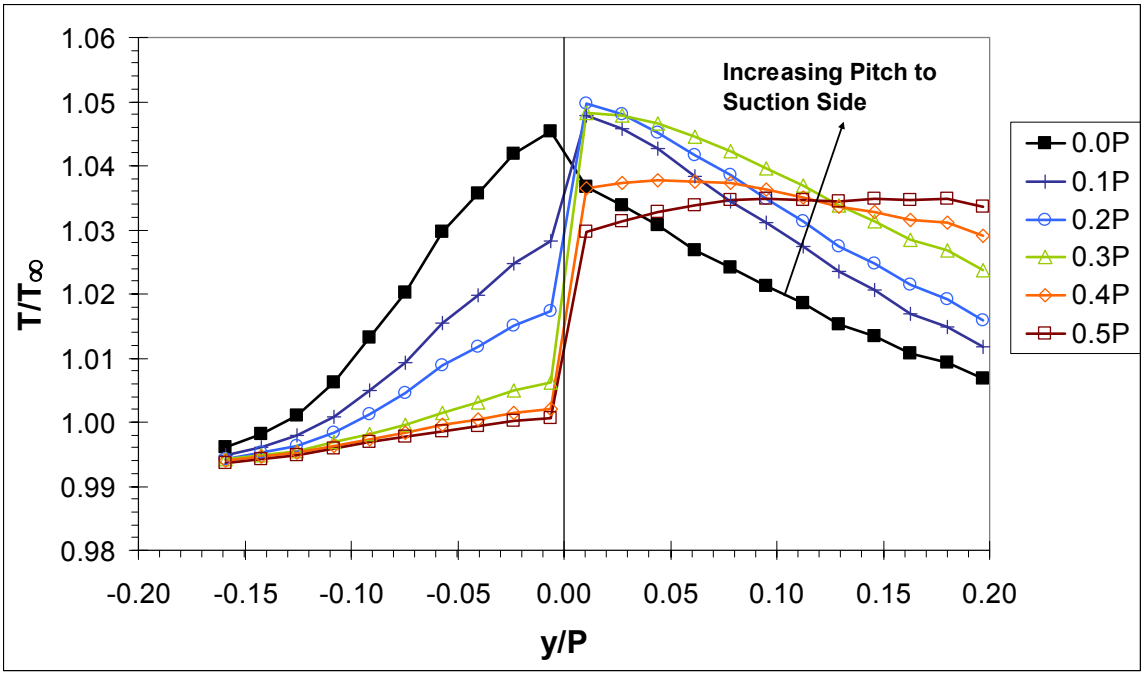

Figure 3.17a: Temperature profiles of the hot streak at Position T with hot streak position varying from 0.0*P* to +0.5*P*, *Tu* = 20%.

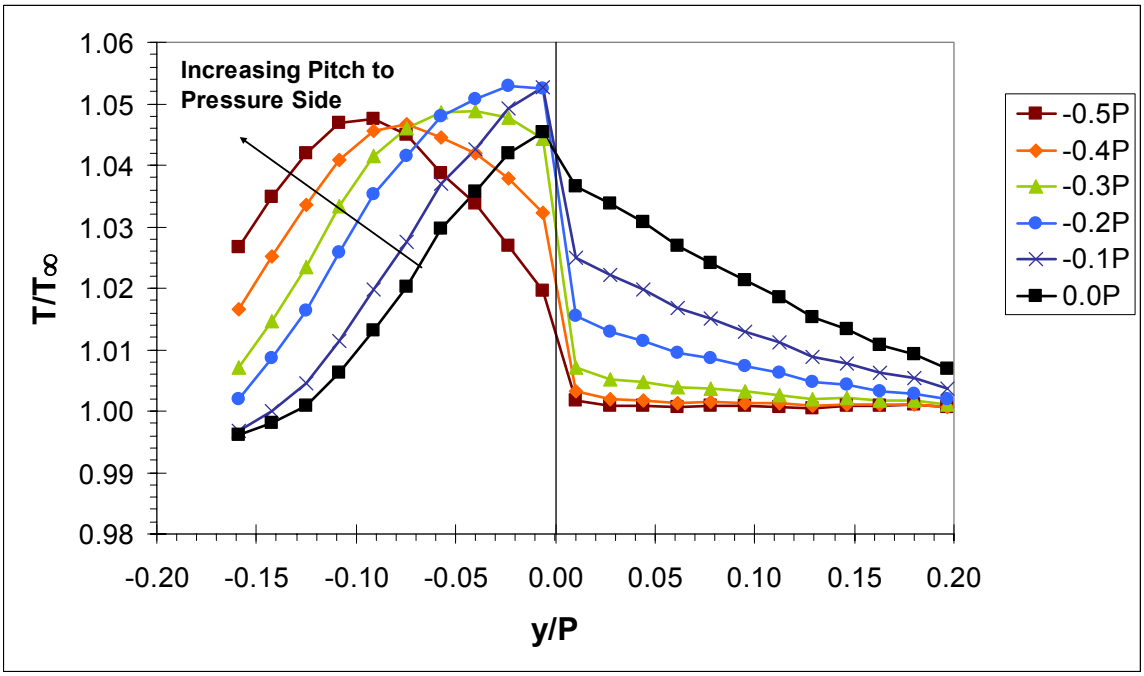

Figure 3.17b: Temperature profiles of the hot streak at Position T with hot streak position varying from -0.5*P* to 0.0*P*, *Tu* = 20%.

positioned to the suction and pressure side of the vane, respectively. Immediately obvious from these figures is the much greater spread of the hot streak relative to the profiles shown for the low mainstream turbulence case in Figure 3.10. On the suction

side at mid-passage (+0.5*P*) the high mainstream turbulence caused an essentially uniform temperature profile from the surface of the vane to the outer wall of the test section located at *y/P* = 0.2 due to the artificial constraint of the tunnel outer wall (see Figure 3.11). For hot streaks positioned closer to the vane on the suction side, at Position T there was an increase in the peak temperature of the hot streak (Figure 3.17a). This may be attributed to the decreased attenuation of the hot streak peak temperature because of the interaction with the vane similar to that discussed previously for the low mainstream turbulence case (§3.4 and Figure 3.10). This interaction with the vane was evidenced by the sharp temperature gradient that occurred at *y/P* = 0.0 for every hot streak positioned on the suction side of the vane. The hot streak temperature profiles at Position T for hot streaks positioned on the pressure side of the vane, Figure 3.17b, also show large temperature gradients at *y/P* = 0.0 indicating interaction with the vane for all profiles except the mid-passage profile (-0.5*P*). Unlike the mid-passage profile on the suction side, this hot streak profile was not uniform.

As is evident in Figures 3.17a and 3.17b, there was a significant decrease in the hot streak temperatures for the hot streak positioned at *y* = 0.0*P* relative to either +0.1*P* or -0.1*P*. Consequently the hot streak was moved with finer resolution about the stagnation line position of 0.0*P*. Hot streak temperature profiles measured at Position T are shown in Figure 3.18. This figure shows a systematic decrease in the hot streak peak temperature for hot streak positions approaching 0.0*P*, but the minimum peak temperature occurred for the hot streak positioned at +0.022*P* on the suction side. For a pitch position of +0.022*P* to the suction side, the greater attenuation on the suction side due to streamline length and compression of streamlines was balanced by the higher incoming temperature profile so that the profile at Position T was nearly the same on both sides of the vane. Due to this effect, at Position T this hot streak pitch position had the lowest peak temperature ratio.

Comparing hot streak temperature ratio profiles for the impinging and mid-passage hot streaks for equal axial positions under conditions of high turbulence in Figure 3.19, the peak temperature ratio was the same for the hot streak positioned at the stagnation line versus passing through the suction side mid-passage, but the profile

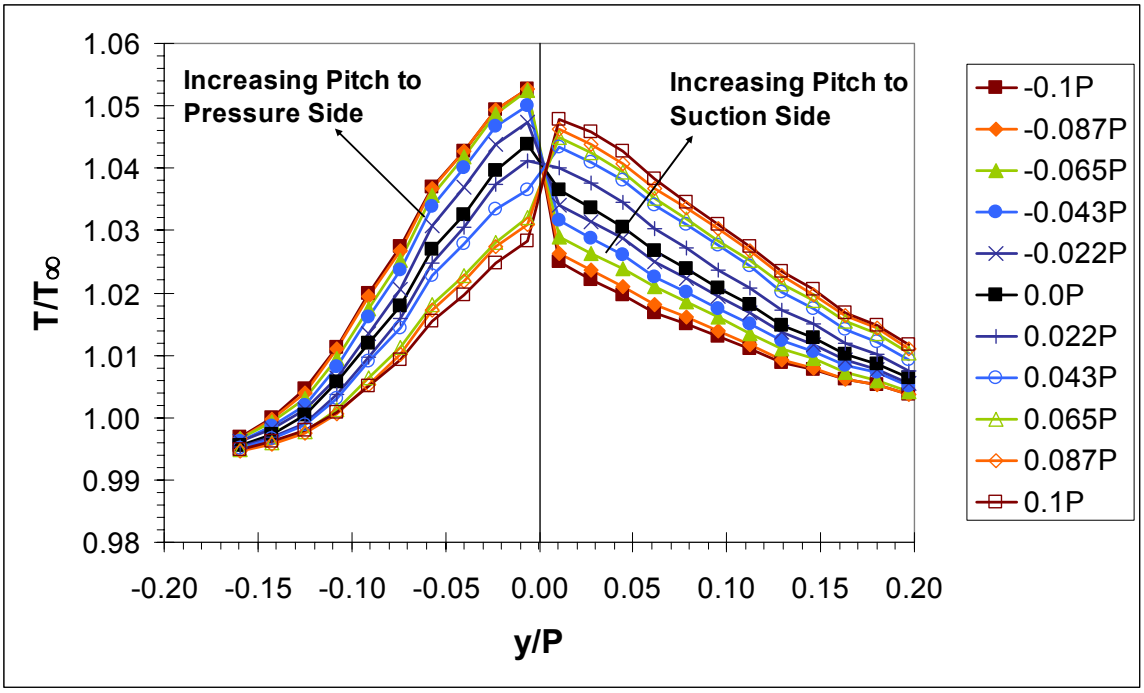

Figure 3.18: Temperature profiles of the hot streak at Position T with hot streak position varying from -0.1*P* to +0.1*P*, *Tu* = 20%.

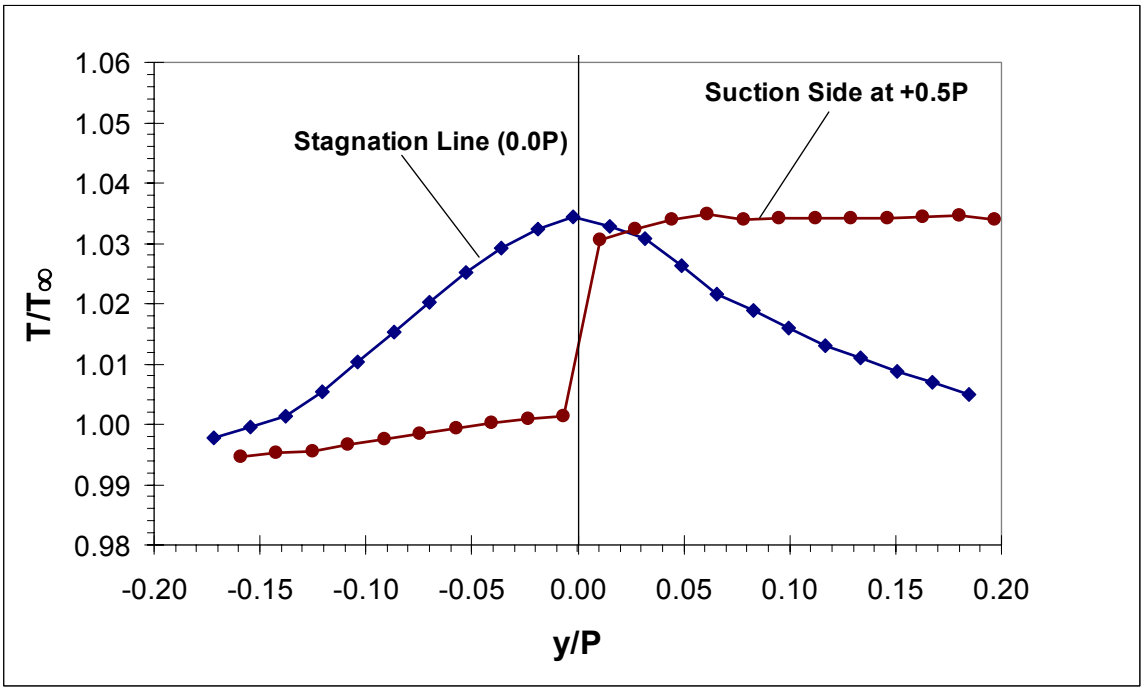

Figure 3.19: Comparison of hot streak profiles impacting the vane at 0.0*P*, and passing through the mid-passage at +0.5*P* at equal axial positions, *Tu* = 20%.

shapes were very different. Although the peak normalized temperature ratios were nearly the same for the impinging and non-impinging hot streak, this result was inconclusive since the hot streak through the suction side passage was artificially constrained by the tunnel outer wall (see Figure 3.14). Due to this, the hot streak shape was significantly different, in contrast to the result under low turbulence conditions.

The contours shown in Figure 3.20 for the same conditions as Figure 3.19 indicate that temperature gradients in the spanwise direction were roughly equivalent for the peak of the stagnation line (Figure 3.20a), and a majority of the width of the hot streak through the suction side mid-passage (Figure 3.20b). The sharp temperature gradient at the trailing edge ($y = 0.0P$) in Figure 3.20b demonstrates how the hot streak

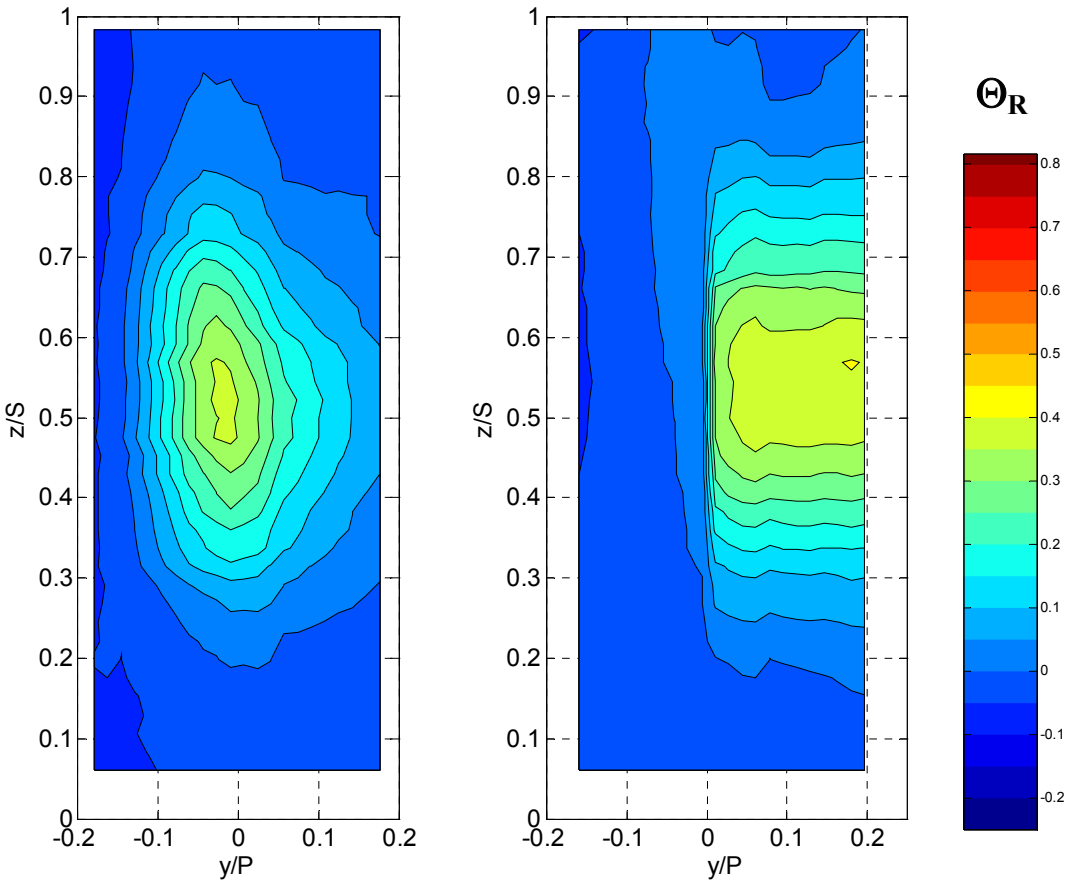

Figure 3.20: Normalized temperature ratio (Θ_R) plot at equal axial positions, high turbulence (Tu = 20%), with hot streak:

a. Impacting the stagnation line

b. Through the mid-passage at +0.5P

was constrained by the vane wall. However, near the edge of the hot streak toward the tunnel outer wall, it is clear that the hot streak was artificially constrained on that side. From the perspective of size, the hot streak passing through the mid-passage appeared stronger since its peak was much wider, which was also an artifact of the wind tunnel configuration. Although for conditions of low mainstream turbulence the equal axial positions in Figure 3.14 showed the equality of impinging and non-impinging hot streaks, it was clear that for conditions of high mainstream turbulence, a different comparison needed to be found to establish the effect of impinging the vane.

Since the effect of the outer wall created an artificial constraint on the growth of the hot streak under conditions of high mainstream turbulence, a comparison between the hot streak positioned to pass through the pressure side passage at -0.5*P*, measured at Position B and measurements at Position T for the hot streak impacting the vane (0.0*P*), was needed. These positions are shown in Figure 3.21, indicating the axial plane intersecting the trailing edge. Since the hot streak through the pressure side mid-passage

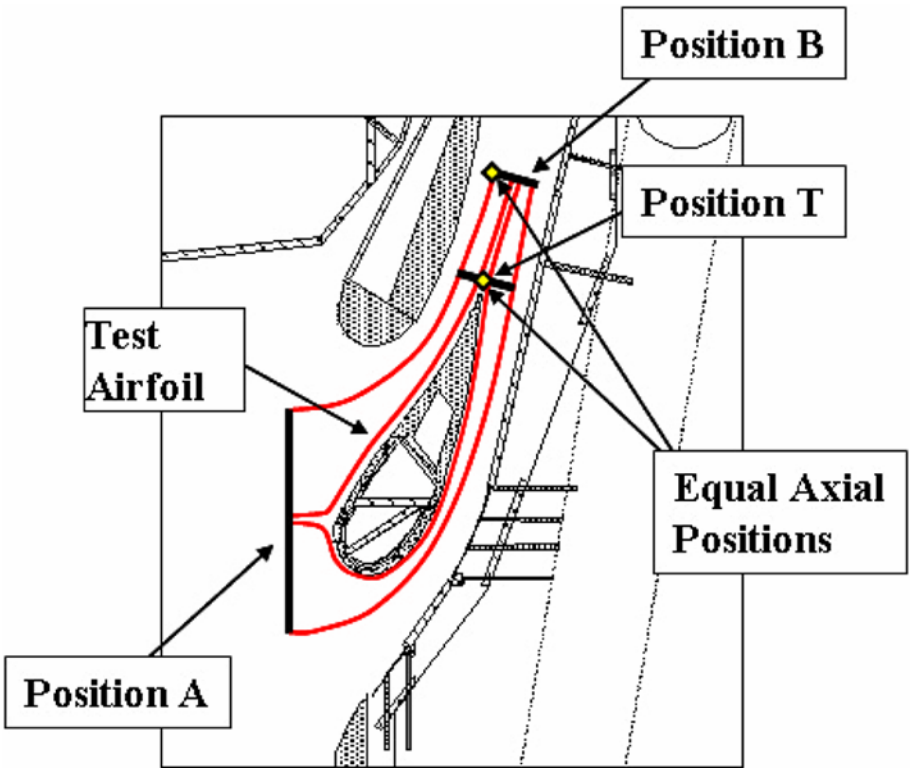

Figure 3.21: Tunnel schematic showing positions along an axial plane for hot streak positions of -0.5*P* and 0.0*P* (axial plane shown with blue dashed line).

was constrained by the vane wall to the pressure side of the test vane, it was a realistic simulation of actual engine conditions, but since it was not at the position of the rotor inlet plane, it was a less desirable comparison in that respect. In Figure 3.22, a comparison of temperature profiles at midspan shows the peaks to be nearly the same for the mid-passage at -0.5*P* and for 0.0*P*. The sharp gradient at 0.0*P*, for the impinging hot streak contributed to the slightly higher value seen at this position. While the peaks were nearly the same, the shape of the profiles was different due the effects of the vane on the shape of the impinging hot streak.

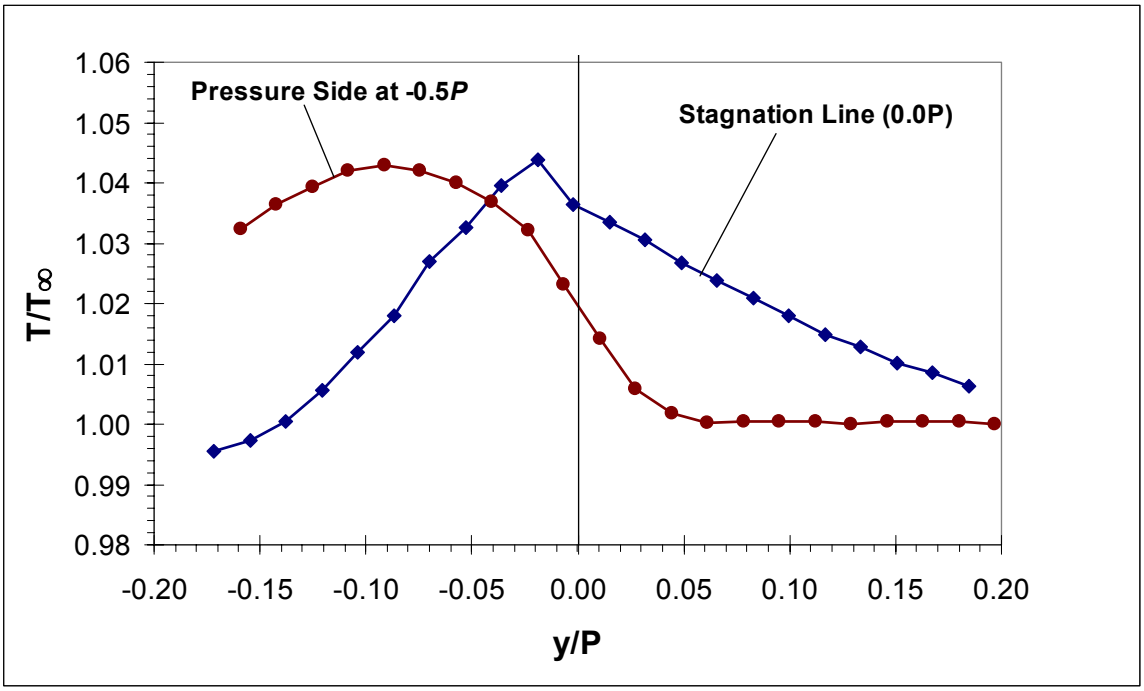

Figure 3.22: Comparison of hot streak profiles passing through the mid-passage at -0.5*P*, and impacting the vane at 0.0*P* at equal axial positions, *Tu* = 20%.

Contour levels for these same pitch positions and measurement locations are shown in Figure 3.23. The sharp temperature gradient was also evident at 0.0*P*, for the impinging hot streak in the warping of contour lines in Figure 3.23b. It was also evident that the impinging hot streak was already slightly constrained by the outer wall to the pressure side as shown in Figure 3.21. Here the line indicating the axial plane indicated where the tunnel outer wall became an artificial constraint even for the stagnation line hot streak, although the effect was small. Overall, the size and shape are fairly similar for the hotter region, $\Theta_R > 0.2$.

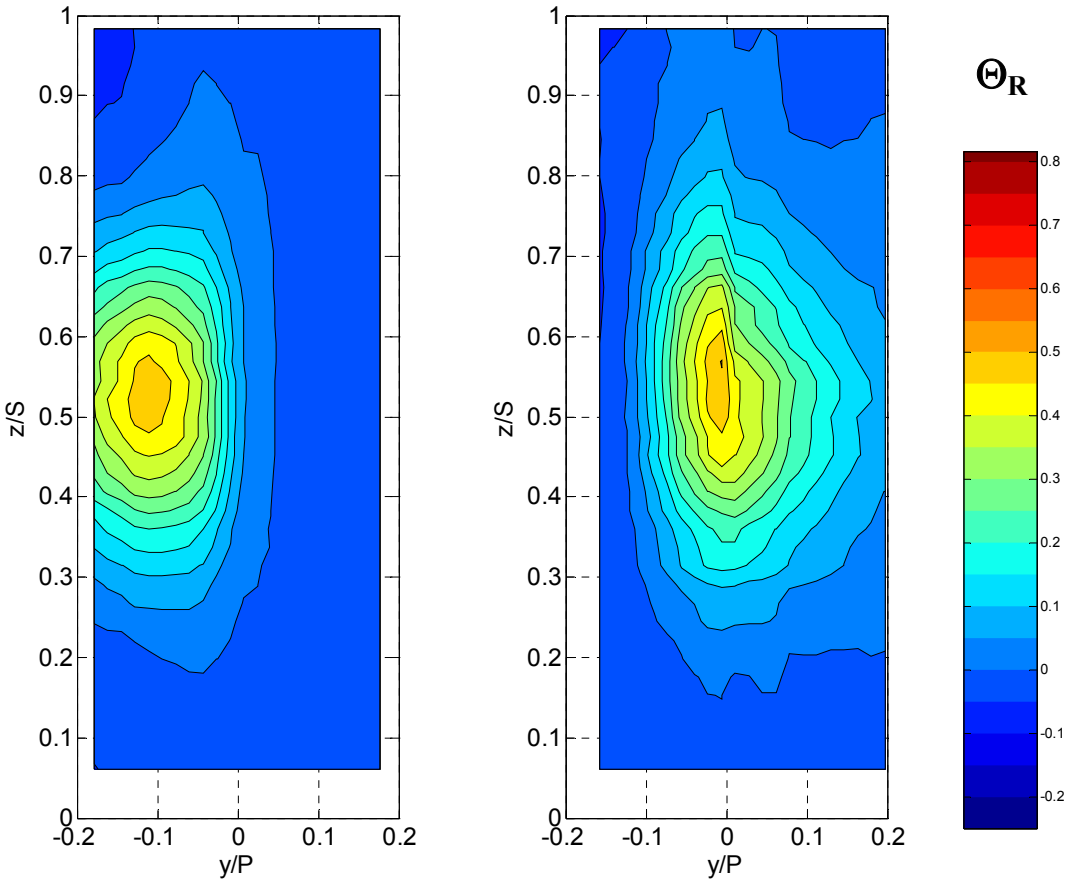

Figure 3.23: Normalized temperature ratio (Θ_R) plot at equal axial positions, high turbulence (*Tu* = 20%), with hot streak:

a. Through the mid-passage at -0.5*P*

b. Impacting the stagnation line

3.6 Effect of Vane Roughness on Hot Streak Attenuation

Based on surveys of in-service vane roughness measurements by Bogard et al [24] and Bons et al. [25], an equivalent sandgrain roughness for adiabatic effectiveness tests of k_s = 55 μm was chosen. Since the vane was scaled 9 times from the actual turbine, the equivalent roughness level was about k_s = 0.5 mm. This roughness level was chosen to simulate a fully rough vane and was an intermediate level of roughness within the range found in the above mentioned references. Sandpaper was chosen with an average roughness diameter of 0.5 mm (36 grit) for these simulations and adhered to the vane

surface. Experiments were performed with the hot streak impinging on the stagnation line to evaluate the effects of roughness on the hot streak at both low and high turbulence, Tu = 3.5% and 20% respectively.

A comparison of the normalized temperature contours in the wake at Position B under conditions of low turbulence indicates little effect of the vane roughness in Figure 3.24. Peaks values of hot streak strength were nearly the same at Θ_R = 0.76 and Θ_R = 0.78 for the smooth and rough vanes respectively. Given that the shape of the hot streak and the peak values were very similar for both cases, it appeared that roughness of the magnitude tested had no discernable effect on the hot streak under conditions of low turbulence.

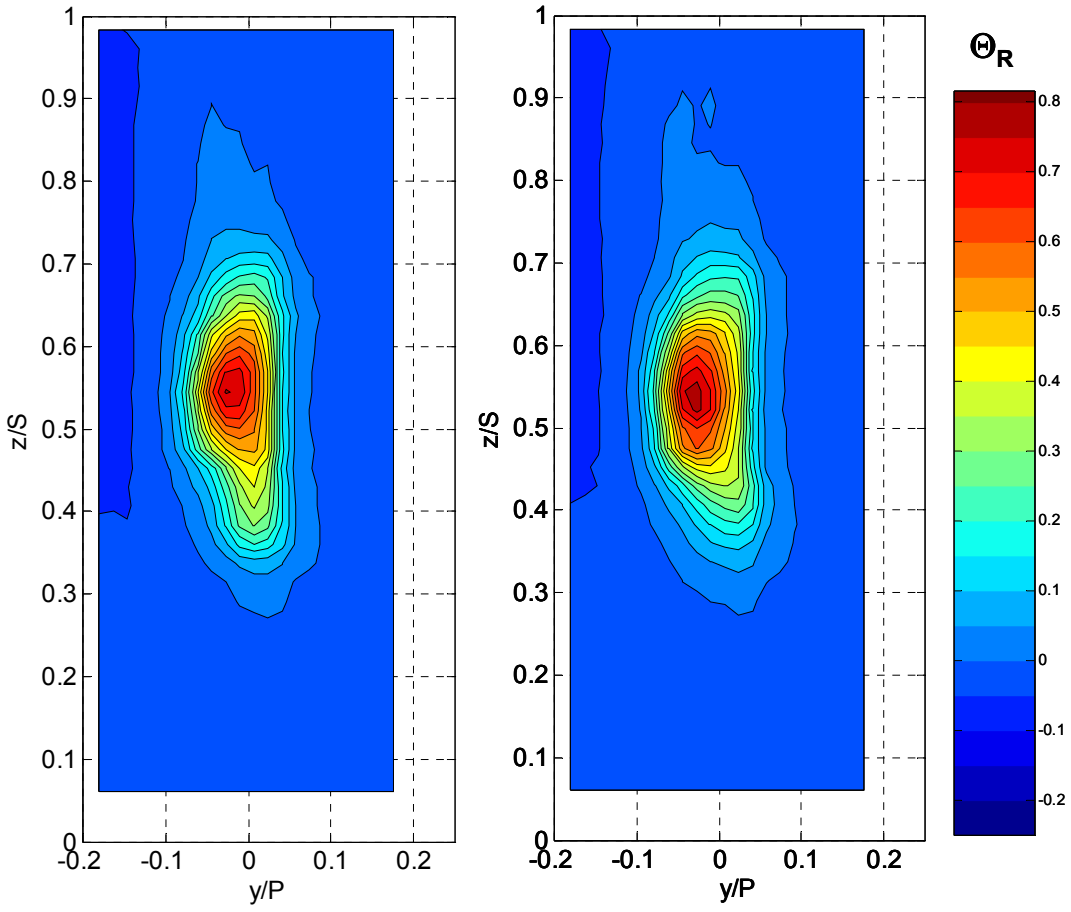

Figure 3.24: Normalized temperature ratio (Θ_R) plot at Position B, with hot streak impacting the stagnation line (0.0P), low turbulence (3.5%):

a. Smooth

b. Rough, k_s = 0.5 mm

Figure 3.25 shows the effects of surface roughness on the downstream hot streak temperature profile for conditions of high turbulence. The peak normalized temperature ratio values differed by very little, and the shape of the hot streak appeared unchanged by interaction with the rough surface.

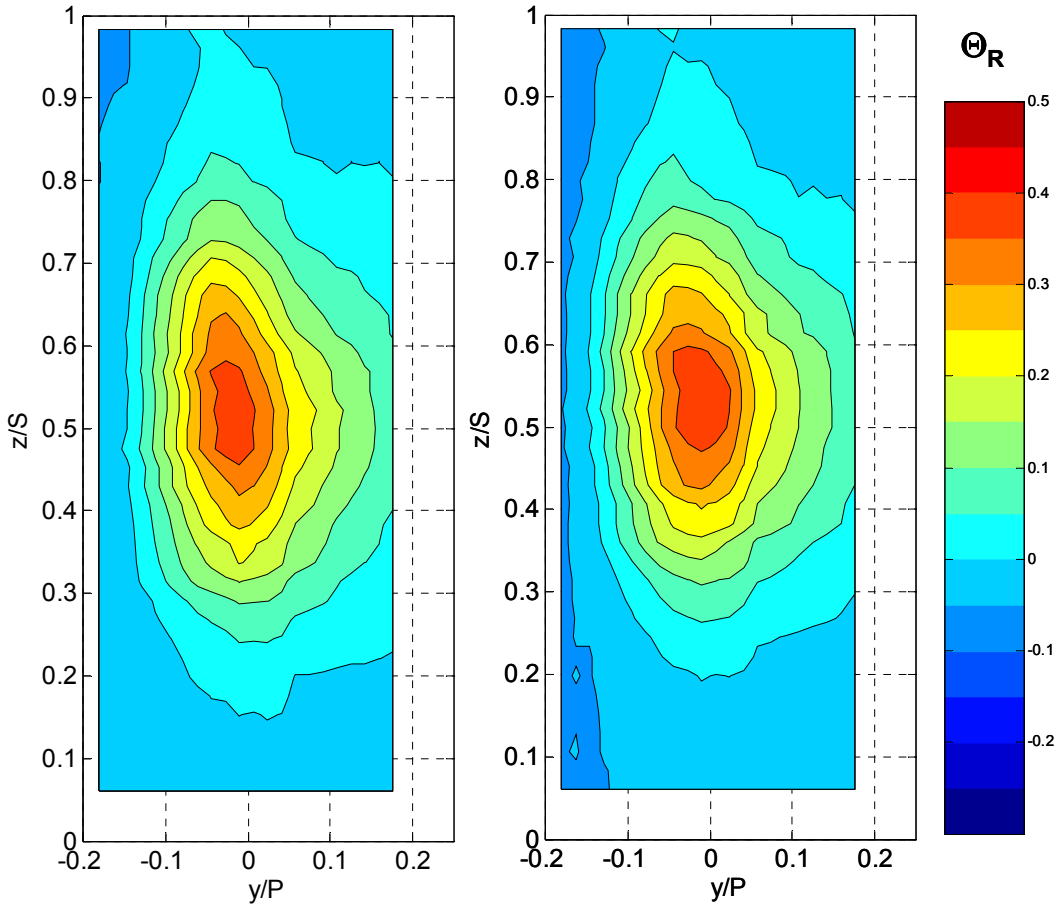

Figure 3.25: Normalized temperature ratio (Θ_R) plot at Position B, with hot streak impacting the stagnation line (0.0*P*), high turbulence (20%):

a. Smooth

b. Rough, k_s = 0.5 mm

Overall, the effect of roughness on the hot streak was not significant. The tests performed showed that very little difference occurred at either low or high turbulence. Clearly the attenuation of the hot streak was dominated by the mainstream turbulence and the additional difference in the boundary layer thickness caused by a rough surface did not have a significant difference in the attenuation of the hot streak.

3.7 Evolution of the Temperature Profile

For the hot streak positioned to impact the stagnation line on the vane, the effects of the difference in flow around the pressure and suction side were apparent from measurements at Position T presented previously. Further temperature profile measurements were made at Positions S1, S2, P1, and P2 along the vane corresponding to 1/3 and 2/3 of the total length along the surface of the vane as shown in Figure 3.1. These measurements were made with a thermocouple rake consisting of 6 E-type thermocouples with a spacing of 14.2 mm. The rake was oriented in a plane normal to the streamlines as shown in Figure 3.1. Immediately upstream of the vane, at Position A, the hot streak had a peak temperature of $T/T_\infty = 1.090$ for high mainstream turbulence (Tu = 20%).

Three-dimensional renderings of the hot streak contours are shown in Figures 3.26a and 3.26b for the suction and pressure sides respectively. A comparison of these two figures demonstrates how the width of the hot streak varied as it passed around the suction and pressure sides of the vane. On the suction side, the hot streak width was reduced substantially due to the compression of streamlines, while the hot streak width on the pressure side was only slightly reduced from that observed at Position A upstream of the stagnation line. As seen in Figure 3.8 previously, streamlines originating from the same distance on either side of the stagnation streamline showed a much greater rate of convergence on the suction side at a position of $s/L = 0.33$ than on the pressure side.

To establish how much the hot streak attenuated between Position A and the stagnation line, measurements were taken at midspan with thermocouples protruding about 1 mm from the surface of the leading edge surrounding the stagnation line. These measurements indicated that the peak normalized temperature ratio was $\Theta_R = 0.85$ at the stagnation line at midspan. Although this drop seems large compared with the distance traveled by the hot streak, i.e. a total of $0.21C$ from Position A to the vane stagnation line, mainstream turbulence levels were very high over this distance and the temperature gradients were equally high, so hot streak attenuation was expected to be large in this region. From Position A to the stagnation line, the hot streak was reduced by about 15% over a distance of 125 mm, or $0.21C$.

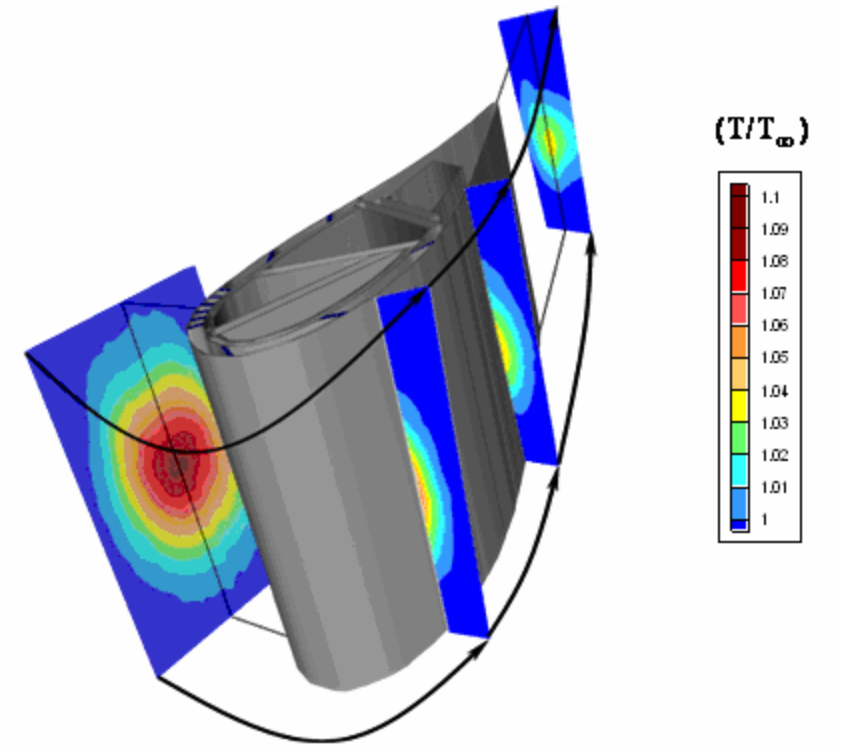

Figure 3.26a: Temperature ratio (T/T_∞) plots around suction side from Position A to 0.33L_S to 0.66L_S to Position B for high turbulence with hot streak impacting the stagnation point.

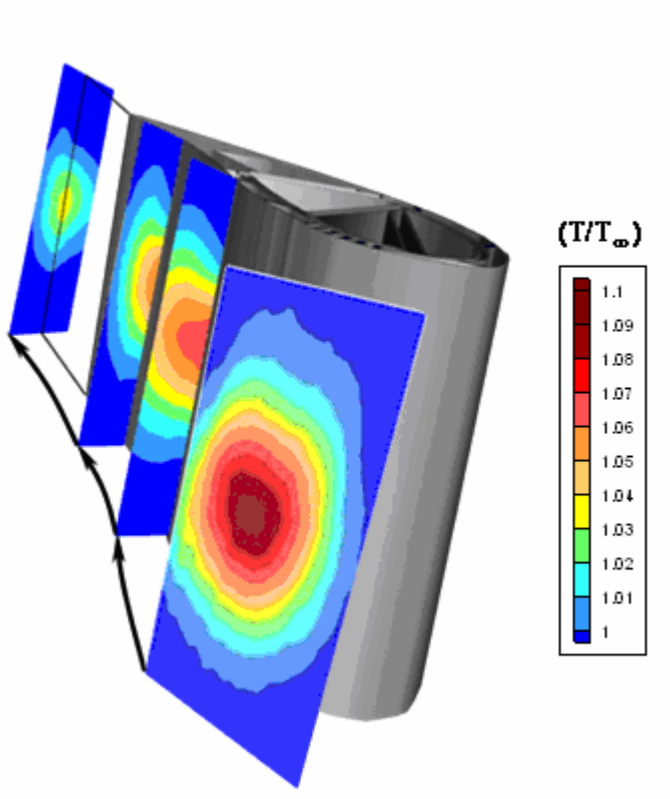

Figure 3.26b: Temperature ratio (T/T_∞) plots around pressure side from Position A to 0.33L_P to 0.66L_P to Position B for high turbulence with hot streak impacting the stagnation point.

Detailed measurements conducted with a single thermocouple probe were made at approximately the same vane surface locations as those shown in Figures 3.26a and 3.26b. The single thermocouple probe was traversed pitchwise in an arc away from the vane surface at midspan by rotating it about its axis of revolution. Due to the size of the thermocouple probe and the position of the access port in the top of the tunnel beside the vane, the nominal positions of the traverses were slightly downstream of those shown in Figures 3.26a and 3.26b. A schematic of the vane and single thermocouple probe is reproduced from Chapter 2 in Figure 3.27 describing the relative location of the measurement planes and arc made by the probe. To differentiate the positions S1, S2, P1, and P2 from those pertaining to the fine scale measurements, the downstream positions for the single thermocouple probe are referred to as S1', S2', P1', and P2', with nominal positions of $0.36L_S$, $0.70L_S$, $0.38L_P$, and $0.71L_P$ respectively. Since the thermocouple probe was traversed in an arc, the position closest to the vane was slightly farther downstream than the position parallel to the vane wall as shown in the schematic in Figure 3.27. However, the maximum range of streamwise displacement for the traverses

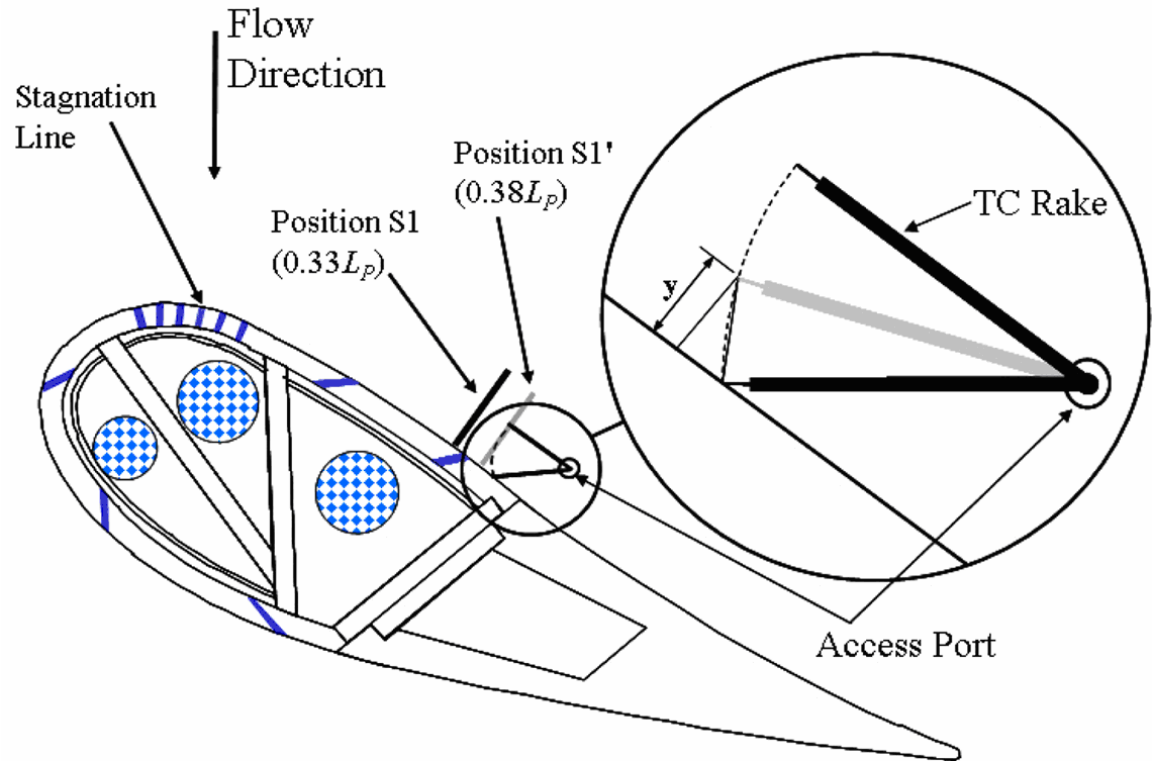

Figure 3.27: Schematic of the single thermocouple probe and its traversing arc.

was $\pm 0.015L_S$ and $\pm 0.02L_P$ for the suction side and pressure side respectively. Since the hot streak attenuation occurred over much larger distances, this range of streamwise displacement was not expected to cause errors in the reported findings.

Evolution of the Θ_R profiles from Positions S1' and P1' to Position B in the wake are shown in Figure 3.28. From the stagnation line to Position S1' (on the suction side), hot streak strength dropped from $\Theta_R = 0.85$ to $\Theta_R = 0.67$ for the thermocouple probe positioned just off the wall, a drop of about 27% over 347 mm (or $0.58C$), roughly 2.5 times the distance as from Position A upstream of the vane to the stagnation line. Although turbulence levels near the wall were suppressed, the attenuating affects of stronger temperature gradients due to compression of streamlines made this a region of relatively high attenuation. Although the temperature ratio was reduced about as much on the pressure side, the drop from $\Theta_R = 0.85$ at the stagnation line to $\Theta_R = 0.66$ at Position P1' just off the wall represented a drop of about 29% over a smaller distance of 277 mm, or $0.47C$. Comparing the drop in near wall hot streak strength normalized by the distance traveled, the pressure side had a larger reduction at about $\Delta\Theta_R = 0.45$ per unit chord compared with the suction side at about $\Delta\Theta_R = 0.33$ per unit chord. Although there was no substantial compression of streamlines to increase the temperature gradient on the pressure side, the turbulence level from the mainstream was also not suppressed to the

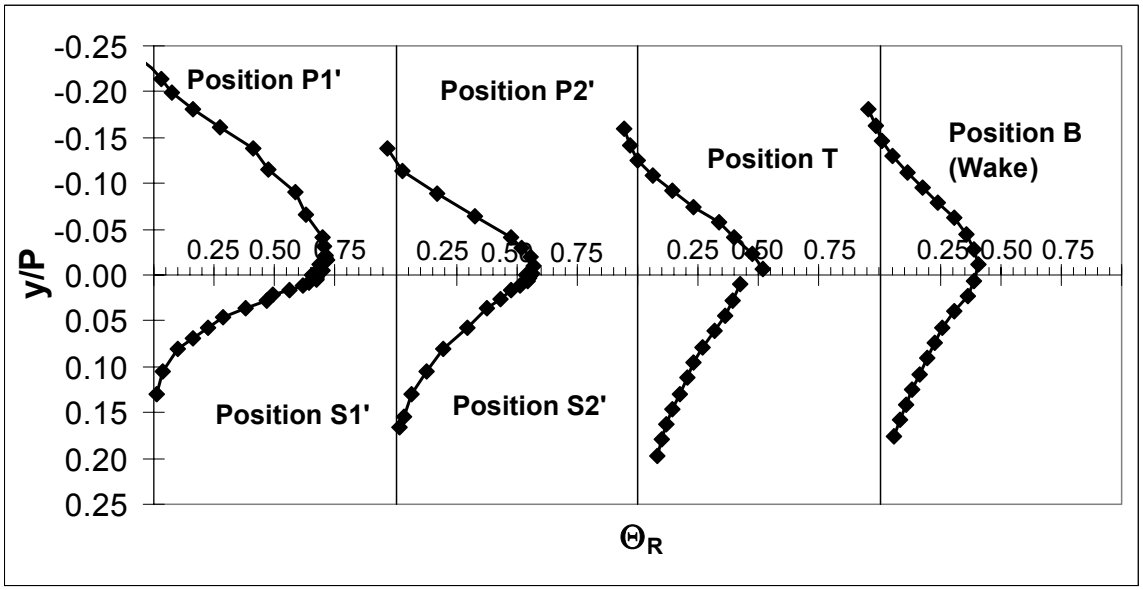

Figure 3.28: Temperature profiles of the hot streak for the hot streak aligned with the stagnation line, *Tu* = 20%.

same extent as on the suction side. This helps to explain why the pressure side hot streak strength was reduced more per unit chord than the suction side.

Between the 1/3*L* and 2/3*L* positions the decay of the hot streak was less on the pressure side; a 24% decrease on the suction side from $\Theta_R = 0.68$ to $\Theta_R = 0.54$ over a distance of 0.45*C*, and an 18% decrease on the pressure side from $\Theta_R = 0.70$ to $\Theta_R = 0.56$ over a distance of 0.32*C*. Again normalizing these reductions by the respective chord length, the reductions in the hot streak were nearly identical at about $\Theta_R = 0.26$ per unit chord. While the pressure side turbulence levels were not suppressed as much as they were on the suction side, the influence of the strong temperature gradient on the suction side made the reductions per unit chord very similar. Finally from the 2/3 position to the trailing edge (Position T) there was a 40% decay on the suction side from $\Theta_R = 0.54$ to $\Theta_R = 0.38$ over 0.45*C*, but less decrease on the pressure side from $\Theta_R = 0.56$ to $\Theta_R = 0.46$ over 0.32*C*. For the last 1/3 of the vane, i.e. from the 2/3*L* position to the trailing edge, the drop in hot streak strength was slightly greater than for the middle 1/3 for both the suction and pressure sides at about $\Theta_R = 0.30$ per vane chord length.

Figure 3.29 shows a comparison of the reduction rates per unit chord between stations, where Position A was the reference. At each station, the reduction between it and the previous station was computed. The trend is clear from this figure; from Position A to the stagnation line the reduction was the greatest for the distance traveled and from the stagnation line to the 1/3*L* position, the pressure side had a greater level of reduction per unit chord, but traveled a much shorter path. From the 1/3*L* position to the 2/3*L* position, and for the last 1/3 of the vane surface, reduction rates per unit chord were nearly the same for the suction and pressure sides. Since the overall reduction of the suction side was much greater than that of the pressure side, this was clearly due to differences in the streamline length around the vane and due to the compression of streamlines on the suction side which created higher gradients.

A closer look at the profiles at Positions S1', S2', P1', and P2' is shown in Figure 3.30. These profiles provide some insight into the mechanism creating a sharp temperature gradient at the trailing edge, Position T, beyond that shown previously in Figure 3.28. While the pressure side profile at Position P1' remained fairly flat with a mild gradient for $y/P < -0.04$ (away from the wall), the suction side profile at Position S1'

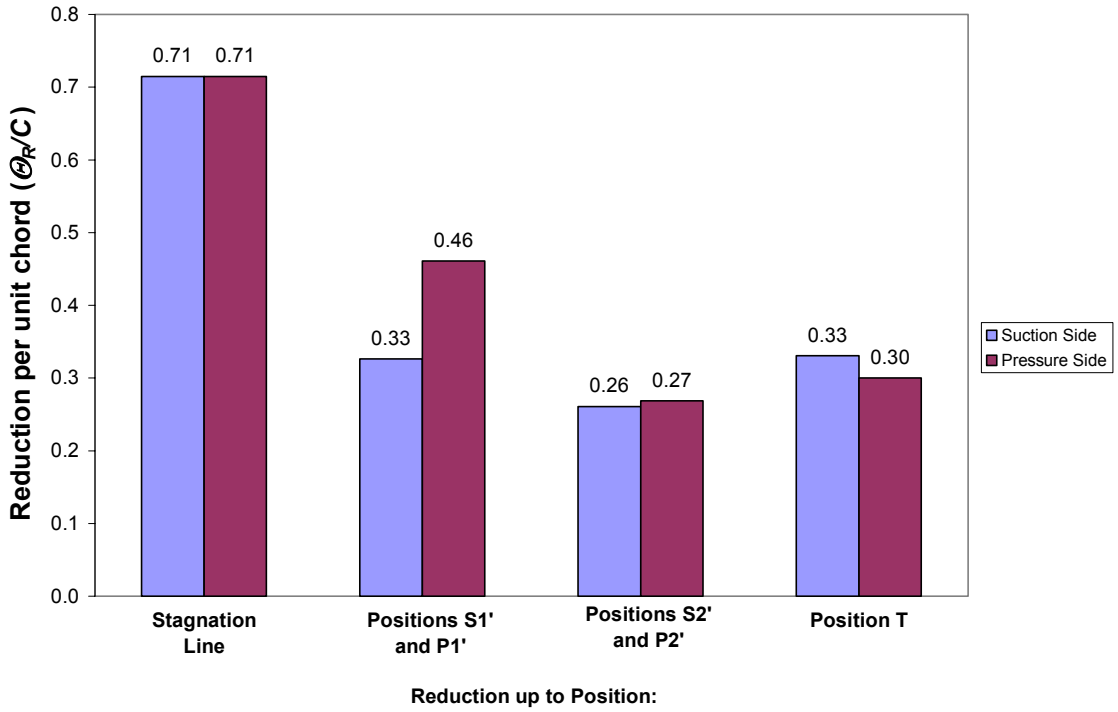

Figure 3.29: Comparison of suction and pressure side reductions per unit chord from Position A to Position T.

showed that the large gradient extended up to the vane wall. This strong temperature gradient accelerated the attenuation process near the wall on the suction side to Position S2', while the strong turbulence levels that were not suppressed as greatly on the pressure side resulted in near wall values that were similar at Position P2'. At Position S1', the temperature gradient farther from the wall ($y/P > 0.02$) was nearly twice as strong as the near wall ($y/P < 0.02$) temperature gradient. Comparing this gradient to the pressure side away from the wall where the pressure side gradient was not flat, the suction side temperature gradient was about three times as strong. By Position S2', the gradient off the wall was about one third as steep as at Position S1' and was wider in the pitchwise direction. Switching again to the pressure side, the gradient was flat near the wall at Position P2', but due to the compression of streamlines at this location on the pressure side, the gradient had increased by about 50% (see Figure 3.8 where Position P2' is roughly across the passage from Position S1 indicated as $0.33L_S$). The fine scale

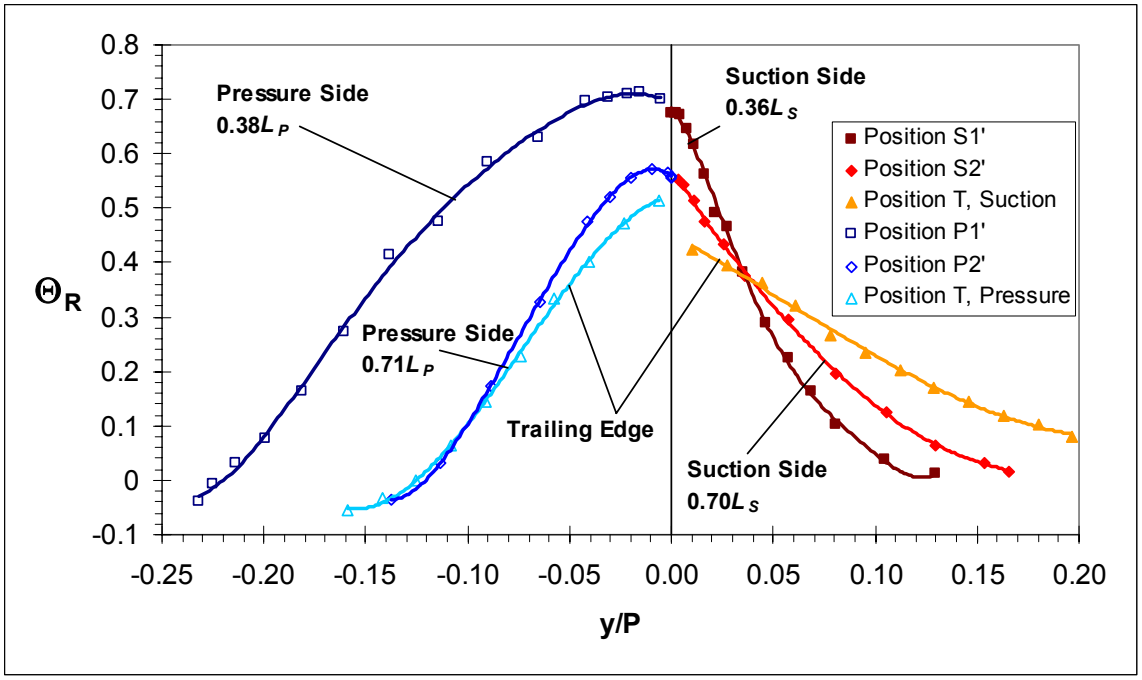

Figure 3.30: Fine scale temperature profiles at Positions P1', P2', S1', and S2' for the hot streak impacting the stagnation line (0.0*P*), *Tu* = 20%.

measurements near to the wall revealed that the profiles had fairly similar values at the wall for corresponding positions of the hot streak, i.e. Position S1' and P1', and Position S2' and P2'. This observation further exposed the nature of the evolution of the sharp temperature gradient at the trailing edge, since the sharp temperature gradient at Position T appeared to occur primarily in the last 1/3 of the vane. The hot streak on the suction side still had a large gradient at Position S2', which relaxed significantly by Position T. The slope of the temperature gradient was about one half as great at Position T as at Position S2'.

The effect of conduction can be evaluated by the gradient near the wall for Positions P1', P2', S1', and S2', since the profile should be flat for a perfectly adiabatic wall. Although surface temperature measurements were not made at these positions, the decrease in the fluid temperature very near the wall was clearly due to conduction into the vane, causing a weak but measurable thermal boundary layer. For Positions P1' and P2', the difference in the peak slightly off the wall and the measurement at the wall was about 0.4° C, but this was localized to less than 1*d* from the wall. For Position S1', the difference was less than 0.1° C and restricted to much less than 0.5*d*, while for Position

S2' the effect was larger at about 0.3° C within 0.5*d* from the wall. As shown in Figure 3.30, this effect was much too small to be detected by the thermocouple rake at Position T since the closest positions were about 1*d* from the wall. As mentioned in Chapter 2, Section 2.4, a small conduction effect of this order was expected.

Surface temperature measurements were made at the trailing edge to show the spanwise variation in surface temperature. These measurements were made with a FLIR ThermaCAM P20 infrared camera, utilizing the large port in the wind tunnel facility used for access to the vane near the trailing edge. The IR camera was used by other researchers for measurements of adiabatic effectiveness and heat transfer. For the square port at the trailing edge a thin plastic film (i.e. Saran Wrap) was used as a window. This plastic film permitted IR wavelength light to be detected from the vane surface, and was needed because the tunnel facility was primarily constructed of Plexiglas which is opaque to IR wavelengths. Calibration of the camera was required despite its capability of converting the raw images to temperature profiles since the thin plastic film interfered with the transmission of IR radiation. An *in situ* calibration for the thin plastic film was performed using 4 ribbon surface thermocouples permitting direct correlation of reported temperatures from the camera to actual temperatures. To perform the transformation of pixel locations on the images to *s/L* and *z/S* physical locations on the vane surface, images were taken of the vane using tape marked with reflective strips at 10 mm increments attached to the vane surface and later used to curve fit data for the transformation. A Matlab program written by James Rutledge, blockscan.m, was used to produce actual temperature values correlated to pixel locations using camera calibration results. More details about this program are available in Rutledge [26]. A second Matlab program, hcontour.m, which plotted normalized surface temperature data by s/L and z/S position on the vane, was developed by this author in collaboration with James Rutledge and Dave Robertson. The "array editor" feature in Matlab was utilized to extract data points for use in normalized temperature profiles.

Temperature measurements for the hot streak impacting the stagnation line under conditions of high mainstream turbulence taken at midspan are shown in Figure 3.31. These data describe the decrease of the hot streak temperature along the vane surface from the stagnation line to the trailing edge on the suction side. Wall-fluid interface

temperatures taken at the stagnation line and at Positions S1', S2', P1', and P2' are shown in the figure along with the surface temperature measurement on the suction side at the trailing edge. The decrease on both sides of the vane was fairly steady, with a larger decrease in the first portion of the vane. This was the same conclusion provided in Figure 3.29, where the reduction per unit chord was higher in the first 1/3 of the vane than farther downstream.

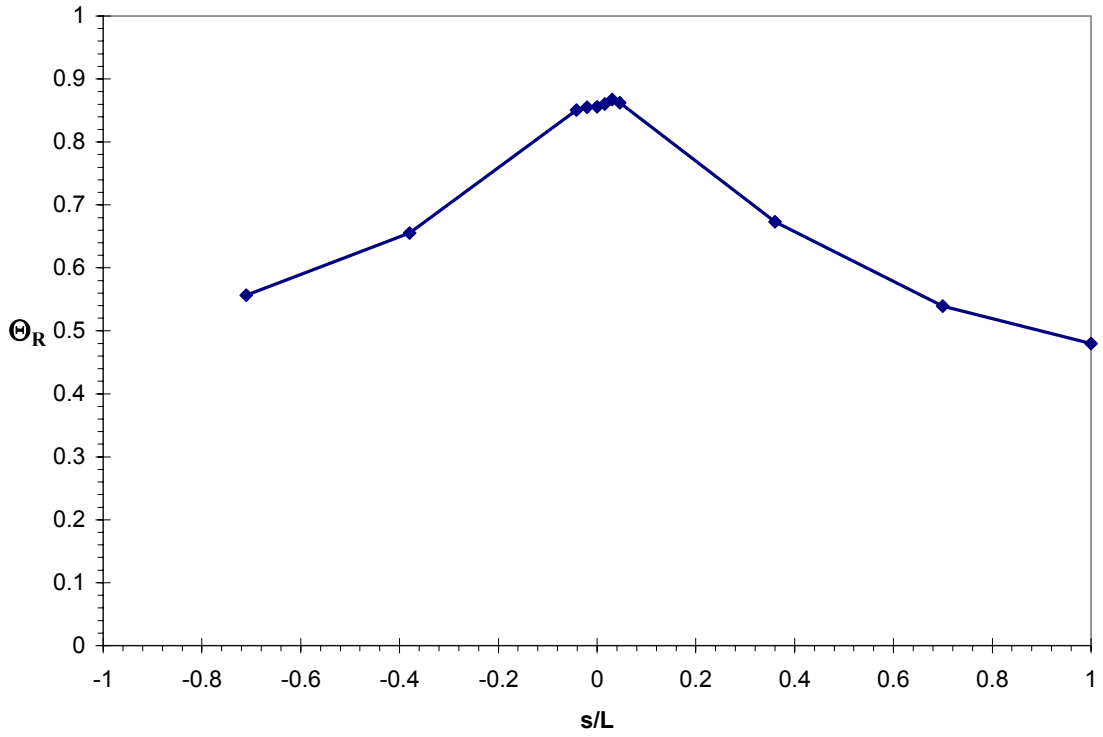

Figure 3.31: Surface temperature measurements along the vane made with a single thermocouple probe or IR camera for the hot streak impacting the stagnation line (0.0*P*), *Tu* = 20%.

Normalized surface temperature contours on the trailing edge for the hot streak impinging on the stagnation line are shown in Figures 3.32a and 3.32b, for low and high mainstream turbulence respectively. Note that the port available at this location limited data to less than the full span; in this case data was taken from about 0.3*S* to about 0.7*S*. These contour plots demonstrate how the spreading of the hot streak affected the adiabatic wall temperature of the vane differently for different mainstream turbulence levels. The much greater spreading of contour levels under conditions of high

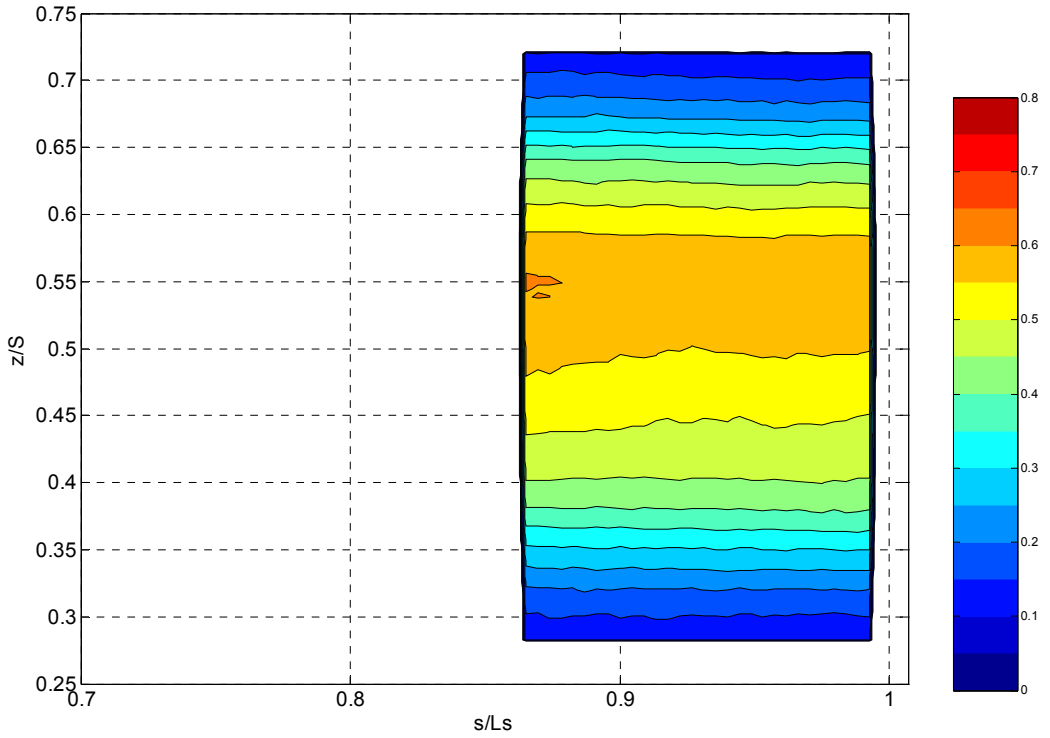

Figure 3.32a: Normalized surface temperature contours (Θ_R) on the trailing edge for the hot streak impacting the stagnation line (0.0*P*), *Tu* = 3.5%.

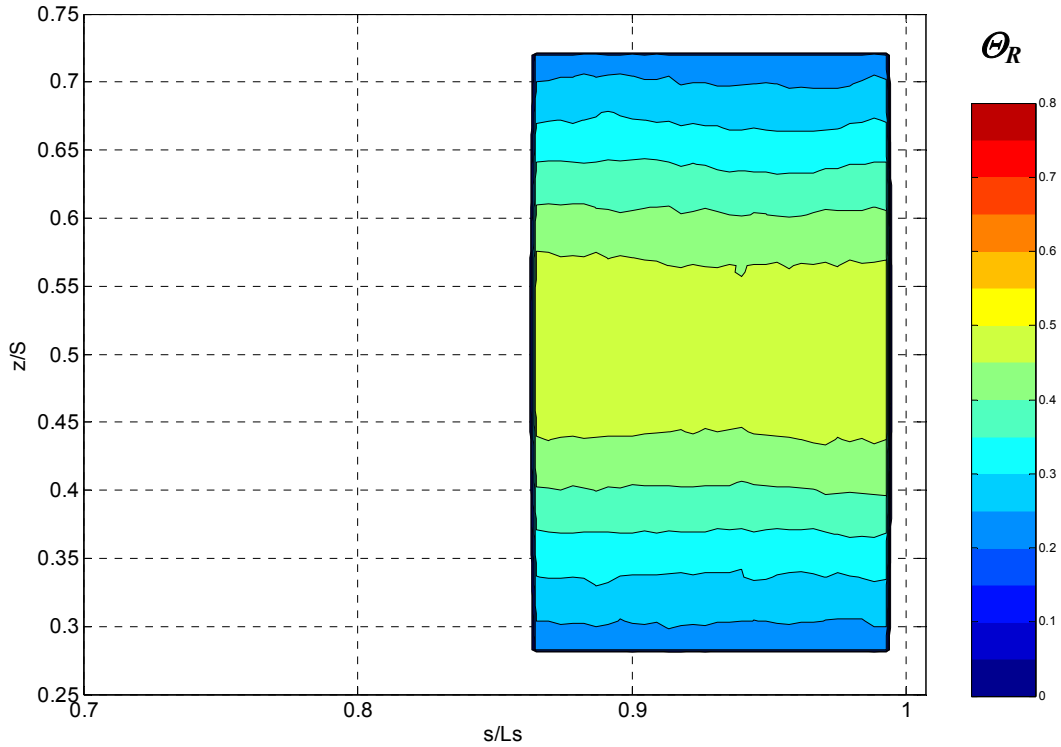

Figure 3.32b: Normalized surface temperature contours (Θ_R) on the trailing edge for the hot streak impacting the stagnation line (0.0*P*), *Tu* = 20%.

mainstream turbulence (Figure 3.32b) was immediately apparent. In Figure 3.32a, the highest temperature contour was slightly above midspan, but this is somewhat exaggerated by the reduced scale in the figure. The same result was shown previously in Figure 3.24a for Position T at the trailing edge for conditions of low mainstream turbulence. The range of the spread of the hot streak on the vane surface also correlated well with fluid temperature contour plots at the trailing edge (see Figure 3.24a and Figure 3.25a.

Data points extracted from the surface temperature measurements at 0.95*Ls* are shown in Figure 3.33. Although these data were limited in the spanwise direction by the size of the port in the tunnel facility, the figure clearly shows the greater spreading and lower peak temperature for high mainstream turbulence.

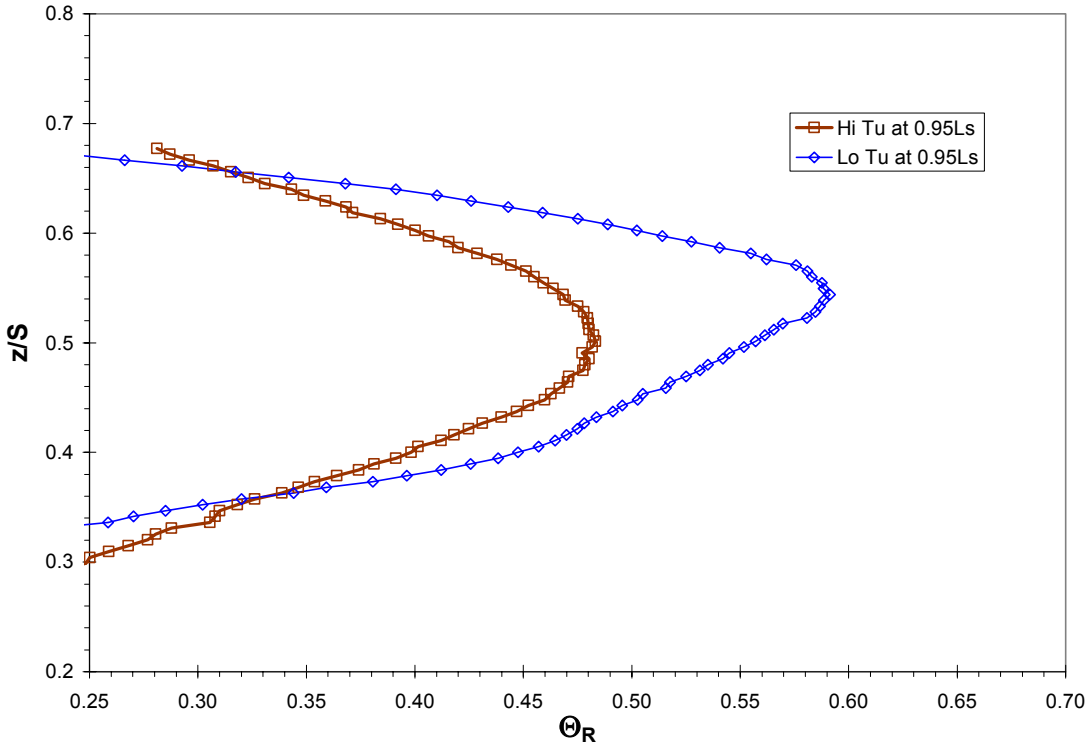

Figure 3.33: Normalized temperature profiles (Θ_R) at 0.95L_s for the hot streak impacting the stagnation line (0.0*P*), *Tu* = 3.5% and 20%.

3.8 Turbulence Effects in the Stator/Rotor Axial Gap at High Mainstream Turbulence

A first look at turbulence effects in the stator/rotor axial gap was shown in Figure 3.28, where measurements at Position B appeared as a smoothing of the sharp temperature gradient present at Position T, 0.32*C* upstream. Additional attenuation of the hot streak coming off the pressure side was seen in the relaxing of the temperature gradient as it mixed with the suction side fluid. A similar sharp temperature gradient was seen at the trailing edge (Position T) for the low mainstream turbulence condition, Tu = 3.5%, as shown in Figures 3.9 and 3.10. Position B, 0.32*C* downstream of the trailing edge, was a particularly relevant position for engine designers since the leading edge of the first stage rotors is usually between about 0.3*C* to 0.5*C* downstream of the first-stage stator. Thus, measurements made at Position B may be considered as fluid temperatures entering the rotor section, and thus affecting rotor heat transfer.

The effects seen in the stator/rotor axial gap downstream of the vane pertaining to hot streak attenuation were twofold. First, attenuation of the hot streak occurred due to the additional distance traveled downstream from Position T to Position B, which was 0.32*C* downstream of the trailing edge. As shown before, reductions for this amount of distance varied widely, but based on reductions per unit chord around the vane a range of about Θ_R = 0.08 to Θ_R = 0.14 were expected. Secondly, further reduction for the portion of the hot streak within the vane wake could reduce the peak even more over a small range in pitch.

A measure of the width of the wake at Position B downstream of the vane was obtained by measuring the stagnation pressure loss profile as shown in Figure 3.34. Here the non-dimensional stagnation pressure loss was defined as $(P_{0,\text{Pos A}} - P_{0,\text{Pos B}})/P_{\text{dyn,Pos A}}$. This measurement showed that the wake profile had a 20% width of about $\delta_{20\%}$ = 0.06*P* for conditions of low mainstream turbulence, which was nearly ½ of the 20% width of the hot streak at the same position downstream of the vane for the narrow hot streak profile at low turbulence (compare to stagnation line profile in Figure 3.15). For conditions of high mainstream turbulence, the wake was measured slightly wider at about $\delta_{20\%}$ = 0.075*P*, but compared to the hot streak width at the same position, it was about ¼

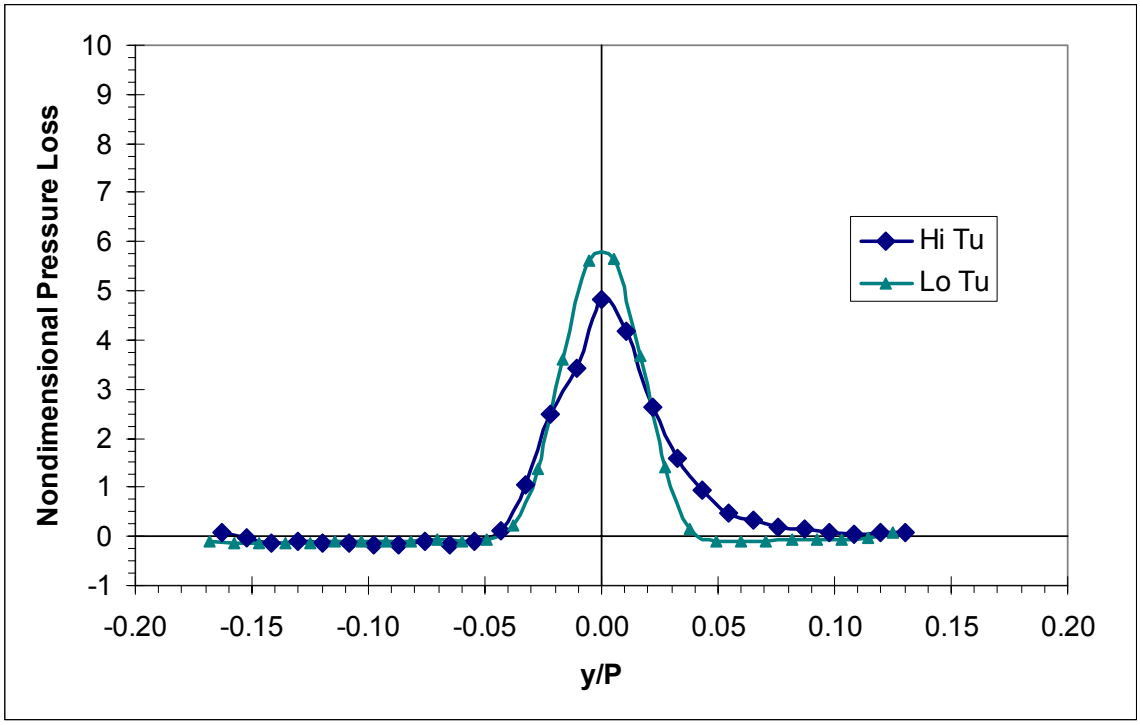

Figure 3.34: Stagnation pressure loss profile taken in the wake of the vane at Position B, *Tu* = 3.5 % and 20%.

of the hot streak 20% width ($\delta_{20\%}$). Most of the extra width was to the suction side and this profile had a slightly lower peak. Therefore, the wake of the vane was expected to cause a greater dispersion of the hot streak in the range $y/P = \pm 0.035$ for low mainstream turbulence and in the range $-0.035 > y/P > +0.050$ for high mainstream turbulence.

The profiles shown in Figure 3.35 demonstrate the effect of erosion of the sharp temperature gradient present at Position T for a pitch position of 0.1*P*, which resulted from splitting the entering hot streak profile as discussed previously. Presumably the vane wake assisted in the erosion of the sharp temperature gradient in the stator/rotor axial gap near $y/P = 0.0$. The drop in peak temperature ratio was substantial, going from $T/T_\infty = 1.053$ at the Position T to $T/T_\infty = 1.042$ at Position B, 0.32*C* downstream, a drop of about 20%. Not only did the peak erode in this region of high gradients, but as a result, the peak was shifted about 0.03*P* to the pressure side. At the position of the peak at Position T ($y/P = -0.006$), the drop was larger at about 25%. For this pitch position, the independent effect of the vane wake could not be separated from the effect of downstream distance.

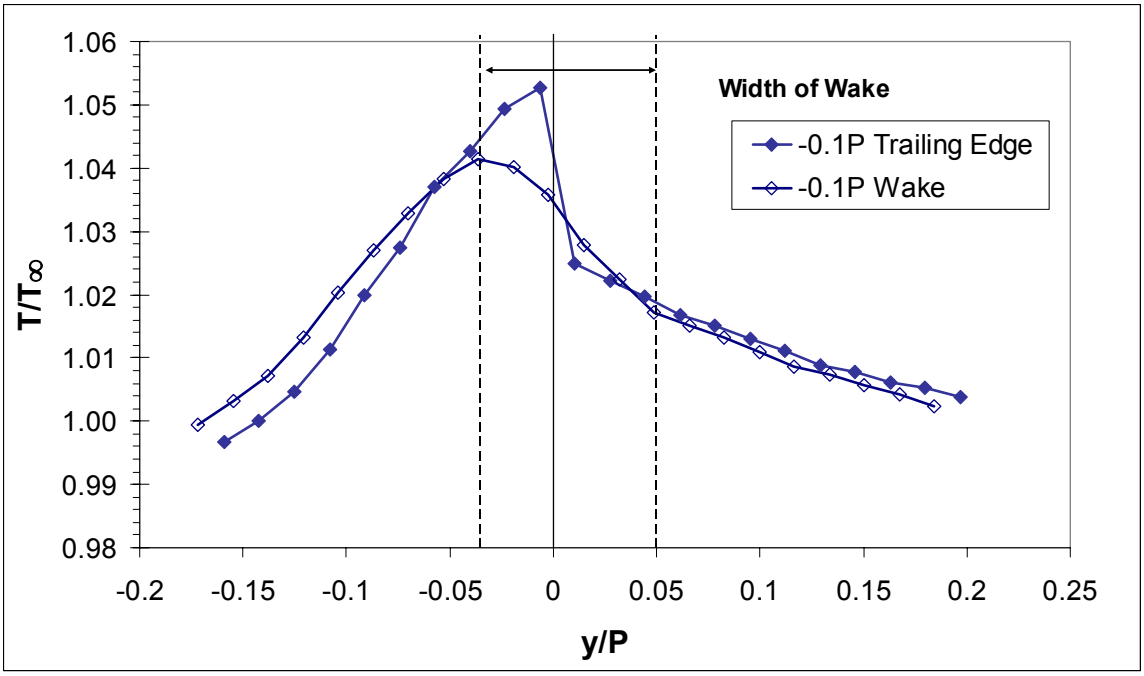

Figure 3.35: Comparison of temperature ratio profiles at Position T (trailing edge) and in the wake at Position B for the hot streak at -0.1*P*, *Tu* = 20%.

The effect of the erosion of the sharp temperature gradients occurred for all pitch positions, as seen in Figures 3.36a and 3.36b, showing suction side and pressure side pitch positions respectively. Here, the sharp temperature gradients present at the trailing edge disappeared, resulting in smooth profiles at Position B, 0.32*C* downstream. These profiles may be compared to those in Figures 3.17a and 3.17b, where the sharp temperature gradients were present at Position T. Note that for the suction side, although the peak temperature ratios for positions on the stagnation line (0.0*P*) and through mid-passage (+0.5*P*) were similar, peak temperature ratios for intermediate positions at +0.2*P* and +0.3*P* were somewhat higher. On the pressure side, intermediate positions (-0.2*P* and -0.3*P*) also had higher values than those found on the stagnation line (0.0*P*) and through the mid-passage (-0.5*P*).

The effect of attenuation over the distance downstream from Position T to Position B is seen in Figure 3.37, for the hot streak profiles at -0.5*P* to the pressure side. Here the sharp temperature gradient at the trailing edge was less of an issue since the approaching temperature profile was mainly on the pressure side. Still, the tail region of the hot streak was attenuated more greatly, resulting in a flat profile at Position T.

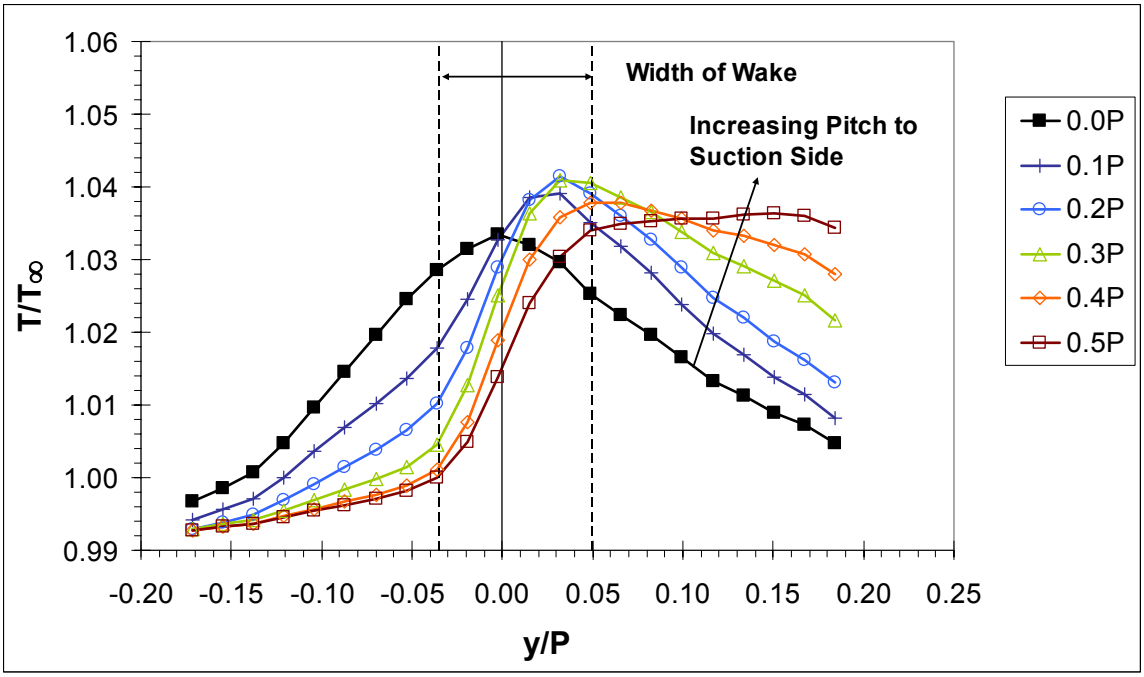

Figure 3.36a: Temperature profiles of the hot streak at Position B with hot streak position varying from 0.0*P* to +0.5*P*, *Tu* = 20%.

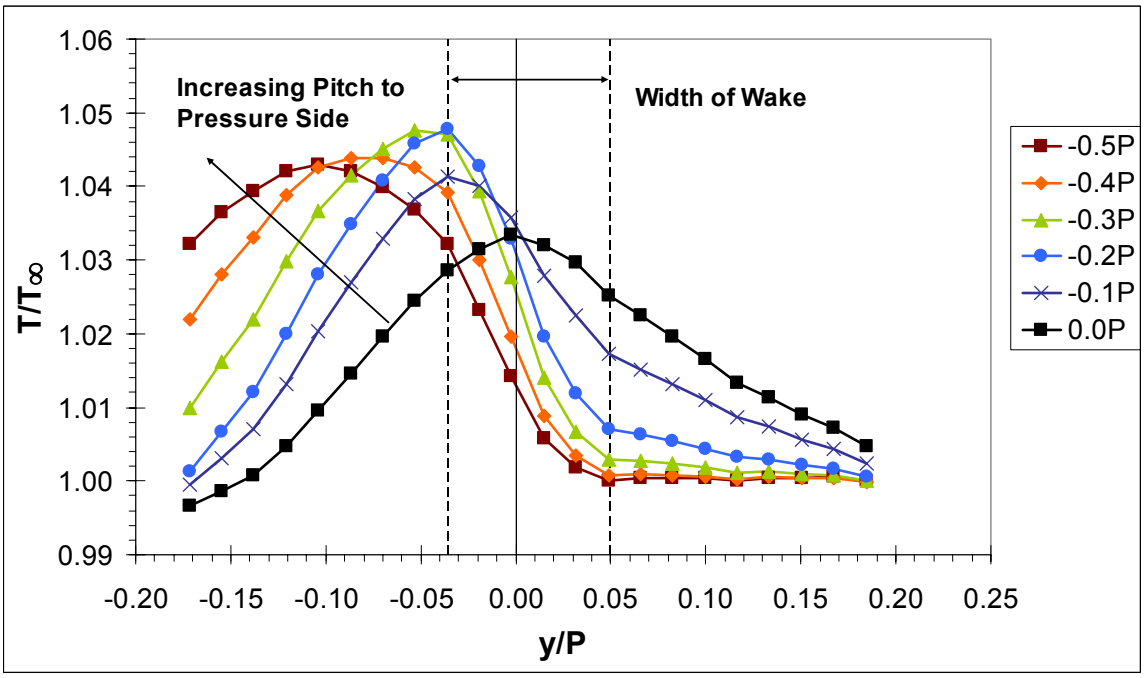

Figure 3.36b: Temperature profiles of the hot streak at Position B with hot streak position varying from -0.5*P* to 0.0*P*, *Tu* = 20%.

Shifting focus to the peak on the pressure side, the more sharply peaked profile at Position T was flattened during its progress downstream to Position B due to mainstream turbulence effects. The drop in peak temperature ratio was about 9% over the 0.32*C* traveled. This compares with a much greater level of attenuation for the hot streak affected by the vane wake. As shown in the figure, for a pitch position of 0.022*P*, the profile at Position T did not have a sharp temperature gradient and the drop in peak temperature ratio was about 18% from Position T to Position B. The significant difference between the attenuation rates for these two pitch positions confirmed that the vane wake had a separate effect from that of the turbulence in the mainstream since turbulence levels were much higher in the vane wake.

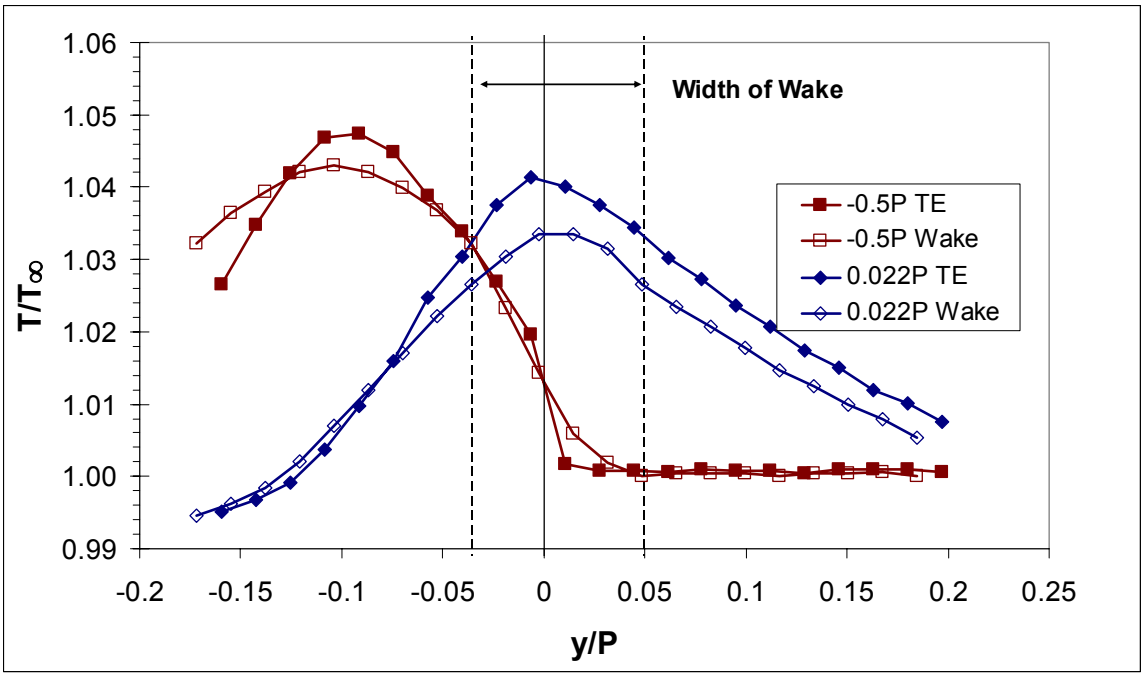

Figure 3.37: Comparison of temperature ratio profiles at the trailing edge and in the wake at Position B for the hot streak at +0.022*P* and -0.5*P*, *Tu* = 20%.

A comparison of the contour levels at -0.5*P* in Figure 3.38 shows a distinct broadening of the hot streak from Position T to Position B. This broadening of contours occurred in all directions, while the peak values dropped from $\Theta_R = 0.56$ at Position T to $\Theta_R = 0.48$ at Position B, due to the turbulence levels in the mid-passage. Evidence of the effect of bounding the hot streak between vanes is also seen in this figure, where there was a sharp gradient at $y/P = 0.0$.

The reduction in hot streak peak through the wake was about twice as much for the hot streak positioned to impact the stagnation line, as shown in Figure 3.39. The sharp temperature gradient shown for the midspan profile in Figures 3.17a and 3.17b for this same pitch position appears as a warping of the temperature contours at y/P = 0.0 in Figure 3.39a at the vane trailing edge. Although the shape and size of the hot streak was essentially unchanged, Figure 3.39b for the hot streak at Position B appears as a step down in contour value for the hotter portions of the hot streak ($\Theta_R > 0.2$).

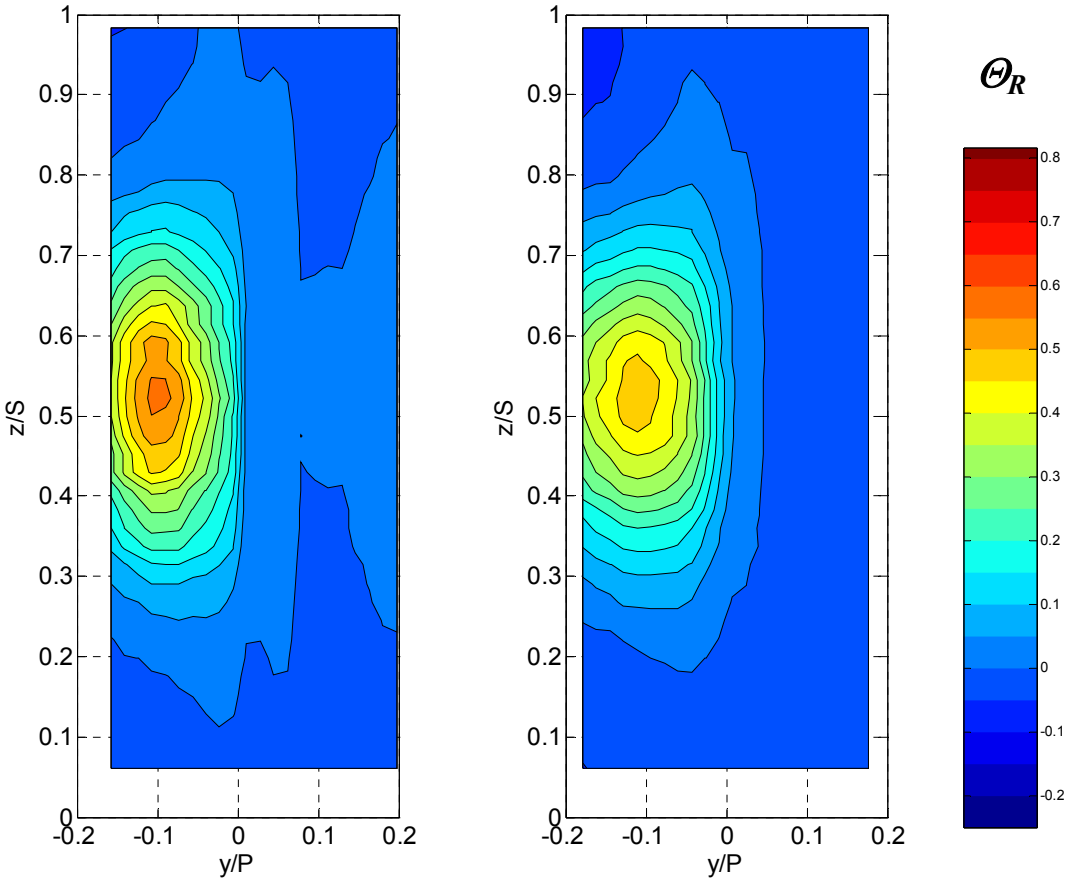

Figure 3.38: Normalized temperature ratio (Θ_R) plot with hot streak passing through the mid-passage (-0.5*P*), high turbulence (*Tu* = 20%), measured at:

a. Position T

b. Position B (0.32*C* downstream)

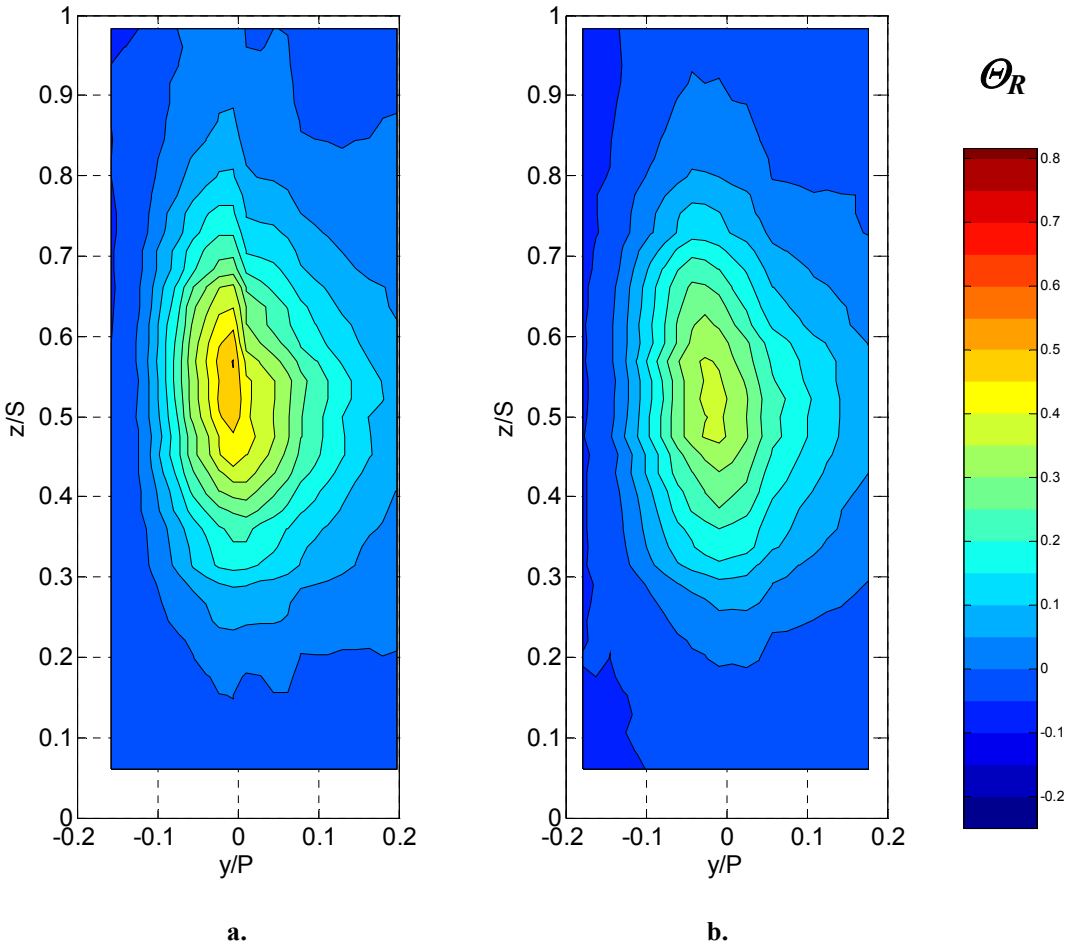

Figure 3.39: Normalized temperature ratio (Θ_R) plot with hot streak impacting the stagnation line (0.0*P*), high turbulence (20%), measured at:

a. Position T

b. Position B (0.32*C* downstream)

3.9 Turbulence Effects in the Stator/Rotor Axial Gap at Low Mainstream Turbulence

Turbulence effects in the stator/rotor axial gap under conditions of low turbulence were similar to that for high turbulence. For a profile at Position T (the trailing edge) with a sharp temperature gradient, the erosion of the sharp temperature gradient left a lower peak and a smooth profile. This effect is shown in Figure 3.40 for a hot streak pitch position of y/P = -0.065. Note that to observe a sharp gradient a Position T, the hot streak was positioned much closer to the stagnation line than for high turbulence, as

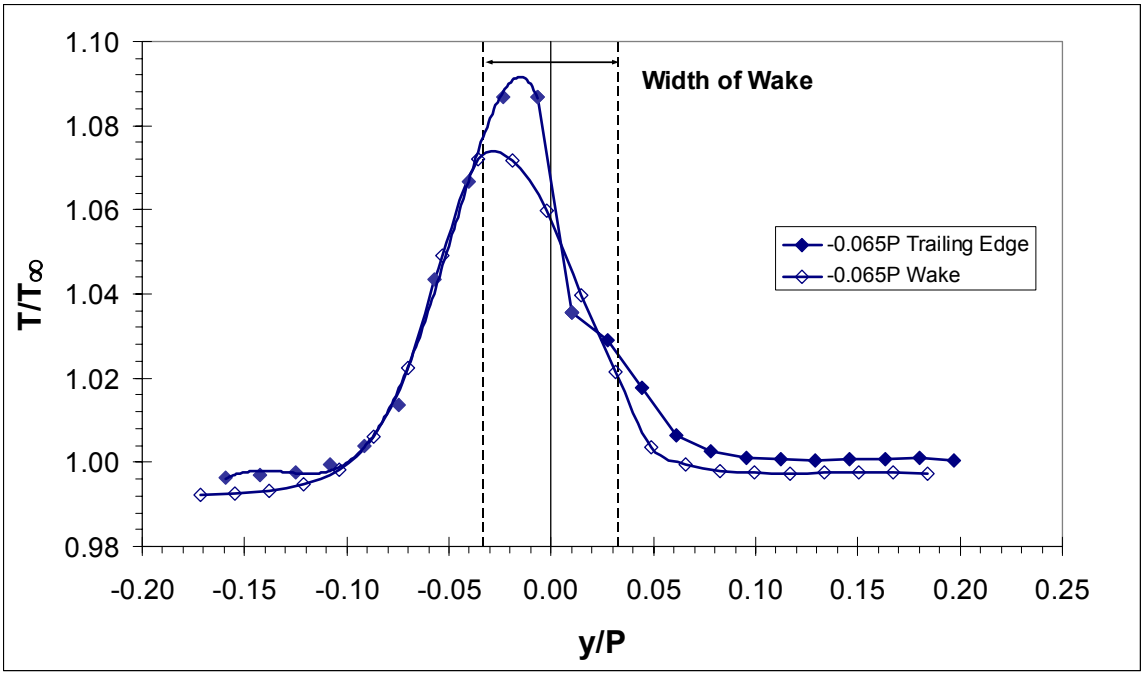

Figure 3.40: Comparison of temperature ratio profiles at Position T (trailing edge) and in the wake at Position B for the hot streak at -0.065*P*, *Tu* = 3.5%.

would be expected given previously discussed results. Here the drop in temperature ratio was about 20% between Position T and Position B although the estimate is a bit less accurate than for high turbulence since the thermocouple rake resolution did not permit a clear identification of the peak.

Figure 3.41 shows the temperature profiles at Position B in the wake for the range of pitch positions between -0.5*P* and +0.5*P*. As was observed under high turbulence, the attenuation in the stator/rotor axial gap smoothed out the temperature profiles for all pitch positions when compared with the profiles at Position T in Figure 3.10.

A comparison of profiles affected only by mainstream turbulence or by the vane wake is shown in Figure 3.42. Here the hot streak positioned at +0.5*P* was completely unaffected by the vane due to its width and decreased from Position T to Position B by approximately 10%. Unlike for the high mainstream turbulence case, there was no pitch position near *y/P* = 0.0 resulting in completely smooth profile at Position T. Since the hot streak was much narrower in the pitchwise direction, all profiles shown at Position T in Figure 3.9 had a sharp gradient due to splitting of the hot streak by the vane. The hot

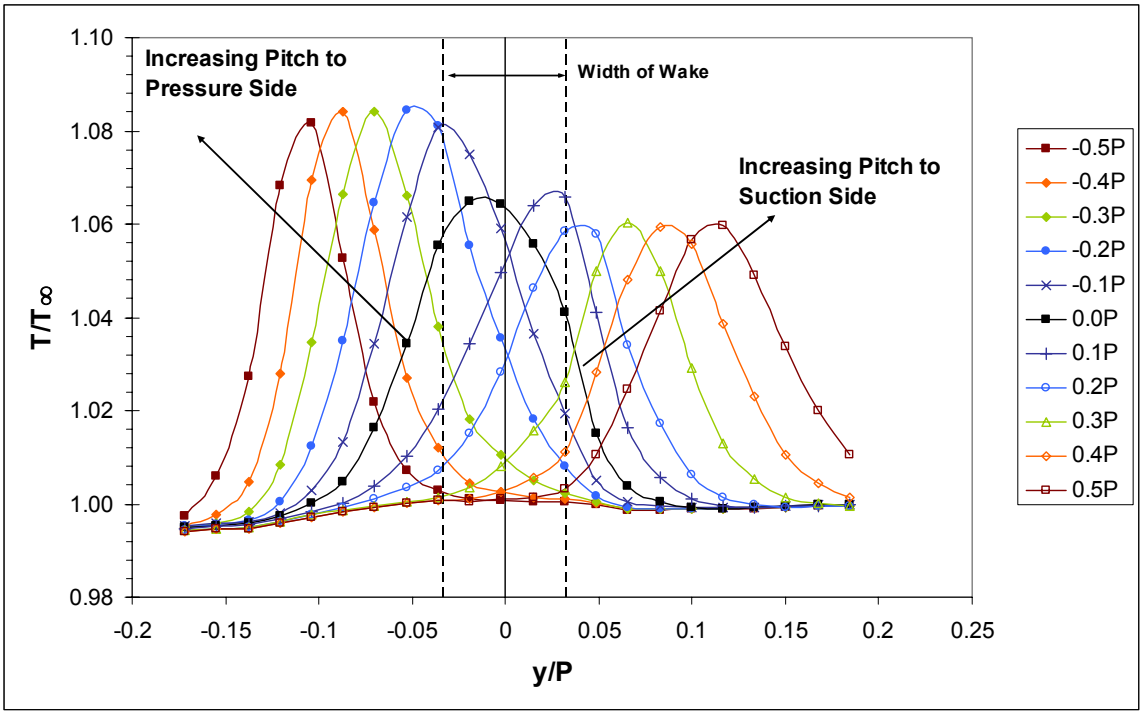

Figure 3.41: Temperature profiles of the hot streak at Position B with hot streak position varying from -0.5*P* to +0.5*P*, *Tu* = 3.5%.

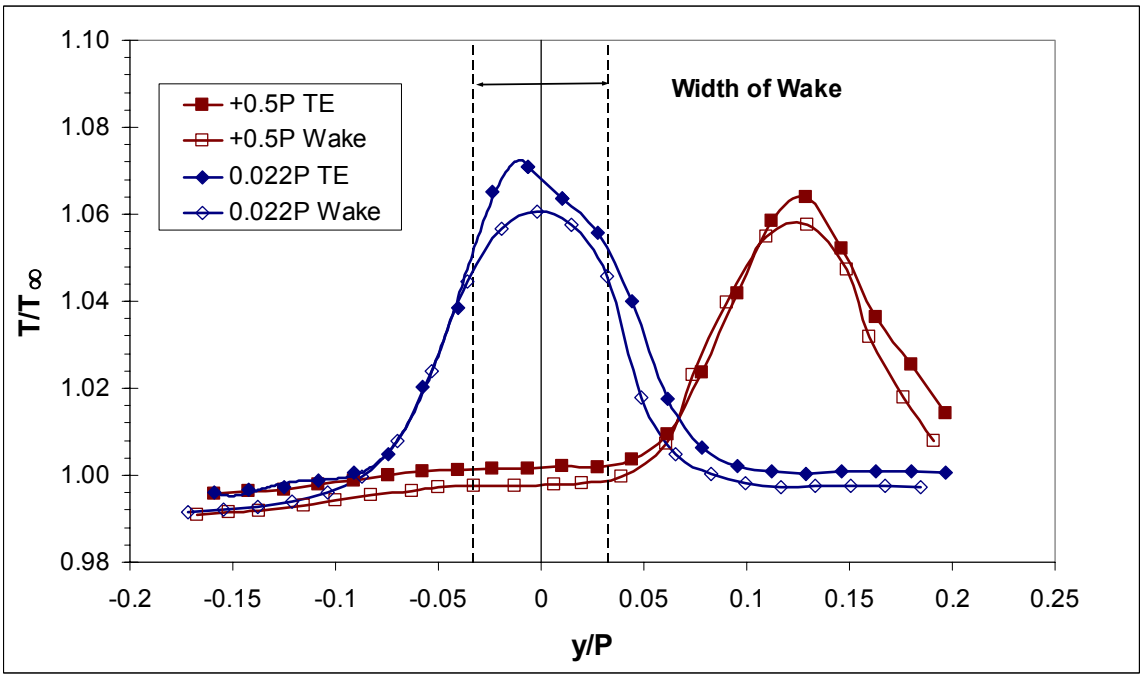

Figure 3.42: Comparison of temperature ratio profiles at the trailing edge and in the wake at Position B for the hot streak at +0.022*P* and +0.5*P*, *Tu* = 3.5%.

streak pitch position of 0.022*P* was chosen for the comparison since that profile had the smallest temperature gradient at the vane trailing edge, slightly less than that for 0.0*P*. The incoming temperature profile, slightly offset to the suction side resulted in the smoothest profile due to the stronger attenuation on the suction side, which was the same effect seen at high turbulence for the same pitch position. As shown in the figure, the reduction of the peak at 0.022*P* was only slightly larger than that for +0.5*P*, estimated at about 15%. It appeared as if the wake was not quite as strong in reducing the hot streak peak relative to mainstream turbulence as it was for the high turbulence case. As the region of effect of the vane wake was smaller at low turbulence, this may have been a factor in the difference in peak reduction. However, since the profile at the trailing edge was not smooth as it was for the high turbulence condition, the independent effect of the vane wake could not be as easily evaluated.

The effect of downstream distance is clear from the contour plots in Figure 3.43 for the hot streak positioned at +0.5*P*. The hot streak size and shape did not vary, but the peak value was reduced from $\Theta_R = 0.62$ to $\Theta_R = 0.53$. Since the hot streak was not wide enough to interact with the vane or wake, the hot streak was attenuated only by mainstream turbulence levels as shown before in the profile comparison of Figure 3.42.

In Figure 3.44 the effect of the vane creating a sharp temperature gradient appears as a warping of contour lines near $y = 0.0P$, but overall the shape and size of the hot streak did not vary from Position T to Position B in the wake. In contrast to the mid-passage hot streak, the peak value at Position T of $\Theta_R = 0.71$ dropped only to $\Theta_R = 0.65$. This may appear to be contrary to the results in the line plots of Figure 3.42, but in the current figure, the pitch position of 0.0*P* is shown as opposed to the +0.022*P* pitch position in the previous figure.

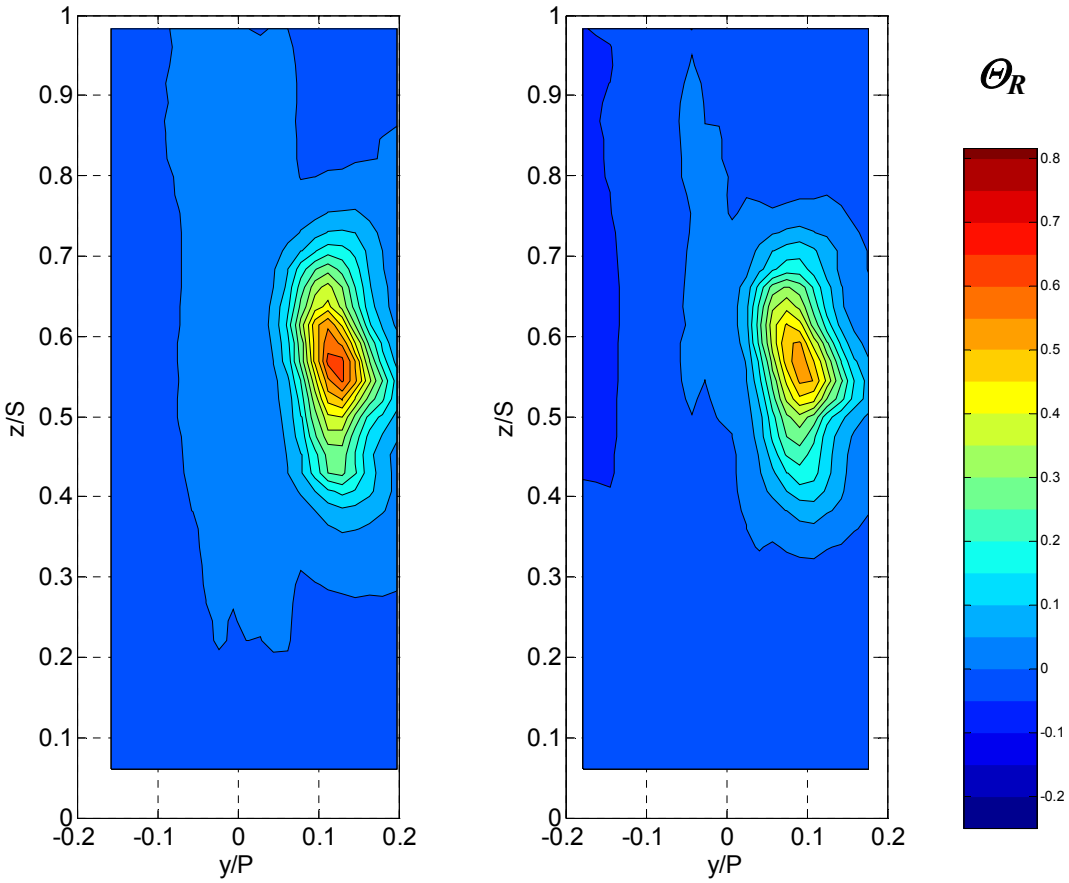

a. **b.**

Figure **3.43: Normalized temperature ratio (Θ_R) plot with hot streak passing through the mid-passage (+0.5*P*), low turbulence (3.5%), measured at:**

a. Position T

b. Position B (0.32*C* downstream)

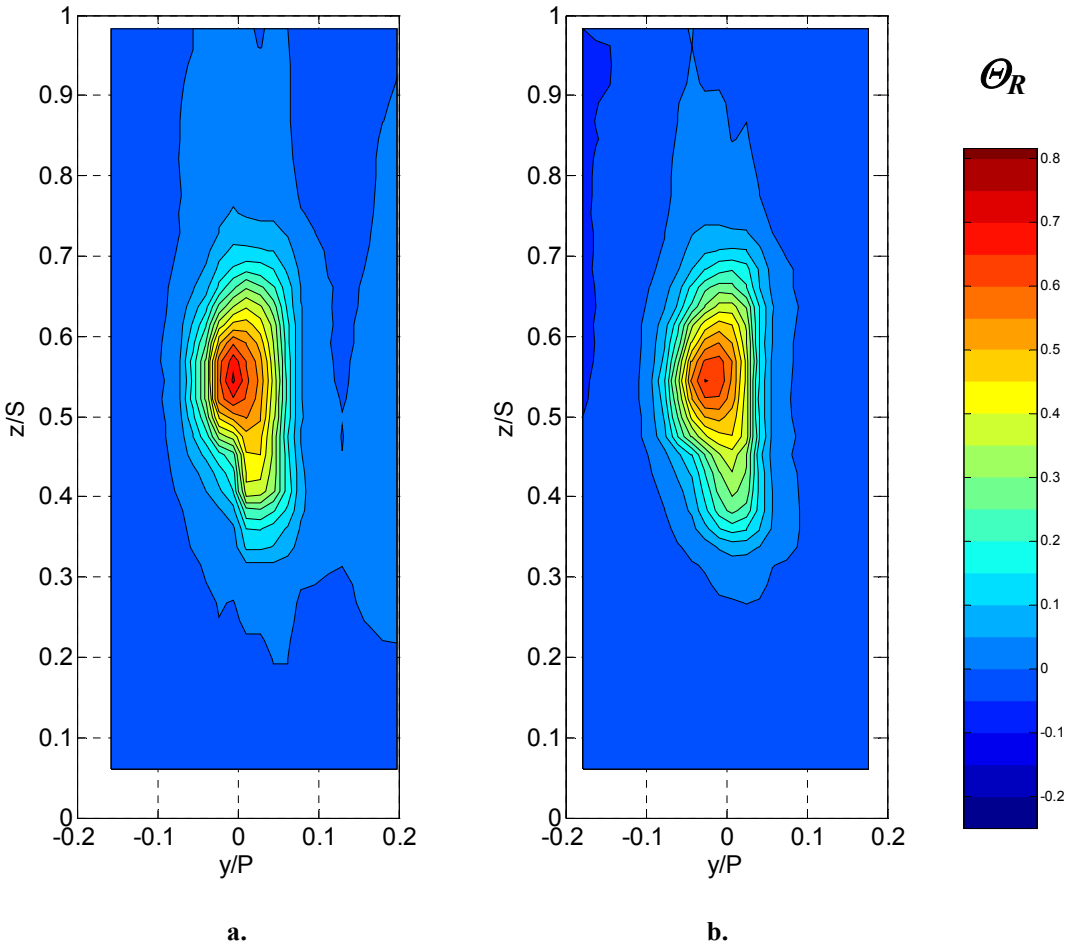

a. **b.**

Figure **3.44: Normalized temperature ratio (Θ_R) plot with hot streak impacting the stagnation line (0.0*P*), low turbulence (3.5%), measured at:**

a. Position T

b. Position B (0.32*C* downstream)

Chapter 4: Effects of Showerhead Film Cooling on Hot Streak Reduction

4.1 Introduction

Additional reduction of the hot streak resulted from mixing of coolant with hot streak fluid. Although the function of coolant is primarily to provide film cooling of the vane surface, a significant reduction in hot streak peak temperature ratio occurred when the coolant interacted with the core of the hot streak. Experiments were performed at high mainstream turbulence to simulate engine operating conditions with film cooling from the showerhead region alone. The showerhead was operated alone to differentiate between effects of the individual coolant regions, which included the showerhead, the suction side, and the pressure side coolant regions from the benefits of hot streak reduction with full coverage film cooling. Covered in separate chapters, each region was operated at a range of blowing ratios to evaluate their region specific effects, as well as in combination, simulating a fully film-cooled turbine vane under actual engine conditions. The nominal blowing ratios for the showerhead were $M^* = 1.4$, 1.6, and 2.0. For full field measurements in the y-z plane, the blowing ratio was held within $M^* = \pm 0.05$ throughout the traverse. The density ratio for the these experiments was set to $DR = 1.6$, also representative of ground-based engine conditions, while a separate study investigated the effect of density ratio to be presented in Chapter 9.

To further investigate how the showerhead coolant mixed with mainstream fluid, measurements were taken at Positions S1', S2', P1', and P2' at midspan for each coolant region. The evolution of the temperature profile due to film cooling was evaluated by comparing those temperature profiles beside the vane with ones at the trailing edge (Position T) and those in the wake at Position B. To determine how turbulence effects in the stator-rotor axial gap affected the coolant distribution, data from the trailing edge and Position B were compared for individual regions and full coverage film-cooling.

4.2 Showerhead Coolant Profiles at the Trailing Edge

Experiments involving showerhead film cooling alone were performed at several blowing ratios, at the optimum blowing ratio for adiabatic effectiveness as determined by Cutbirth, et al [27] and blowing ratios above and below this level. As described in

Section 2.1, the showerhead consisted of 102 film cooling holes in six rows, where three rows were on the suction side of the stagnation line, and two rows on the pressure side, while the stagnation line split the remaining row as shown in Figure 4.1. The overlap region, where the injection angle of 25% was angled upwards as shown in the figure, resulted in a greater concentration of coolant in this area. This showerhead configuration was partially chosen due to manufacturing constraints, where holes on the lower portion of the span could not be made from below due to interference with the endwall. The design of the overlap region, however, did not anticipate any specific benefit due to hot streak reduction. In Figure 4.2, contours of the normalized temperature ratio show the accumulation of coolant at a spanwise position of about z/S = 0.3. These data were measured at Position T (at the trailing edge) for conditions of high mainstream turbulence with a showerhead blowing ratio of M^* = 1.6 and a density ratio of DR = 1.6.

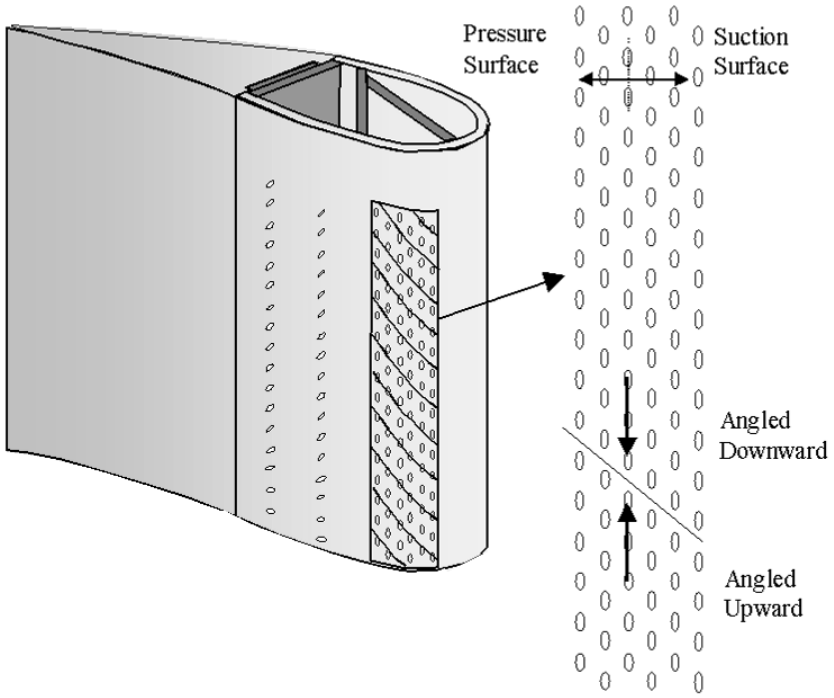

Figure 4.1: Showerhead and pressure side cooling holes.

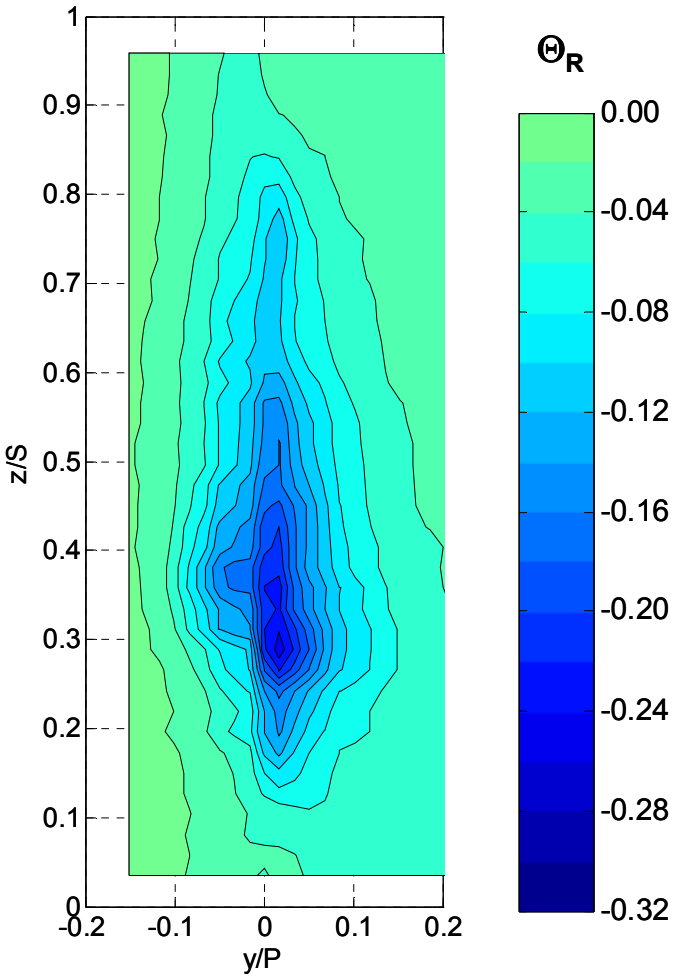

Figure 4.2: Normalized temperature ratio (Θ_R) contours at Position T for showerhead blowing at M^* = 1.6, high mainstream turbulence (Tu = 20%).

Measurements were taken in increments of 12.7 mm (0.023S) in the spanwise direction and thermocouple spacing on the rake was 7.8 mm (0.017P) in the pitchwise direction for data presented in the y-z plane. Since the lowest temperature ratio due to coolant accumulation from the overlap region was well below the midspan, a majority of coolant was not expected to interact with the hot streak fluid. Note that a Θ_R scale containing only negative values was used in this figure for coolant measurements. A comparison of coolant temperatures at midspan (z/S = 0.5) vs. those at z/S = 0.29 in Figure 4.3 shows how much lower the coolant temperatures were due to the overlap region. At midspan, where the temperature ratio of the hot streak was the highest, Θ_R = -0.16 while at z/S =

0.29, Θ_R = -0.25, more than 50% lower, representing a larger capacity for reducing hot streak strength in this region. Since the design of the overlap region was primarily for manufacturing reasons, it was not positioned to interact with a hot streak.

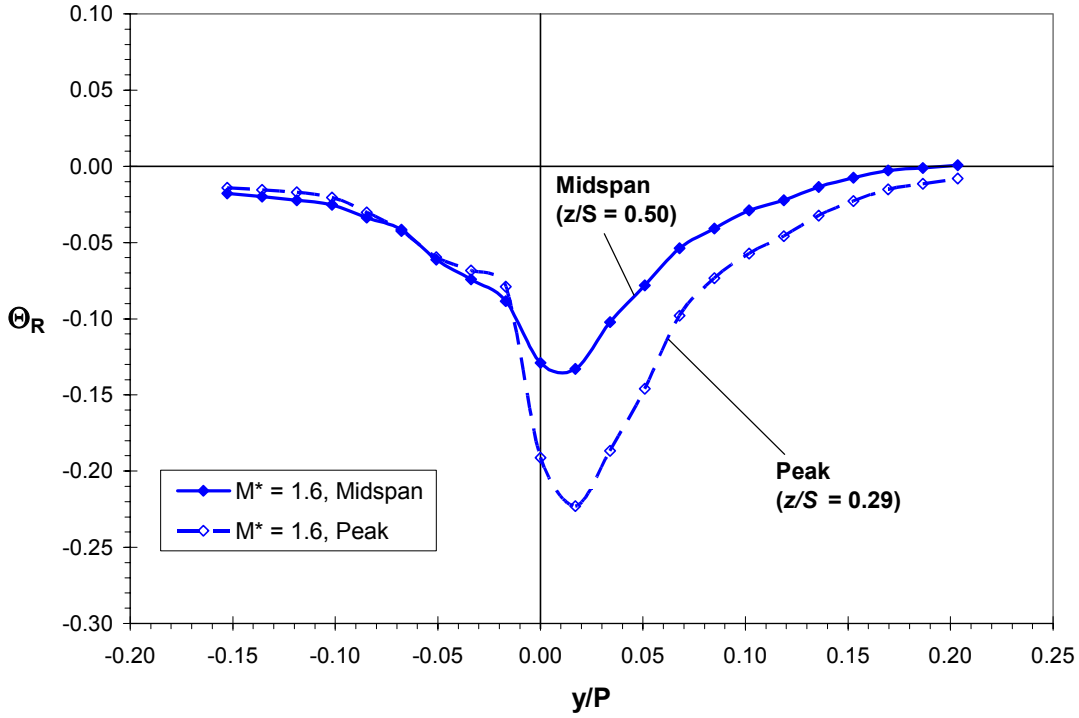

Figure 4.3: Normalized temperature ratio (Θ_R) profiles at Position T for showerhead blowing at M^* = 1.6, high mainstream turbulence (Tu = 20%).

4.3 Effects of Showerhead Film Cooling on Hot Streak Reduction

Subsequently, the hot streak was activated along with showerhead coolant and measurements made at Position T. These results are shown as contours in Figure 4.4, where the hot streak was reduced significantly, especially in the lower region where additional coolant collected due to the overlap region. In the figure, a comparison with the uncooled hot streak showed that the central portion around z/S = 0.5 was reduced significantly while the lower portion, around z/S = 0.30, was reduced to mainstream temperatures and as low as Θ_R = -0.12 at about z/S = 0.2. The peak temperature ratio dropped from Θ_R = 0.51 to Θ_R = 0.33 and was at a slightly higher position with showerhead film cooling since somewhat more coolant was found in the lower portion of the measurement plane. Overall, given that showerhead coolant was distributed on both

sides of the vane and spread well away from the vane surface by the trailing edge, the hot streak was reduced in a fairly uniform manner across the pitch, reducing the hot streak temperature ratios by one or two contour levels. At midspan, showerhead blowing reduced the hot streak peak about 45%, as shown in Figure 4.5, and had a broad effect, reducing the hot streak across nearly the full width.

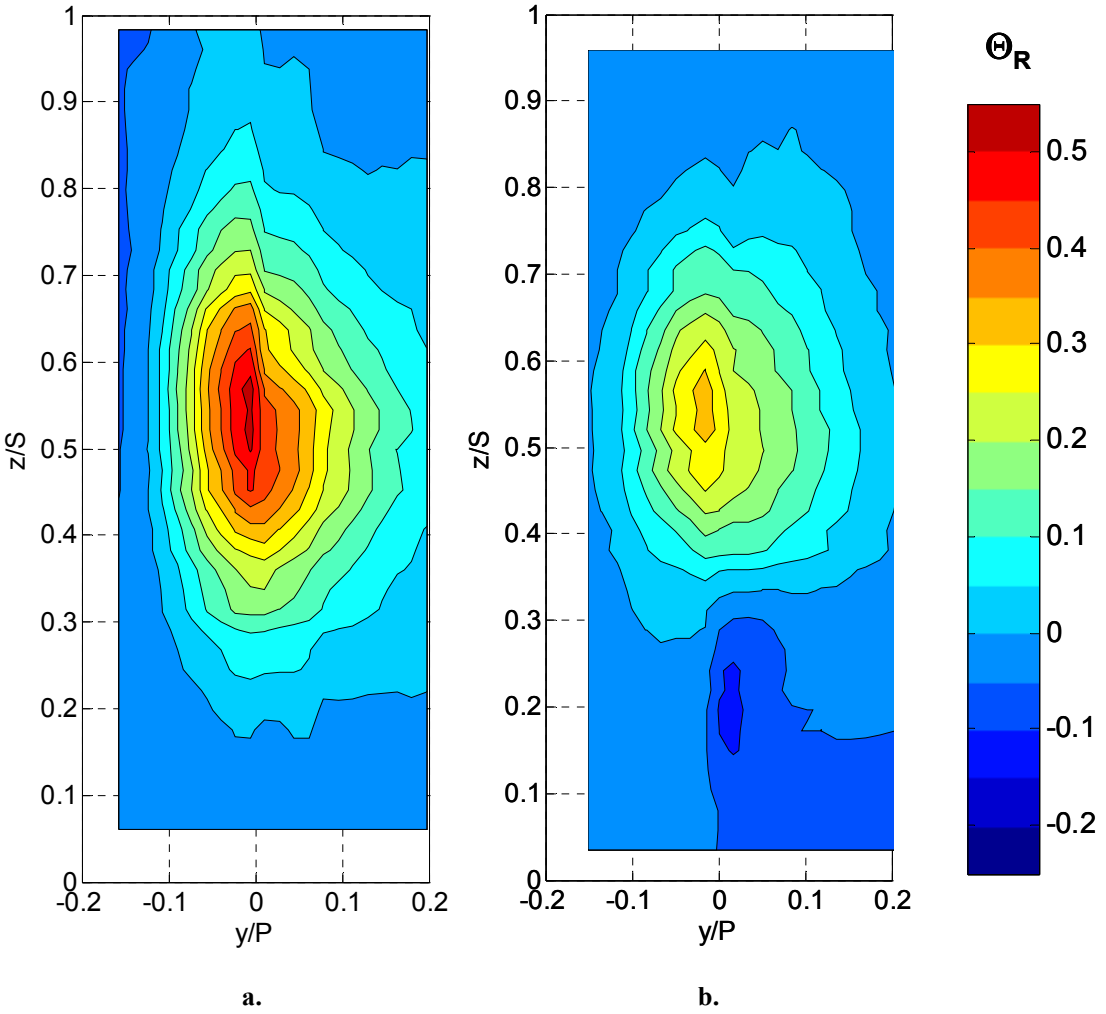

Figure 4.4: Normalized temperature ratio (Θ_R) contours at PositionT, hot streak at stagnation line, high mainstream turbulence (Tu = 20%):

a. No coolant

b. Showerhead on at M^* = 1.6, DR = 1.6.

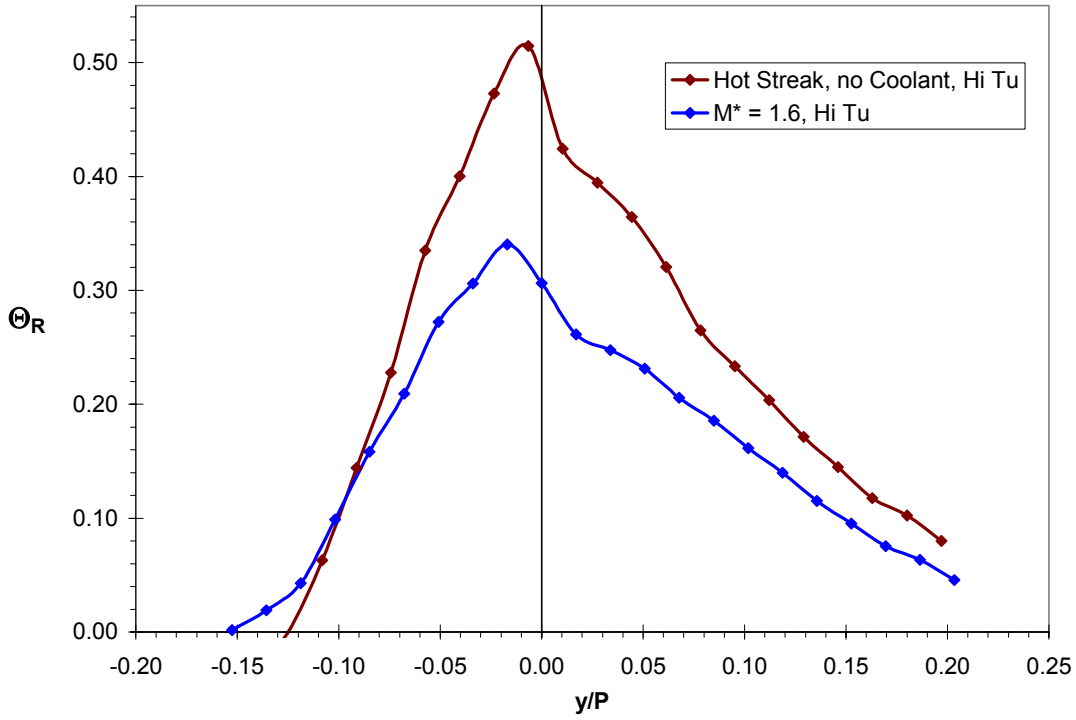

Figure 4.5: Normalized temperature ratio (Θ_R) profiles at Position T for the hot streak impacting the stagnation line without coolant and with showerhead blowing at M^* = 1.6, high mainstream turbulence (Tu = 20%).

4.4 Effect of Varying Showerhead Blowing Ratio

The effect of varying blowing ratio was investigated by measuring temperature profiles at Position T for showerhead blowing ratios of M^* = 1.4, 1.6, and 2.0 representing the range of blowing ratios that still provided reasonable adiabatic effectiveness. As mentioned previously, a blowing ratio of M^* = 1.6 was the optimum blowing ratio for adiabatic effectiveness, while M^* = 1.4 was below optimum. A blowing ratio of M^* = 2.0 actually provided slightly greater adiabatic effectiveness, but required a great deal more coolant to achieve this (Cutbirth [27]). Therefore, in the balance of providing cooling to the stagnation region versus the loss in engine efficiency due to compressor bleed, this higher blowing ratio was unwarranted. In general, for the showerhead, higher blowing ratios continue to provide greater adiabatic effectiveness up to the highest value tested by Cutbirth [27] at M^* = 2.8, however a distinctive increase in effectiveness was observed just below M^* = 1.6. Increasing the blowing ratio from M^* =

1.4 to 1.6 resulted in almost a 15% improvement in adiabatic effectiveness for roughly the same percent increase in blowing ratio. However, increasing the blowing ratio from M^* = 1.6 to 2.0 resulted in just below an 8% increase in effectiveness with an increase of 25% in blowing ratio, representing much more coolant usage for the improvement in effectiveness. A blowing ratio of M^* = 2.0 represented the limit of diminishing returns with higher blowing ratios by simply using greater amounts of compressor bleed with the associated lower efficiency for smaller returns in adiabatic effectiveness. A blowing ratio of M^* = 1.4 was chosen to represent the lower range of reasonable adiabatic effectiveness since below this value the adiabatic effectiveness dropped off steadily.

Contour plots showing the coolant distribution for blowing ratios of M^* = 1.4, 1.6, and 2.0 are shown in Figure 4.6. While the pattern of the coolant distribution was similar among the three blowing ratios, the greater decrease in fluid temperature at Position T was evident with higher blowing ratio. The area of greatest influence

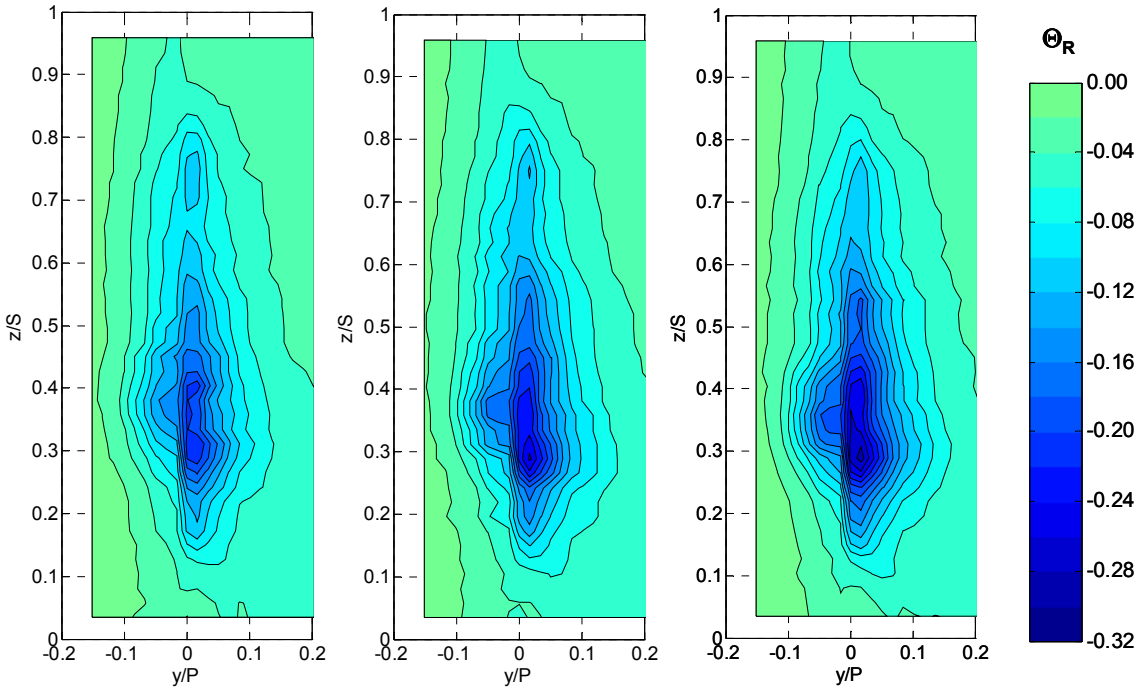

Figure **4.6: Normalized temperature ratio (Θ_R) contours at Position T, high mainstream turbulence (Tu = 20%) for showerhead blowing at:**

a. M^* = 1.4
b. M^* = 1.6
c. M^* = 2.0

remained at y/P = 0.0 and about z/S = 0.3 independent of the blowing ratio, and the size of the region with normalized temperature ratios below Θ_R = -0.05 also grew with increasing blowing ratio.

Since the peak of the hot streak occurred at midspan, the most relevant coolant temperatures were at this location as well. In Figure 4.7, line profiles for the coolant at midspan for blowing ratios of M^* = 1.4, 1.6, and 2.0 show how the coolant spread away from the vane surface at y/P = 0.0 and extended well into the passage. Significant amounts of coolant were measured as far as -0.08 < y/P < +0.10 with the higher levels of coolant to the suction side due to the greater number of coolant rows toward that side. Also on this figure are line profiles for the spanwise position of the peak coolant levels, which all occurred at about y/P = 0.30. The peak value at 0.30S varied from Θ_R = -0.22 to Θ_R = -0.31 for M^* = 1.4 to 2.0, all a little more than 50% lower than the value at midspan. On the pressure side, only the highest blowing ratio resulted in more coolant

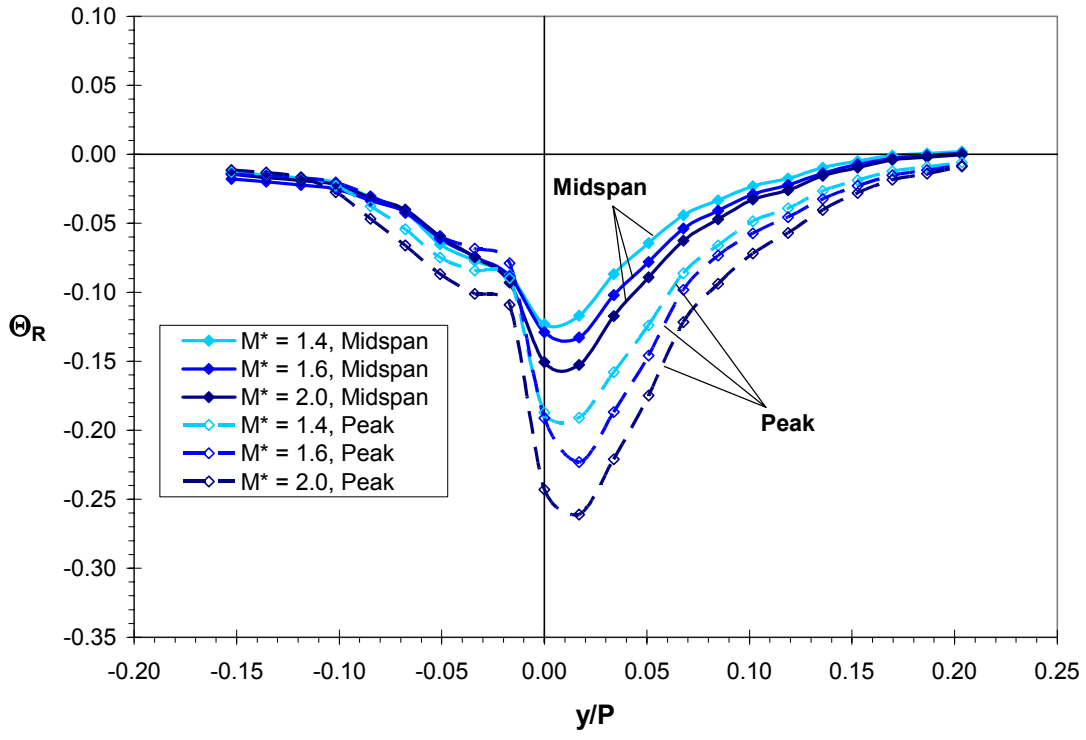

Figure 4.7: Normalized temperature ratio (Θ_R) profiles at Position T at midspan (z/S = 0.50) and the position of peak coolant (z/S = 0.29) for showerhead blowing at M^* = 1.4, 1.6, and 2.0, high mainstream turbulence (Tu = 20%).

away from the vane surface for the peak profile, since at 0.3*S* the overlap region primarily directed additional fluid to the suction side. Because of this, on the suction side the peak profiles had lower values for all blowing ratios than at midspan.

The effect of varying blowing ratios on the hot streak peak values at midspan were as expected based on coolant profiles in Figure 4.7. In Figure 4.8, profiles with the hot streak activated show a substantial decrease of about 40% for all showerhead blowing ratios where higher blowing ratios had a larger effect. For a blowing ratio of $M^* = 1.9$, the peak value at midspan has a temperature ratio of $\Theta_R = 0.29$, down from $\Theta_R = 0.51$ with no film cooling. Recall that the peak temperature ratio was found to be slightly higher than midspan for showerhead film cooling at $M^* = 1.6$ as shown in Figure 4.4 previously. The blowing ratios for this set of experiments were $M^* = 1.47$, 1.55, and 1.92, so it is not surprising that the two lower blowing ratios had nearly the same effect on the hot streak as they differed by only a small amount.

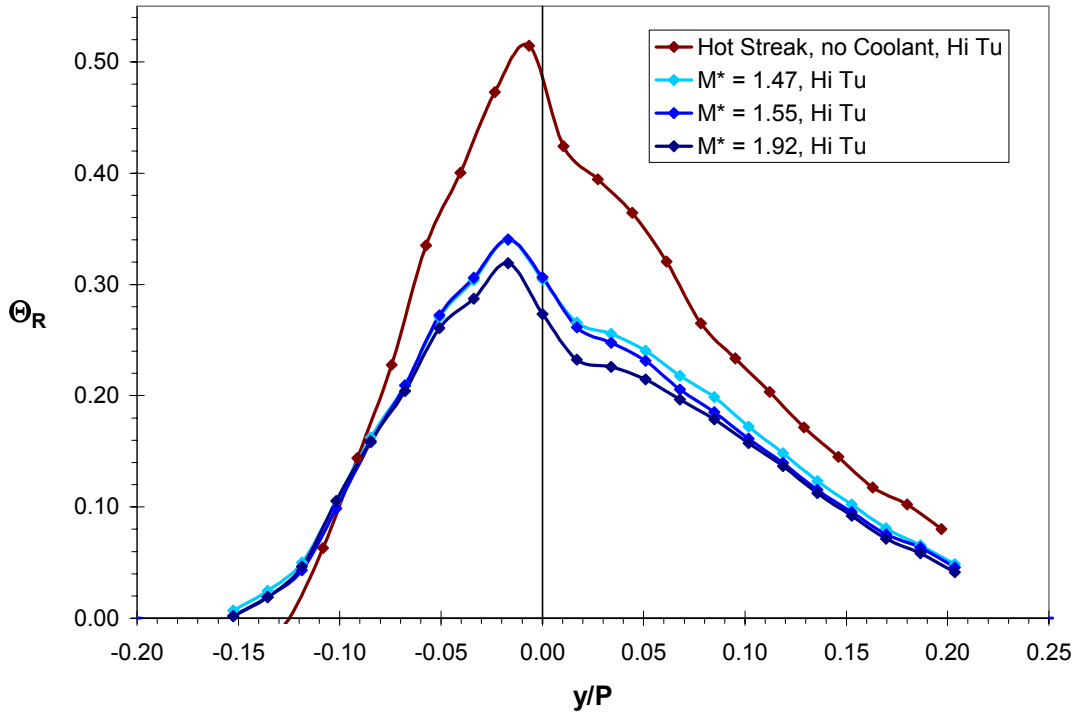

Figure 4.8: Normalized temperature ratio (Θ_R) profiles at Position T for the hot streak impacting the stagnation line without coolant and with showerhead blowing at $M^* = 1.4$, 1.6, and 2.0, high mainstream turbulence ($Tu = 20\%$).

4.5 Evolution of the Showerhead Coolant Profile

To further investigate how the coolant profile at Position T evolved from the showerhead coolant holes, measurements were taken at Positions S1', S2', P1', P2', and T' for the optimum adiabatic effectiveness blowing ratio of $M^* = 1.6$ under conditions of high mainstream turbulence. The measurements were made with the single thermocouple probe as described in §2.2.7 (shown schematically in Figure 2.15) and previously used for fine scale hot streak measurements in §3.6. Position T' was about $0.08C$ downstream of the trailing edge due to the length of the single thermocouple probe.

The coolant profile shown in Figure 4.3 at midspan at Position T was a result of showerhead coolant mixing with the mainstream and advecting downstream around the vane. High mainstream turbulence levels spread the coolant well away from the vane surface, and as shown in Figure 4.9, this process occurred gradually over a relatively large distance. On the pressure side, coolant temperatures were very low near the wall, and the temperature gradient was relatively steep until about $y = 1.5d$ from the wall,

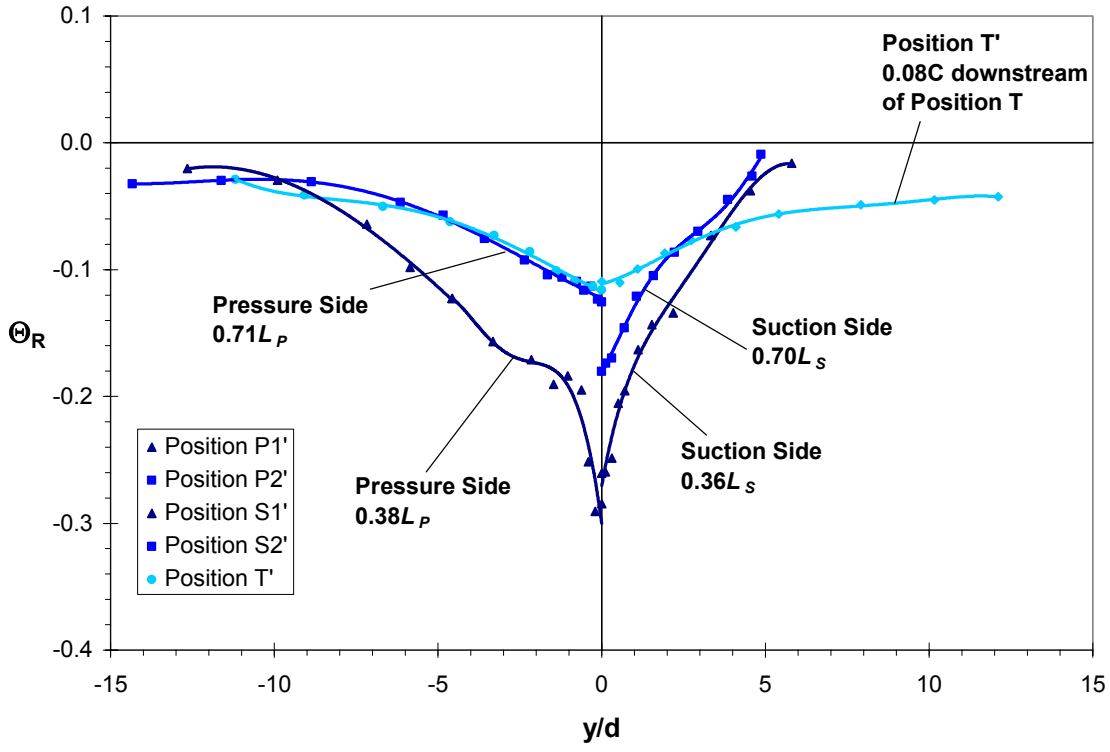

Figure 4.9: Profiles of showerhead coolant at Positions S1', S2', P1', P2', and T' at midspan (z = 0.5S), high mainstream turbulence (Tu = 20%), showerhead blowing at $M^* = 1.6$.

where d is the coolant hole diameter. Mixing with the mainstream occurred relatively rapidly between the stagnation line and Position P1' at $0.38L_P$, with appreciable amounts of coolant as far as $y = 6d$ from the wall. Further downstream on the pressure side, the coolant was much more greatly dispersed. Coolant temperatures varied from $\Theta_R = -0.12$ at the wall to $\Theta_R = -0.04$ at about $y = 6d$ from the wall. Further away from the wall the coolant profile was flat. On the suction side, due partially to a greater compression of streamlines, the coolant temperature profile had a steep gradient from the wall at $\Theta_R = -0.25$ to almost $6d$ from the wall with $\Theta_R = 0.0$. Further downstream, the coolant profile had approximately the same gradient, but the coolant temperature was only $\Theta_R = -0.17$ at the wall. It appeared as if the coolant continued to advect spanwise due to the downward velocity component (negative z-direction) imparted by the showerhead coolant hole orientation. Slightly downstream of the trailing edge, at Position T', the coolant profile was continuous across $y/d = 0.0$ and had reached the same general shape shown previously in Figures 4.3 and 4.7. At Position T', the peak coolant temperature was $\Theta_R = -0.10$ at $y/d = 0.0$ and slowly decreased to about $\Theta_R = -0.02$ on the pressure side at $y/d = -10$ and to about $\Theta_R = -0.03$ on the suction side at $y/d = 12$. This profile was slightly different from that seen at the trailing edge (Position T) in Figure 4.3 since it was taken slightly farther downstream. On the suction side, the coolant profile was steep until near the trailing edge, while the pressure side profile was nearly the same at $0.71L_P$ (Position P2') and at Position T'. The spreading of the coolant away from the vane surface helped to explain why the showerhead coolant had an overall diminishing effect on the hot streak. The coolant mixed in a uniform fashion with the hot streak fluid, resulting in a lower peak and lower values over a wide area (see Figure 4.4 for reference).

4.6 Turbulence Effects in the Stator/Rotor Axial Gap with Showerhead Film Cooling

At Position T, the coolant profiles at midspan for showerhead film cooling seen in Figures 4.3 and 4.7 showed a strong decrease in the magnitude of the coolant profile to the pressure side, i.e. $y/P < 0.0$, which lessened away from the vane surface. At high mainstream turbulence, turbulence and vane effects in the stator/rotor axial gap served to redistribute the coolant across a greater pitchwise width. As shown in the midspan

profiles in Figure 4.10, coolant was moved toward the pressure side, while the peak coolant strength lessened somewhat. This effect can be clarified in the *y-z* contours of Figure 4.11, where the large amount of additional coolant far above midspan and far to the pressure side was evidence of the action of the passage vortex. This three dimensional flow feature is well known in the literature, and was shown by Reinmoller et al [28] to move coolant injected at 80% span (20% h/H for their configuration) and impinging on the vane leading edge from near the vane surface to the pressure side across the passage. This flow phenomenon is shown schematically in Figure 4.12 from Sauer et al [29]. In addition to the movement of coolant by the passage vortex, coolant spread nearly the full pitch between adjacent vanes. Attenuation of the magnitude of the coolant peak was on the order of 25%.

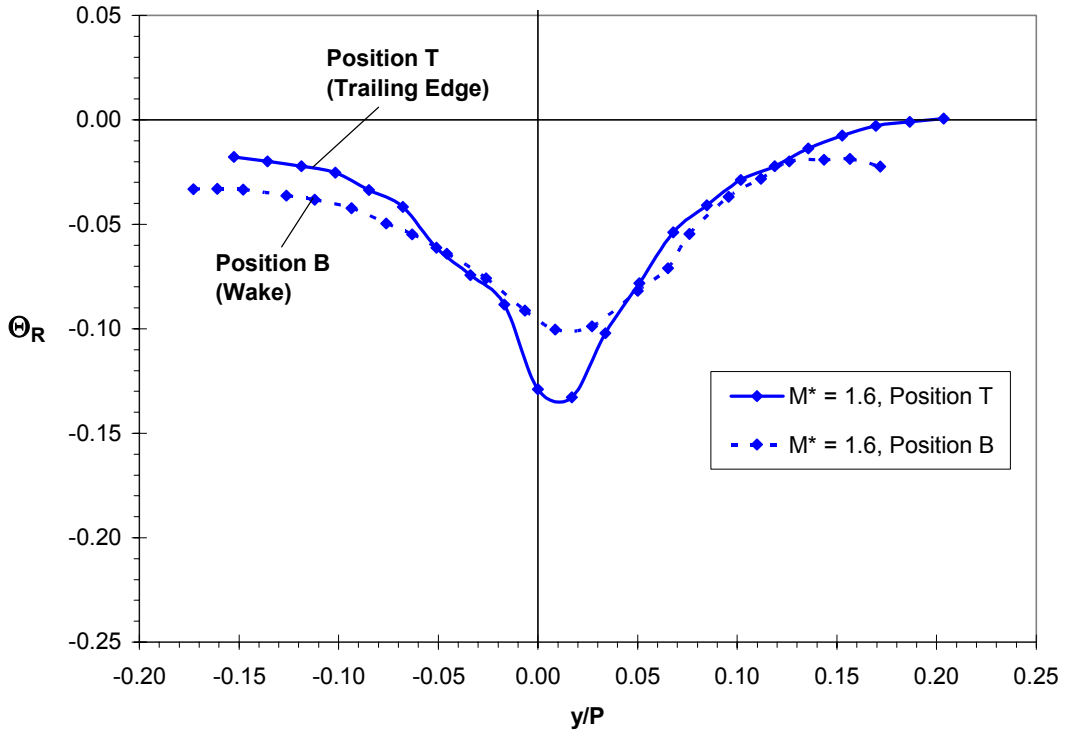

Figure 4.10: Normalized temperature ratio (Θ_R) profiles at Position T and Position B at midspan (z/S = 0.5) for showerhead blowing at M^* = 1.4, 1.6, and 2.0, high mainstream turbulence (Tu = 20%).

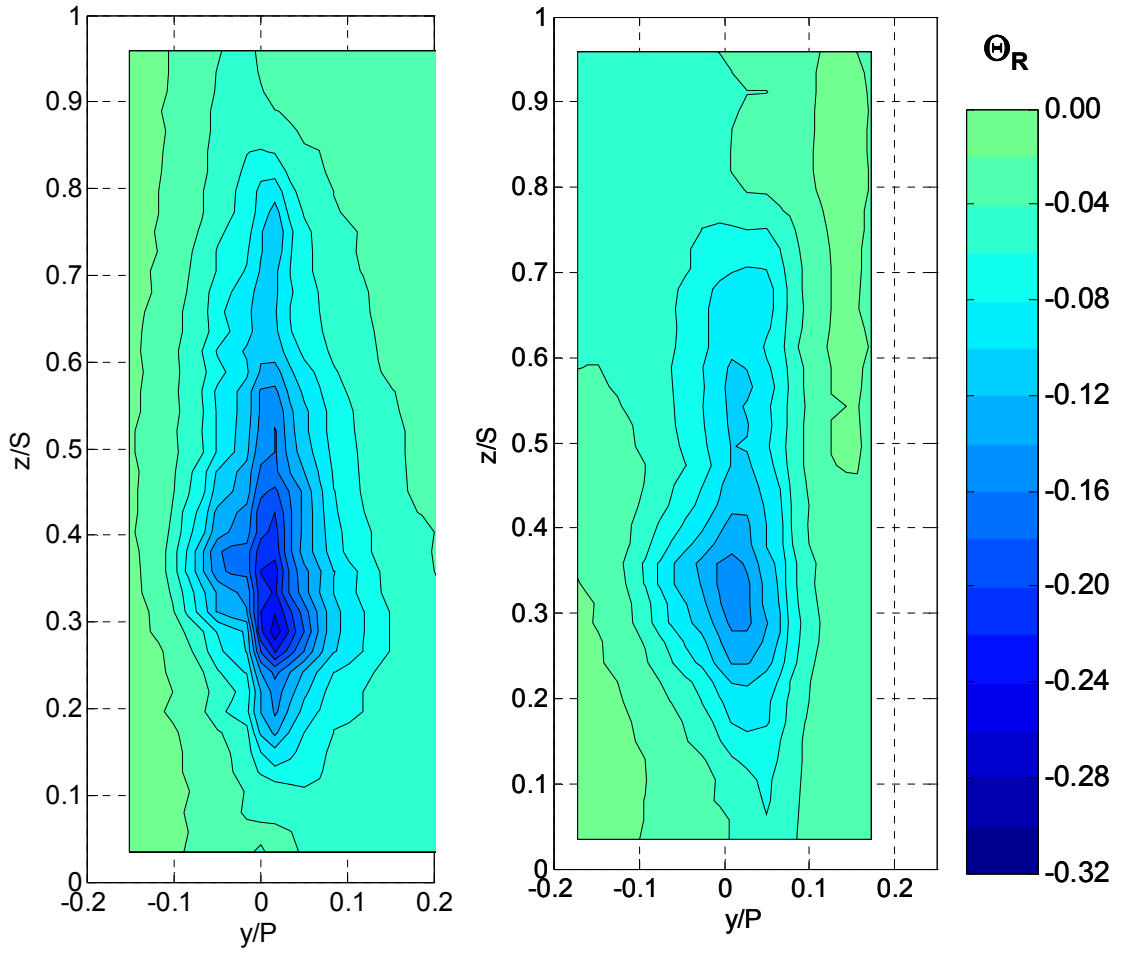

a. **b.**

Figure 4.11: Normalized temperature ratio (Θ_R) contours for showerhead blowing at $M^* = 1.6$, high mainstream turbulence (Tu = 20%) at:

a. Position T

b. Position B

Spreading of coolant (and the hot streak) was also apparent in the midspan profiles with the hot streak activated. In Figure 4.13, profiles at Position B in the wake are shown with dotted lines. The profiles for showerhead blowing at $M^* = 1.6$ indicate little change on the suction side of the vane ($y/P > 0.0$) while the pressure side of the hot streak was substantially reduced in the stator/rotor axial gap. At about $y/P = -0.03$, the hot streak was reduced by an additional 25% between Positions T at the trailing edge and Position B in the wake. Coolant was redistributed across $y/P = 0.0$ and sharp gradients

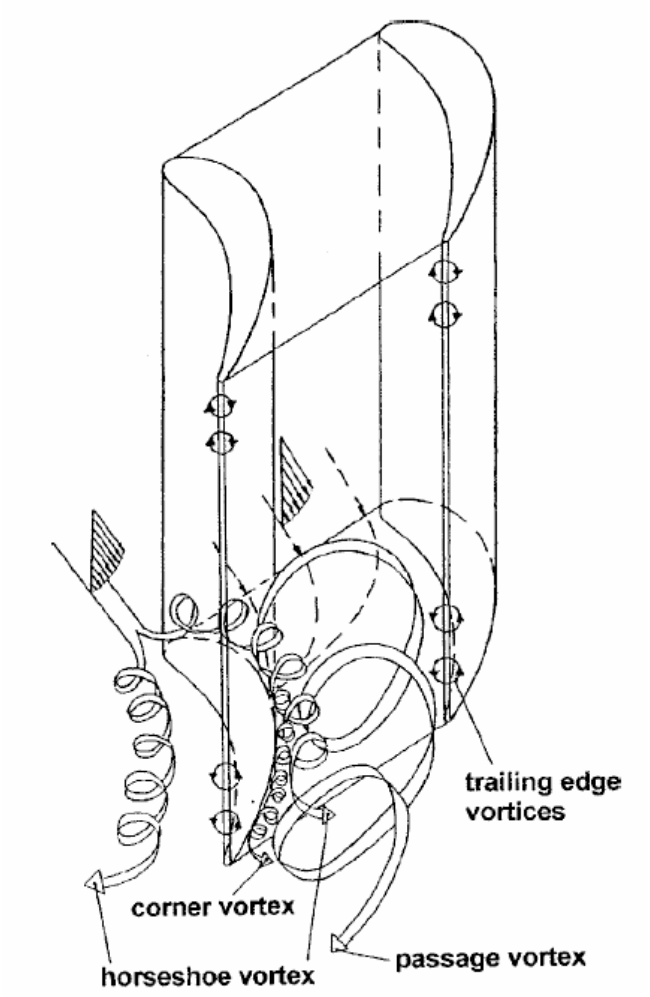

Figure 4.12: Schematic of secondary flows in a turbine cascade (from Sauer [29]).

present at Position T were removed. Turbulence and vane effects in the stator/rotor axial gap were also evident in the difference between the profiles for the hot streak with no film cooling also shown in this figure.

A comparison of contour plots for Position T and Position B is shown in Figure 4.14, both with showerhead blowing at $M^* = 1.6$. The peak, positioned slightly above midspan, as noted previously, was reduced by more than one contour level ($\Delta\Theta_R = 0.05$ for these figures) from $\Theta_R = 0.33$ to $\Theta_R = 0.27$ for a total decrease of 73% from Position A upstream of the vane to Position B in the wake. As noted earlier, Position B lies at approximately the axial position of the rotor inlet plane, so this result is a direct indication of the total effect of high mainstream turbulence and the additional effect of showerhead film cooling at the optimum adiabatic effectiveness blowing ratio.

Compared with no film cooling, with the same position and turbulence conditions, showerhead film cooling provided about a 20% improvement in hot streak peak temperature ratio reduction.

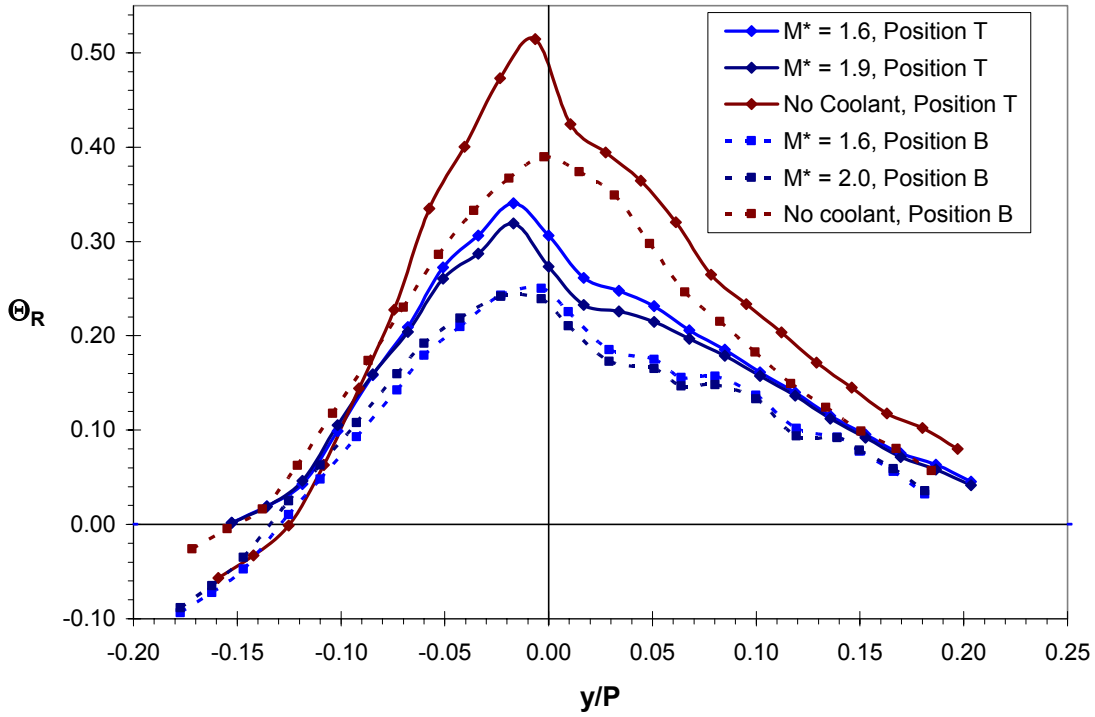

Figure 4.13: Normalized temperature ratio (Θ_R) profiles at Position T and Position B at midspan (z/S = 0.5) with the hot streak activated and with showerhead blowing at M^* = 1.6 and 2.0, high mainstream turbulence (Tu = 20%).

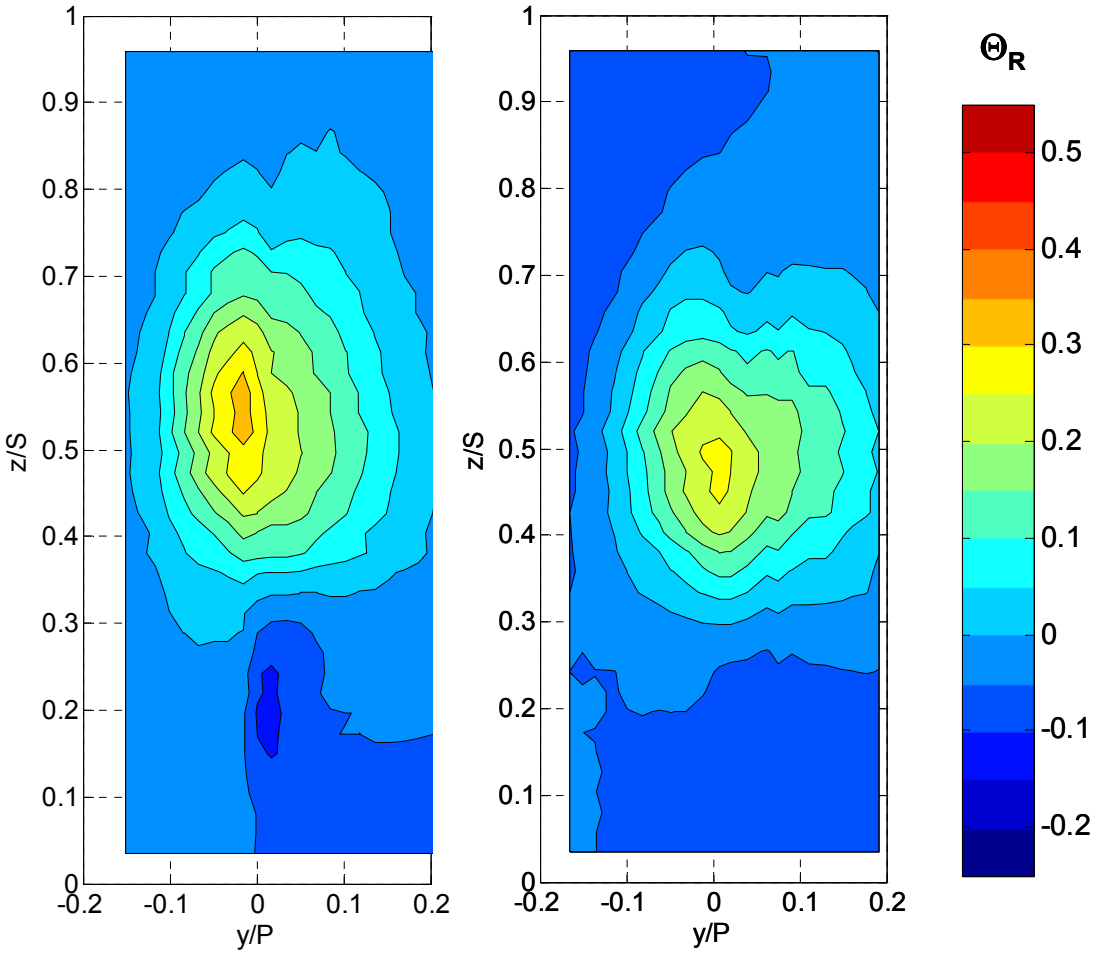

Figure **4.14: Normalized temperature ratio (Θ_R) contours for showerhead blowing at M^* = 1.6, DR = 1.6, high mainstream turbulence (Tu = 20%):**

a. Position T (Trailing Edge)

b. Position B (Wake)

Chapter 5: Effects of Suction Side Film Cooling on Hot Streak Reduction

5.1 Introduction

As for showerhead film cooling, the suction side coolant region was operated alone to investigate the independent effects of that film cooling region on hot streak attenuation. Measurements were made at Position T (at the trailing edge) with and without the hot streak activated to determine how coolant profiles related to hot streak reduction. For suction side film cooling, average blowing ratios were set at M_{avg} = 0.5, 0.7, and 1.0, representing below optimum, optimum, and above optimum blowing ratios with respect to adiabatic effectiveness. These blowing ratios are later referred to as "low," "standard," and "high" blowing ratios to avoid confusion between what was optimum with respect to adiabatic effectiveness versus optimum for hot streak reduction. Each of the three film cooling rows, shown in Figure 5.1 had a slightly different blowing ratio due to differing external velocities at the coolant row exit and a common plenum supplying coolant as described in Chapter 2. Calculations were carried out using an

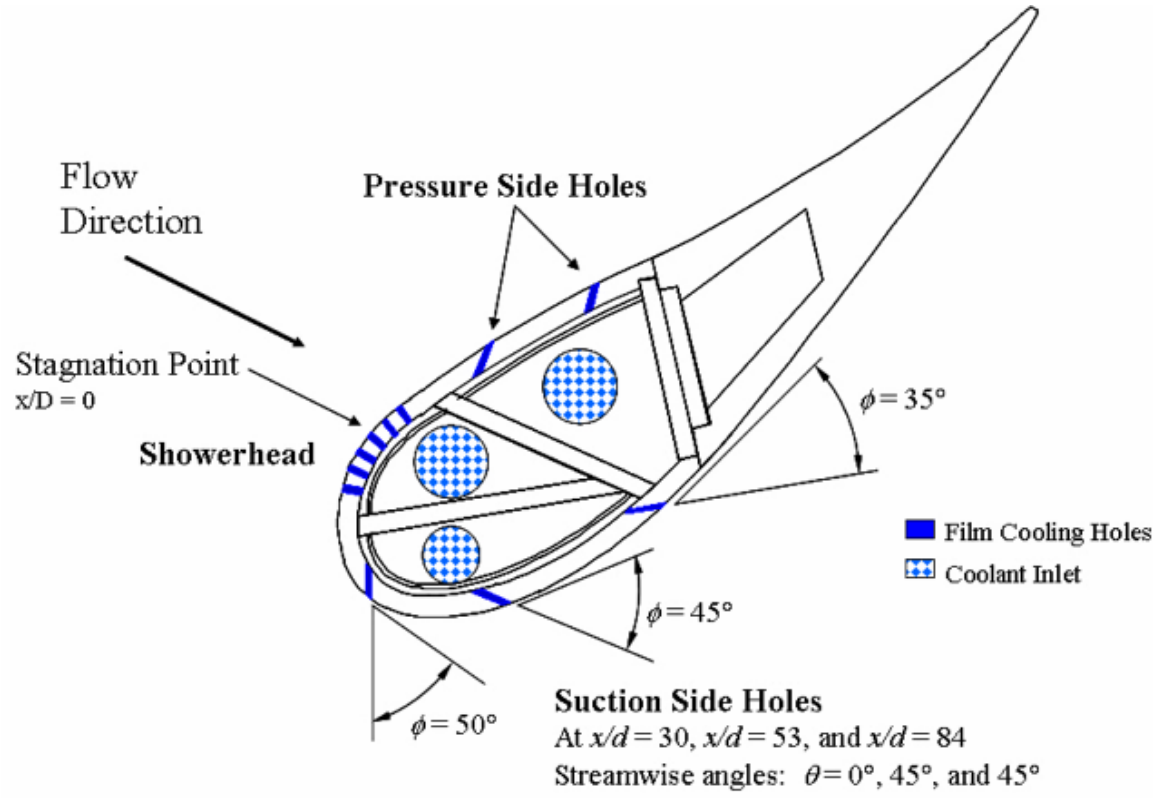

Figure 5.1: Schematic of film cooling hole configuration showing suction side hole parameters.

iterative method to find the local blowing ratio at each row of holes based on the overall average blowing ratios of M_{avg} = 0.5, 0.7, and 1.0 also described in Chapter 2. These blowing ratios are listed in Table 5.1.

	Row 1	Row 2	Row 3
M_{avg} = 0.5	0.32	0.52	0.56
M_{avg} = 0.7	0.64	0.69	0.71
M_{avg} = 1.0	1.05	0.96	0.94

Table 5.1: Local blowing ratios for suction side coolant holes

Measurements were also made along the vane at positions S1' and S2' to determine how the coolant spread away from the vane wall at the standard blowing ratio (M_{avg} = 0.7). As mentioned before, measurements were made at the trailing edge, allowing for a clear understanding of how the suction side film cooling affected the hot streak without the additional effects in the stator/rotor axial gap. Measurements were taken at Position B of the coolant alone, as well as with the hot streak activated to determine how turbulence effects in the stator/rotor axial gap assisted in spreading suction side coolant.

5.2 Suction Side Coolant Profiles at the Trailing Edge

Under conditions of high mainstream turbulence, coolant from the suction side rows of holes resulted in a concentrated pattern of coolant at the trailing edge as shown in Figure 5.2. The coolant was split into three regions due to coolant hole blockage, which was a result of the suction side film cooling hatch developed to study differing vane and hole geometries for adiabatic effectiveness studies. This hatch prevented several holes that were visible on the vane surface from flowing coolant due to the position of the flange used to mount the hatch on the vane. These holes are shown in the diagram filled in black. Other holes were sealed over completely by previous researchers and are not shown on the diagram, but this explains the gaps in the uniformly spaced hole configuration. As mentioned in Chapter 2, the first row of coolant holes had a streamwise angle of $\theta = 0°$, while the second and third rows (labeled SS5 and SS6) had streamwise angles of $\theta = 45°$ downward. Due to the arrangement of coolant holes and

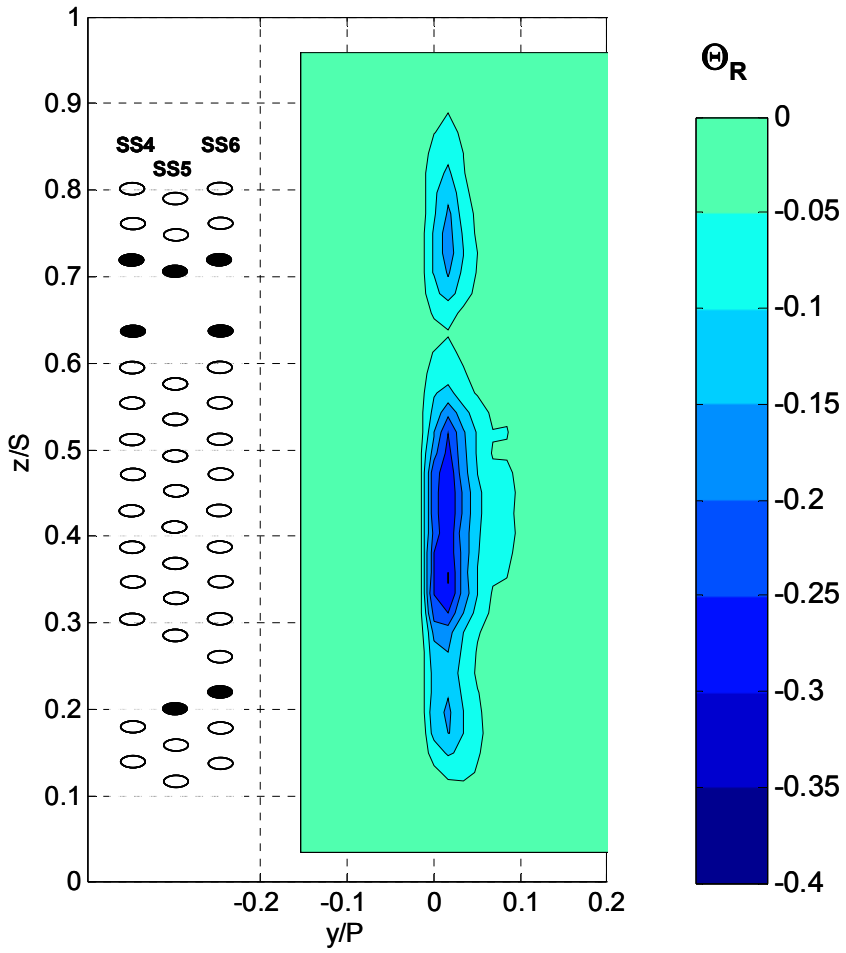

Figure 5.2: Normalized temperature ratio (Θ_R) coolant contours at Position T for suction side blowing at M_{avg} = 0.7, high mainstream turbulence (Tu = 20%).

streamwise injection angles, coolant from the top set of holes was observed between about 0.70 < z/S < 0.85 for an average blowing ratio of M_{avg} = 0.7. As noted in Table 5.1, the local row blowing ratios were M_{local} = 0.64, 0.69, and 0.70 for the 1st, 2nd, and 3rd rows of suction side holes respectively (SS4, SS5, and SS6). The middle spanwise set of holes produced concentrations of coolant between 0.30 < z/S < 0.55, spreading somewhat continuously into the coolant from the lowest group which extended down to about z/S = 0.15. As opposed to the remainder of the holes, the bottom two coolant holes in the 2nd and 3rd rows (SS5 and SS6) were angled incrementally towards the streamwise direction. For all of the coolant holes shown in Figure 5.2, coolant remained fairly close to the vane wall with the edge of the Θ_R = -0.05 contour extending only to about y/P = 0.10 with the lowest Θ_R values very near to the trailing edge and mostly below midspan (between 0.3 <

$z/S < 0.5$). For this reason, the effect on the hot streak was expected to be strongest in the lower half since a majority of the coolant was below midspan. Presumably, if there were no missing or blocked coolant holes, the suction side coolant contours would be fairly uniform across most of the span.

In contrast to showerhead film cooling, the coolant profile at midspan was nearly the same as the profile where the peak overall coolant temperatures were found. As shown in Figure 5.3, for an average blowing ratio of M_{avg} = 0.7, the coolant profile dipped sharply on the suction side of the trailing edge with near wall values of Θ_R = -0.18. Note that although the profile is shown as continuous across the trailing edge, coolant was not found on the pressure side as implied by the curve fit between points on the trailing edge and just to the pressure side. At midspan, the coolant reached a peak at Θ_R = -0.27 near the wall at y/P = 0.015 (about 1.5d where d was the coolant hole diameter), but the lowest portion of the peak region diminished by y/P = 0.07 (about 8d), gradually merging with the mainstream beyond that point. The overall peak occurred at a spanwise position of z/S = 0.36, but the peak here was only slightly lower at Θ_R = -0.30.

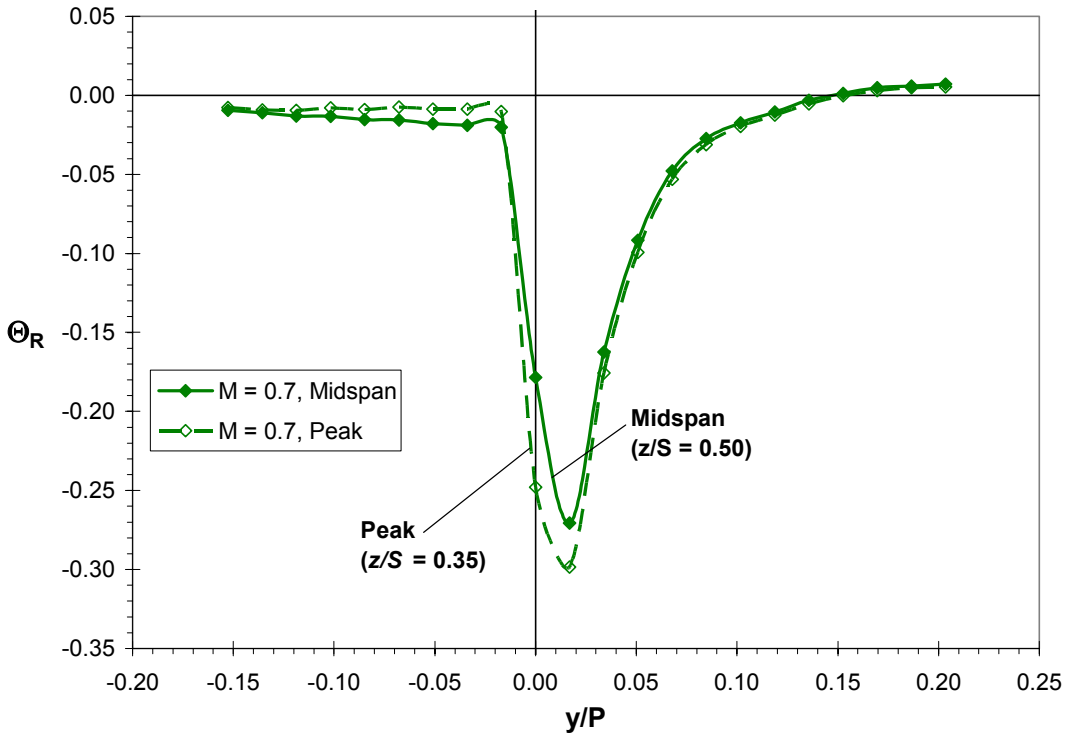

Figure 5.3: Normalized temperature ratio (Θ_R) coolant profiles at Position T for suction side blowing at M_{avg} = 0.7, high mainstream turbulence (Tu = 20%).

5.3 Effect of Suction Side Film Cooling on Hot Streak Reduction

As expected from the coolant profiles, suction side film cooling had a substantial effect on the lower half of the hot streak on the suctions side, but no effect on the pressure side. As shown in Figure 5.4, the portion of the hot streak to the suction side was reduced considerably with a lesser effect above midspan than below. A large blob of extra coolant was seen below the remaining hot streak well below midspan at about z/S = 0.15. Overall, the hot streak was reduced to a maximum value of Θ_R = 0.42 due to the effect of coolant on the suction side, but this value occurred at about midspan just to the pressure side of the trailing edge. On the suction side where coolant interacted with the

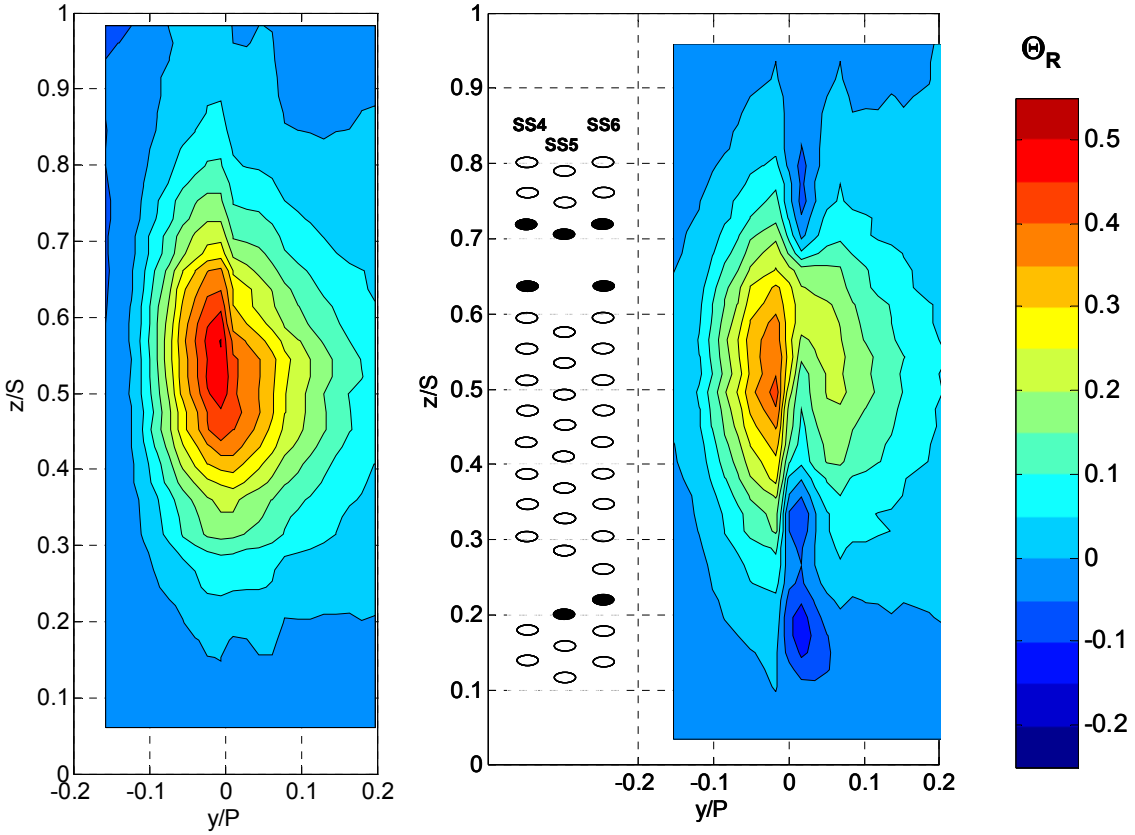

a. b.

Figure 5.4: Normalized temperature ratio (Θ_R) contours at Position T with the hot streak at the stagnation line, high mainstream turbulence (Tu = 20%):

a. No coolant

b. Suction side blowing at M_{avg} = 0.7, DR = 1.6.

hot streak, the peak was much lower at Θ_R = 0.22 at a position just above midspan. Given the pattern of the suction side cooled hot streak, it is clear that suction side cooling had a greater effect on the lower half of the hot streak. It is expected that a coolant array with no blocked or missing holes would reduce the hot streak in a more uniform manner across the span on the suction side. Most likely the lower half of the hot streak represents how this would occur, given the coolant profiles in Figure 5.2. For the lower half of the hot streak on the suction side of the trailing edge in Figure 5.4, the maximum value was Θ_R = 0.19, below that on the suction side overall. The position of this peak was well away from the trailing edge at y/P = 0.07 where the tightly focused coolant profile had diminished significantly.

At midspan, profiles shown in Figure 5.5 demonstrate how drastically the hot streak was reduced on the suction side near the trailing edge, but unaffected on the pressure side. Suction side coolant reduced the hot streak near the trailing edge to a local

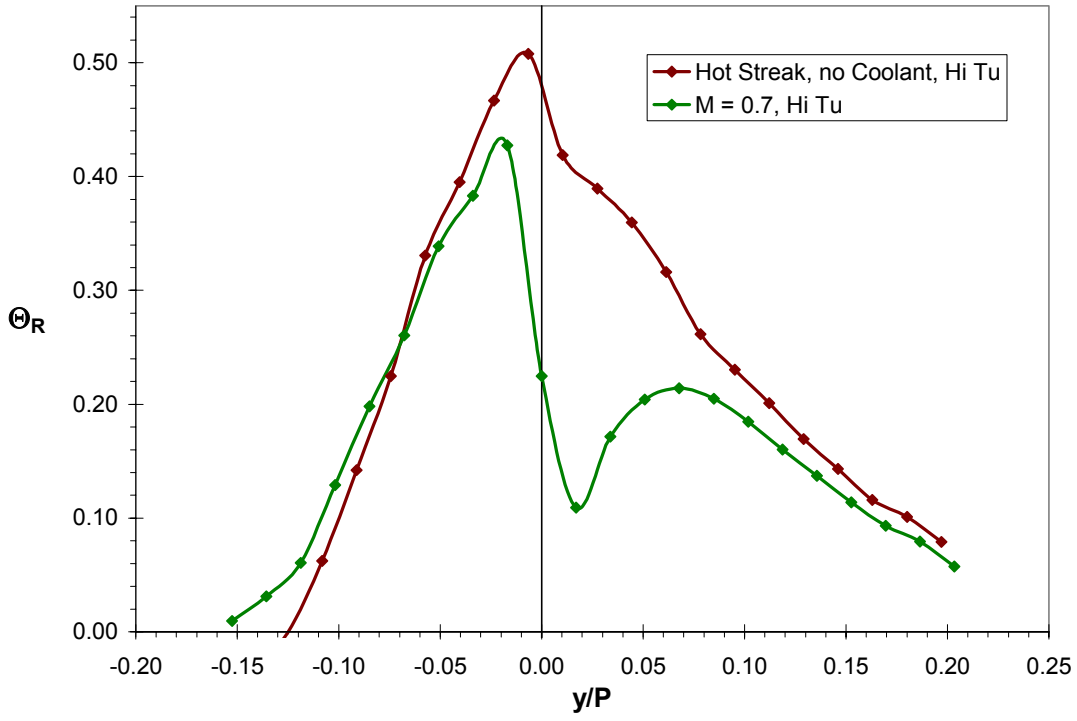

Figure 5.5: Normalized temperature ratio (Θ_R) profiles at Position T for the hot streak impacting the stagnation line without coolant and with suction side blowing at M_{avg} = 0.7, high mainstream turbulence (Tu = 20%).

minimum of Θ_R = 0.11 at y/P = 0.015 (about 1.5d) with little or no coolant benefit past y/P = 0.07 (about 8d). These effects are precisely what would be expected given the midspan coolant profiles in Figure 5.3. A slight effect of mixing of coolant with the pressure side of the hot streak at the trailing edge can be seen just to the pressure side of 0.00P since the thermocouple rake was positioned about 5 mm downstream of the trailing edge.

5.4 Effect of Varying Suction Side Blowing Ratio

Measurements were made for three suction side blowing ratios, M_{avg} = 0.5, 0.7, and 1.0, and, in general, the effect of increasing the blowing ratio was to increase the size and intensity of the coolant areas as demonstrated in Figure 5.6. At a contour level of Θ_R = -0.05, the central region of coolant at Position T grew in width from about 0.06P (6.5d)

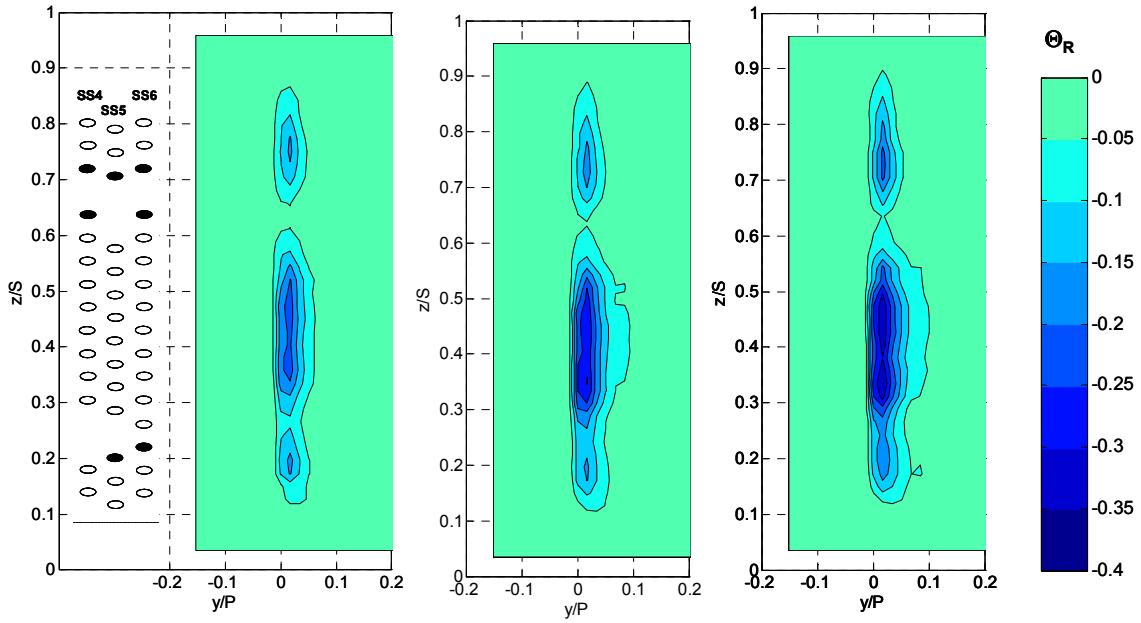

a. **b.** **c.**

Figure 5.6: Normalized temperature ratio (Θ_R) coolant contours at Position T, high mainstream turbulence (Tu = 20%) for suction side blowing at:

a. M_{avg} = 0.5

b. M_{avg} = 0.7

c. M_{avg} = 1.0

at the lowest blowing ratio to 0.11P (12d) at the highest blowing ratio, while the peak coolant value increased from Θ_R = -0.22 to -0.36. For the highest blowing ratio (Figure 5.6c), the upper and central regions of coolant nearly merged at a contour level of Θ_R = -0.05, while the lower region of coolant appeared as an extension of the central region.

At midspan, the coolant profiles in Figure 5.7a show the gradual decrease of the peak coolant level, and increase in coolant profile width, both representing a greater capacity for hot streak reduction. In Figure 5.7b, profiles at the spanwise position of the peak coolant level (z/S = 0.35) were added in dashed lines, showing values only to the suction side of the trailing edge (y/P > 0.0). While at the lowest blowing ratio there was virtually no difference between midspan and peak coolant profiles, at the highest blowing ratio (M_{avg} = 1.0) the difference was greater.

In Figure 5.8, the effect of increased blowing ratio on hot streak reduction was unsurprisingly greater. In this figure, midspan profiles for blowing ratios of M_{avg} = 0.5 and 0.7 are shown with the larger blowing ratio reducing the near wall portion of the hot

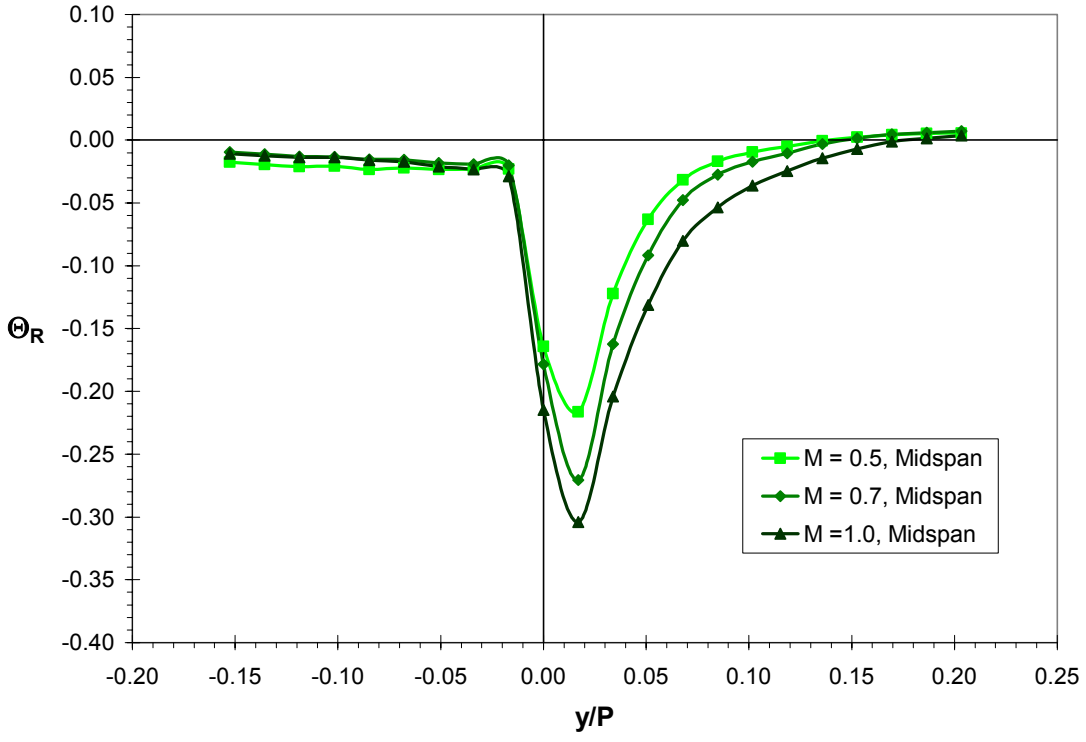

Figure 5.7a: Normalized temperature ratio (Θ_R) coolant profiles at Position T at midspan (z/S = 0.50) for suction side blowing at M_{avg} = 0.5, 0.7, and 1.0, high mainstream turbulence (Tu = 20%).

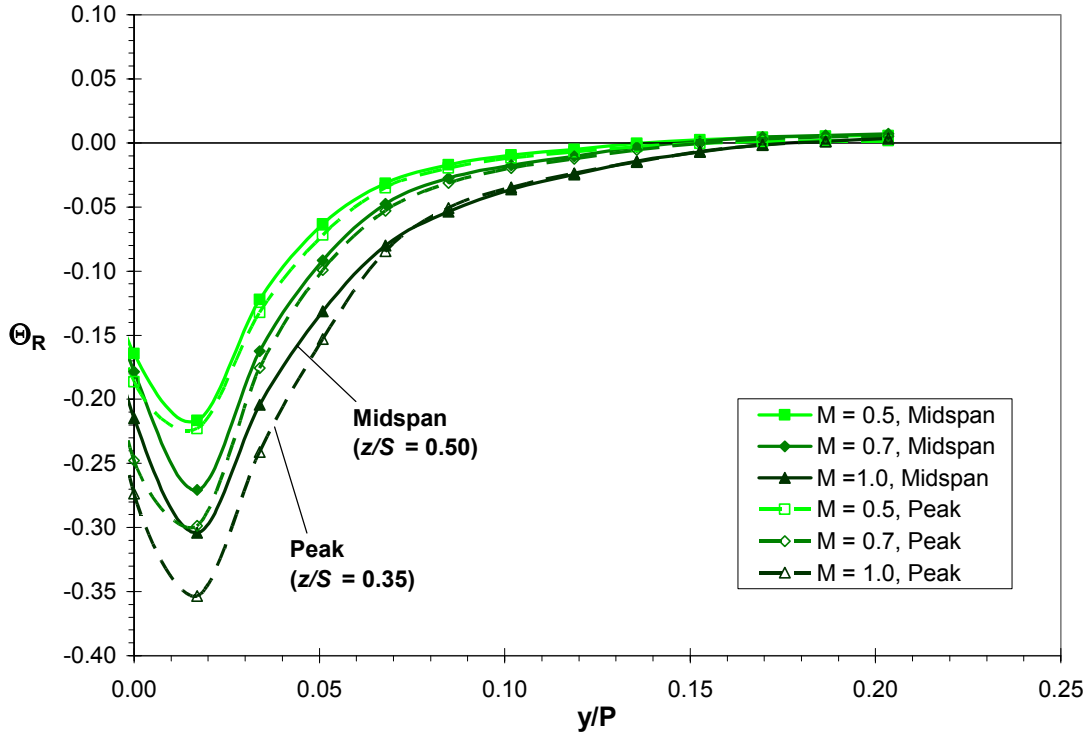

Figure 5.7b: Normalized temperature ratio (Θ_R) coolant profiles at Position T at midspan (z/S = 0.50) and at the spanwise position of the peak coolant level (z/S = 0.35) for suction side blowing at M_{avg} = 0.5, 0.7, and 1.0, high mainstream turbulence (Tu = 20%).

streak much more, however, farther from the wall on the suction side where the local hot streak peak occurred (near y/P = 0.07) the values were nearly the same since the coolant was greatly diluted at that point.

5.5 Evolution of the Suction Side Coolant Profile

Measurements were made at Positions S1', S2', and T' with a single thermocouple probe as described in Chapter 2 with suction side blowing at M_{avg} = 0.7. The measurement positions and their relation to coolant row locations are shown in Figure 5.9. As shown in Figure 5.10, suction side coolant slowly spread away from the wall to give the Position T profiles shown in previous figures. At Position S1', the coolant profile was steep and extended only about 3d from the wall. As shown in Figure 5.9, Position S1' was downstream of the first two rows of coolant holes. By Position S2', more coolant had been added through the third row of holes, producing a fuller coolant

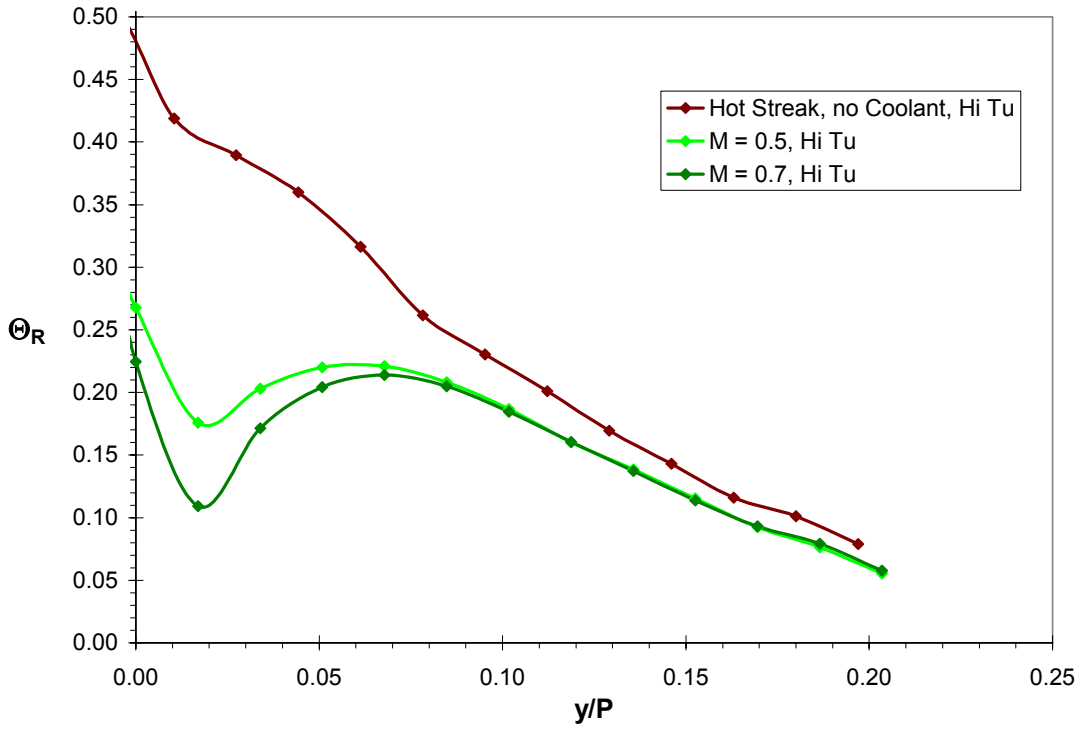

Figure 5.8: Normalized temperature ratio (Θ_R) profiles at Position T for the hot streak impacting the stagnation line without coolant and with suction side blowing at M_{avg} = 0.5 and 0.7, high mainstream turbulence (Tu = 20%).

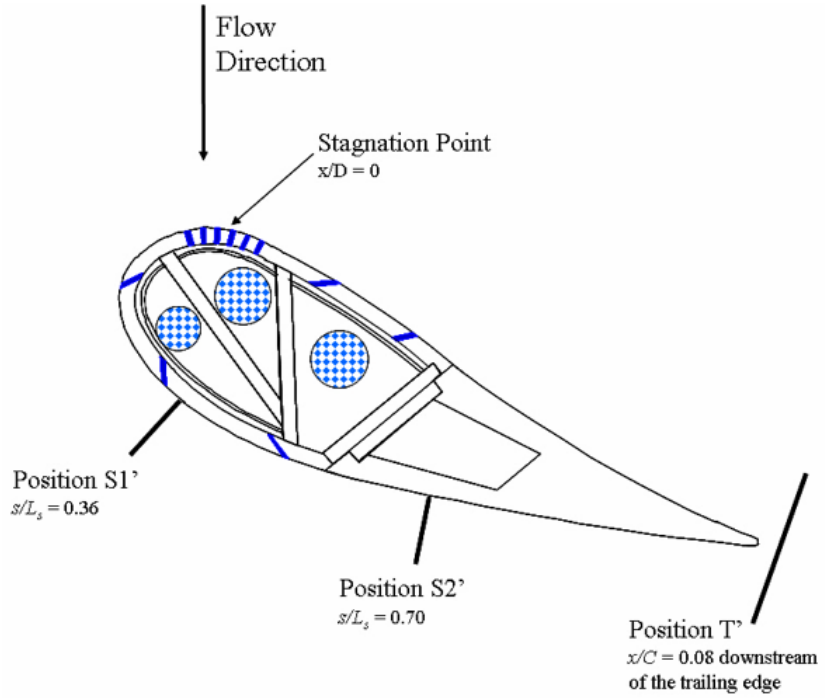

Figure 5.9: Schematic of single thermocouple probe measurement positions for suction side film cooling.

profile that extended slightly farther from the vane wall. Progressing downstream between Positions S1' and S2' the wall coolant temperature rose slightly from Θ_R = -0.74 to -0.60, however off the wall at about 2*d*, the normalized coolant temperature was nearly four times lower, representing a much larger cooling potential.

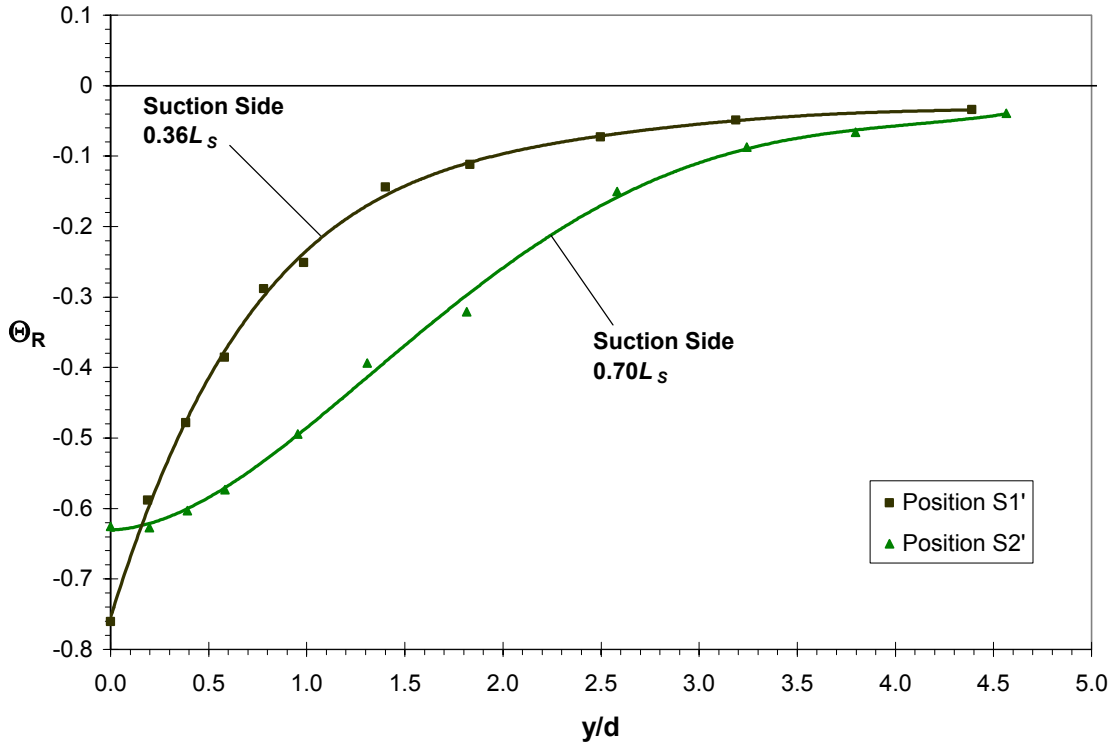

Figure 5.10: Profiles of suction side coolant at Positions S1' and S2' at midspan (z = 0.5*S*), high mainstream turbulence (*Tu* = 20%), for suction side blowing at M_{avg} = 0.7.

Measurements made at Positions T and T' are included in Figure 5.11, where the evolution of the coolant profile downstream past the trailing edge can be observed. The sharply peaked profiles at Positions S1' and S2' broadened into the Position T profile at the trailing edge, which was much flatter but still extended only about 7*d* from the wall. The thermocouple rake at Position T was positioned such that the thermocouple at y/P = 0.0 was within 1 mm of the trailing edge of the vane, and therefore measured a temperature that was a mixture of pressure side and suction side fluid temperatures. For this reason the temperature recorded for this thermocouple was higher than that measured to the suction side of the trailing edge. Clearly, temperature profiles on the pressure side

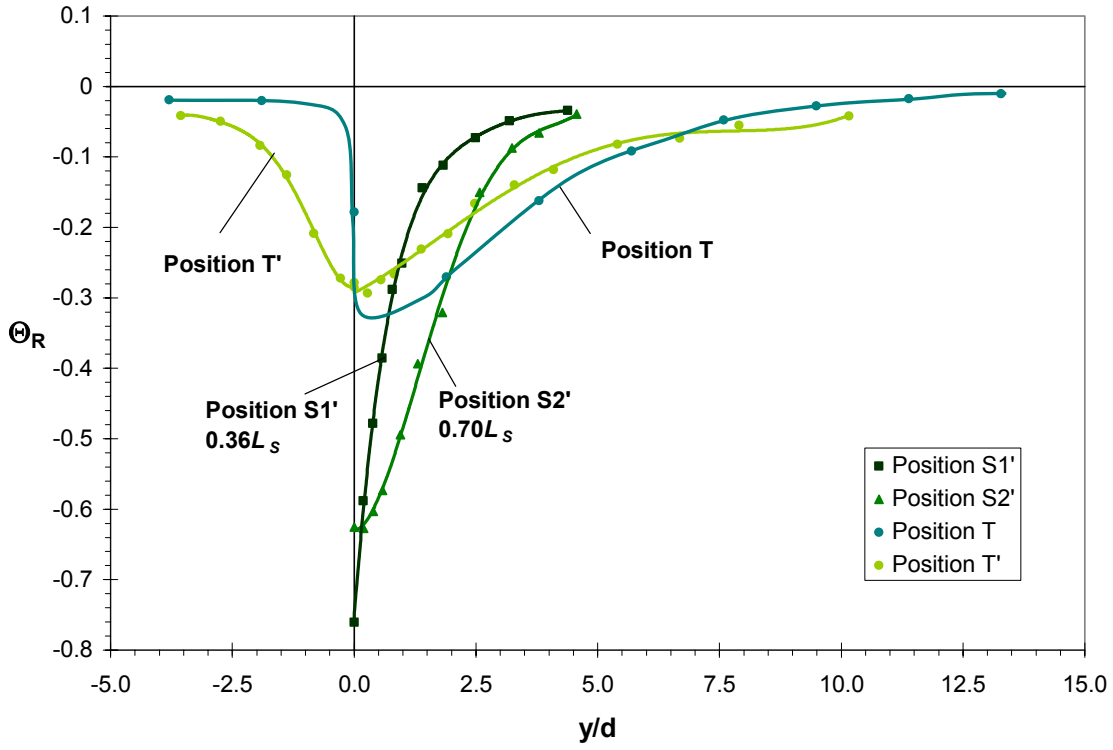

Figure 5.11: Profiles of suction side coolant at Positions S1', S2', T, and T' at midspan (z = 0.5S), high mainstream turbulence (Tu = 20%), for suction side blowing at M_{avg} = 0.7.

at Positions P1' and P2' would be flat at Θ_R = 0.0, since there was no coolant on that side of the vane. This created a strong temperature gradient at the trailing edge of the vane as indicated by the curve fit through points for Position T. Slightly downstream at Position T' (at 0.08C downstream from the trailing edge) the sharp temperature gradient had already relaxed slightly and coolant was observed up to 2.5d from the trailing edge toward the pressure side.

Comparing the Position S1' profiles for the suction side and showerhead permits a clearer understanding of how the two coolant regions differ. Mass flow rates for the two regions were fairly comparable. In terms of a percentage of the mainflow total flow rate per unit span, the showerhead was 0.85% and the suction side was 0.65% of the mainflow for one vane pitch, therefore the total suction side mass flow rate was about 77% of the total showerhead mass flow rate for suction side blowing at M_{avg} = 0.7 and showerhead blowing at M^* = 1.6. However, about 40% of the showerhead coolant was directed toward the pressure side due to the configuration of showerhead holes (see Figure 5.1

where the stagnation line is indicated). For profiles upstream of the trailing edge, the suction side mass flow rate was therefore about 130% of the showerhead mass flow rate on the suction side of the vane. In Figure 5.12a, it is evident that the suction side produced a much stronger temperature gradient near the wall, while the showerhead coolant extended further from the wall. The peak coolant value at the vane wall for suction side blowing was about 3 times lower at Θ_R = -0.74 compared with Θ_R = -0.26 for showerhead blowing, which is understandable since the showerhead coolant had advected much further downstream to reach the measurement plane at Position S1'. Further downstream at Position S2', in Figure 5.12b, the situation was similar. Again the suction side coolant profile had a much lower peak and the showerhead profile was flatter, but at this position along the vane both coolant profiles extend to about the same distance from the wall. As seen in Figure 5.12c, at Position T', something quite different happened. While the suction side coolant at Positions S1' and S2' was blocked by the vane, at Position T' a fair amount of coolant had washed over to the pressure side in the developing wake. Compared with the showerhead coolant, the profile was steep and restricted to very near y/P = 0.0, where showerhead coolant reached more than 10d from the wall with a fairly small gradient. On the suction side of y/P = 0.0, the showerhead coolant spread far from the wall, but the suction side coolant profile was also broad extending past 8d from the wall. As shown in Figure 4.3 in the previous chapter, showerhead coolant reached nearly 20d at Position T (equivalent to y/P = 0.17 in the figure), well outside of the range of the single thermocouple probe used at Position T'. The showerhead, with its broad coverage and reasonably low Θ_R values, and the suction side, with its tightly focused coolant near the vane surface, made a powerful combination for reducing the strength of an impinging hot streak.

5.6 Turbulence Effects in the Stator/Rotor Axial Gap with Suction Side Film Cooling

The vane wake and turbulent advection over the distance between Positions T and B was expected to broaden the coolant profile and lower the magnitude of its peak value, and is exactly what is shown in the midspan profiles of Figure 5.13. For the three

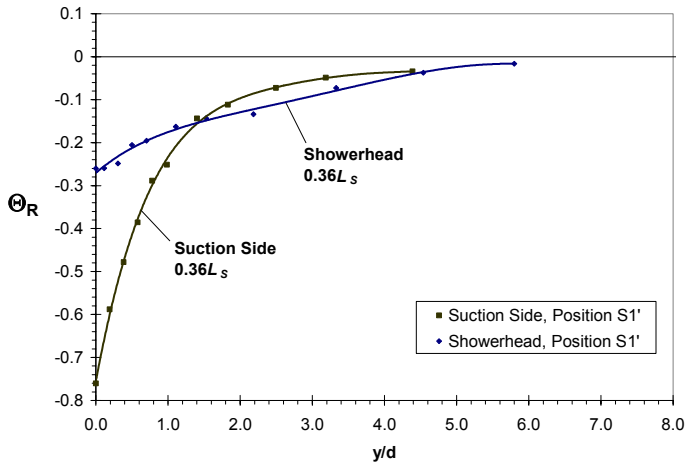

Figure **5.12a: Coolant profiles at Position S1' at midspan ($z = 0.5S$) for suction side blowing at M_{avg} = 0.7 and showerhead blowing at $M^* = 1.6$, high mainstream turbulence ($Tu = 20\%$).**

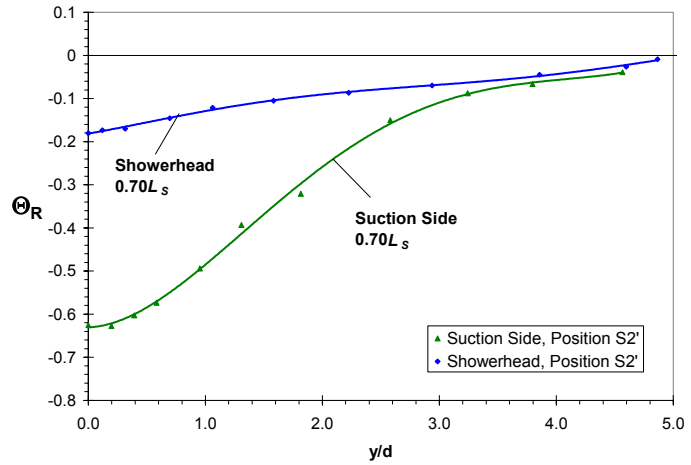

Figure **5.12b: Coolant profiles at Position S2' at midspan ($z = 0.5S$) for suction side blowing at M_{avg} = 0.7 and showerhead blowing at $M^* = 1.6$, high mainstream turbulence ($Tu = 20\%$).**

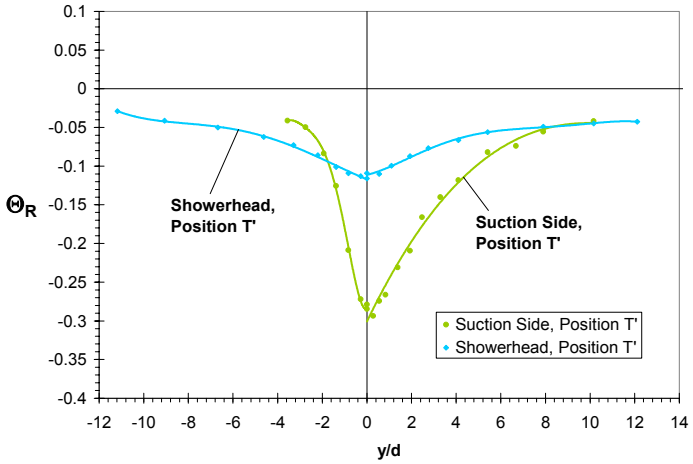

Figure 5.12c: Coolant profiles at Position T' at midspan ($z = 0.5S$) for suction side blowing at M_{avg} = 0.7 and showerhead blowing at $M^* = 1.6$, high mainstream turbulence ($Tu = 20\%$).

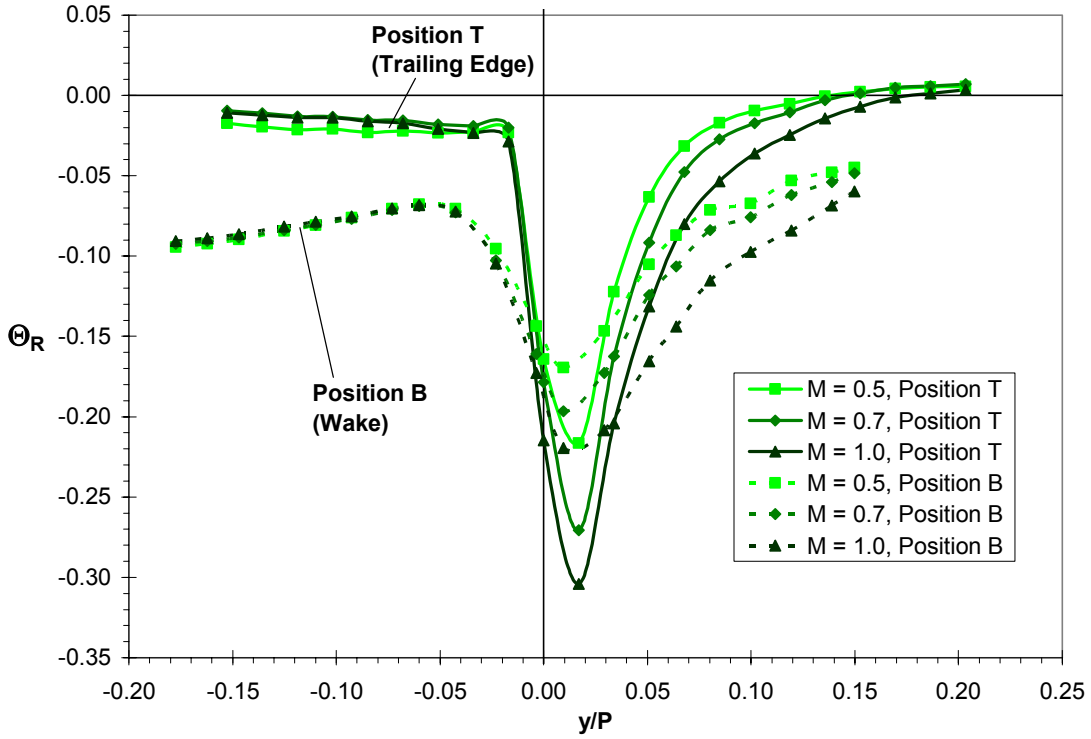

Figure 5.13: Coolant profiles at the trailing edge (Position T) and in the wake at Position B at midspan (z = 0.5S) for suction side blowing at M_{avg} = 0.5, 0.7, and 1.0, high mainstream turbulence (Tu = 20%).

blowing ratios tested, each profile was broadened by a factor of two and the peak lessened by about the same amount. For a suction side blowing ratio of M_{avg} = 0.7, the magnitude of the peak dropped about 30% between the trailing edge and Position B in the wake from Θ_R = -0.27 to -0.20. The other two blowing ratios were affected similarly. The effect of the passage vortex in transporting coolant from near the vane surface to the opposite side of the passage was seen for the suction side as well as the showerhead (see §4.5). This effect is seen even more clearly in the y-z contours in Figure 5.14, where coolant appeared near the opposite vane wall at Position B at midspan and above.

With the hot streak activated, effects of the vane wake and additional downstream distance in the stator/rotor axial gap are illustrated with midspan profiles in Figure 5.15. Midspan profiles at Positions T and B with no film cooling are also included in the figure to demonstrate how the hot streak profile was reduced without coolant. For suction side

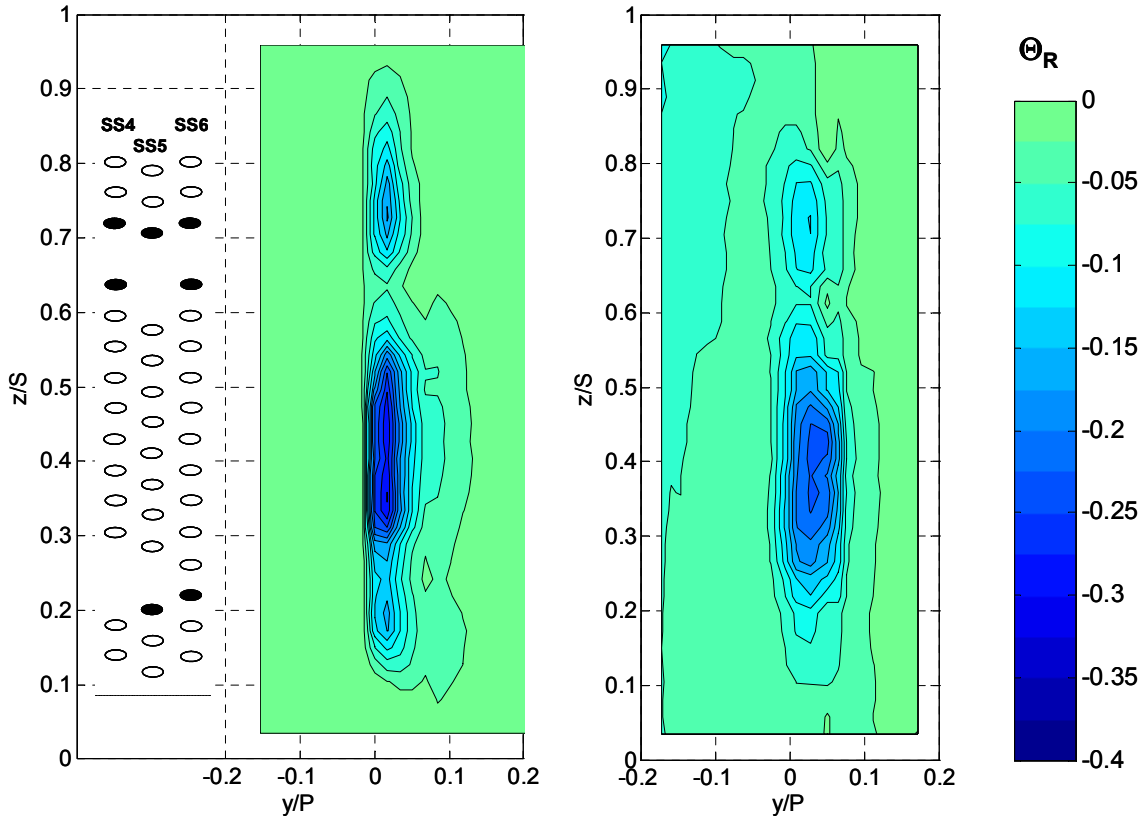

a. **b.**

Figure 5.14: Normalized temperature ratio (Θ_R) contours for suction side blowing at M_{avg} = 0.7, high mainstream turbulence (Tu = 20%) at:

a. Position T

b. Position B

blowing at M_{avg} = 0.7, the hot streak profile at Position T, with a large dip to the suction side near the vane wall, was flattened out by Position B. On the pressure side, the large peak had also diminished considerably.

Looking at temperature contours in Figure 5.16, it is clear that the strong gradients at the trailing edge were dissolved in the stator/rotor axial gap over the span of the hot streak. While the hot streak was reduced to levels below Θ_R = 0.22 to the suction side of y/P = 0.0, to the pressure side the hot streak was attenuated much more. The hot streak peak on the pressure side at Position T was reduced nearly 35% to Θ_R = 0.28 at Position B.

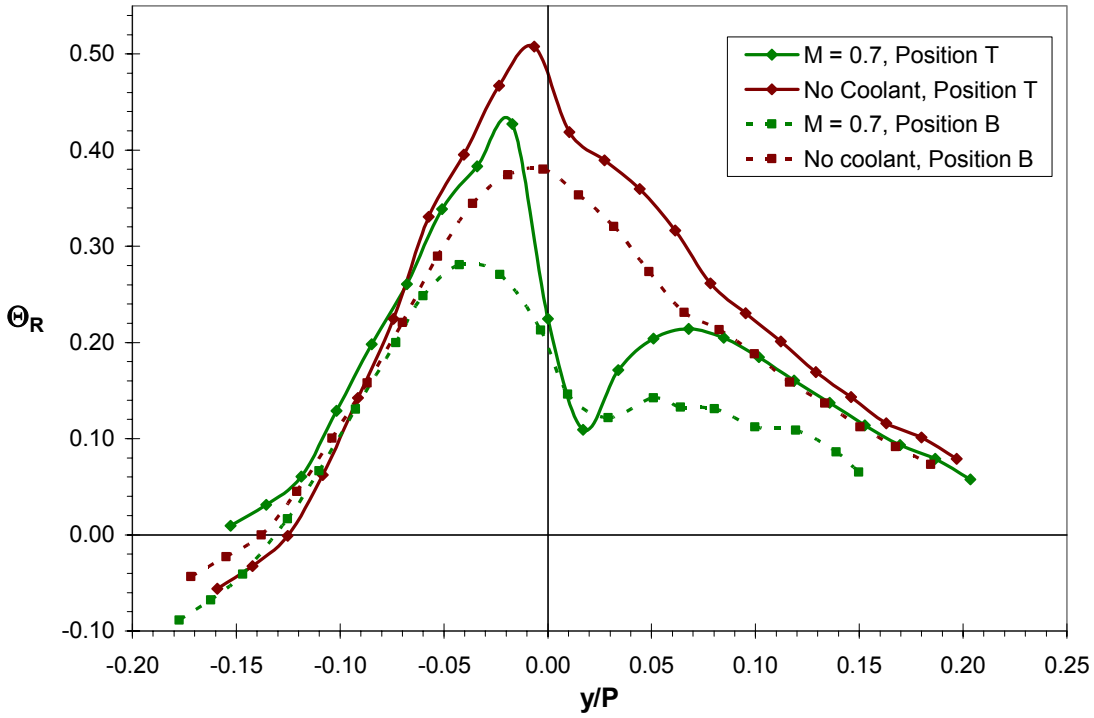

Figure 5.15: Normalized temperature ratio (Θ_R) profiles at Position T and Position B for the hot streak impacting the stagnation line without coolant and with suction side blowing at M_{avg} = 0.7, high mainstream turbulence (Tu = 20%).

Including turbulence effects in the stator/rotor axial gap, suction side blowing was nearly as effective at reducing the hot streak as the showerhead shown in Chapter 4. Even though at the trailing edge, the suction side coolant had only reduced one side of the hot streak, further attenuation of the strong temperature gradients created by suction side film cooling in the stator/rotor axial gap reduced the hot streak peak to Θ_R = 0.28. This was just 5% higher than the result for showerhead film cooling at M^* = 1.6. A comparison of Position B results is shown in Figure 5.17. The main differences were the location of the hot streak peak and the size and shape of the hottest region, i.e. $\Theta_R > 0.25$. The size of the remaining hot streak overall ($\Theta_R > 0.0$) was very similar between the two blowing conditions. This implies that broad reduction and highly focused reduction of the hot streak may be equally effective at the rotor inlet plane given the attenuation of strong temperature gradients in the stator/rotor axial gap.

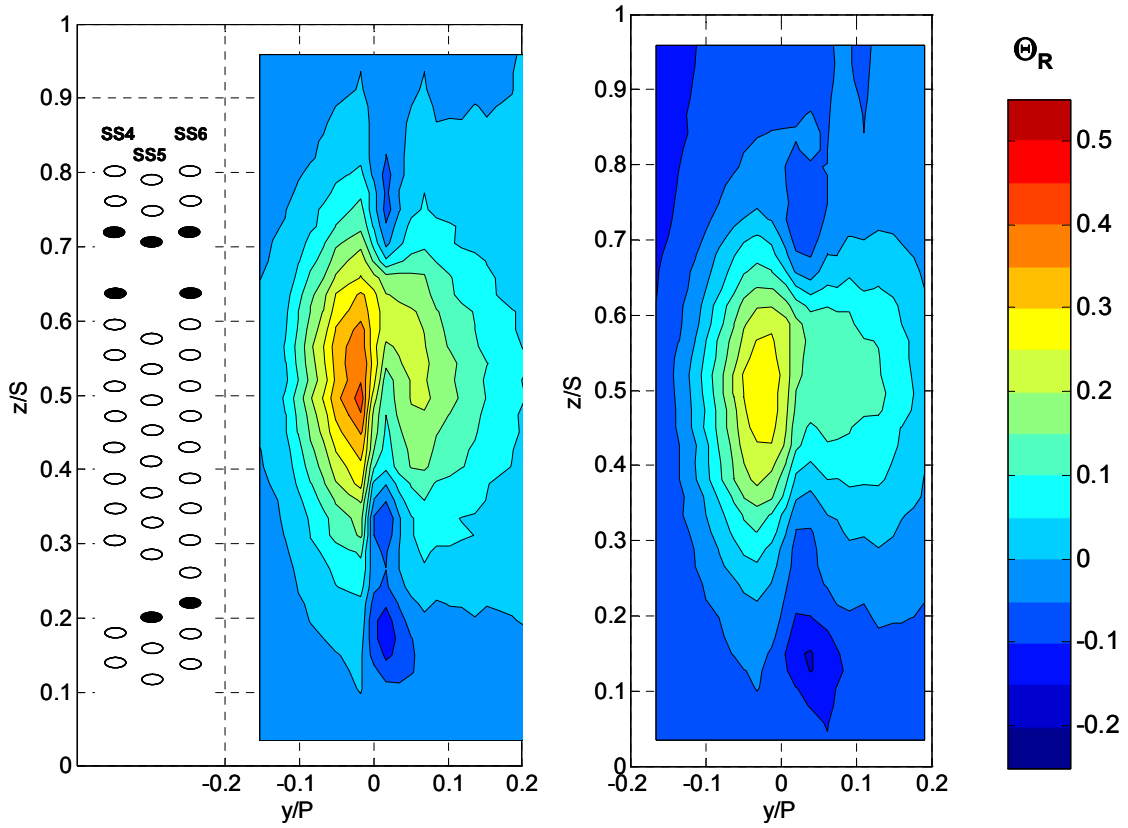

a. b.

Figure **5.16: Normalized temperature ratio (Θ_R) contours for suction side blowing at M_{avg} = 0.7, high mainstream turbulence (Tu = 20%):**

a. Position T (Trailing Edge)

b. Position B (Wake)

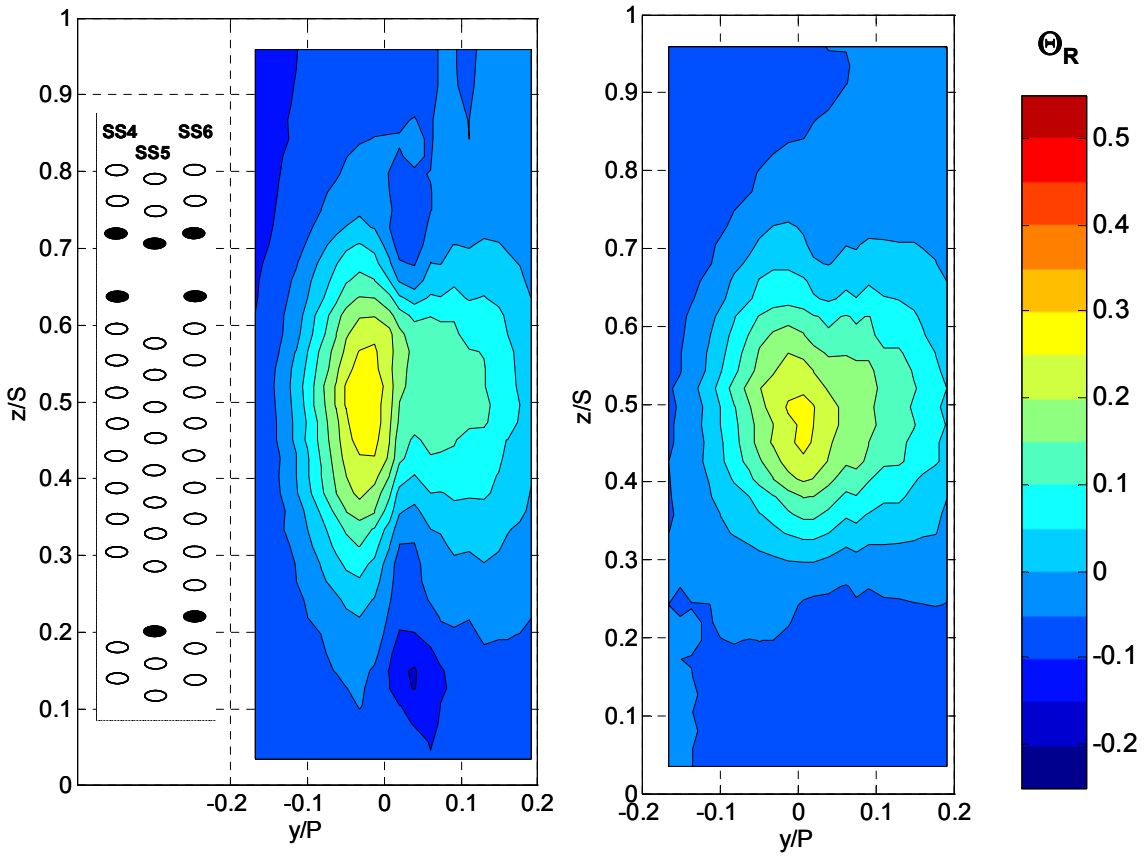

a. **b.**

Figure **5.17: Normalized temperature ratio (Θ_R) contours at Position B, high mainstream turbulence (*Tu* = 20%) for:**

a. Suction side blowing at M_{avg} = 0.7

b. Showerhead blowing at M^* = 1.6

Chapter 6: Effects of Pressure Side Film Cooling on Hot Streak Reduction

6.1 Introduction

The effect of pressure side film cooling on hot streak reduction was significantly smaller than either film cooling from the showerhead or suction side. Coolant was ejected from two rows of coolant holes as shown in Figure 6.1, angled at an injection angle of $\phi = 30°$ and a streamwise angle of $\theta = 45°$. The pressure side was operated at three blowing ratios, M_{avg} = 0.4, 0.6, and 1.0, representing below optimum, optimum, and above optimum levels with respect to adiabatic effectiveness later referred to as low, standard, and high blowing ratios as in previous chapters. As for the suction side, the pressure side rows of holes were fed by a common plenum. As a result, local blowing ratios for each row of holes were different from the overall average as presented in Table 6.1.

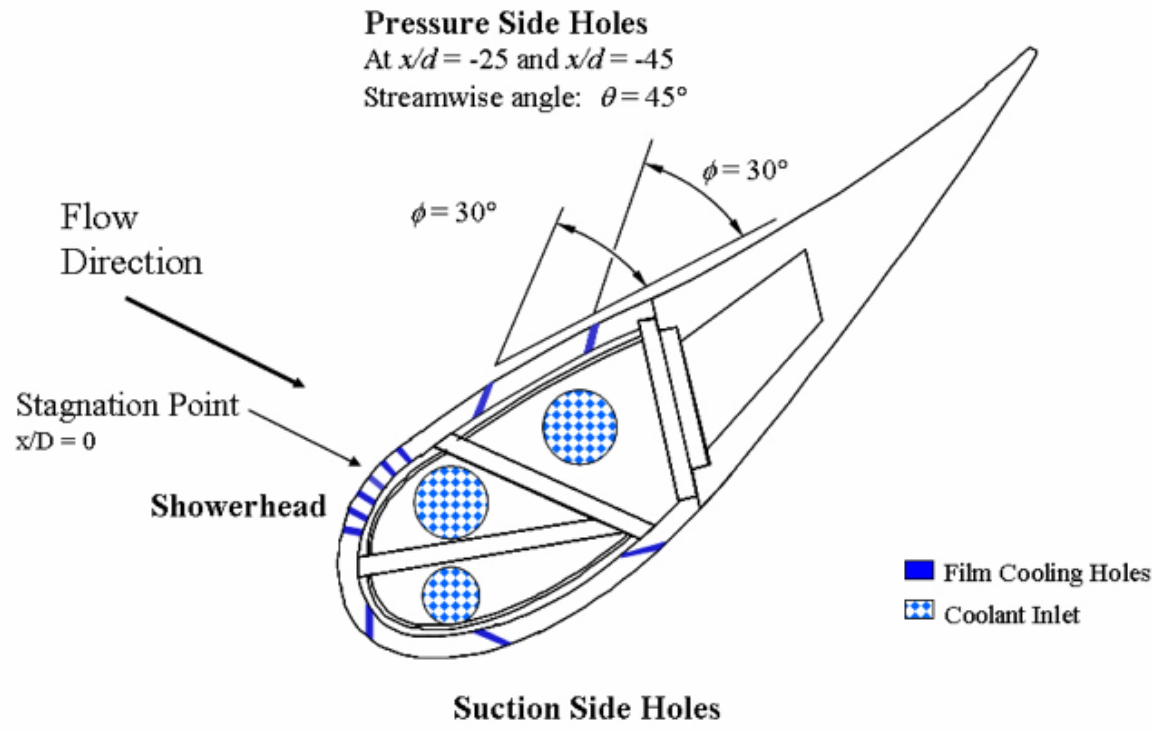

Figure 6.1: Schematic of film cooling hole configuration showing pressure side hole parameters.

Measurements were made at the trailing edge for each blowing ratio, both with and without the hot streak. Additional measurements were made at Positions P1' and P2' clarifying how coolant profiles evolved from the coolant holes to the trailing edge. The effect of the wake was also quantified for pressure side film cooling with the hot streak activated.

	Row 1	Row 2
M_{avg} = 0.4	0.26	0.51
M_{avg} = 0.6	0.55	0.64
M_{avg} = 1.0	1.06	0.95

Table 6.1: Local blowing ratios for pressure side coolant holes

6.2 Pressure Side Coolant Profiles at the Trailing Edge

As seen in Figure 6.2, very little evidence of coolant was observed at the trailing edge for the adiabatic effectiveness optimum blowing ratio of M_{avg} = 0.6 compared with

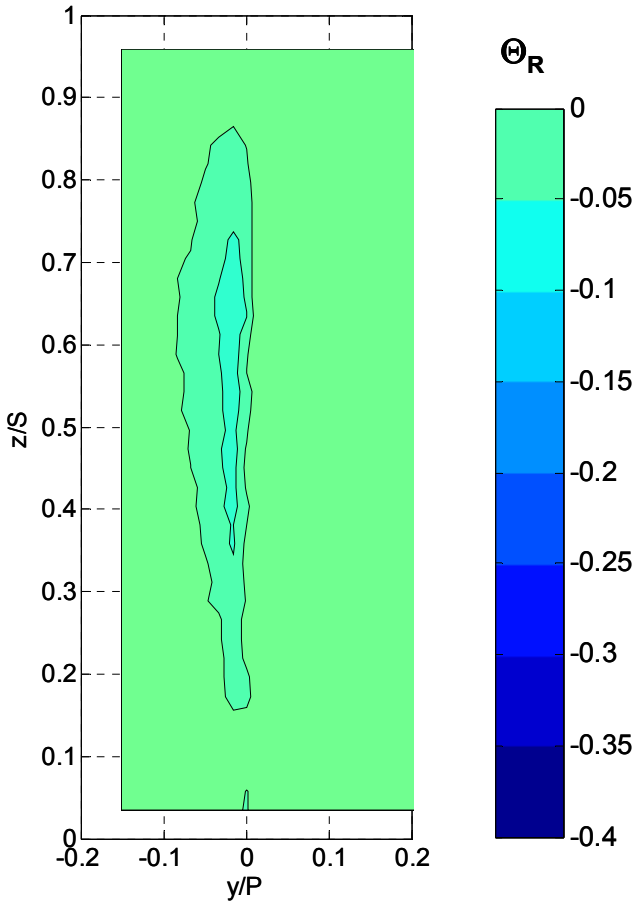

Figure 6.2: Normalized temperature ratio (Θ_R) coolant contours at Position T for pressure side blowing at M_{avg} = 0.6, high mainstream turbulence (Tu = 20%).

the hot streak peak temperature ratio of Θ_R = 0.51, or the showerhead and suction sides with Θ_R values 3 to 4 times as low. In the figure, the peak contour level of the coolant profile was close to the trailing edge at about y/P = 0.02 and was centered spanwise between about 0.35 < z/S < 0.75. Although the position of the coolant was well suited for hot streak reduction, there was simply not a sufficient amount to expect it to be effective.

Figure 6.3 shows how small the coolant peak was at midspan, reaching a maximum of only Θ_R = -0.05 close to the wall. This figure also shows how the peak profile, found spanwise at z/S = 0.63, was nearly identical to the midspan profile for this blowing ratio. Overall, the profile was fairly flat at Position T, indicating that coolant spread far from the vane surface, however, with values this close to zero, it was unclear where the coolant edge occurred due to uncertainty in the mainstream.

A direct comparison in Figure 6.4 between the pressure side, suction side, and showerhead profiles at standard blowing ratios reveals how much lower the peak on the suction side was than the pressure side. The peak magnitude of the suction side coolant

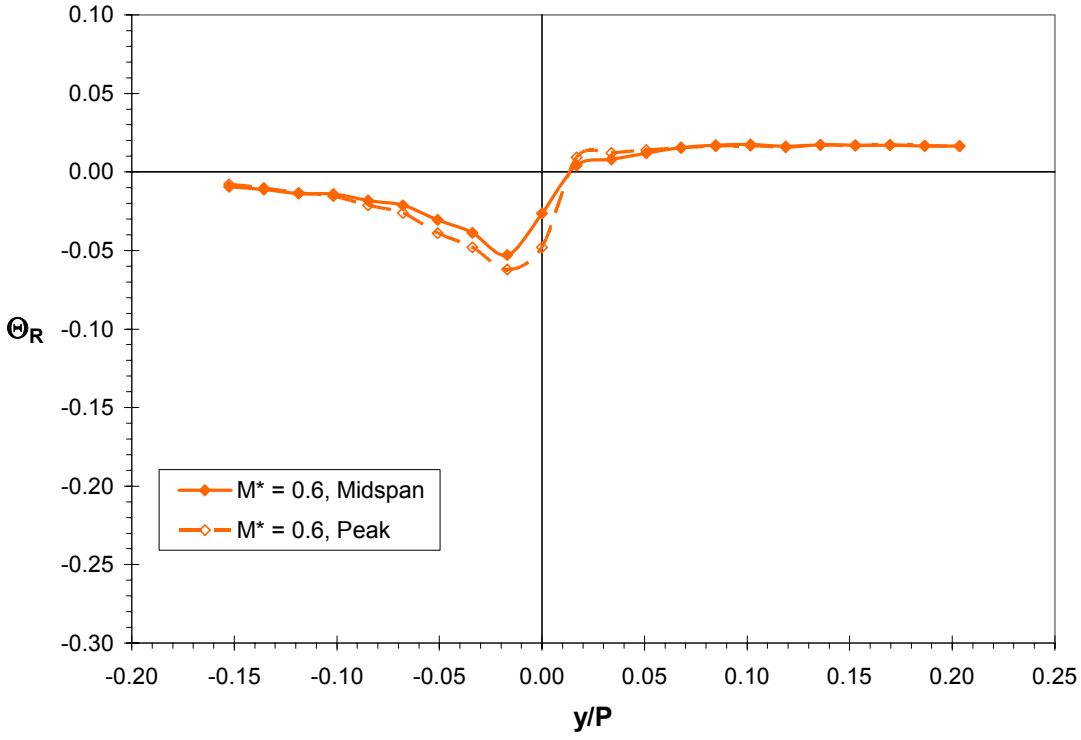

Figure 6.3: Normalized temperature ratio (Θ_R) coolant profiles at Position T for pressure side blowing at M_{avg} = 0.6, high mainstream turbulence (Tu = 20%).

profile was about four times lower than the pressure side profile. While the showerhead coolant profile peak magnitude was not as large, its broad shape indicated a much greater amount of coolant at midspan. The pressure side profile had by far the lowest amount of coolant at the trailing edge, primarily due to the lower coolant mass flow rate. Using the area between the curves and $\Theta_R = 0.0$ as a measure of coolant quantity, the showerhead had the most coolant with the suction side a close second at about 85% of the showerhead, while the pressure side profile had about 30% as much as the showerhead. These percentages compare fairly well with mass flow rates, where the suction side mass flow rate was 77% of the showerhead mass flow rate, and the pressure side mass flow rate was 16% of the showerhead mass flow rate. Since the test vane was the only cooled vane, these percentages are per unit pitch. These sets of percentages differ primarily because a great deal of showerhead coolant was observed well below midspan as described in §4.2, therefore it was not surprising that relatively more coolant was

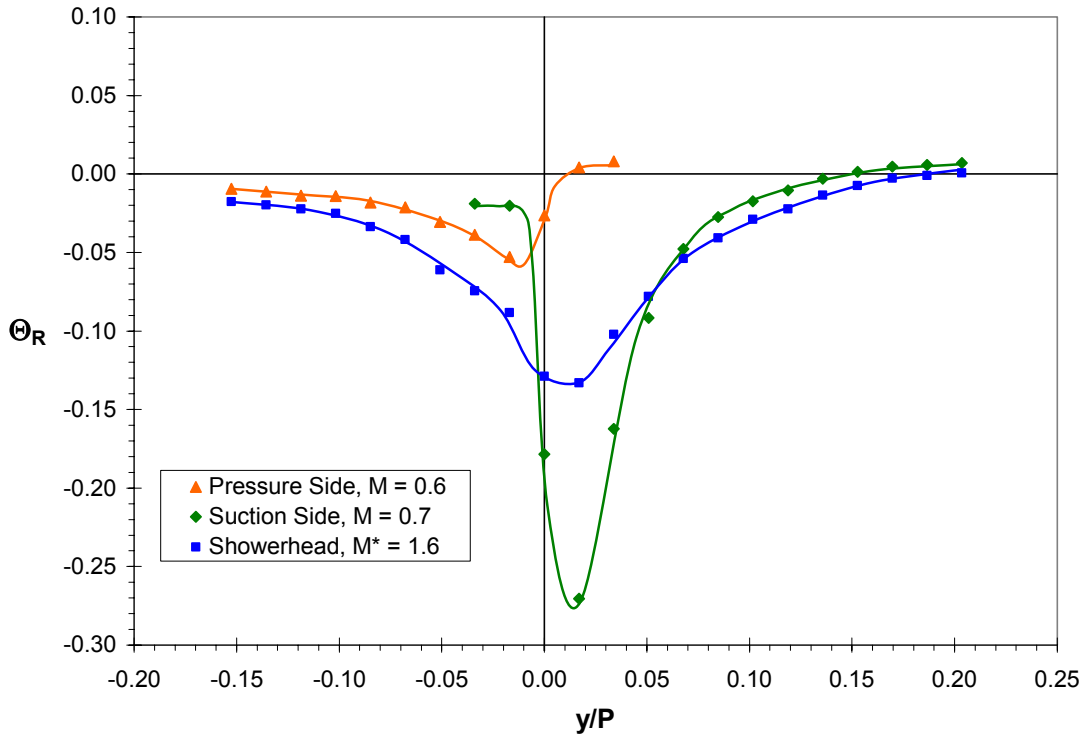

Figure 6.4: Normalized temperature ratio (Θ_R) coolant profiles at Position T comparing pressure side blowing ($M_{avg} = 0.6$), suction side blowing ($M_{avg} = 0.7$), and showerhead blowing ($M^* = 1.6$), high mainstream turbulence ($Tu = 20\%$).

estimated at midspan for the suction side and pressure side than represented in mass flow rates. On a per hole basis, the mass flow rate for the pressure side was 25% of the mass flow rate for the suction side on average. Although there were blocked holes on the suction side due to the hatch, there were three rows on the suction side and only two rows on the pressure side, so the total number of holes was nearly the same. Therefore, the primary difference causing different mass flow rates at nearly the same blowing ratio on the pressure and suction sides was the external velocity. Comparing with the showerhead, there were exactly three times as many holes on the showerhead as the pressure side, with 102 holes compared with 34 respectively. In addition, the mass flow rate per hole on the pressure side was about 50% of the mass flow rate on the showerhead. This, along with the greater number of holes made the showerhead coolant profile much colder than the pressure side profile.

6.3 Effect of Pressure Side Film Cooling on Hot Streak Reduction

Looking at the effect of pressure side film cooling on hot streak reduction in Figure 6.5, only a small benefit was observed. The size of the peak contour level was smaller with reductions on the pressure side near the trailing edge ($y/P = 0.0$). The peak hot streak value was reduced just over 20% to $\Theta_R = 0.40$ at the trailing edge. This was about the same as the maximum reported for suction side film cooling, which was also positioned to the side opposite of the film cooling region. Comparing results for suction and pressure side blowing for their respective portions of the hot streak, pressure side blowing reduced the hot streak on the pressure side of the trailing edge by about 15% while suction side blowing reduced the hot streak on the suction side of the trailing edge by about 40%.

Midspan profiles in Figure 6.6 for pressure side blowing at $M_{avg} = 0.6$ show how little effect this film cooling region has on hot streak reduction. The pressure side coolant did remove the highest part of the peak, but had significantly less effect than either the showerhead or suction side.

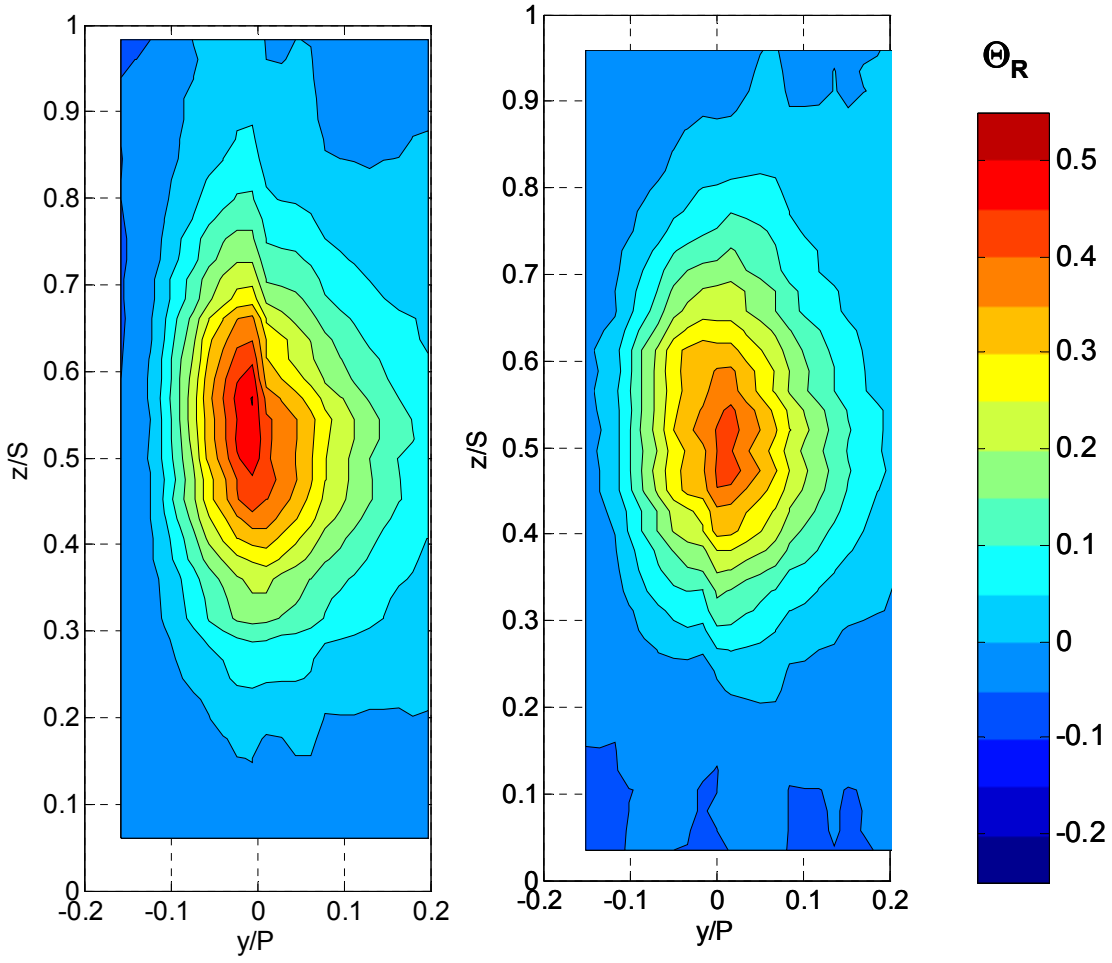

Figure 6.5: Normalized temperature ratio (Θ_R) contours at Position T with the hot streak at the stagnation line, high mainstream turbulence (Tu = 20%):

a. No coolant

b. Pressure side blowing at M_{avg} = 0.6, DR = 1.6.

6.4 Effect of Varying Pressure Side Blowing Ratio

Given the meager performance of the pressure side at the adiabatic effectiveness optimum blowing ratio, a below optimum blowing ratio would seem unlikely to provide effective levels of coolant. However, the above optimum blowing ratio did provide more significant levels of coolant as shown in Figure 6.7. The maximum coolant level was Θ_R = -0.09 at a blowing ratio of M_{avg} = 1.0 (Figure 6.7c), but at the lowest blowing ratio of

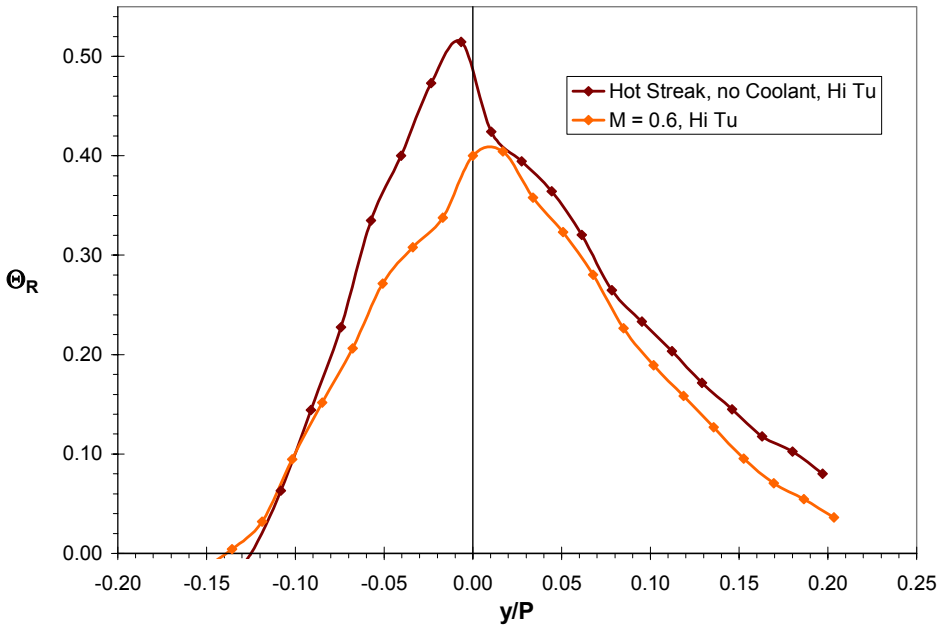

Figure 6.6: Normalized temperature ratio (Θ_R) profiles at Position T for the hot streak impacting the stagnation line without coolant and with pressure side blowing at M_{avg} = 0.6, high mainstream turbulence (Tu = 20%).

M_{avg} = 0.4 (Figure 6.7a), coolant levels were very low, barely different from the mainstream temperature. For the highest blowing ratio, the coolant appeared as a continuous strip across most of the span, just to the pressure side of the trailing edge (y/P = 0.0). Since the coolant holes for both rows of pressure side holes were located between 0.15S and 0.80S and they had a streamwise angle of θ = 45°, coolant was restricted to about the same range. Midspan profiles in Figure 6.8 show the same trend with peak values ranging from near mainstream at the lowest blowing ratio to Θ_R = -0.07 for M_{avg} = 1.0.

6.5 Evolution of the Pressure Side Coolant Profile

Coolant profiles were measured at Positions P1' and P2' as shown in the schematic in Figure 6.9. These profiles indicated how the coolant mixed with mainstream fluid, and since Position P1' was located immediately downstream (less than 1d) of a coolant hole, a comparison of the profiles at these positions demonstrates how

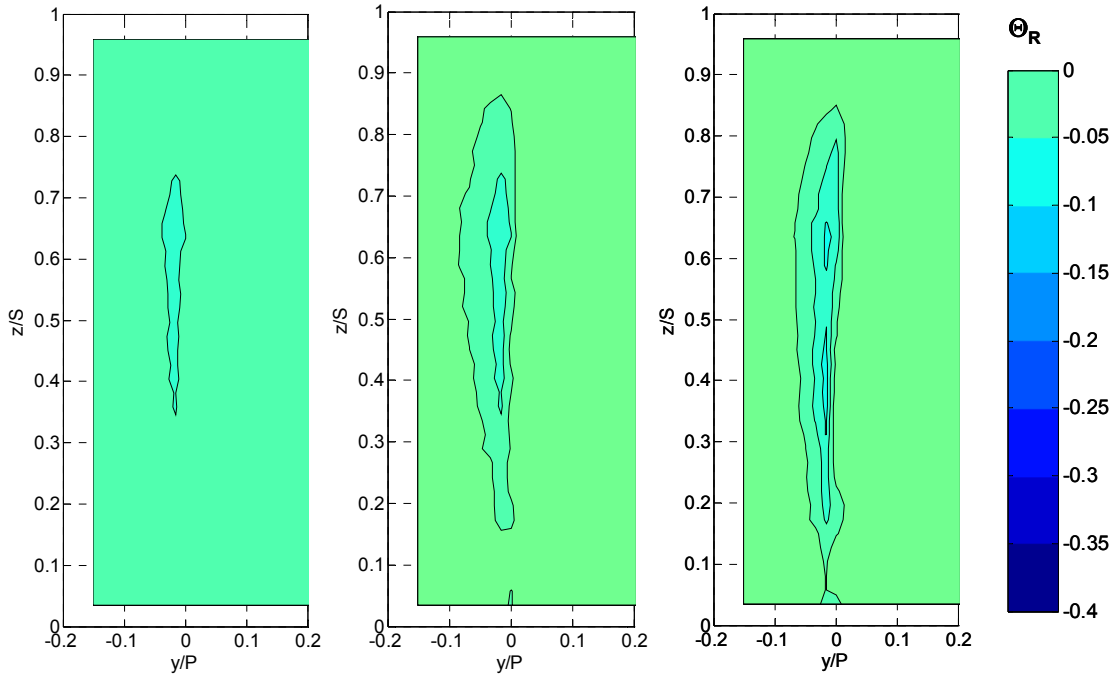

Figure 6.7: Normalized temperature ratio (Θ_R) coolant contours at Position T, high mainstream turbulence (Tu = 20%) for pressure side blowing at:

a. M_{avg} = 0.4

b. M_{avg} = 0.6

c. M_{avg} = 1.0

the strong profile weakened as it progressed downstream (Figure 6.10). At the coolant hole exit (Position P1'), values topped out at Θ_R = -0.42 on the wall and were as high as Θ_R = -0.16 at just over 0.5d from the wall. The edge of the coolant profile appeared to be a little more than 1d from the wall at Position P1'. Downstream at Position P2', the coolant profile was nearly flat, peaking at the wall at Θ_R = -0.10. At this position, it was difficult to determine where the edge of the coolant profile was located since the coolant had mixed thoroughly with mainstream fluid between Positions P1' and P2'. As shown previously in Figure 6.3, the peak coolant value dropped even further to Θ_R = -0.06 at Position T.

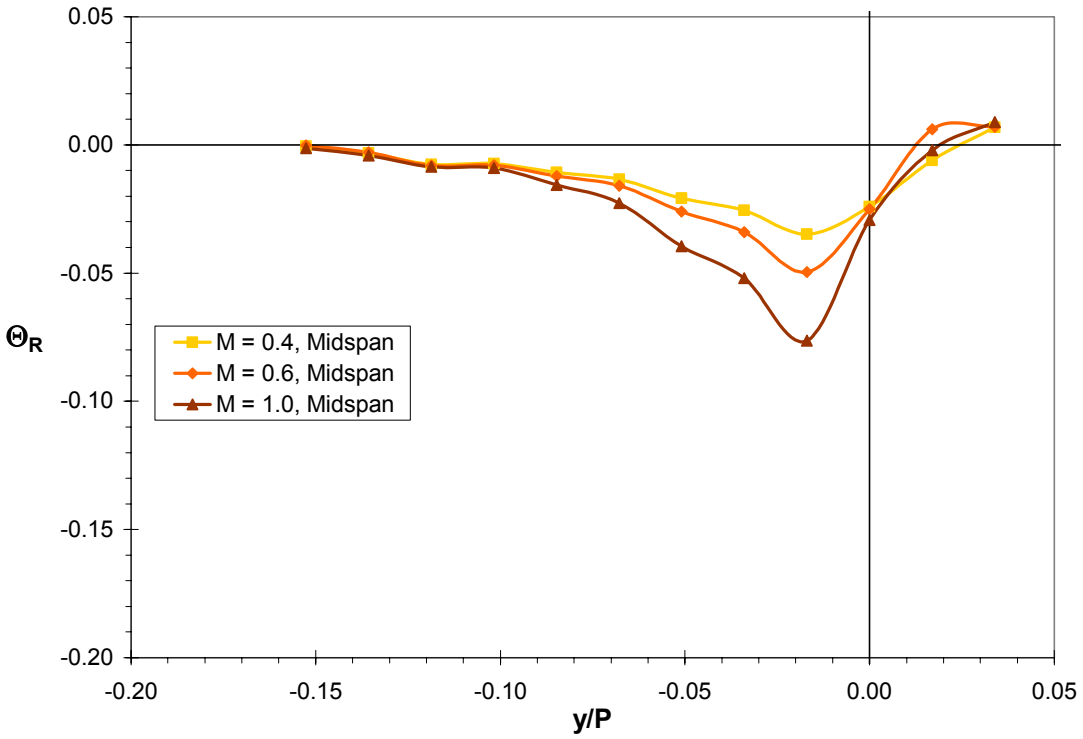

Figure 6.8: Normalized temperature ratio (Θ_R) coolant profiles at Position T at midspan (z/S = 0.50) for pressure side blowing at M_{avg} = 0.4, 0.6, and 1.0, high mainstream turbulence (Tu = 20%).

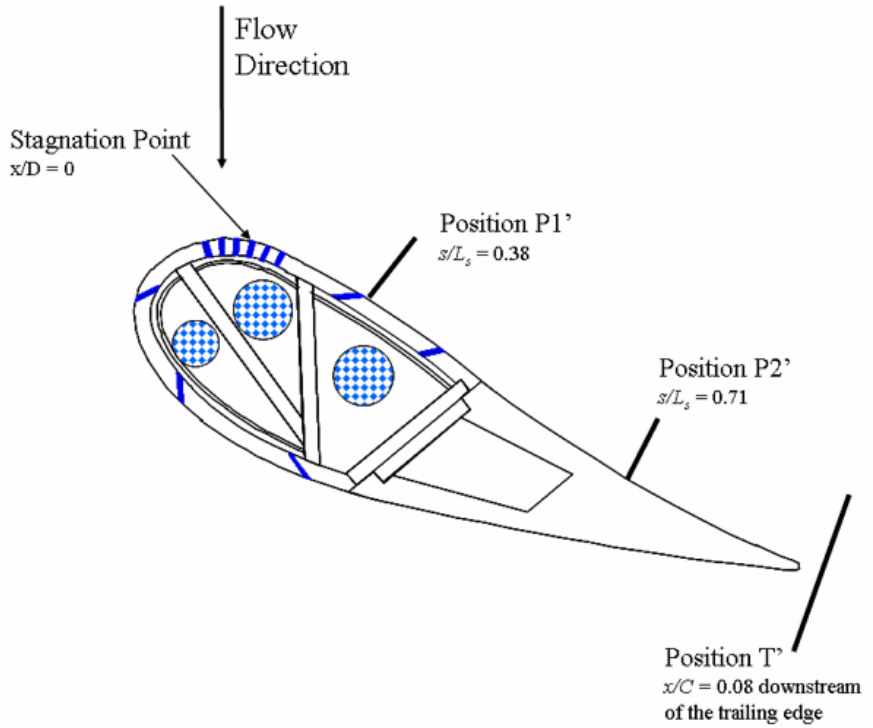

Figure 6.9: Schematic of single thermocouple probe measurement positions for pressure side film cooling.

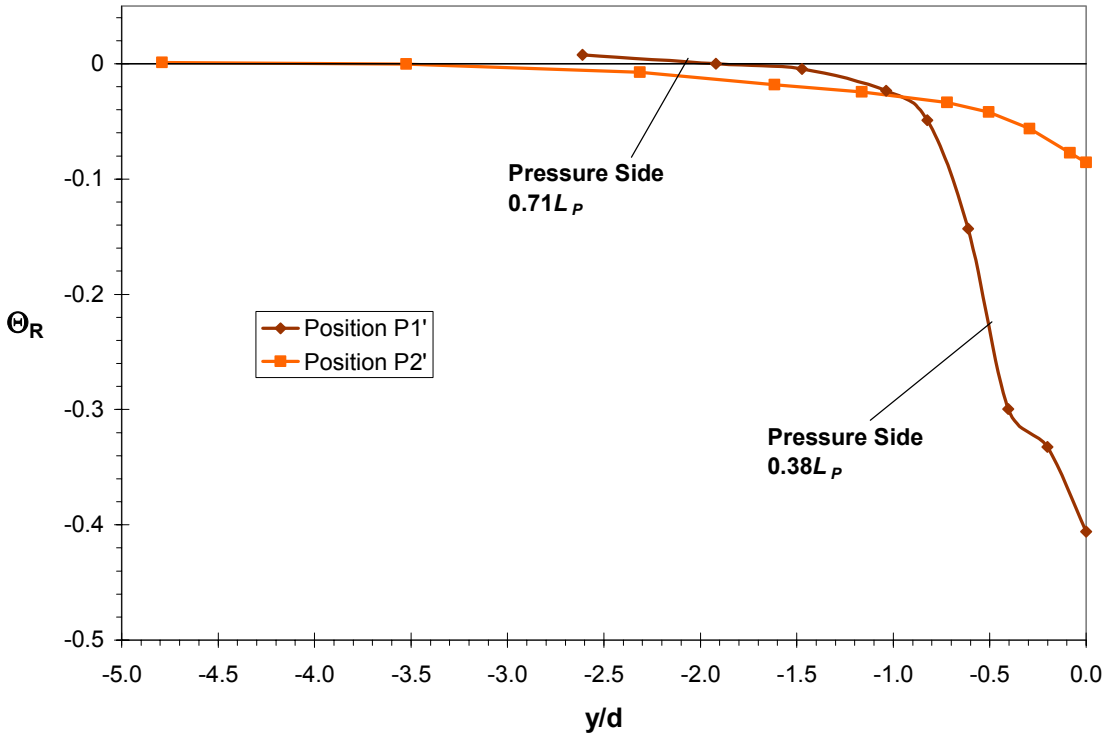

Figure 6.10: Profiles of pressure side coolant at Positions P1' and P2' at midspan ($z = 0.5S$), for pressure side blowing at $M_{avg} = 0.6$, high mainstream turbulence ($Tu = 20\%$).

6.6 Turbulence Effects in the Stator/Rotor Axial Gap with Pressure Side Film Cooling

Turbulence effects in the stator/rotor axial gap attenuated the hot streak with no film cooling much more than the effect of pressure side film cooling as demonstrated in Figure 6.11. The peak of the hot streak was reduced nearly 25% without the aid of film cooling while pressure side film cooling reduced the peak an additional 5%. At the trailing edge the benefit due to pressure side film cooling appeared much greater. Clearly the vane wake and additional downstream distance was the dominant factor in reducing the hot streak for pressure side film cooling.

Pressure side film cooling was observed to remove the sharp gradients at the trailing edge since it acted on the hotter side of the profile (see Figure 6.5). Comparing contour plots in Figure 6.12 shows that the attenuation in the wake was fairly uniform over the entire hot streak since no inversions or sharp gradients in the temperature profile existed at the trailing edge due to pressure side film cooling.

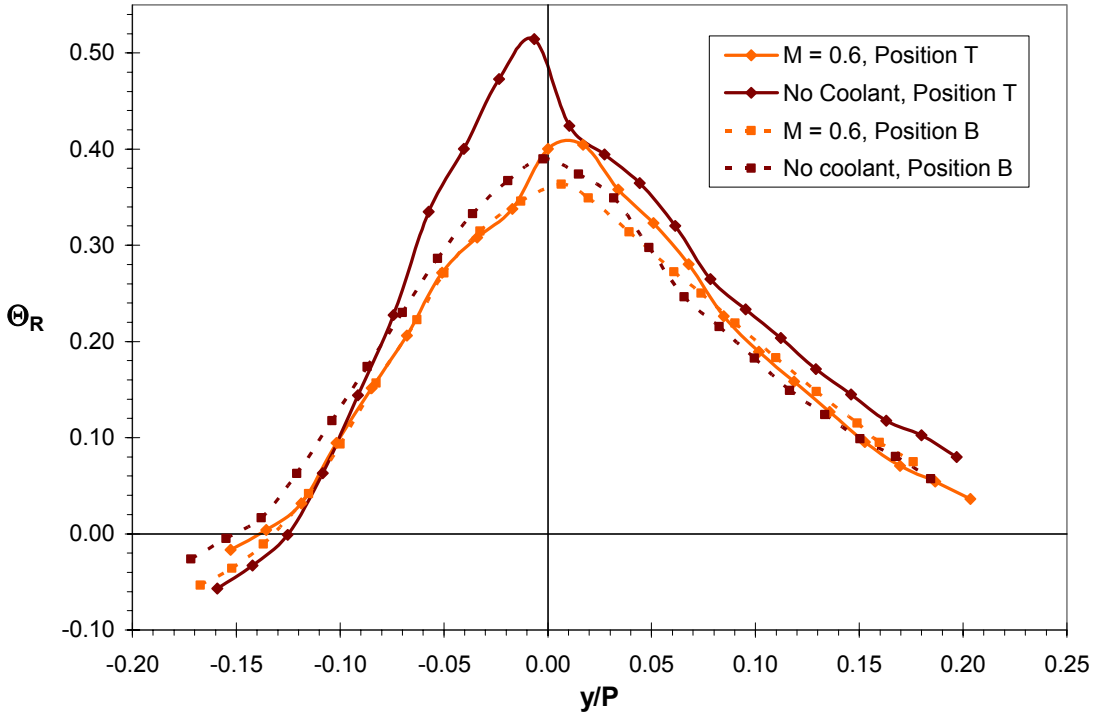

Figure **6.11: Normalized temperature ratio (Θ_R) profiles at Position T and Position B for the hot streak impacting the stagnation line without coolant and with pressure side blowing at M_{avg} = 0.6, high mainstream turbulence (Tu = 20%).**

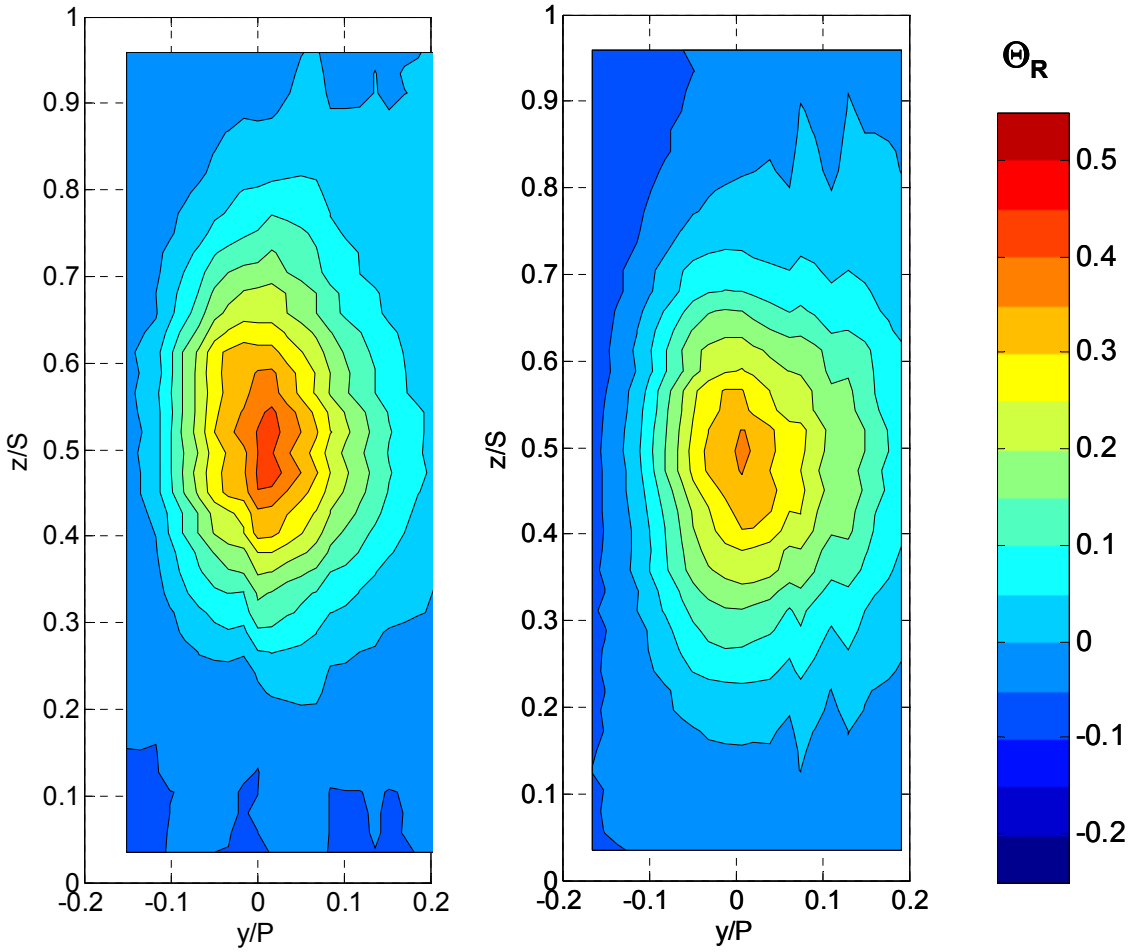

Figure **6.12: Normalized temperature ratio (Θ_R) contours for pressure side blowing at M_{avg} = 0.6, high mainstream turbulence (Tu = 20%) at:**

a. Position T (Trailing Edge)

b. Position B (Wake)

Chapter 7: Effects of Full Coverage Film Cooling on Hot Streak Reduction

7.1 Introduction

Given the substantial reductions in hot streak strength with cooling from the showerhead and suction sides individually, and the slight benefit from the pressure side, combining all three regions promised to provide significant cooling of the hot streak. Two sets of blowing ratios were used, adiabatic effectiveness optimum and above optimum blowing ratios as tested for the individual cooling regions separately. Blowing ratios for optimum levels were $M^* = 1.6$ for the showerhead, $M_{avg} = 0.7$ for the suction side, and $M_{avg} = 0.6$ for the pressure side. Above optimum blowing ratios were $M^* = 2.0$ for the showerhead, $M_{avg} = 1.0$ for the suction side, and $M_{avg} = 1.0$ for the pressure side. These blowing ratio sets are later referred to as the "standard" blowing ratios and "high" blowing ratios to prevent confusion between what is optimum for adiabatic effectiveness and optimum for hot streak reduction. Just as for the individual regions separately, experiments were run with coolant only and with the hot streak activated, and measurements were also taken both at the trailing edge (Position T) and in the wake at Position B. Measurements of coolant profiles were made at midspan at Positions P1', P2', S1', S2', and T' to study the evolution of the full coverage coolant profile.

An ancillary set of experiments were conducted with blowing ratios corresponding to an earlier experimental set of data to examine the effect of coolant on a hot streak positioned well away from the vane at a position of $0.4P$ to the suction side. The blowing ratios for this set of experiments were $M^* = 1.4$ for the showerhead, $M_{avg} = 1.0$ for the suction side, and $M_{avg} = 1.0$ for the pressure side.

Figure 7.1 shows the pressure side of the vane with the showerhead and pressure side coolant holes, while Figure 7.2 shows the film cooling schematic. A full description of the film cooling configuration may be found in §2.1.

7.2 Full Coverage Coolant Profiles at the Trailing Edge

Contours for full coverage film cooling at standard blowing ratios ($M^*_{showerhead} = 1.6$, $M_{avg,\ suction} = 0.7$, and $M_{avg,\ pressure} = 0.6$) are shown in Figure 7.3. A large mass of

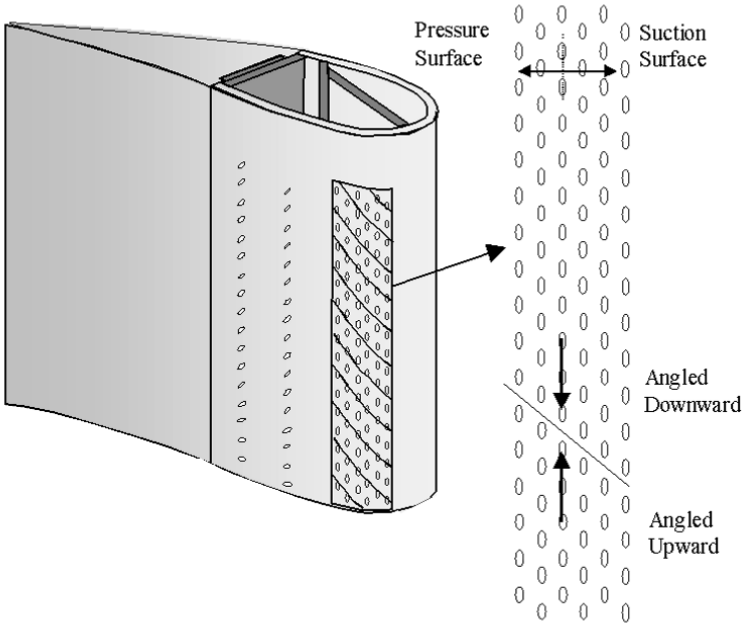

Figure 7.1: Showerhead and pressure side cooling holes.

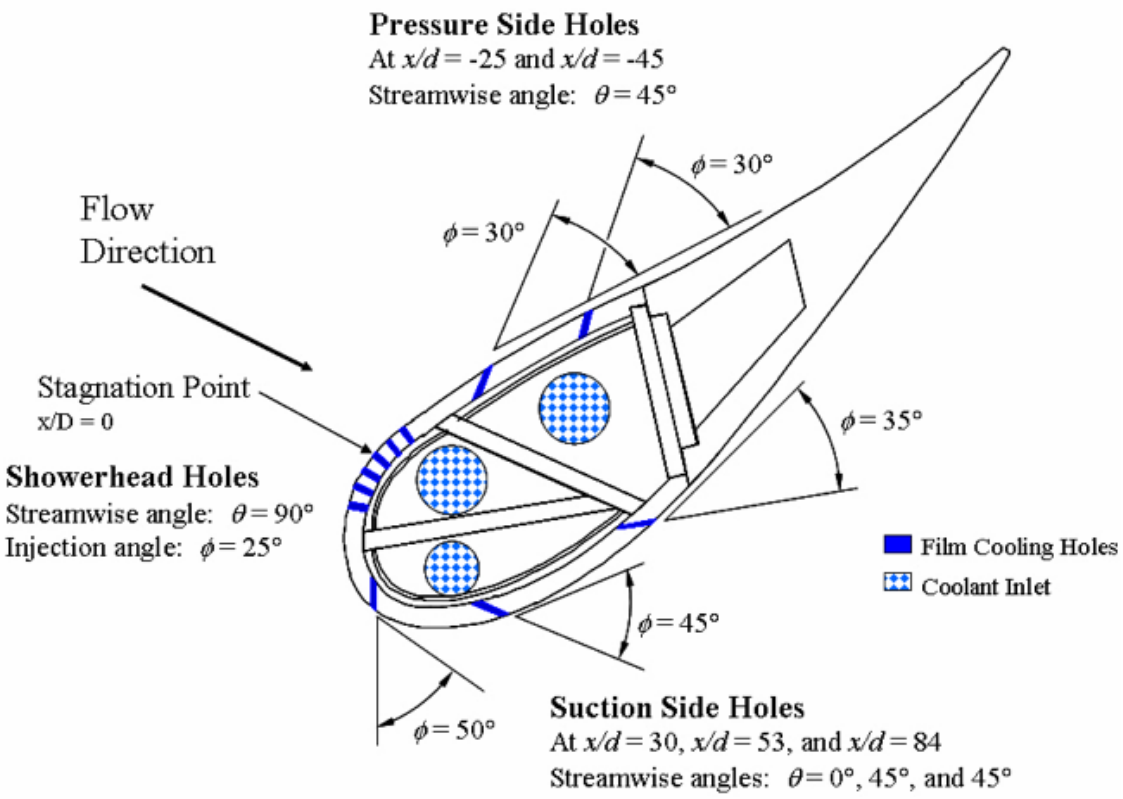

Figure 7.2: Schematic of film cooling hole configuration.

coolant was centered pitchwise at the trailing edge and well below midspan at about z/S = 0.3. This region of low coolant temperatures (below the Θ_R = -0.16 contour) stretched spanwise between 0.2 < z/S < 0.6 with a pitchwise width that varied between about 6 to 13d (0.06 to 0.12P). The peak coolant temperature of Θ_R = -0.42 coincided with the widest portion well below midspan at about 0.35S. Another large region of coolant was observed above midspan at about z/S = 0.7.

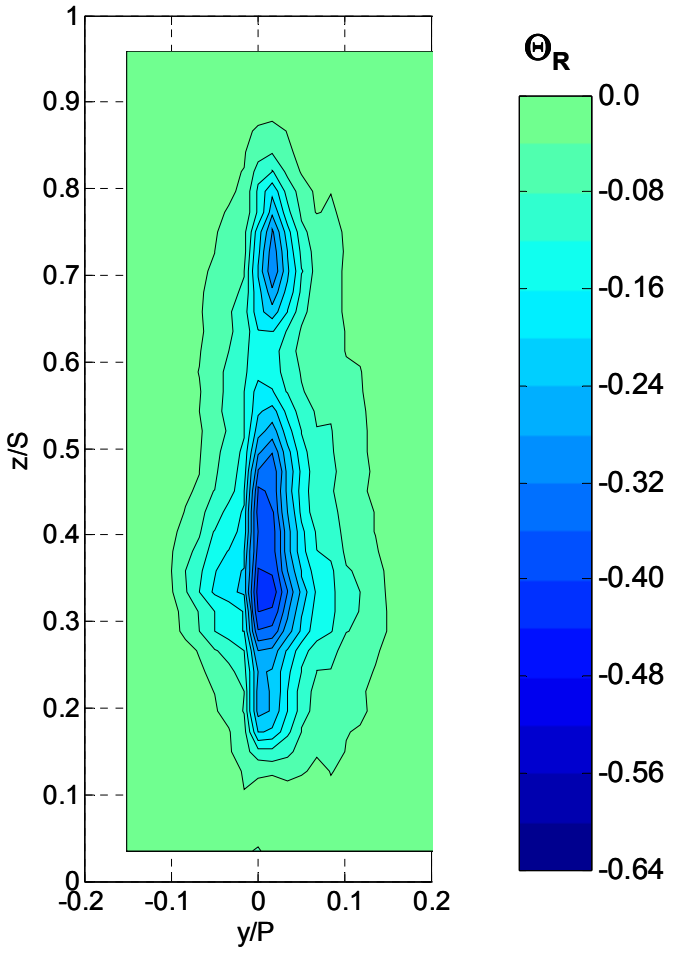

Figure 7.3: Normalized temperature ratio (Θ_R) coolant contours at Position T for full coverage blowing at $M^*_{showerhead}$ = 1.6, $M_{avg,\ suction}$ = 0.7, and $M_{avg,\ pressure}$ = 0.6, high mainstream turbulence (Tu = 20%).

A comparison of full coverage film cooling results with results from individual regions at the same blowing ratios in Figure 7.4 shows that full coverage blowing had significantly lower Θ_R levels. Figure 7.4 also demonstrates that full coverage contours retain the characteristics of both the showerhead and the suction side. The largest region

of coolant occurred due to the co-mingling of showerhead coolant from the crossover region (Figure 7.4a) and the tightly focused coolant profile of the suction side (Figure 7.4b). Even the slight performance of the pressure side can be seen in the widening of the contours to the pressure side of the trailing edge (y/P = 0.0). The upper area of coolant primarily came from the suction side, augmented by showerhead and pressure side coolant.

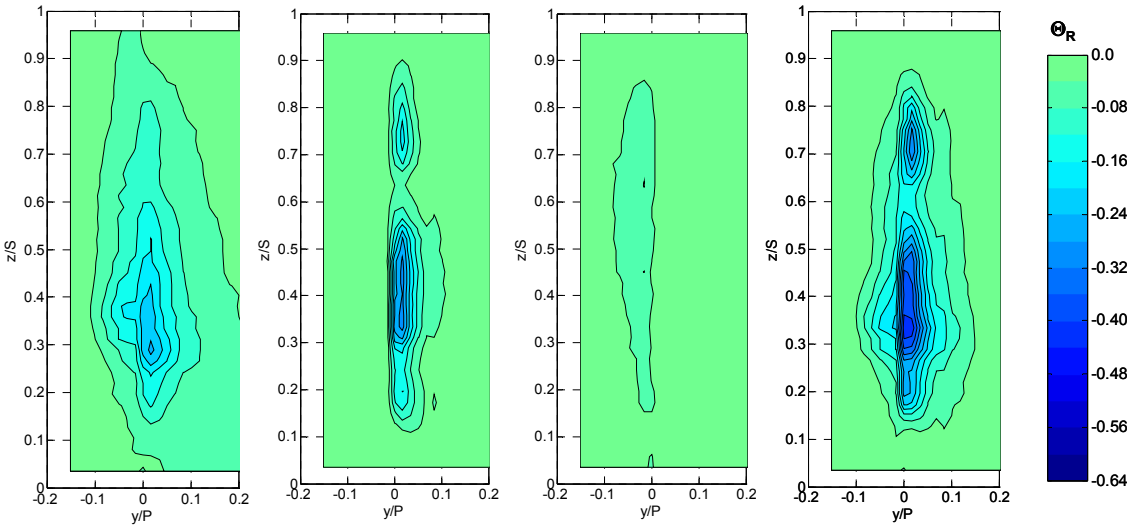

Figure 7.4: Normalized temperature ratio (Θ_R) coolant contours at Position T, high mainstream turbulence (Tu = 20%) for:

a. Showerhead blowing at M^* = 1.6
b. Suction side blowing at M_{avg} = 0.7
c. Pressure side blowing at M_{avg} = 0.6
d. Full coverage blowing at $M^*_{showerhead}$ = 1.6, $M_{avg,\ suction}$ = 0.7, and $M_{avg,\ pressure}$ = 0.6

Turning to midspan and peak profiles in Figure 7.5, the shape of the full coverage profiles becomes evident. Fortunately, at midspan where the hot streak was strongest, coolant levels were fairly low due to the combination of showerhead and suction side coolant. The coolant profile at midspan dipped to Θ_R = -0.32 with a 20% width of nearly 17d (0.15P) at Θ_R = -0.06. The spanwise position of peak coolant was well below midspan at 0.33S, which was about the same as for the showerhead (see §4.2). At this spanwise position, the coolant profile was nearly 50% wider than the midspan profile and peaked more than 35% lower at Θ_R = -0.43. This suggests a very large potential for hot

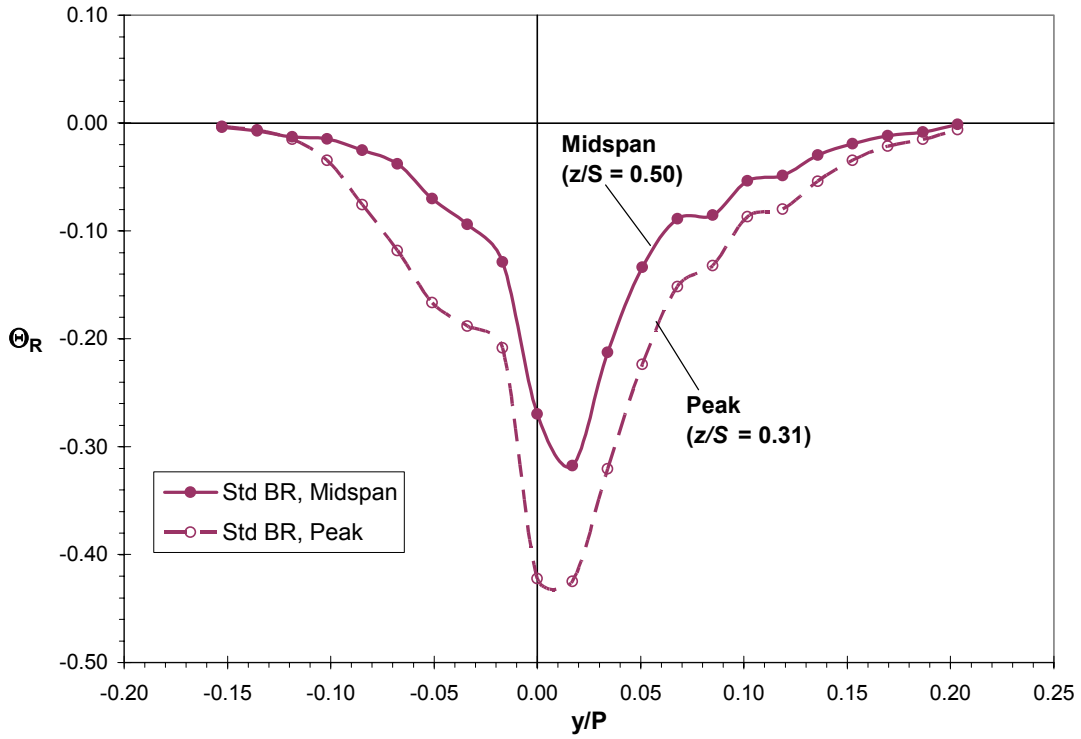

Figure 7.5: Normalized temperature ratio (Θ_R) coolant profiles at Position T at midspan (z/S = 0.50) and at the spanwise position of the peak coolant level (z/S = 0.31) at standard blowing ratios ($M^*_{showerhead}$ = 1.6, $M_{avg,\ suction}$ = 0.7, and $M_{avg,\ pressure}$ = 0.6), high mainstream turbulence (Tu = 20%).

streak reduction if the center of the hot streak were positioned at approximately 1/3 span. For the current spanwise position of the hot streak, these results suggest that positioning the hot streak just to the suction side of vane would provide a slight benefit as compared to the stagnation line at y/P = 0.0, since the peak of the coolant profile was at y/P = 0.02. Recalling the discussion of vane effects without film cooling (§3.5), a hot streak pitch position of y/P = 0.022 was found to have the lowest peak, although the difference between this position and the stagnation line was small (about Θ_R = 0.03). As such, full coverage film cooling could be expected to reduce the hot streak even more with the hot streak positioned slightly to the suction side.

7.3 Effect of Full Coverage Film Cooling on Hot Streak Reduction

The effect of full coverage film cooling on the hot streak was considerable. As shown in Figure 7.6, only a small portion of the hot streak remained at significant levels.

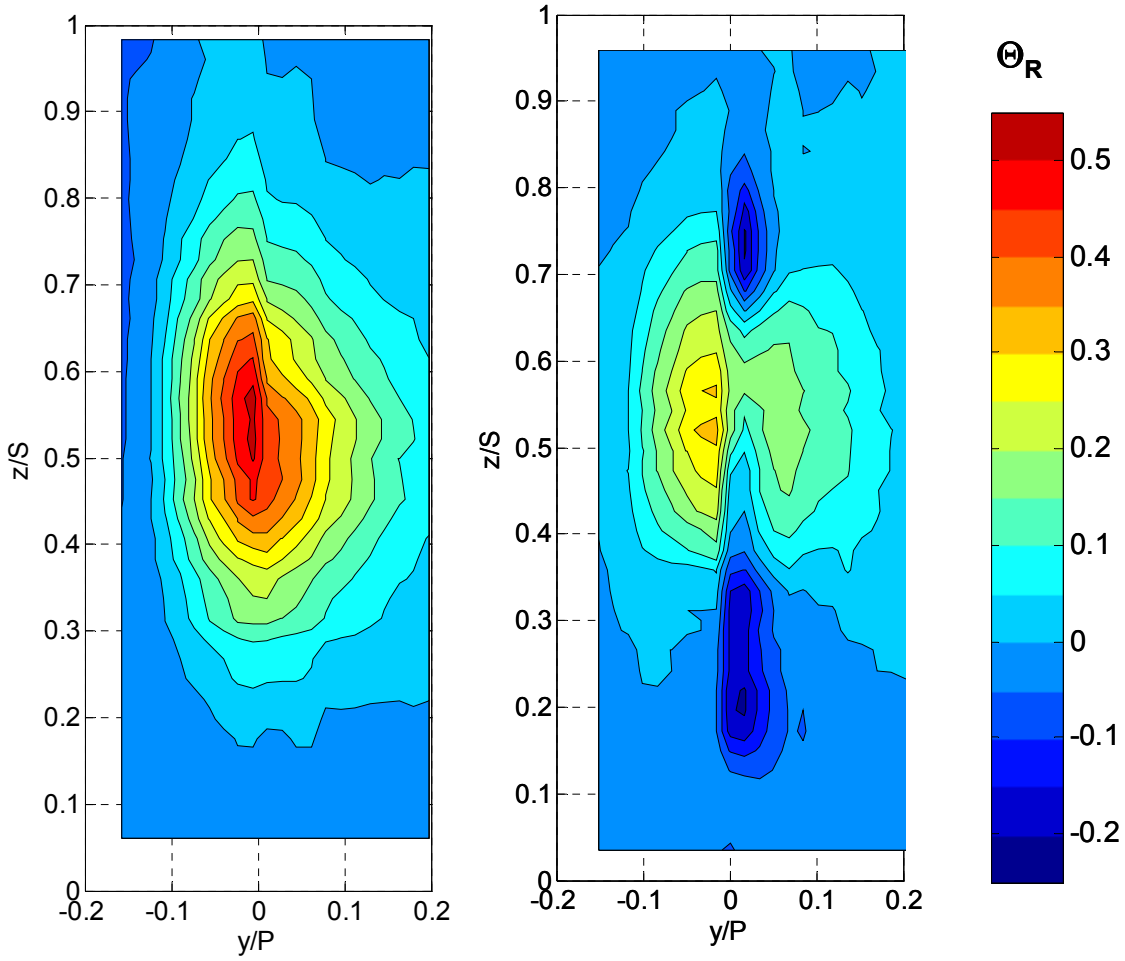

a. **b.**

Figure 7.6: Normalized temperature ratio (Θ_R) contours at Position T with the hot streak at the stagnation line, high mainstream turbulence (Tu = 20%):

a. No coolant

b. Full coverage blowing at $M^*_{showerhead}$ = 1.6, $M_{avg,\ suction}$ = 0.7, and $M_{avg,\ pressure}$ = 0.6

The reduced hot streak peaked at Θ_R = 0.33 just to the pressure side of the vane at midspan, with a small region surrounding the peak at a contour level of Θ_R = 0.30. Overall, the reduction in the hot streak peak was 35% compared with no film cooling, while the reduction in the hot streak with respect to the reference position (Position A) upstream of the vane was 67%. Large amounts of excess coolant appeared above and below the hot streak to the suction side well below and above midspan, while the hot streak on the suction side was reduced to Θ_R = 0.19.

Looking at midspan profiles of the hot streak with full coverage film cooling in Figure 7.7, it is clear that additional coolant on the pressure side would help diminish the remainder of the hot streak on that side. On the suction side, the peak at midspan was Θ_R = 0.17, while on the pressure side it was more than 70% higher at Θ_R = 0.29. Coolant also had an effect on the hot streak much further away from the vane on the suction side than on the pressure side.

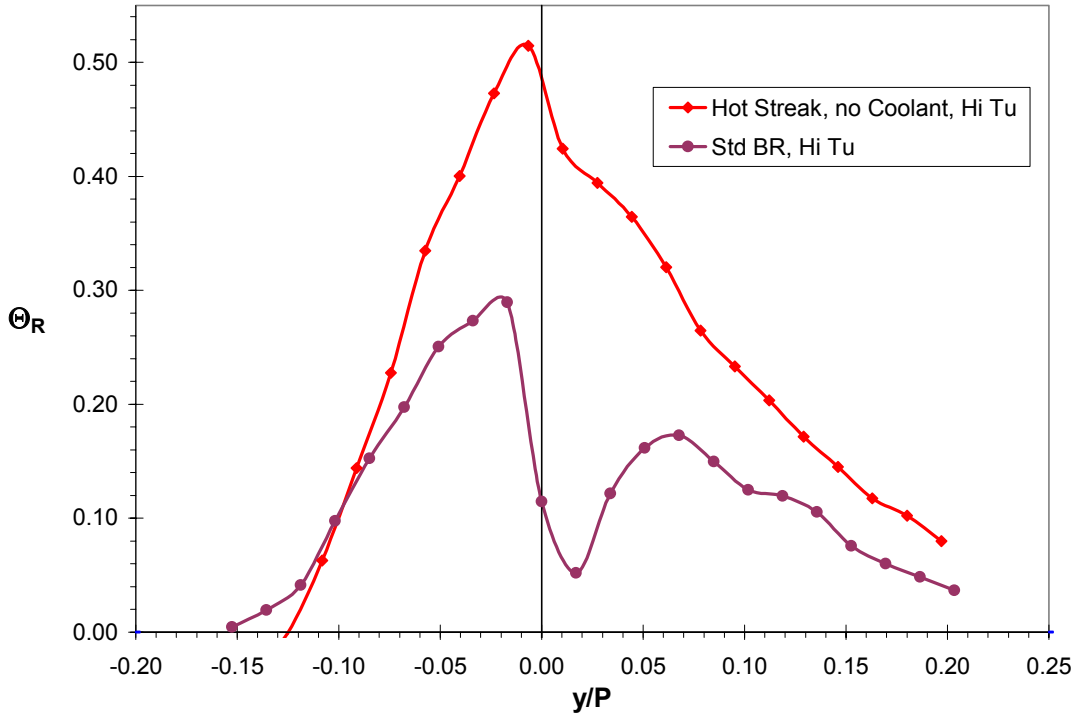

Figure 7.7: Normalized temperature ratio (Θ_R) profiles at Position T for the hot streak impacting the stagnation line without coolant and with full coverage blowing at $M^*_{showerhead}$ = 1.6, $M_{avg,\ suction}$ = 0.7, and $M_{avg,\ pressure}$ = 0.6, high mainstream turbulence (Tu = 20%).

Figure 7.8 demonstrates how much additional coolant was available at the position of the coolant profile peak (0.33S). The uncooled hot streak profile for this spanwise position is also shown in the figure. Since there was very little hot streak at this location, the film cooled hot streak profile reached at magnitude of Θ_R = -0.17, just to the suction side of the trailing edge.

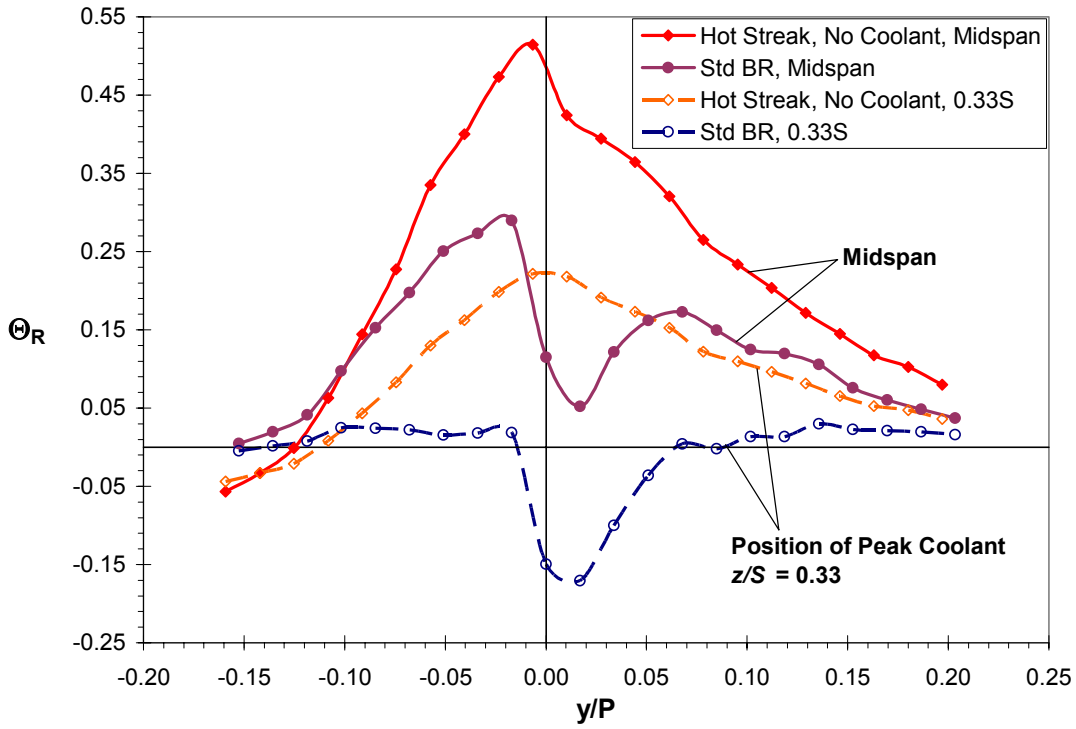

Figure 7.8: Normalized temperature ratio (Θ_R) profiles at Position T at midspan (z/S = 0.50) and at the spanwise position of the peak coolant level (z/S = 0.33) for the hot streak impacting the stagnation line without coolant and with full coverage blowing at $M^*_{showerhead}$ = 1.6, $M_{avg,\ suction}$ = 0.7, and $M_{avg,\ pressure}$ = 0.6, high mainstream turbulence (Tu = 20%).

7.4 Effect of Varying Full Coverage Blowing Ratios

As mentioned previously, two sets of full coverage blowing ratios were tested, corresponding to the optimum (standard) and above optimum (high) blowing ratios with respect to adiabatic effectiveness. The high blowing ratios had 35% more total mass flow rate than the standard blowing ratios. With respect to the approach flow to the vane, total coolant mass flow rates were 1.65% and 2.25% of the core flow for one vane pitch. Lower than optimum blowing ratios were not tested in combination since they would not provide nearly as high a level of hot streak reduction, and due to the difficulty of achieving stable conditions with all regions blowing.

Figure 7.9 compares coolant profiles for standard blowing ratios ($M^*_{showerhead}$ = 1.6, $M_{avg,\ suction}$ = 0.7, and $M_{avg,\ pressure}$ = 0.6) and high blowing ratios ($M^*_{showerhead}$ = 2.0, $M_{avg,\ suction}$ = 1.0, and $M_{avg,\ pressure}$ = 1.0). While the shapes of the contours were similar

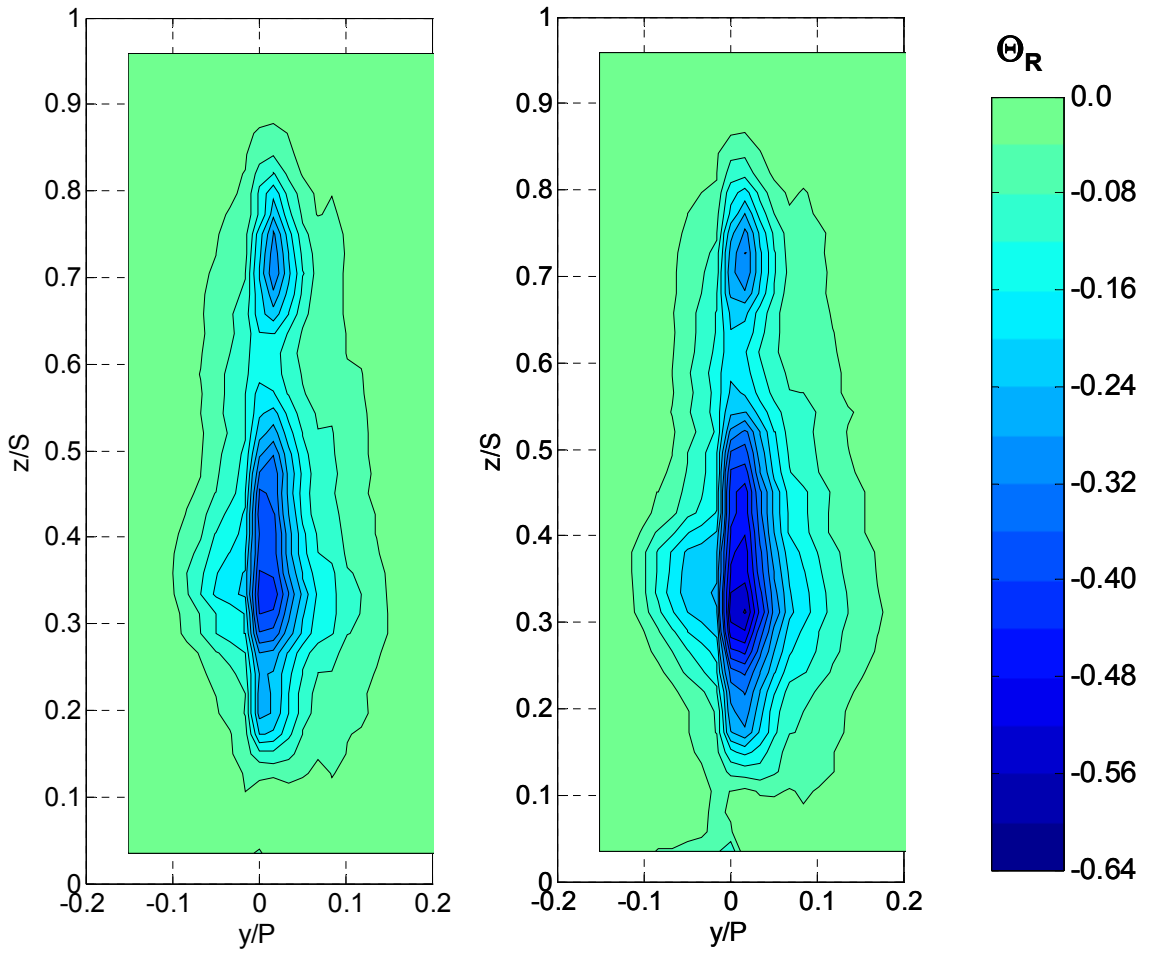

Figure 7.9: Normalized temperature ratio (Θ_R) coolant contours at Position T, high mainstream turbulence (Tu = 20%) for full coverage blowing at:

a. $M^*_{showerhead}$ = 1.6, $M_{avg,\ suction}$ = 0.7, and $M_{avg,\ pressure}$ = 0.6

b. $M^*_{showerhead}$ = 2.0, $M_{avg,\ suction}$ = 1.0, and $M_{avg,\ pressure}$ = 1.0

with a large area of coolant centered below midspan and a small area of coolant above midspan, the main difference was the magnitude of the peak and size of the areas of coolant at a given contour level. For optimum blowing ratios, the peak was Θ_R = -0.43, while the peak for above optimum blowing ratios was almost 40% lower at Θ_R = -0.56. In the small area of coolant above midspan, the magnitude of the coolant peak only increased slightly with increased blowing ratio. With increased showerhead blowing ratio in Chapter 4, this region of coolant was relatively unchanged with increasing blowing ratio, likely due to the angle of showerhead holes which directed coolant

downward. With increased momentum at higher blowing ratios, the significant increases in coolant levels were only observed below 0.6*S* (see Figure 4.6). Therefore the primary source of increased coolant levels was the suction side, where small increases were observed for the upper coolant area with an increase in blowing ratio from $M_{avg,\ suction}$ = 0.7 to 1.0 (see Figure 5.6).

Midspan and peak coolant profiles are shown in Figure 7.10 where the effect of increased blowing is immediately evident. A marked increase in cooling potential occurred for high blowing ratios, where the peak decreased nearly 25%, from Θ_R = -0.32 to -0.38. As discussed for showerhead and full coverage film cooling, the peak coolant level well below midspan had a large potential for hot streak reduction. At a maximum of Θ_R = -0.56 for the highest set of blowing ratios, the coolant would have the potential to more than eliminate the hot streak peak (with a value of Θ_R = 0.51) if it were positioned correctly.

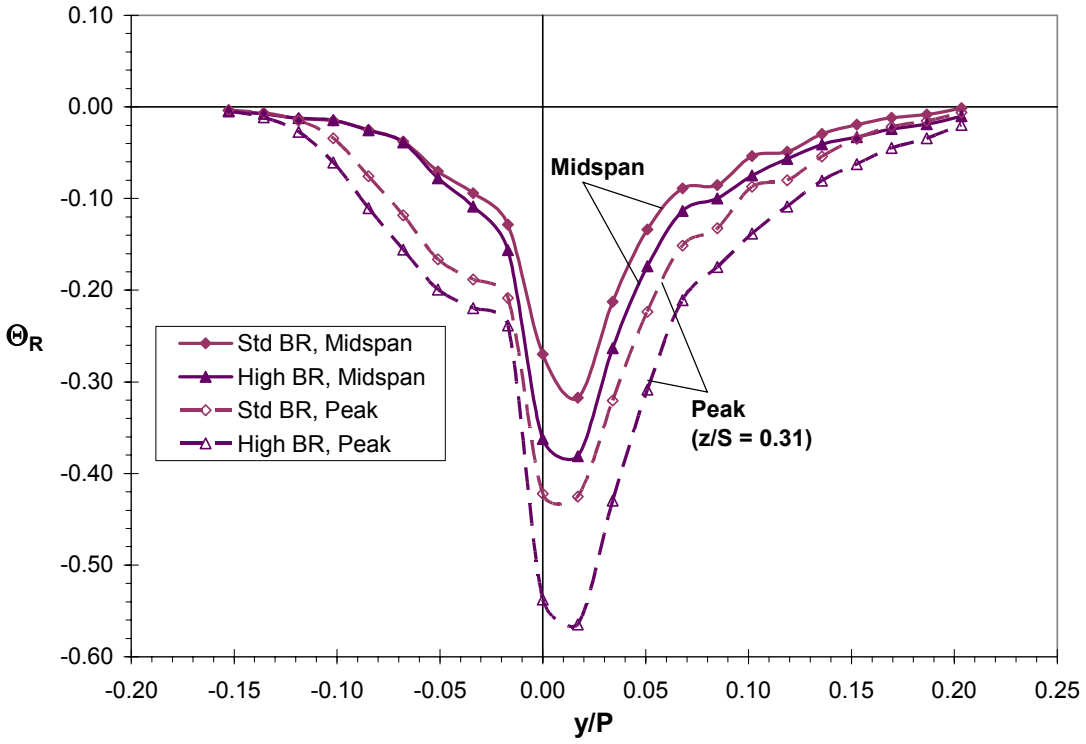

Figure 7.10: Normalized temperature ratio (Θ_R) coolant profiles at Position T at midspan (z/S = 0.50) and at the spanwise position of the peak coolant level (z/S = 0.31) for adiabatic effectiveness optimum blowing ratios ($M^*_{showerhead}$ = 1.6, $M_{avg,\ suction}$ = 0.7, and $M_{avg,\ pressure}$ = 0.6) and above optimum blowing ratios ($M^*_{showerhead}$ = 2.0, $M_{avg,\ suction}$ = 1.0, and $M_{avg,\ pressure}$ = 1.0), high mainstream turbulence (Tu = 20%).

Contour plots in Figure 7.11 show the reduction in the hot streak due to full coverage blowing, with increased coolant levels above and below the hot streak with increased blowing ratio. There was also a decrease in the size and magnitude of the remaining hot streak. At above optimum blowing ratios the peaks were reduced by at least one contour level ($\Delta\Theta_R$ = 0.05). Significant decreases in the hot streak peak were not observed, primarily due to the nature of the individual coolant regions. The remaining hot streak was on the pressure side of the trailing edge, which was the case with showerhead blowing only. As shown in Figure 4.8 previously, increasing the showerhead blowing ratio had little effect on the pressure side of the hot streak at midspan. This was due to the same effect mentioned with regard to Figure 7.9; an increase in the showerhead blowing ratio led to higher coolant momentum resulting in higher coolant levels below midspan (also shown clearly in Figure 4.7). This additional

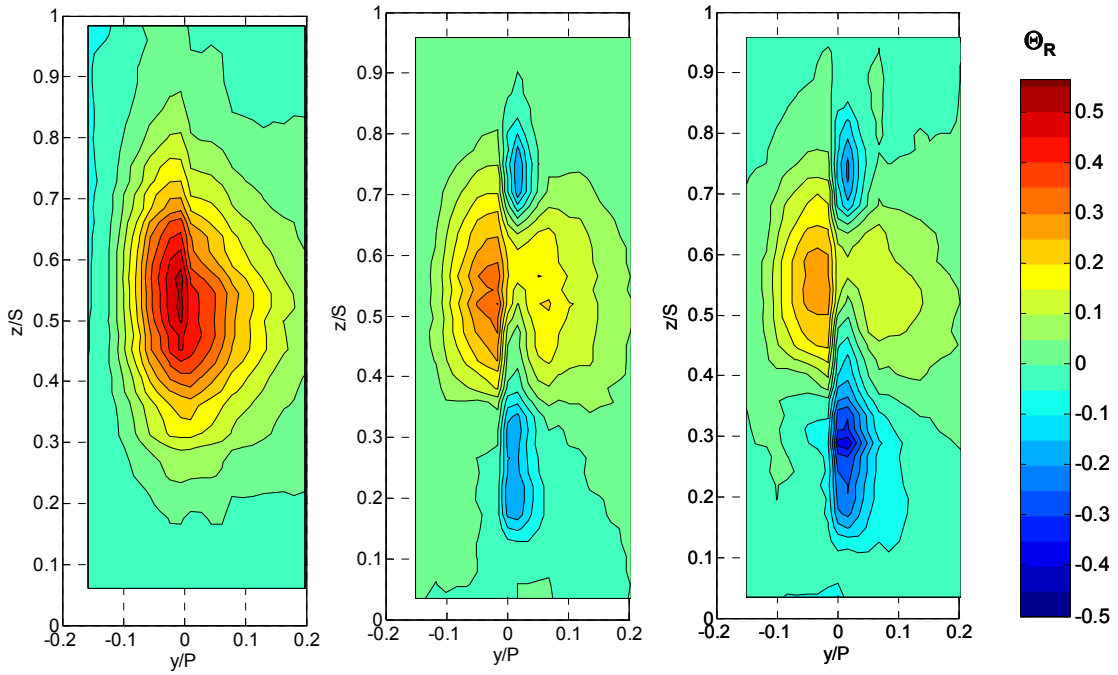

Figure 7.11: Normalized temperature ratio (Θ_R) contours at Position T with the hot streak at the stagnation line, high mainstream turbulence (Tu = 20%):

a. No coolant

b. Full coverage blowing at $M^*_{showerhead}$ = 1.6, $M_{avg,\ suction}$ = 0.7, and $M_{avg,\ pressure}$ = 0.6

c. Full coverage blowing at $M^*_{showerhead}$ = 2.0, $M_{avg,\ suction}$ = 1.0, and $M_{avg,\ pressure}$ = 1.0

coolant contributed to the considerable drop in fluid temperature at about 0.3*S*, from Θ_R = -0.21 to Θ_R = -0.38. As discussed in Chapter 6, pressure side coolant had very little impact on hot streak attenuation, while suction side blowing had a substantial effect, but only to the suction side of the trailing edge as shown in Figure 7.11. This helps to explain why the significant increase in mass flow did not have a correspondingly large effect on the hot streak peak value.

At midspan, in Figure 7.12, a considerable decrease in the hot streak was apparent to the suction side where values dropped to mainstream temperatures. As shown in the contour plots of Figure 7.11, the remaining peak was on the pressure side where the meager amount of pressure side coolant was insufficient to augment showerhead coolant and reduce this portion of the hot streak further. A smaller peak was observed on the suction side, well away from the vane wall where the hot streak was less

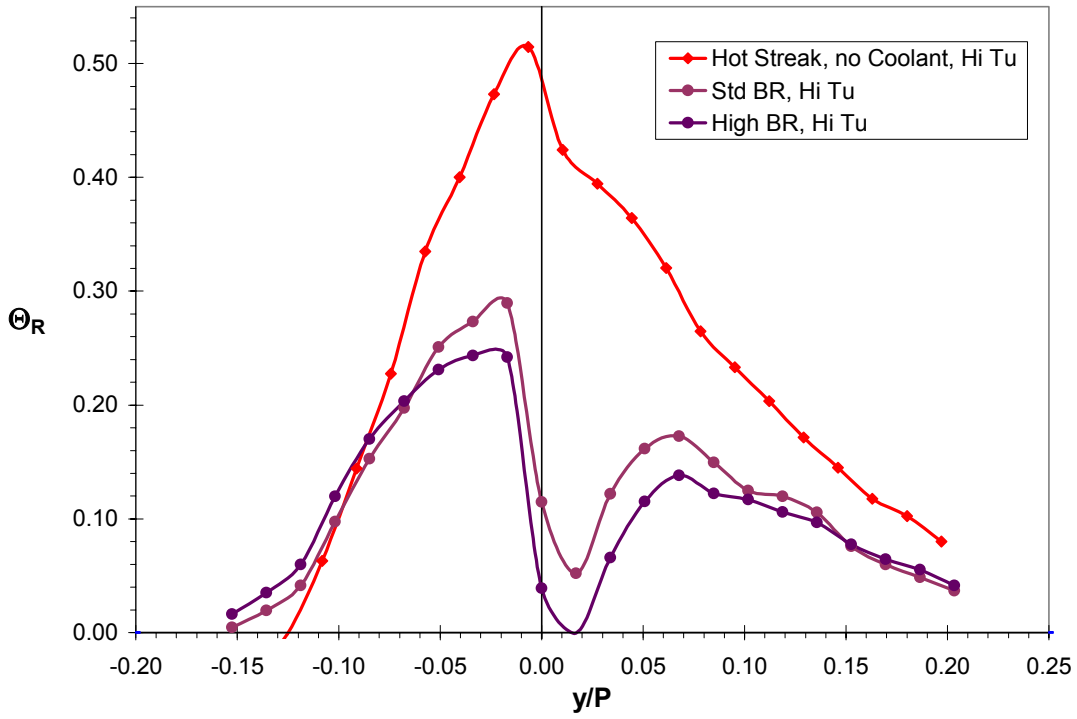

Figure 7.12: Normalized temperature ratio (Θ_R) profiles at Position T for the hot streak impacting the stagnation line without coolant and with full coverage blowing at adiabatic effectiveness optimum blowing ratios ($M^*_{showerhead}$ = 1.6, $M_{avg,\ suction}$ = 0.7, and $M_{avg,\ pressure}$ = 0.6) and above optimum blowing ratios ($M^*_{showerhead}$ = 2.0, $M_{avg,\ suction}$ = 1.0, and $M_{avg,\ pressure}$ = 1.0), high mainstream turbulence (*Tu* = 20%).

affected, due to the tightly focused nature of the suction side coolant. Both peaks were reduced by an additional 15% to 20% with the higher blowing ratios. Further increasing the blowing ratios would likely reduce these peaks even more, however a great deal more coolant would be required to eliminate the peak on the pressure side. Based on observations of the nature of suction side coolant distributions, the current suction side coolant hole configuration would be unlikely to permit elimination of the peak to the suction side since suction side coolant tended to stay tightly focused near the wall.

7.5 Evolution of the Full Coverage Coolant Profile

To investigate the evolution of the full coverage coolant profile, standard blowing ratios of $M^*_{showerhead} = 1.6$, $M_{avg,\ suction} = 0.7$, and $M_{avg,\ pressure} = 0.6$ were used. These were also the blowing ratios used for individual regions, so direct comparisons could be made between full coverage and individual region profiles. Measurements were taken along the vane at Positions P1', P2', S1', S2', and T' as shown in the schematic in Figure 7.13 to track the development of the trailing edge profile and explore the interactions of the three coolant regions.

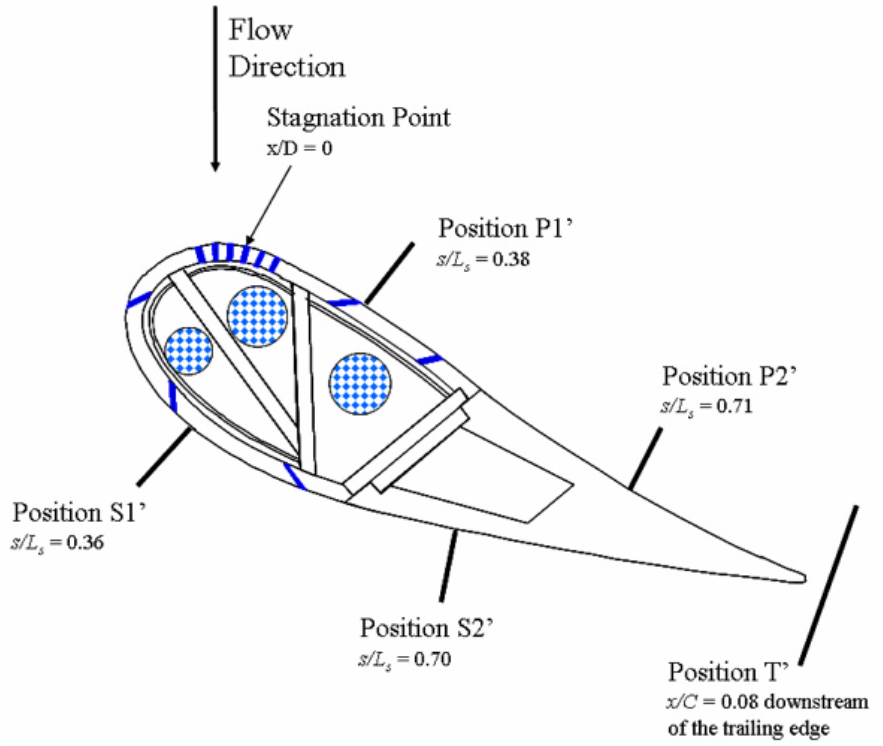

Figure 7.13: Schematic of single thermocouple probe measurement positions for full coverage film cooling.

Figure 7.14 presents a comparison of the film cooling profiles from individual regions with the full coverage profile, all at standard blowing ratios. The full coverage profile derived its width and peak primarily from the showerhead and suction side as previously discussed, while the pressure side added a small amount. However, it was not clear why the suction side profile and full coverage profile had similar peak magnitudes, while the full coverage profile was wider than either the suction side or showerhead profiles. An investigation into the evolution of the full coverage trailing edge coolant profile and its relation to individual region profiles provided some clarity into these issues.

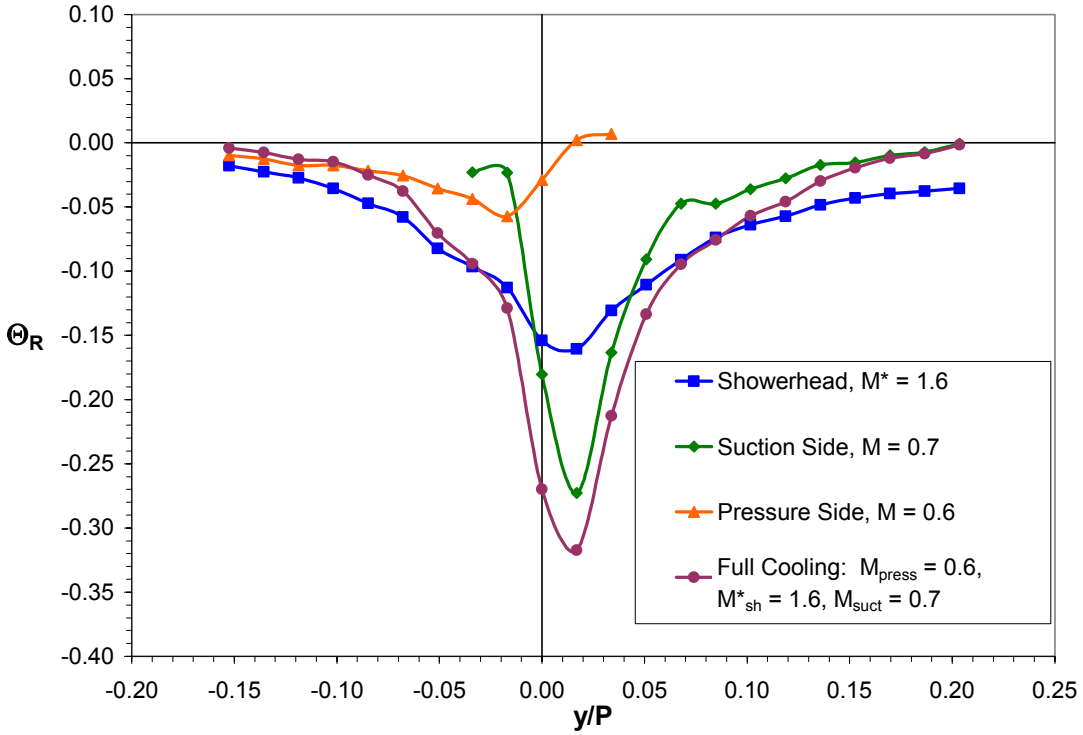

Figure 7.14: Normalized temperature ratio (Θ_R) coolant profiles at Position T at midspan (z/S = 0.50) comparing showerhead blowing (M^* = 1.6), suction side blowing (M_{avg} = 0.7), pressure side blowing (M_{avg} = 0.6), and full coverage blowing ($M^*_{showerhead}$ = 1.6, $M_{avg,\ suction}$ = 0.7, and $M_{avg,\ pressure}$ = 0.6), high mainstream turbulence (Tu = 20%).

Beginning with full coverage coolant profiles at Positions P1', P2', S1', S2', and T in Figure 7.15, the development of the trailing edge profile at Position T is demonstrated fairly well, although there was one issue that required further explanation. The profile at Position P1' had an extremely low peak on the wall, especially in

comparison with the profile at Position P2'. This was caused by the positioning of the thermocouple probe, which was directly downstream (within 1*d*) of the coolant hole exit of the 1st row of pressure side coolant holes as shown in Figure 7.13. Due to this, the profile was much steeper and had a much lower peak. The pressure side profile alone peaked at Θ_R = -0.42 for a blowing ratio of M_{avg} = 0.6, so it was not surprising to observe a value well below that with pressure side and showerhead blowing. However, the profile at Position P2' revealed how the coolant profile appeared well away from the coolant holes with a peak at the wall of Θ_R = -0.39. Referring to the schematic in Figure 7.13, Position S1' was located downstream of the 2nd row of suction side holes and was also positioned closer to the 2nd suction side row than Position S2' was to the 3rd row. As a result, the downstream profile (Position S2') was about twice as broad and had lower values at positions farther from the wall. For example, at about 2*d* from the vane wall, the Θ_R value in the Position S2' profile had about twice the magnitude of that in the

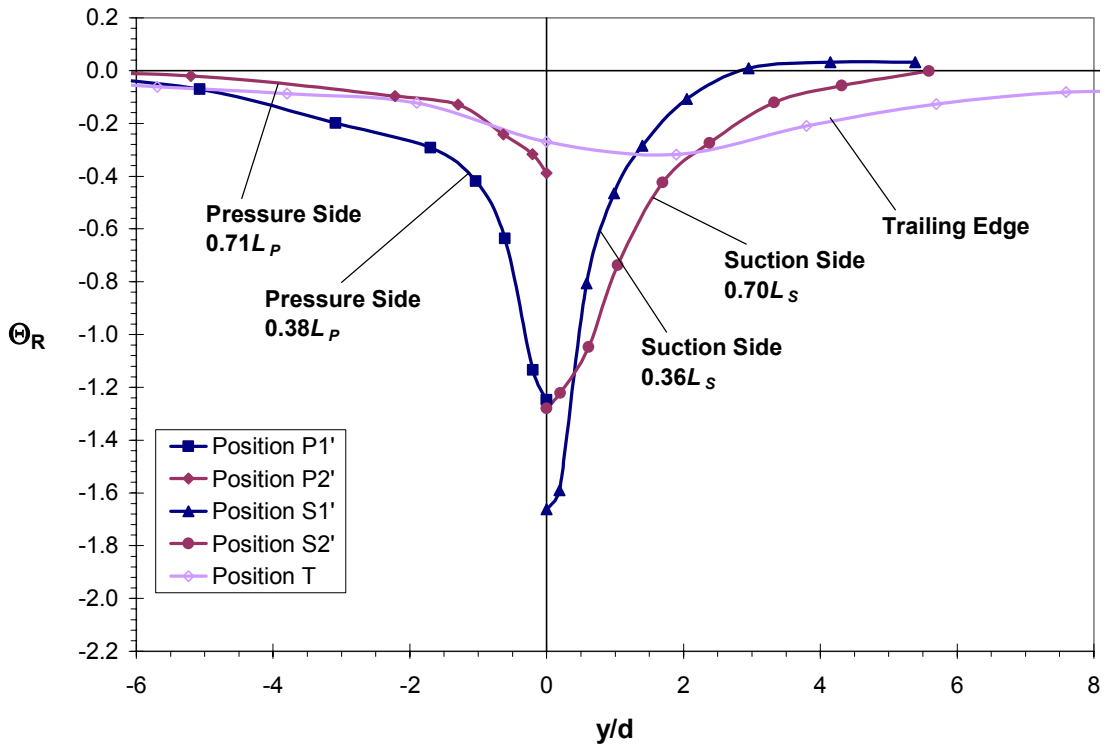

Figure 7.15: Profiles of full coverage coolant at Positions P1', P2', S1', S2', and T' at midspan (z = 0.5S), for full coverage blowing at $M^*_{showerhead}$ = 1.6, $M_{avg,\ suction}$ = 0.7, and $M_{avg,\ pressure}$ = 0.6, high mainstream turbulence (Tu = 20%).

Position S1' profile. The Position T profile peaked on the suction side at Θ_R = -0.32, while on the pressure side, the Position T profile was similar to the Position P2' profile upstream, but without as strong a temperature gradient next to the wall. From these profiles, it appears that there was considerable decay of the Position S2' profile up to the trailing edge. This was also observed with the hot streak, as shown in Figure 3.30, and with the showerhead coolant profiles in Figure 4.9. Suction side profiles comparing the Position S2' profile in Figure 5.10 with the trailing edge profile in Figure 5.3 also showed this trend. Although the decrease in magnitude was larger for the full coverage profiles, the gradient was also steeper near the wall than for the other three cases.

A comparison of profiles for full coverage film cooling with profiles from individual coolant regions provided some explanation of how the shape and magnitude of the full coverage profiles at Positions P1', P2', S1', and S2' came about. At Position P1' in Figure 7.16, as mentioned before, the pressure side dominated due to the location of

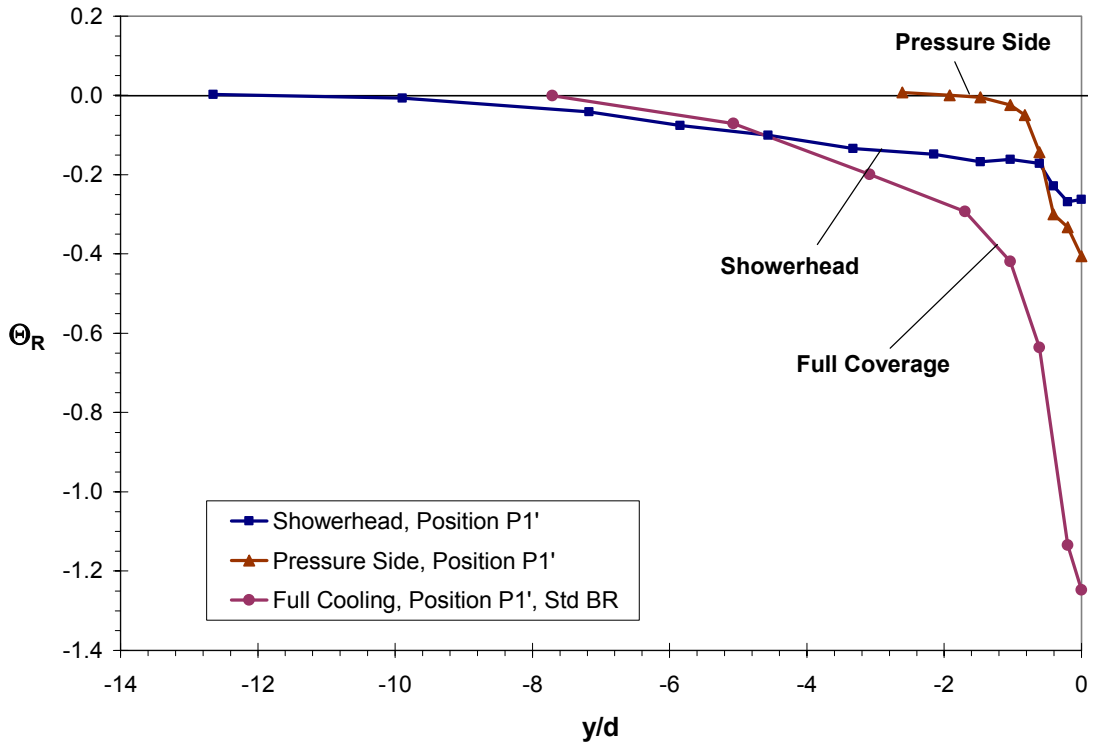

Figure 7.16: Profiles of full coverage coolant at Positions P1' at midspan (z = 0.5S), comparing showerhead blowing (M^* = 1.6), suction side blowing (M_{avg} = 0.7), pressure side blowing (M_{avg} = 0.6), and full coverage blowing ($M^*_{showerhead}$ = 1.6, $M_{avg,\ suction}$ = 0.7, and $M_{avg,\ pressure}$ = 0.6), high mainstream turbulence (Tu = 20%).

the thermocouple probe directly behind a 1st row pressure side coolant hole. Since the thermocouple probe was so close to the coolant hole exit, differences in the full coverage profile and the pressure side profile were likely due to slight differences in the spanwise position of the thermocouple probe, since a positioning error in the spanwise direction of less than 0.5 mm would put the probe into or away from the centerline of the coolant jet. While the showerhead contribution was a thick profile extending well away from the wall, the pressure side coolant provided the steep profile near the wall, resulting in the very sharply peaked but wide profile for full coverage cooling.

At Position P2' (Figure 7.17), the diffused pressure side profile contributed less at positions farther from the wall, but had a peak at about the same magnitude as the showerhead. Still, an additive combination of the two individual profiles gave a good approximation of the full coverage profile for positions away from the wall.

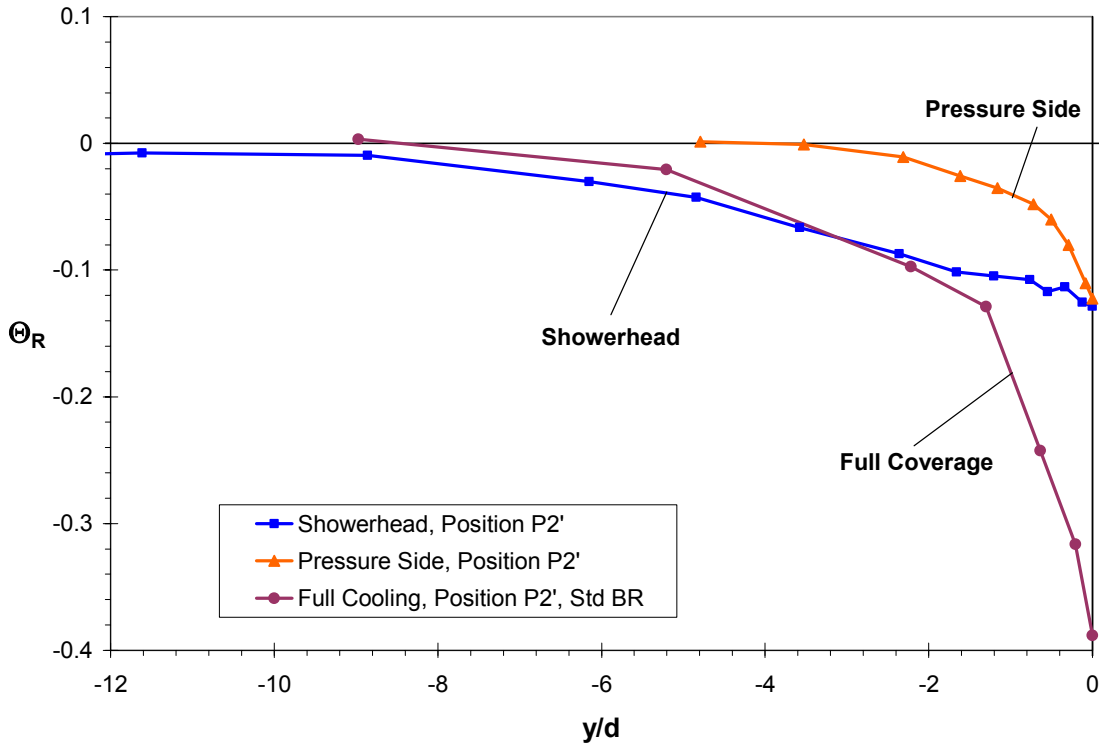

Figure 7.17: Profiles of full coverage coolant at Positions P2' at midspan ($z = 0.5S$), comparing showerhead blowing ($M^* = 1.6$), suction side blowing ($M_{avg} = 0.7$), pressure side blowing ($M_{avg} = 0.6$), and full coverage blowing ($M^*_{showerhead} = 1.6$, $M_{avg,\ suction} = 0.7$, and $M_{avg,\ pressure} = 0.6$), high mainstream turbulence ($Tu = 20\%$).

For Position S1', in Figure 7.18, the full coverage profile had a much lower value at the wall than the additive combination of the suction side and showerhead profiles. With blowing from individual regions, the strong gradient near the wall was reduced quickly, as this fluid was in a thin layer near the vane surface. It is likely that the showerhead coolant acted like a buffer layer, protecting suction side coolant from the mainstream, and permitted the coolant temperatures very near to the wall, i.e. much less than 0.5*d*, to remain much lower. By about 0.5*d* from the wall, the additive combination of the suction side and showerhead coolant was about the same as the magnitude of the full coverage coolant. Farther away the comparison was even better.

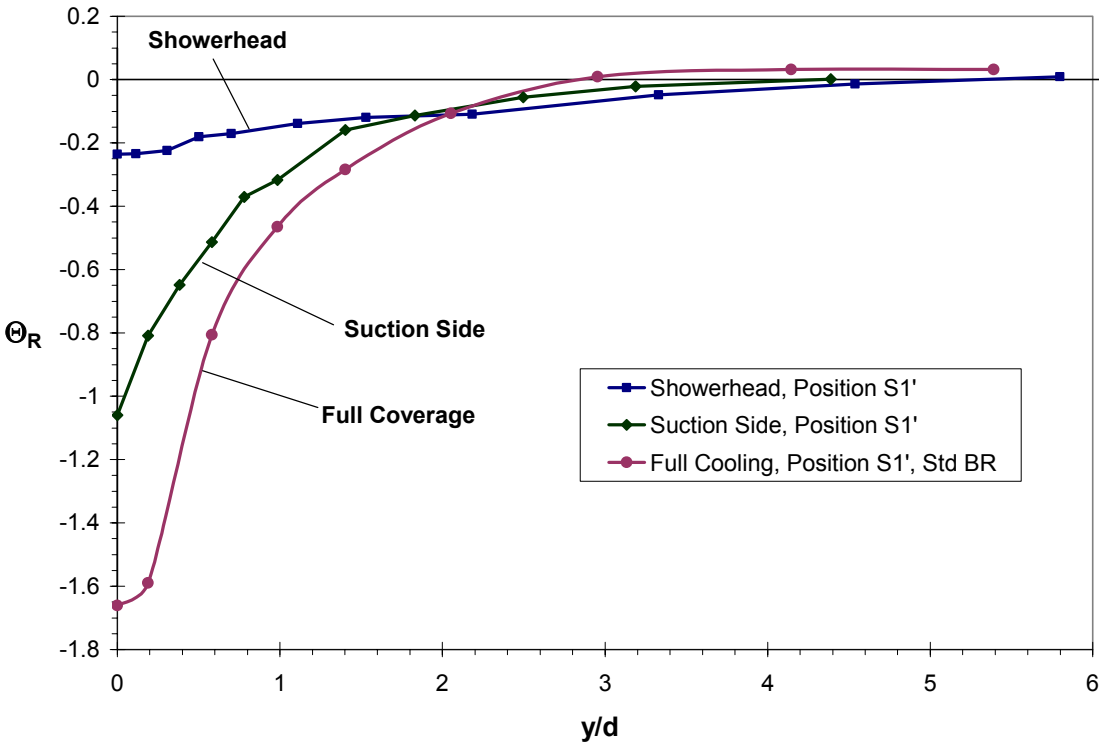

Figure 7.18: Profiles of full coverage coolant at Positions S1' at midspan (z = 0.5S comparing showerhead blowing (M^* = 1.6), suction side blowing (M_{avg} = 0.7), pressure side blowing (M_{avg} = 0.6), and full coverage blowing ($M^*_{showerhead}$ = 1.6, $M_{avg,\ suction}$ = 0.7, and $M_{avg,\ pressure}$ = 0.6), high mainstream turbulence (Tu = 20%).

At Position S2', the same trend was observed, as shown in Figure 7.19. Again, the full coverage profile had lower values near to the wall, up to about 1*d*. At this position the coolant also spread farther from the wall as previously shown in Figure 7.15.

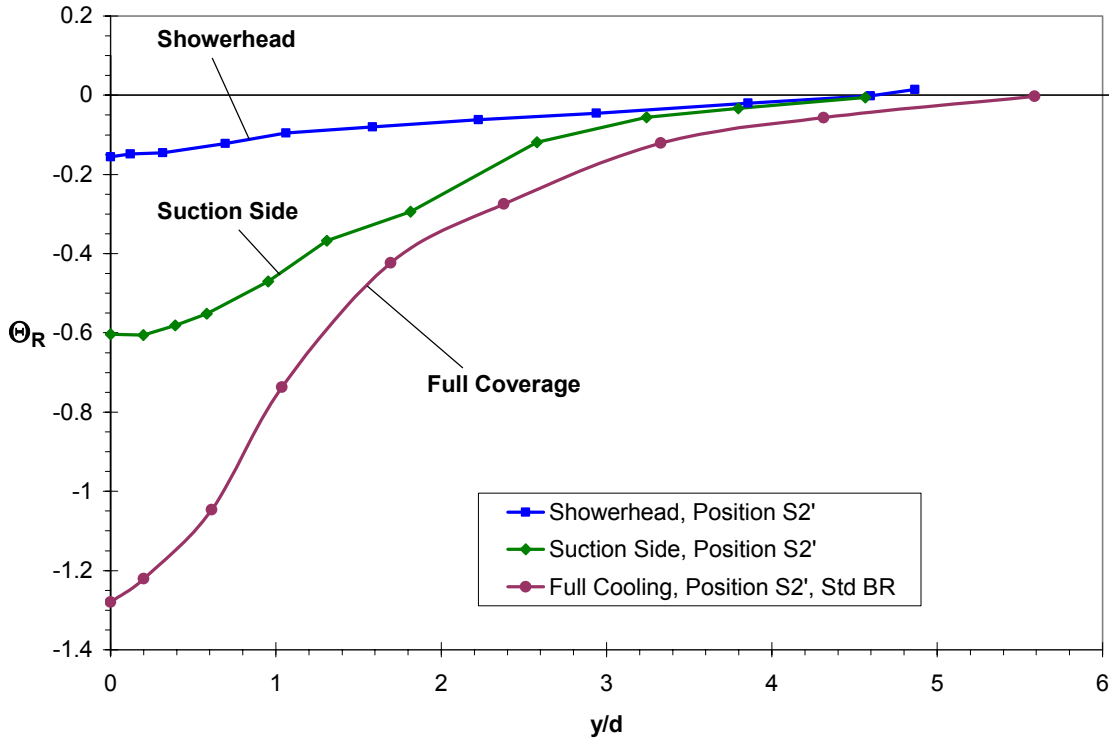

Figure 7.19: Profiles of full coverage coolant at Positions S2' at midspan (z = 0.5S), comparing showerhead blowing (M^* = 1.6), suction side blowing (M_{avg} = 0.7), pressure side blowing (M_{avg} = 0.6), and full coverage blowing ($M^*_{showerhead}$ = 1.6, $M_{avg,\ suction}$ = 0.7, and $M_{avg,\ pressure}$ = 0.6), high mainstream turbulence (Tu = 20%).

7.6 Turbulence Effects in the Stator/Rotor Axial Gap with Full Coverage Film Cooling

The contrast between contour plots at the trailing edge and at Position B in the wake for full coverage film cooling in Figure 7.20 indicated that the coolant was strongly diffused in the stator/rotor axial gap. Blowing ratios for these experiments were the high set of blowing ratios at $M^*_{showerhead}$ = 2.0, $M_{avg,\ suction}$ = 1.0, and $M_{avg,\ pressure}$ = 1.0. The vane wake and downstream distance between Positions T and B caused the region of coolant located well above midspan (0.7S) to blend into the main region, while the larger region, focused below midspan at 0.3S at the trailing edge was reduced significantly in magnitude. In addition, the peak coolant position moved slightly upwards between the trailing edge and Position B, with its magnitude dropping almost 50% to Θ_R = -0.31. Comparing these reductions in coolant strength with reductions in the stator/rotor axial

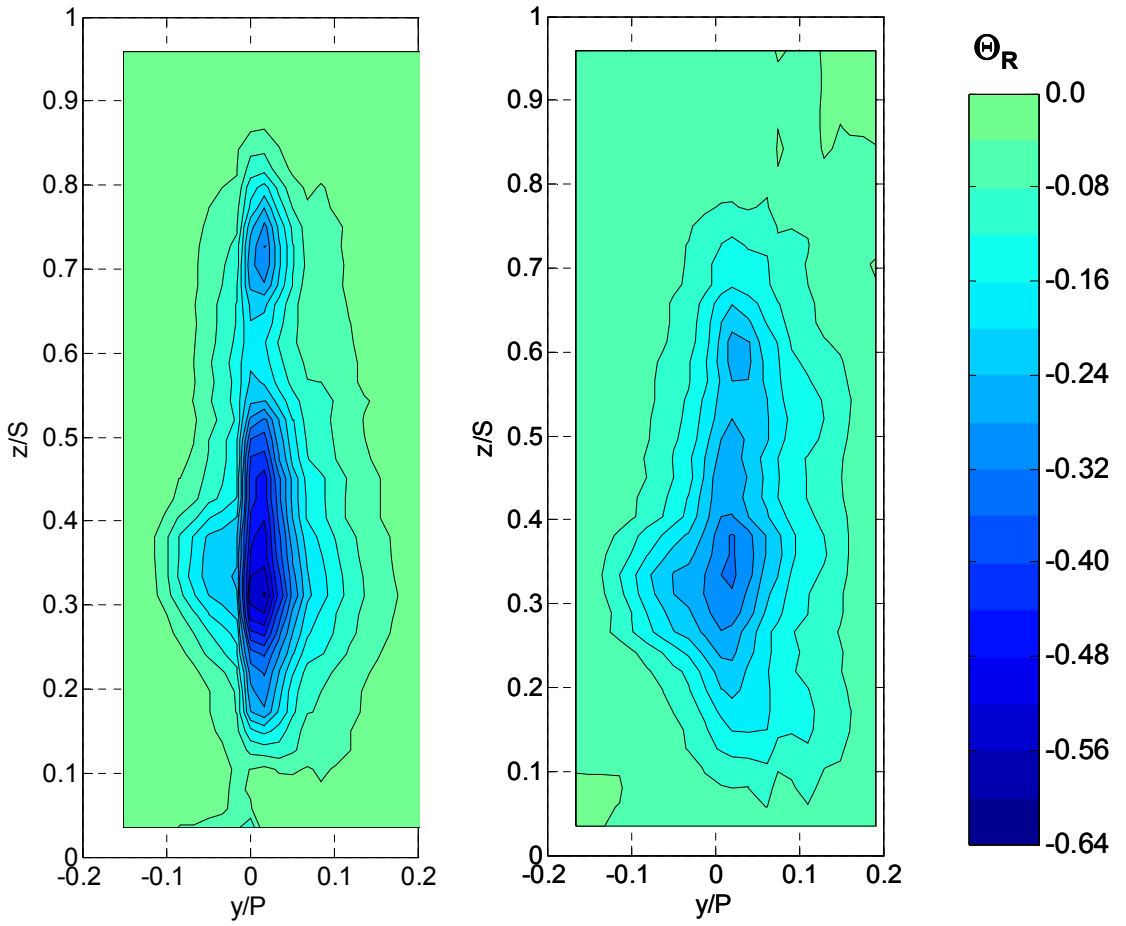

Figure 7.20: Normalized temperature ratio (Θ_R) coolant contours at Position T for full coverage blowing at $M^*_{showerhead}$ = 2.0, $M_{avg,\ suction}$ = 1.0, and $M_{avg,\ pressure}$ = 1.0, high mainstream turbulence (Tu = 20%) at:

a. Position T (Trailing Edge)

b. Position B (Wake)

gap of the hot streak, the hot streak strength dropped from Θ_R = 0.51 at the trailing edge to Θ_R = 0.38 at Position B in the wake (see §3.8 and Figure 3.39). The difference between the two decay rates may be explained by the difference in the steepness of the temperature gradients, where the full coverage coolant profile at the trailing edge had much steeper gradients than the hot streak at the same position. Coolant centered about the trailing edge at Position T between 0.2S and 0.5S spread noticeably in the stator/rotor axial gap and provides some justification for the conclusion that the vane wake contributed in spreading coolant across the pitch. The effect of the passage vortex,

shown to be a factor in transporting coolant across the passage for showerhead and suction side blowing (see Figures 4.11 and 5.14 respectively) was not as obvious in Figure 7.20. This was due to the contour level increments used for the figure, since similar Θ_R values of about Θ_R = -0.07 were observed for all three cases in the upper left region of the figures.

Even at midspan, the gradient in the trailing edge coolant profile was very steep, as shown in Figure 7.21. The magnitude of this gradient, especially within the range of the vane wake between ± 0.035P played a role in the nearly 40% drop in coolant strength between the trailing edge and Position B. The 20% width of the profile increased more than 75% between the two measurement planes. Here the 20% width was used in the same way as described in Chapter 3.

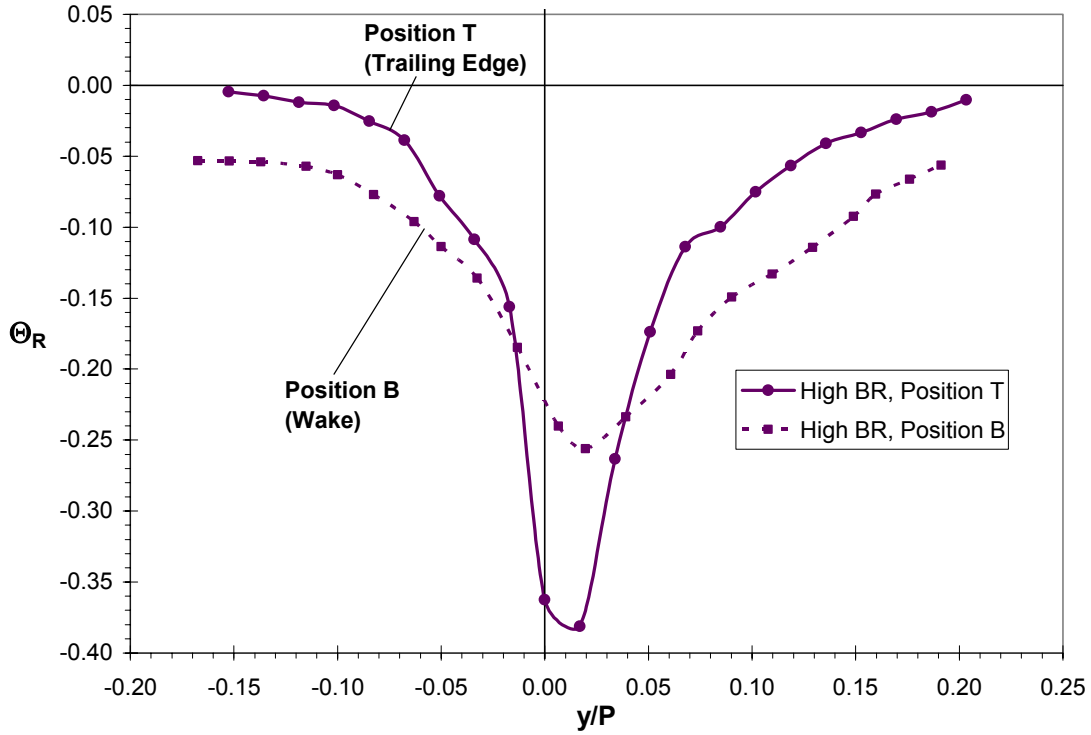

Figure 7.21: Coolant profiles at the trailing edge (Position T) and in the wake at Position B at midspan (z = 0.5S) for full coverage blowing at $M^*_{showerhead}$ = 2.0, $M_{avg,\ suction}$ = 1.0, and $M_{avg,\ pressure}$ = 1.0, high mainstream turbulence (Tu = 20%).

The rapid decline in coolant strength has important implications for hot streak reduction. However, as opposed to reducing the potential for hot streak reduction, the

strong temperature gradients in the coolant profiles at Position T imply that there would be strong temperature gradients in the film cooled hot streak as well (shown previously in Figure 7.7). The dissipation in the stator/rotor axial gap caused a significant drop in the sharply peaked trailing edge profile, as seen in the midspan profiles shown in Figure 7.22. The dip in the film cooled hot streak profile just to the suction side of the trailing edge was mixed out in the wake region, along with flattening out the smaller peak to that side. Meanwhile, the peak on the pressure side was reduced an additional 40% in the wake to a value of $\Theta_R = 0.17$. While the erosion of a strong temperature gradient was a prominent theme in the discussion of wake effects on the hot streak in Chapter 3, here the strong temperature gradients at the trailing edge were caused by coolant.

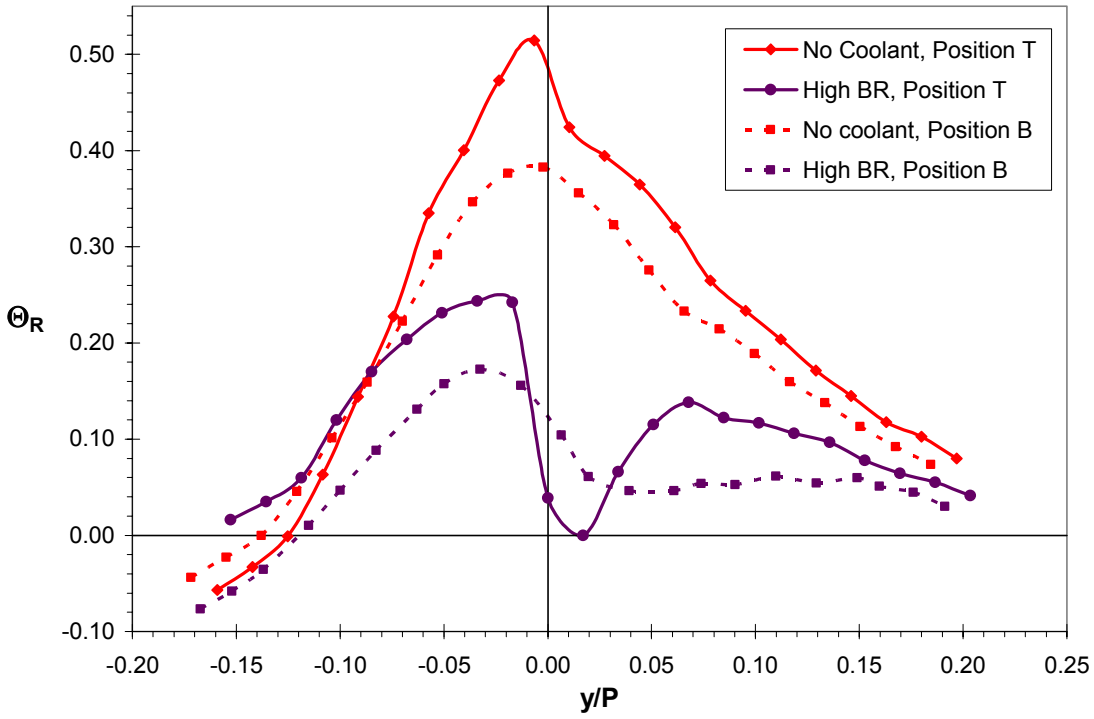

Figure 7.22: Normalized temperature ratio (Θ_R) profiles at Position T and Position B for the hot streak impacting the stagnation line without coolant and with full coverage blowing at $M^*_{showerhead}$ = 2.0, $M_{avg,\ suction}$ = 1.0, and $M_{avg,\ pressure}$ = 1.0, high mainstream turbulence (Tu = 20%).

Contour plots in Figure 7.23 show that the peak at midspan at Position B was also the overall peak. Here the full potential of film cooling in the wake was realized, with the hot streak reduced to a small region of low strength to the pressure side of the vane.

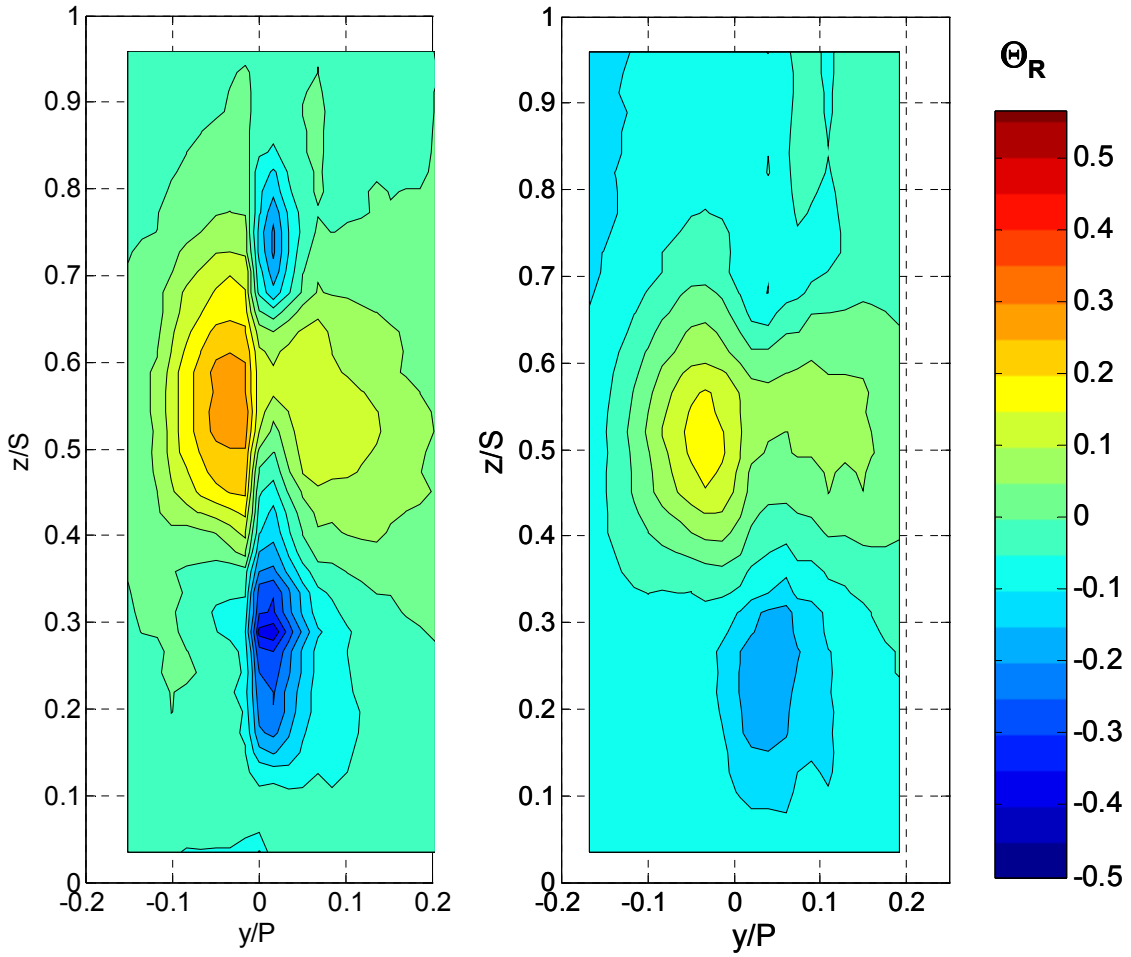

a. **b.**

Figure 7.23: Normalized temperature ratio (Θ_R) contours for full coverage blowing at $M^*_{showerhead}$ = 2.0, $M_{avg,\ suction}$ = 1.0, and $M_{avg,\ pressure}$ = 1.0, high mainstream turbulence (Tu = 20%):

a. Position T (Trailing Edge)

b. Position B (Wake)

A large region of coolant was centered at about 25% span and to the suction side. This figure emphasizes the importance of the role of the vane wake in reducing the strength of the hot streak. At the trailing edge, regions of the remaining hot streak with high gradients were separated by the trailing edge, with moderately strong gradients along the boundaries of regions of coolant. By Position B in the wake, these areas were all diffused into one another, leaving much weaker gradients and considerably reducing the hot streak. The peak hot streak at Θ_R = 0.17 represented a reduction in hot streak strength of

83% compared with the upstream reference at Position A, and a 55% reduction in the hot streak compared with no film cooling at Position B.

7.7 Effect of Full Coverage Film Cooling on a Passage Hot Streak

Experiments were carried out to determine the effect of full coverage film cooling on a hot streak passing through the mid-passage. The hot streak was positioned to pass through the passage on the suction side of the test vane at +0.4*P* from the stagnation line. This position corresponded to the position used for previous hot streak measurements, and as compared with a pitch position of 0.5P, was weighted in favor of coolant/hot streak interaction.

Since the blowing ratios for this set of experiments corresponded to a prior data set and therefore were slightly different than the blowing ratios in the current study, it is instructive to compare coolant profiles for the current study with those used for the passage hot streak. In Figure 7.24, a comparison of coolant profiles for high blowing ratios at $M^*_{showerhead} = 2.0$, $M_{avg,\ suction} = 1.0$, and $M_{avg,\ pressure} = 1.0$ and passage hot streak blowing ratios at $M^*_{showerhead} = 1.4$, $M_{avg,\ suction} = 1.0$, and $M_{avg,\ pressure} = 1.0$ demonstrates that the main difference was in the magnitude of the coolant strength near the trailing edge. The showerhead blowing ratio was responsible for this difference, with a lower blowing ratio at $M^* = 1.4$. Overall, the spread of the coolant at lower contour levels was slightly higher for the passage hot streak blowing ratios, but the positioning of the coolant peaks was similar.

In Figure 7.25, the peak normalized hot streak temperature ratio was about $\Theta_R = 0.43$ for the hot streak with no film cooling, indicating a drop in strength of just over 55% from the upstream value, and was slightly lower than the value of $\Theta_R = 0.51$ for the hot streak at the stagnation line. Since measurements were made at the trailing edge of the vane, the results indicate a sharp gradient at y/P = 0.0 due to the vane isolating the hot streak from flow on the pressure side of the test vane as discussed in Chapter 3. The effect of film cooling on the peak hot streak value is apparent in Figure 7.25b. Here the hot streak was further attenuated by full coverage film cooling despite having been positioned at 0.4*P* to the suction side of the test vane. The peak normalized hot streak

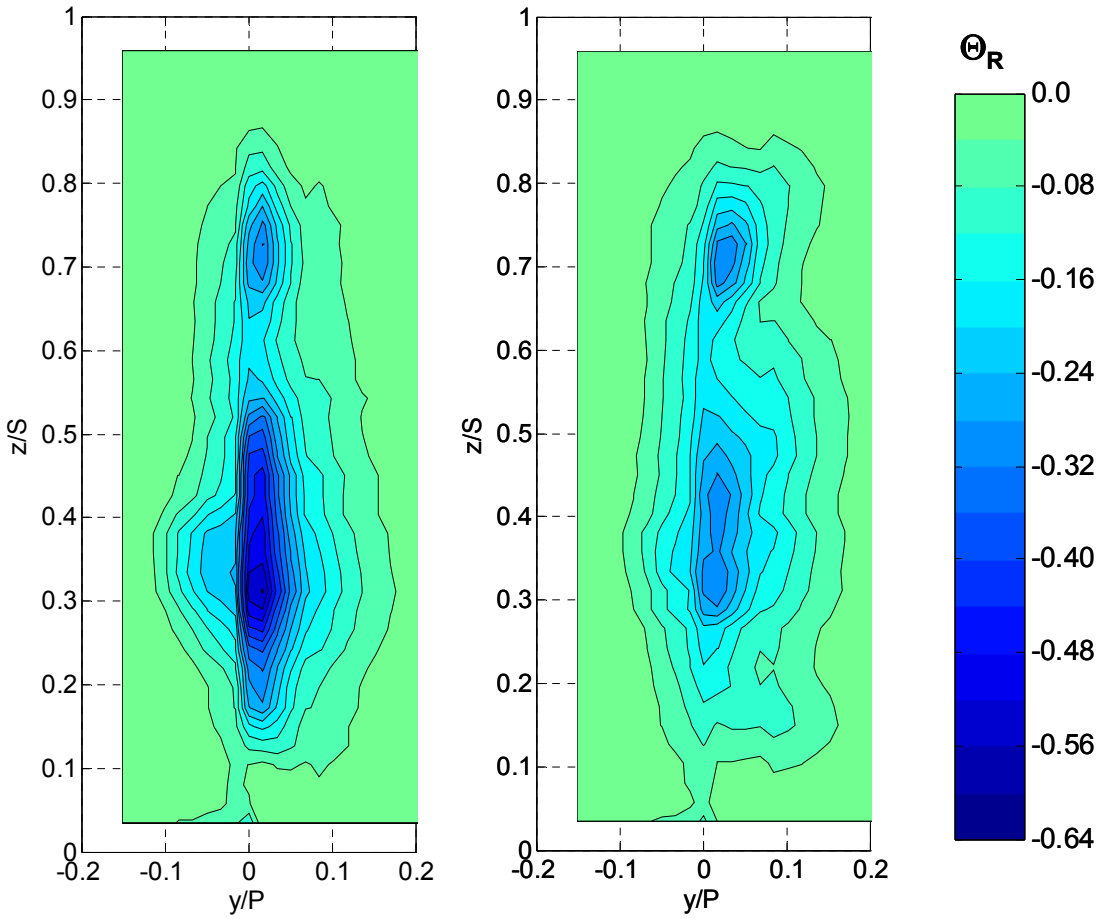

Figure 7.24: Normalized temperature ratio (Θ_R) coolant contours at Position T, high mainstream turbulence (Tu = 20%) for full coverage blowing at:

a. $M^*_{showerhead}$ = 2.0, $M_{avg,\ suction}$ = 1.0, and $M_{avg,\ pressure}$ = 1.0

b. $M^*_{showerhead}$ = 1.4, $M_{avg,\ suction}$ = 1.0, and $M_{avg,\ pressure}$ = 1.0

temperature ratio in this case was Θ_R = 0.30, and coolant pushed this peak about 0.12P further from the stagnation line. The large quantity of coolant for y/P < 0.0 primarily was from the showerhead since the pressure side had relatively low mass flow rate compared with the showerhead even at the blowing ratios used.

Insight into why the hot streak was so greatly attenuated was given by the contour plot of the coolant alone at the same blowing ratios, which was shown in Figure 7.24b. Here the coolant extended far from the vane surface. The coolant had a large effect on

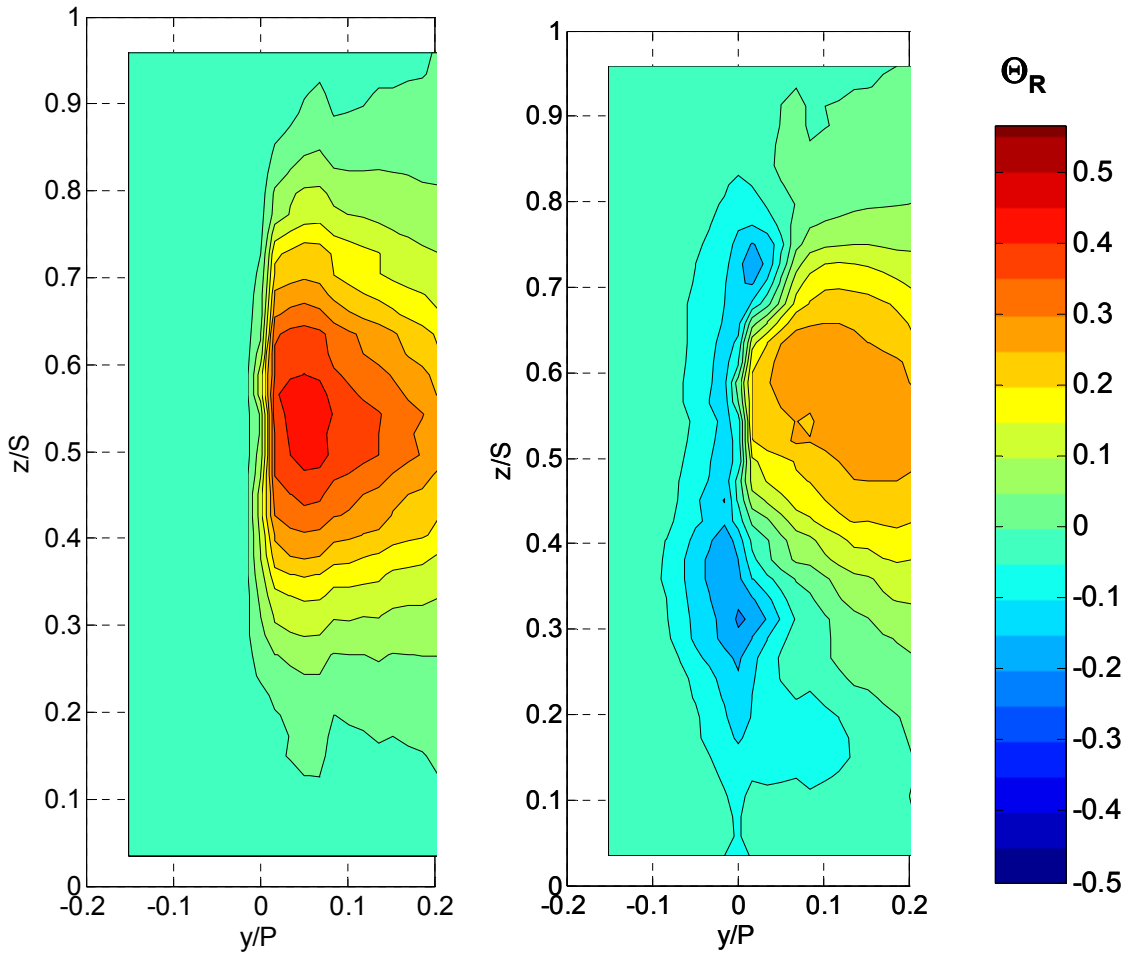

a. **b.**

Figure 7.25: Normalized temperature ratio (Θ_R) contours at Position T with the hot streak at 0.4*P* to the suction side, high mainstream turbulence (*Tu* = 20%):

a. No coolant

b. Full coverage blowing at $M^*_{showerhead}$ = 1.4, $M_{avg,\ suction}$ = 1.0, and $M_{avg,\ pressure}$ = 1.0

the temperature field as far as 0.15P from the centerline, while the hot streak peak was located at about 0.05P. High turbulence effects were primarily responsible for extending the range of the coolant's effect.

Profiles taken at midspan indicate how coolant reduced the hot streak, shown in Figure 7.26. The coolant extended considerably toward the edge of the passage, thereby diminishing the peak of the hot streak which was relatively near the vane. The shape of the uncooled hot streak profile may be attributed to the decreased attenuation of the hot streak near the wall as discussed in Chapter 3. At midspan, the hot streak peak at Θ_R =

0.42 was reduced significantly by coolant that had a coolant only peak of Θ_R = -0.23 relatively near the hot streak peak. The coolant reduced hot streak was diminished less for positions well away from the vane where it peaked at only Θ_R = 0.27.

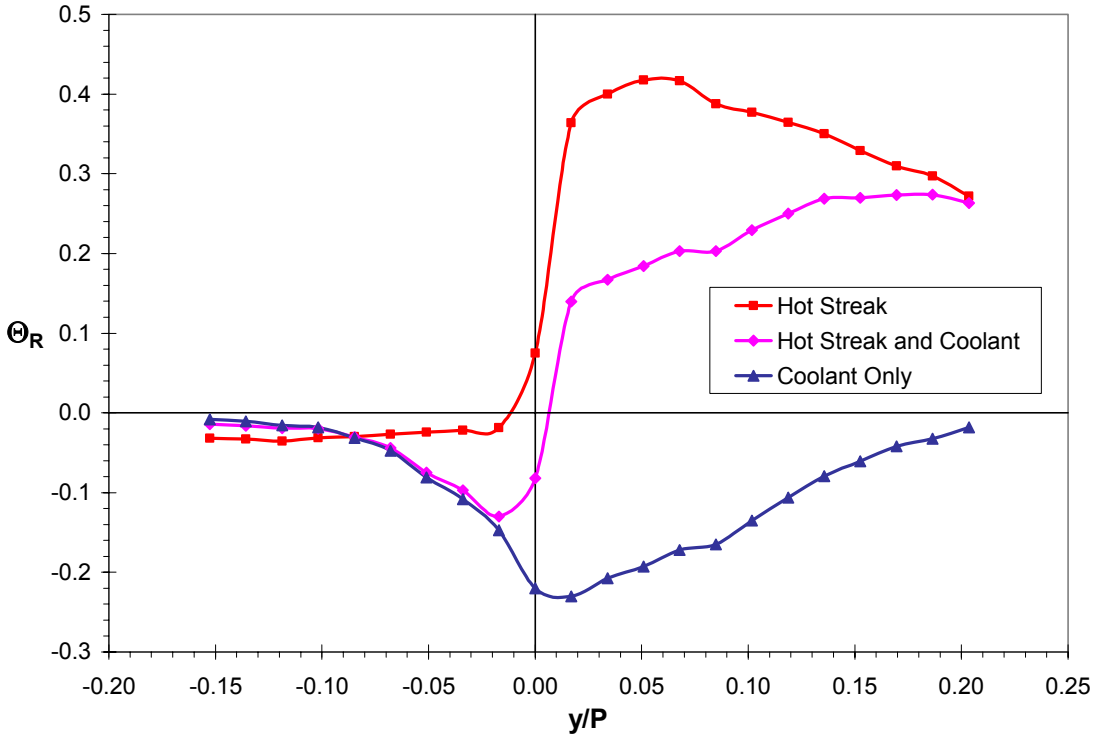

Figure 7.26: Normalized temperature ratio (Θ_R) profiles at Position T for the hot streak at 0.4*P* to the suction side showing the hot streak with no cooling, with full coverage blowing at $M^*_{showerhead}$ = 1.4, $M_{avg,\ suction}$ = 1.0, and $M_{avg,\ pressure}$ = 1.0, and the coolant only profile, high mainstream turbulence (*Tu* = 20%).

Overall, the effect of coolant on the hot streak passing through the mid-passage at 0.4P to the suction side of the test vane was relatively high. This was due to two factors. The spread of the coolant due to high turbulence in the mainstream and boundary layer served to greatly attenuate the hot streak peak, which was relatively close to the vane due to other turbulence effects. The hot streak positioned to impact the vane was even more greatly attenuated, however, even with a pitch position of +0.5P, the coolant extended far enough away from the vane to have a significant effect at that hot streak pitch position as well.

Chapter 8: Effects of Turbulence Level

8.1 Introduction

Although high mainstream turbulence is the engine representative condition, comparisons of results at high and low mainstream turbulence permitted analysis of the function of turbulence level in dispersing coolant and how this affected hot streak reduction. Coolant profiles were measured for all three coolant regions individually and for full coverage film cooling, however the blowing ratios tested were carefully selected among the larger high mainstream turbulence data set to provide the best understanding of turbulence effects.

Since the upstream hot streak reference was different for high and low mainstream turbulence levels, a direct comparison between coolant distributions was not possible using Θ_R. Therefore, for direct comparisons of coolant profiles at different turbulence levels, the normalized coolant temperature, Θ_C, was used.

8.2 Effect of Turbulence Level on Showerhead Coolant Dispersion

The effect of mainstream turbulence level was investigated for showerhead film cooling to determine how the coolant dispersed without the aid of additional turbulent mixing and advection. In Figure 8.1, the effect is clear. Under conditions of low mainstream turbulence (Figure 8.1a) the coolant was restricted to a very narrow range around the trailing edge, with much lower temperature levels. The effect of the overlap region was clear as well, where on the suction side ($y/P > 0.0$) a mass of coolant reached $\Theta_C = -0.12$ (equivalent to $\Theta_R = -0.40$ for low turbulence) at $z/S = 0.30$. In contrast to the high mainstream turbulence result, on the pressure side, due to the angle of the overlap region (shown in Figure 4.1 previously), coolant advecting to the pressure side from the overlap region collected at about $z/S = 0.4$. Under conditions of high mainstream turbulence, the turbulence levels dispersed this smaller amount of coolant, presumably merging it with the larger mass found at about $z/S = 0.30$, although some indication of the pressure side overlap region was seen in Figure 4.5c of Chapter 4, at the highest blowing ratio.

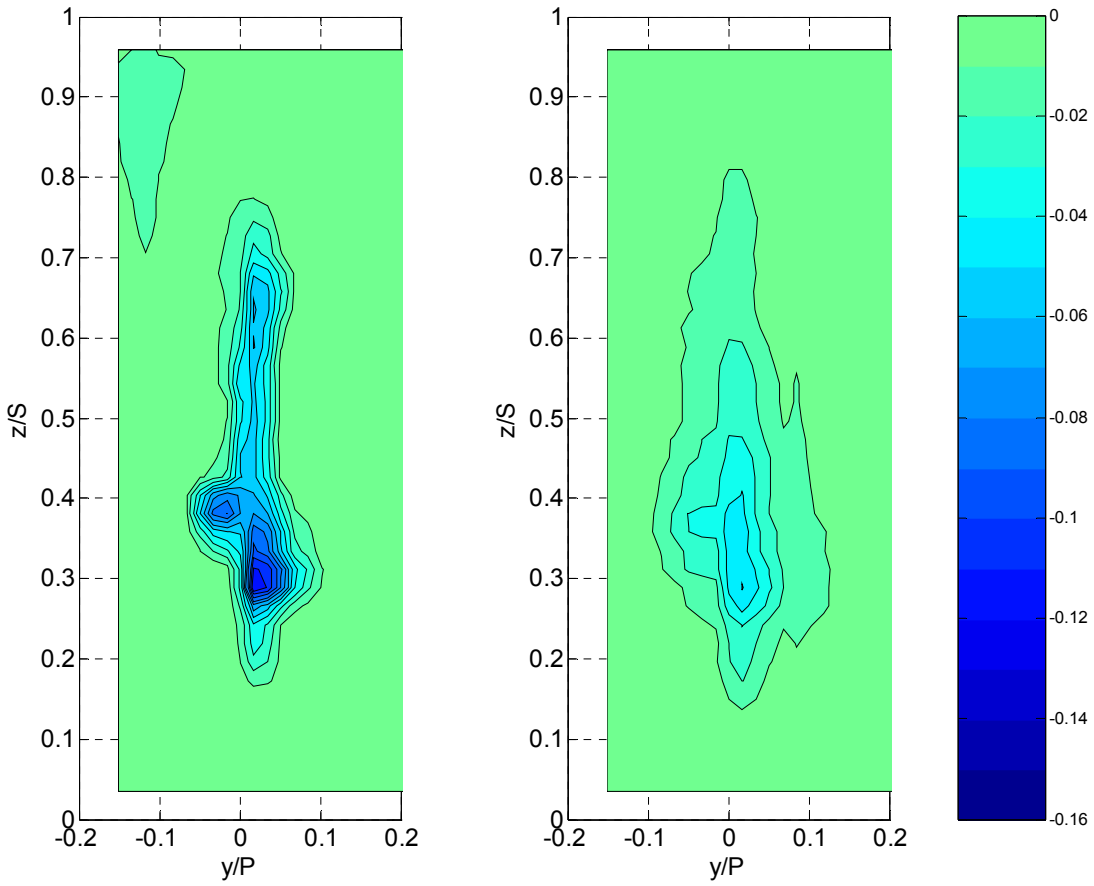

Figure 8.1: Normalized coolant temperature (Θ_C) contours for showerhead blowing at $M^* = 1.6$, $DR = 1.6$ for:

a. Low mainstream turbulence ($Tu = 3.5\%$)

b. High mainstream turbulence ($Tu = 20\%$)

Comparing midspan profiles at high and low mainstream turbulence for the range of blowing ratios gives a clearer indication of how much greater the spread of coolant was at the high mainstream turbulence level. In Figure 8.2, the profiles for low mainstream turbulence are much narrower and peaked than the broader profiles for high mainstream turbulence, shown with dotted lines. The 20% width of the coolant profile for low mainstream turbulence was about $0.08P$, while the 20% width at high mainstream turbulence was about $0.18P$, a little more than twice as wide. The peak coolant temperature ratio was also lower at $\Theta_C = -0.05$ for $M^* = 1.6$ for the low turbulence case

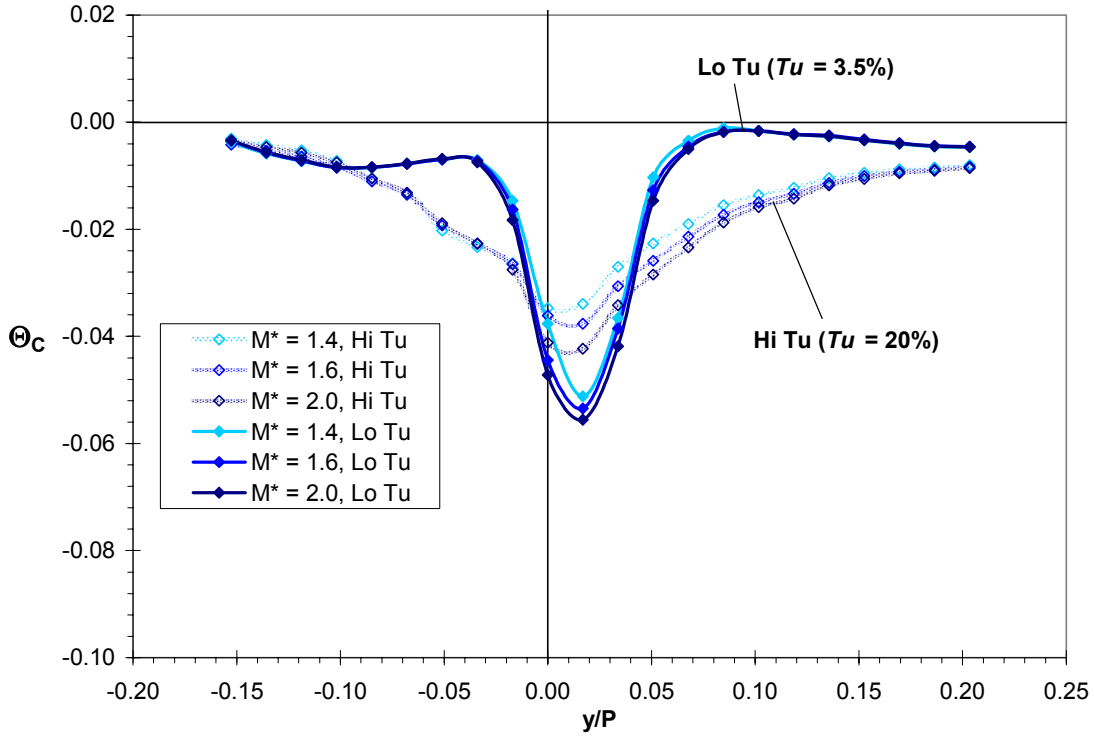

Figure 8.2: Normalized coolant temperature (Θ_C) profiles for at Position T at midspan (z/S = 0.50) for showerhead blowing at M^* = 1.4, 1.6, and 2.0, for low turbulence (Tu = 3.5%) and high turbulence (Tu = 20%).

(equivalent to Θ_R = -0.17) compared with Θ_C = -0.03 for the high turbulence case (equivalent to Θ_R = -0.12 for high turbulence). Note that for the low mainstream turbulence profiles on the outer edges, the non-zero values were due to inconsistencies in the bulk mainstream temperature field as discussed in Chapter 2, but were not related to the presence of coolant coming from the vane.

The effect of showerhead film cooling at low mainstream turbulence on the hot streak was fairly similar to that at high mainstream turbulence. Since the hot streak was more compact under the low mainstream turbulence condition, the less dispersed coolant reduced the peak of the hot streak in a similar fashion for both turbulence levels. In Figure 8.3, there was a large region of coolant due to the overlap region below the remaining hot streak, and a different resulting shape of the showerhead cooled hot streak (compare to Figure 4.4). The peak of the hot streak was reduced from Θ_R = 0.71 with no

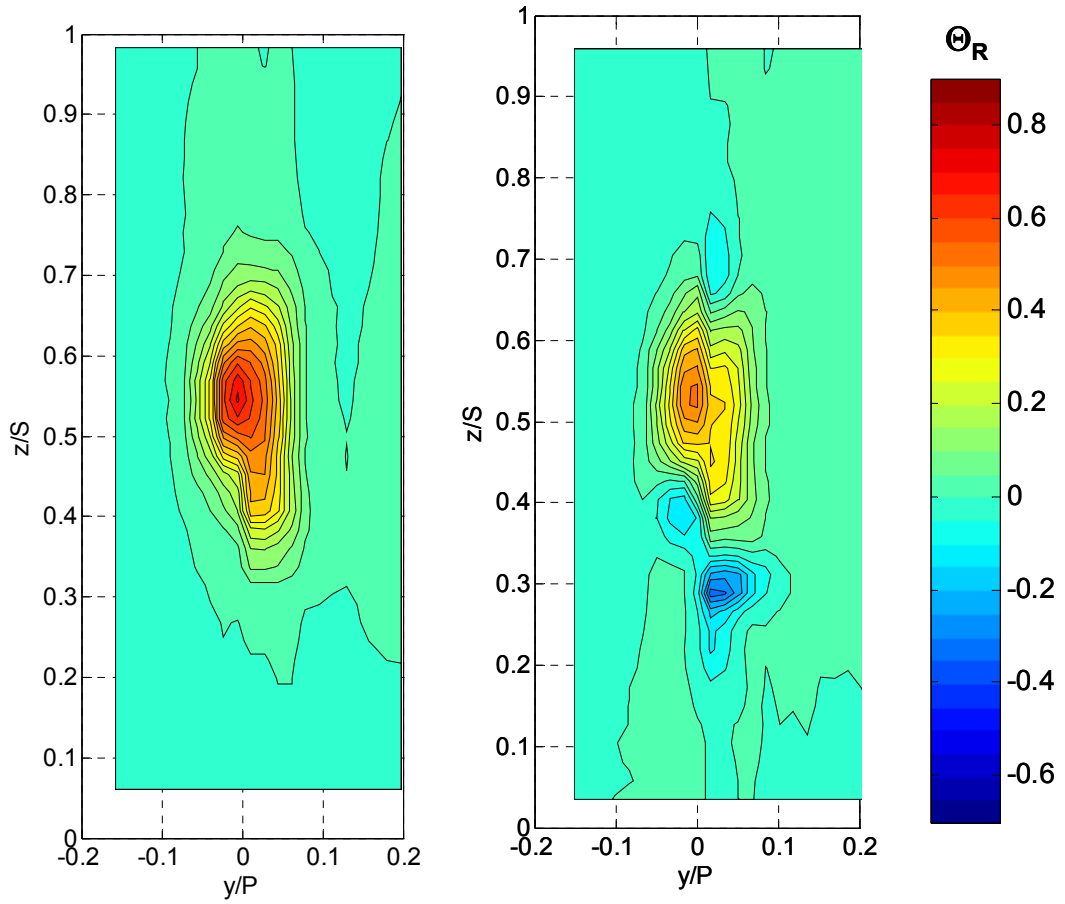

a. **b.**

Figure 8.3: Normalized temperature ratio (Θ_R) contours at Position T with the hot streak at the stagnation line, low mainstream turbulence (Tu = 3.5%):

a. No coolant

b. Showerhead blowing at M^* = 1.6

film cooling to Θ_R = 0.51 with showerhead film cooling at a blowing ratio of M^* = 1.6. Fairly similar values were found in the drop in hot streak peak temperature ratio at about 30% at low mainstream turbulence as compared to 25% for the high mainstream turbulence condition. Under conditions of low turbulence the position of the peak hot streak temperature ratio was slightly above midspan due to the pattern of coolant holes and the coolant interaction with the hot streak. In general, the showerhead film cooling behaved in a fairly similar manner at both turbulence levels, with an overall reduction of temperature values and a greater reduction of the lower portions of the hot streak.

Line profiles taken at midspan, in Figure 8.4, indicate a reduction over the width of the hot streak, growing with increased blowing ratio. At midspan, the peak was reduced to about Θ_R = 0.45 for M^* = 1.90, for a reduction of almost 30%, while under conditions of high mainstream turbulence, the reduction was slightly more for the same spanwise position and the same blowing ratio (see Figure 4.8). The profiles indicate a sharp gradient at the trailing edge, similar to Figure 4.8 for high mainstream turbulence. Since the hot streak alone had this sharp gradient with lower temperatures on the suction side, and since slightly larger quantities of coolant passed to the suction side (40% more as noted earlier), it was not surprising that the sharp gradient was increased with showerhead film cooling.

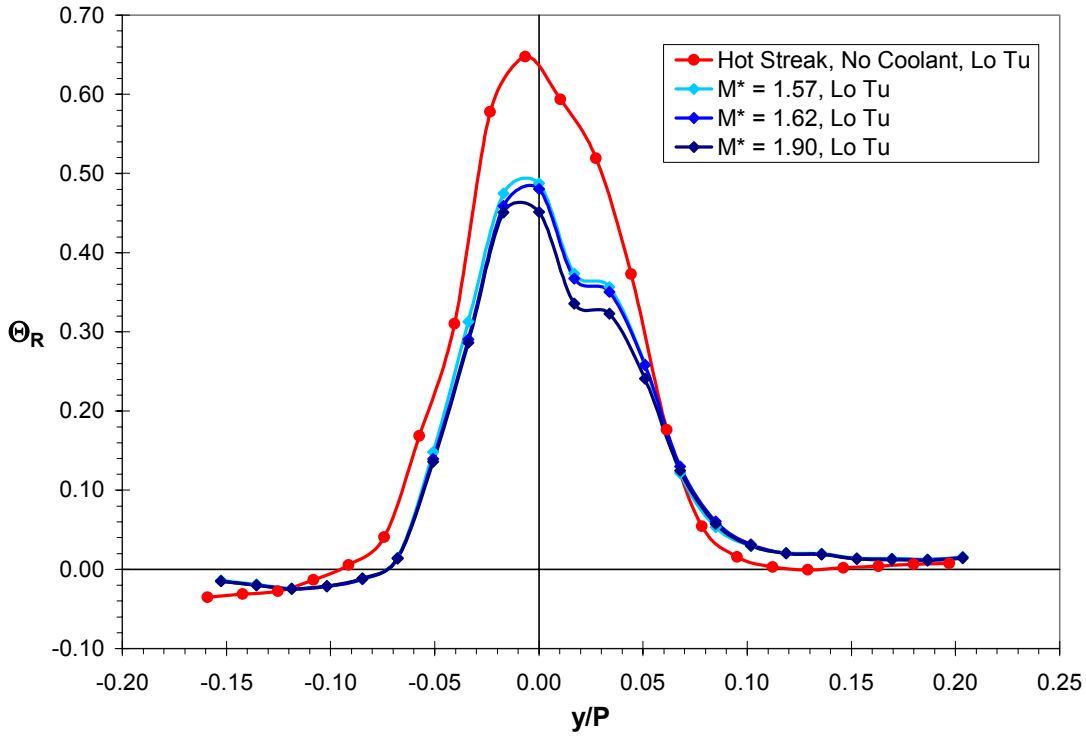

Figure 8.4: Normalized temperature ratio (Θ_R) profiles at Position T for the hot streak impacting the stagnation line without coolant and with showerhead blowing at M^* = 1.4, 1.6, and 2.0, low mainstream turbulence (Tu = 3.5%).

Further investigation of the origin of the Position T profiles was performed by making additional measurements at Positions S1', P1', S2', and P2' under conditions of low mainstream turbulence, shown in Figure 8.5. At Position P1', coolant reached

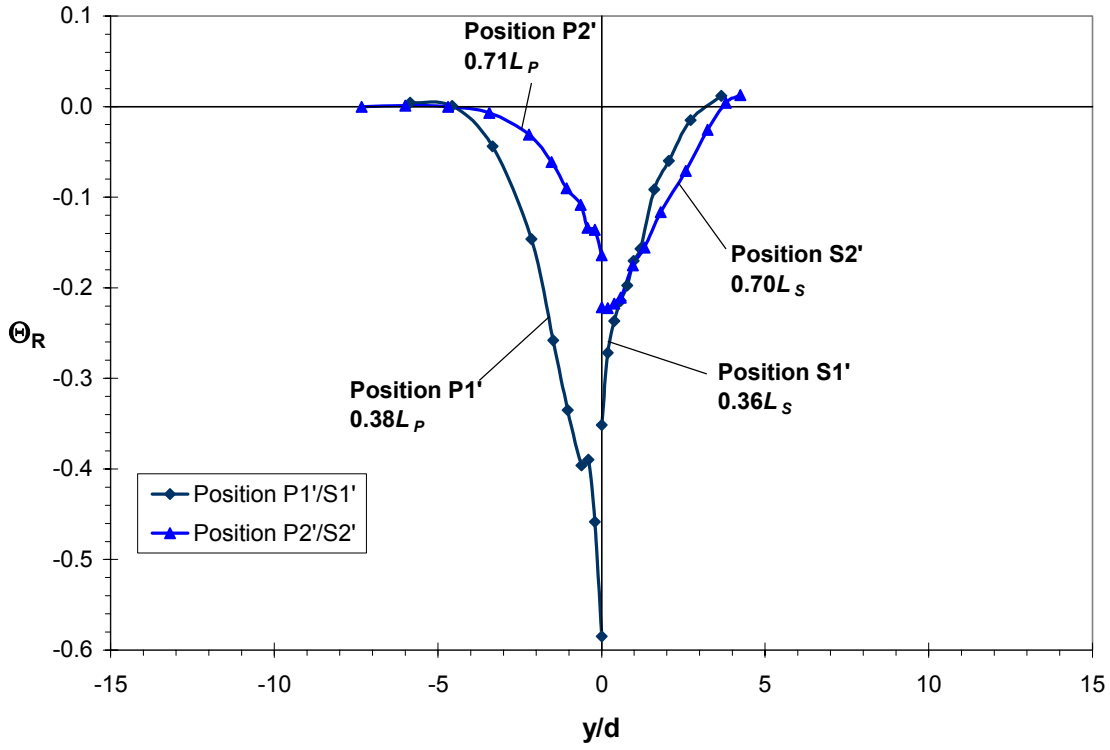

Figure 8.5: Profiles of showerhead coolant in terms of Θ_R, at Positions S1', S2', P1', P2', and T' at midspan (z = 0.5S), low mainstream turbulence (Tu = 3.5%), showerhead blowing at M^* = 1.6.

nearly Θ_R = -0.60, but only extended a little more than 4d from the wall. Further downstream, the pressure side profile was somewhat less steep, but still the coolant extended only a short distance from the vane wall. There appeared to be less coolant at Position P2', which was due to the compression of streamlines between Positions P1' and P2'. Since the coolant did not mix quickly with the mainstream, the coolant profile appeared thinner. The difference between Position P1' on the pressure side and Position S1' on the suction side was also due to differences in the compression of streamlines. Even though there was more coolant passing to the suction side (3 ½ rows compared to 2 ½) the coolant profile appeared narrower, as if there were less coolant. For this reason, the profile had an even steeper slope than on the pressure side, and barely extended 2d from the wall at $s = 0.36L_S$ (Position S1'). Again, further downstream on the suction side the coolant profile was slightly more relaxed, extending to almost 3d from the wall. These coolant profiles help to explain why the profiles for showerhead film cooling were so peaked at Position T in Figure 8.2.

Although the coolant profiles in this figure may be compared with Figure 4.9 shown previously in Chapter 4 for high mainstream turbulence, a one-to-one comparison with values normalized by the same parameter is more instructive. These values are shown in Figure 8.6 in terms of Θ_C, the coolant reference temperature as defined in Chapter 2, as opposed to the upstream hot streak peak temperature. The difference in the effect of turbulence level is very clear in this figure, with large departures in slope on the pressure side at Position P1'. As shown previously, the coolant reached just past 4*d* from the wall at low turbulence, but under high turbulence it reached more than twice as far from the wall. The effect of turbulence level on the suction side was less pronounced, presumably due to the compression of streamlines which limited the dispersion of showerhead coolant for both turbulence levels. Nonetheless, the coolant extended about 1*d* farther from the wall at Position S1' and the overall coolant profile was about twice as

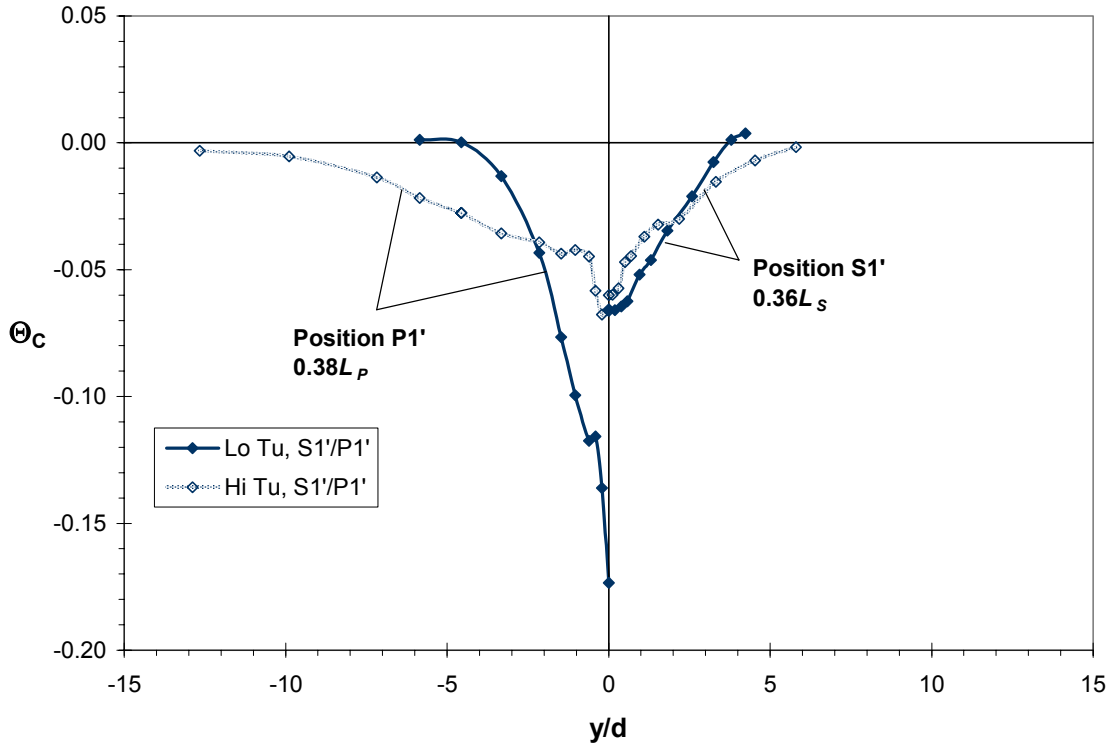

Figure 8.6: Profiles of showerhead coolant in terms of Θ_C, at Positions S1' and P1' at midspan (z = 0.5S), comparing low mainstream turbulence (*Tu* = 3.5%) with high mainstream turbulence (*Tu* = 20%), showerhead blowing at *M = 1.6.**

steep for the low turbulence case. At Positions S2' and P2' in Figure 8.7, a similar comparison can be made. The profile at P2' under low turbulence conditions sloped strongly up to 3.5*d* away from the vane wall, while the high turbulence profile was nearly flat and extended well past 6*d* from the wall. On the suction side, the low turbulence profile reached a peak of Θ_C = -0.10 at the vane wall where the high turbulence profile reached less than half that value. Additionally, coolant was present nearly twice as far from the vane wall under conditions of high mainstream turbulence as compared with low turbulence at Position S2'.

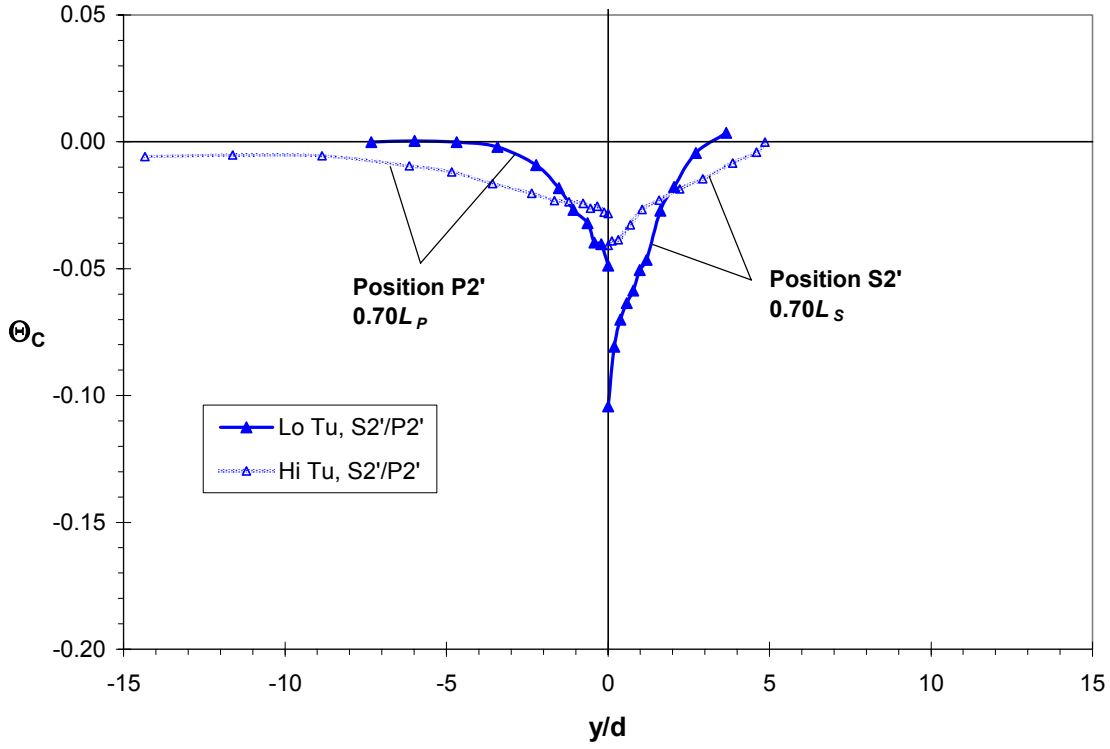

Figure 8.7: Profiles of showerhead coolant in terms of Θ_C, at Positions S2' and P2' at midspan (z = 0.5S), comparing low mainstream turbulence (*Tu* = 3.5%) with high mainstream turbulence (*Tu* = 20%), showerhead blowing at *M = 1.6.**

8.3 Effect of Turbulence Level on Suction Side Coolant Dispersion

As seen for the showerhead, coolant distributions at the trailing edge for suction side film cooling differed for the two mainstream turbulence levels. Figure 8.8 shows the normalized coolant temperature distributions for a suction side blowing ratio of M_{avg} = 0.7. Here the main difference was the degree of spreading of the coolant, mainly in the

pitchwise direction. The low turbulence distribution appeared to be somewhat narrower, but the width at the lowest contour level of Θ_C = -0.01 was fairly similar for both turbulence levels (about 0.06*P* for low turbulence and 0.08*P* for high turbulence). The main difference was in the larger negative peak under low mainstream turbulence conditions. This was due to the levels of dispersion which spread the coolant farther into the mainstream under high turbulence conditions, resulting in levels indistinguishable from the mainstream temperature.

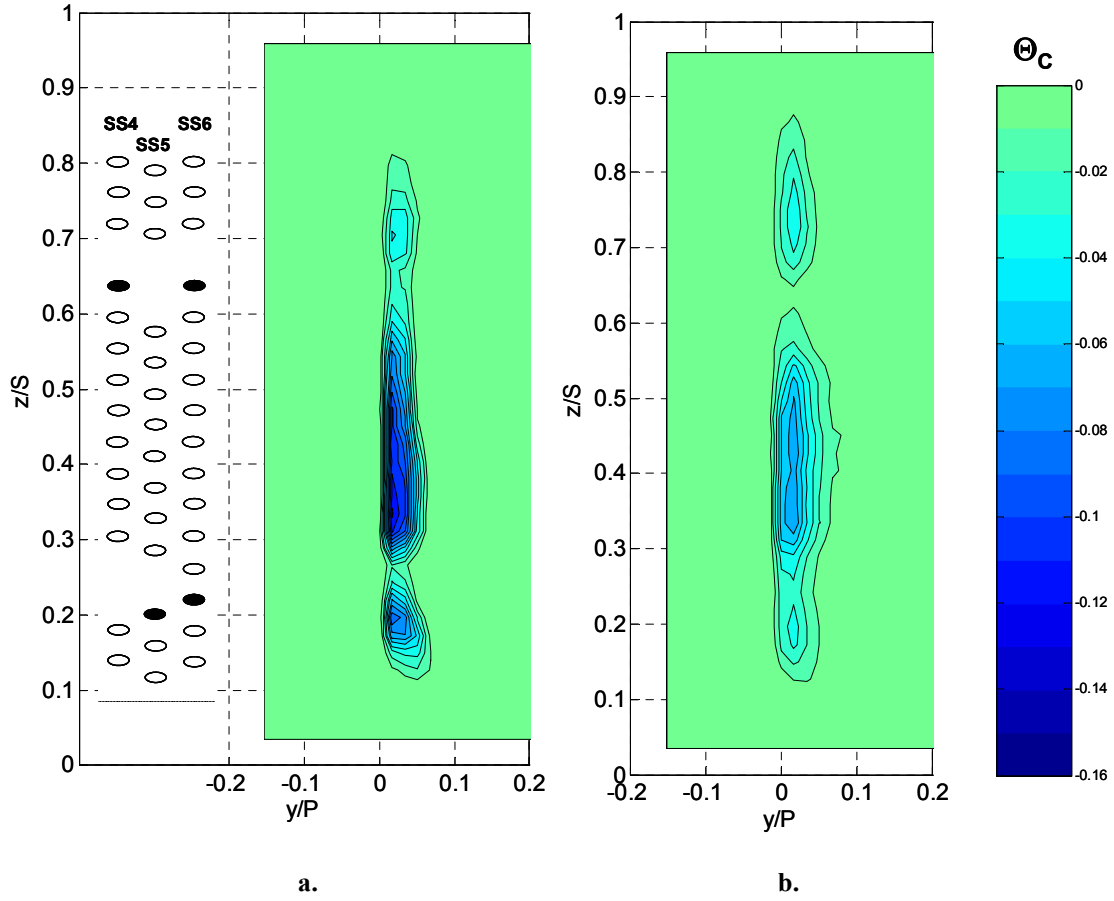

Figure 8.8: Normalized coolant temperature (Θ_C) contours for suction side blowing at M_{avg} = 0.7, *DR* = 1.6 for:

a. Low mainstream turbulence (*Tu* = 3.5%)

b. High mainstream turbulence (*Tu* = 20%)

Midspan profiles for M_{avg} = 0.5, 0.7, and 1.0 at both turbulence levels are shown in Figure 8.9. For each blowing ratio the peak coolant level was distinctly lower for the lower turbulence level. In fact, the peaks for low mainstream turbulence at M_{avg} = 0.5

and high mainstream turbulence at M_{avg} = 1.0 were nearly the same. Over the set of blowing ratios tested, low mainstream turbulence resulted in peaks about 30% larger than for high mainstream turbulence for each blowing ratio. The coolant profiles for high mainstream turbulence were also wider, since the same amount of coolant was ejected from coolant holes for a given blowing ratio under both turbulence conditions. All three low turbulence coolant profiles had about the same width, but the width of the high turbulence profiles varied more. The 20% width for the high turbulence profile was about 50% wider than for the low turbulence profile.

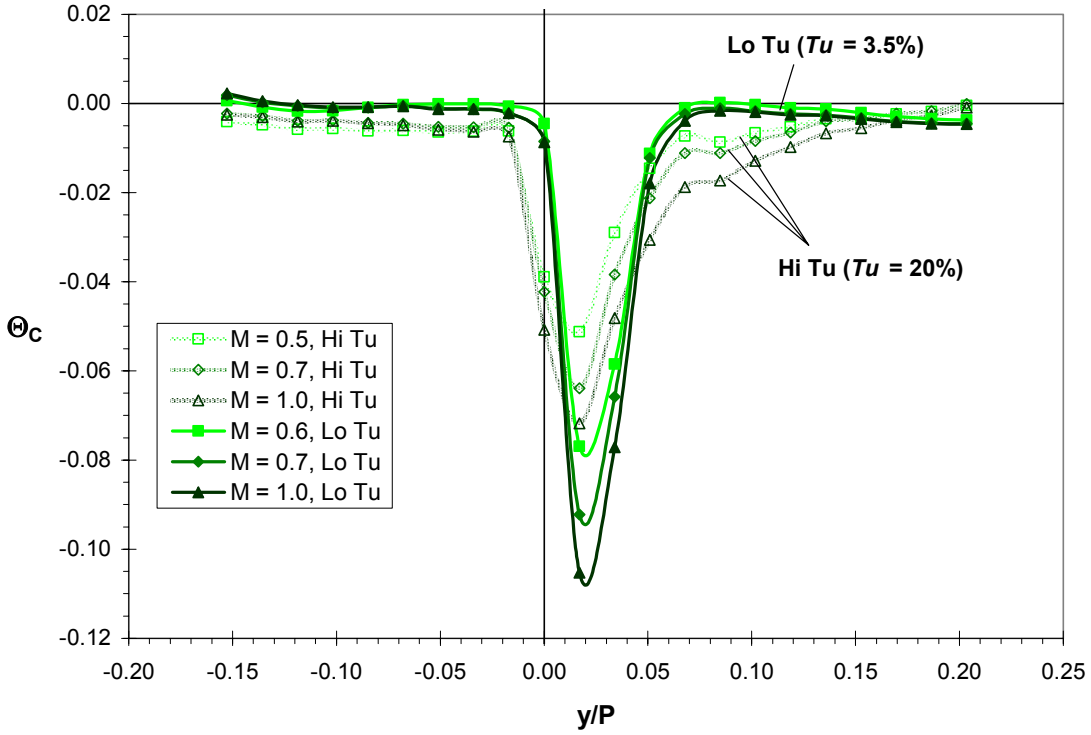

Figure 8.9: Normalized coolant temperature (Θ_C) profiles for at Position T at midspan (z/S = 0.50) for suction side blowing at M_{avg} = 0.5, 0.7, and 1.0, for low turbulence (Tu = 3.5%) and high turbulence (Tu = 20%).

The effects of suction side film cooling on the hot streak at low mainstream turbulence were more pronounced than at high mainstream turbulence since the coolant distribution was more tightly focused. Figure 8.10 shows how the hot streak was drastically reduced on the suction side while unaffected on the pressure side. The hot

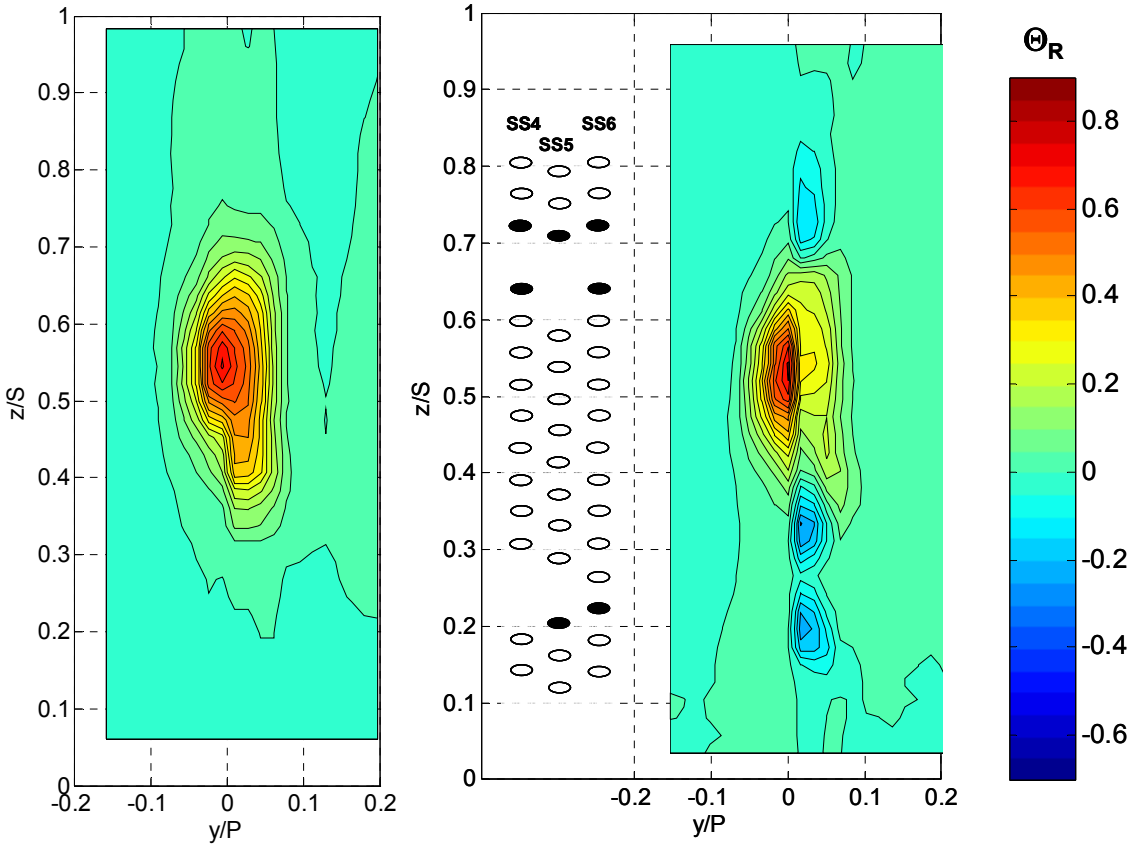

Figure 8.10: Normalized temperature ratio (Θ_R) contours at Position T with the hot streak at the stagnation line, low mainstream turbulence (Tu = 3.5%):

a. No coolant

b. Suction side blowing at M_{avg} = 0.7

streak peak was unchanged at Θ_R = 0.71 as the hot streak peak was slightly to the pressure side of the trailing edge. On the suction side of the trailing edge, the peak was Θ_R = 0.31, a reduction of 50% from the same position without film cooling. The significant reduction in the hot streak on the suction side also created a very strong gradient along the trailing edge. Since coolant shown in Figure 8.8a was strongest between 0.3S and 0.6S, while the hot streak was strongest between higher spanwise positions, between 0.4S and 0.7S, contours indicating excess coolant were observed below the range of the uncooled hot streak between 0.3S and 0.4S to the suction side of the trailing edge. Excess coolant was also observed well above and well below the hot

streak, but this would be expected given the coolant distributions in Figure 8.8 and the absence of significant hot streak fluid in these locations. Comparing the low mainstream turbulence result to high mainstream turbulence (see Figure 5.4), there was a stronger effect of suction side film cooling to the suction side of the trailing edge with a 50% reduction at low turbulence versus about a 40% reduction at high turbulence. As discussed in §5.3, the lower half of the suction side was more representative of film cooling effects on an actual vane since this area was less affected by hole blockage. In this region, the hot streak was again reduced by about 10% more with low turbulence than with high turbulence.

The very sharp gradient at the trailing edge can be seen clearly in the midspan profiles in Figure 8.11. The effect of suction side film cooling at low mainstream turbulence was a large decrease in the hot streak just to the suction side of the trailing edge, gradually lessening farther from the wall. As expected, larger blowing ratios

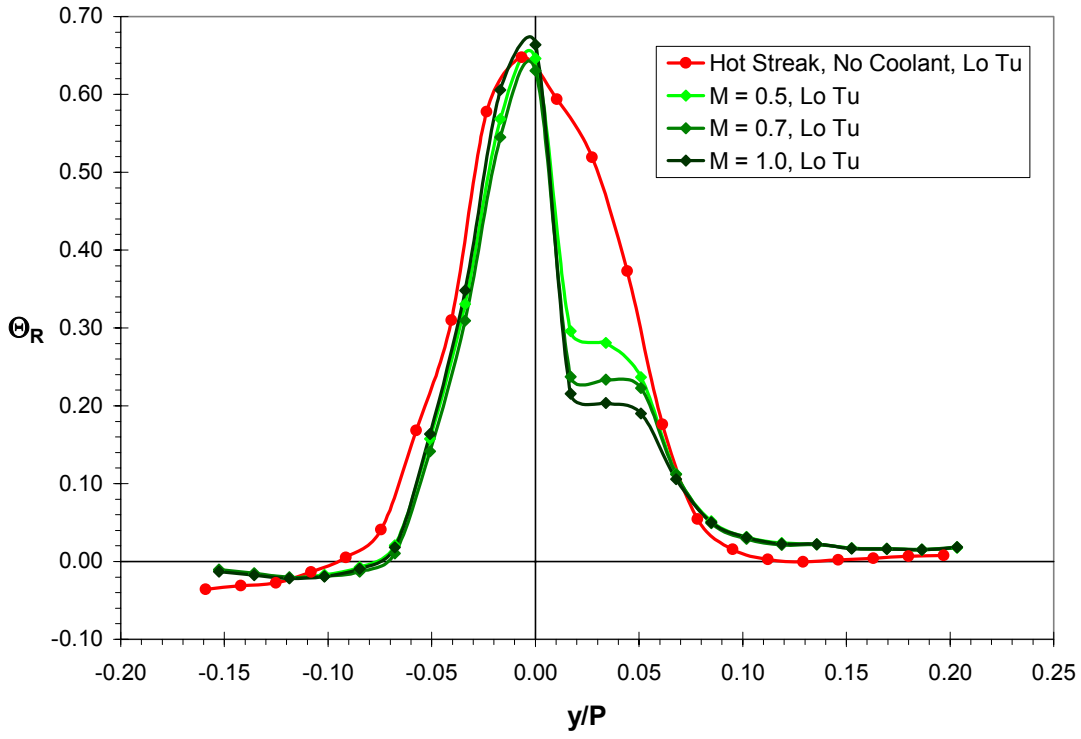

Figure 8.11: Normalized temperature ratio (Θ_R) profiles at Position T for the hot streak impacting the stagnation line without coolant and with suction side blowing at M_{avg} = 0.5, 0.7, and 1.0, low mainstream turbulence (Tu = 3.5%).

caused a larger reduction in the hot streak strength. For a position just off the wall, at y/P = 0.03, the highest blowing ratio reduced the hot streak by almost 30% more than the lowest blowing ratio.

8.4 Effect of Turbulence Level on Pressure Side Coolant Dispersion

Since the pressure side was much less effective at reducing the hot streak strength due to the lower mass flow rates and wider hot streak over the pressure side, only coolant profiles at midspan are compared for low versus high mainstream turbulence. Figure 8.12 shows the profiles for both turbulence levels at midspan for blowing ratios of M_{avg} = 0.4, 0.6, and 1.0. Coolant from the pressure side film cooling holes remained much closer to the wall for low mainstream turbulence than for high mainstream turbulence peaking about 1d from the wall (y/P = -0.005), while the peak for high mainstream turbulence was at about 2.5d from the wall (y/P = -0.02). Peaks were also about twice as

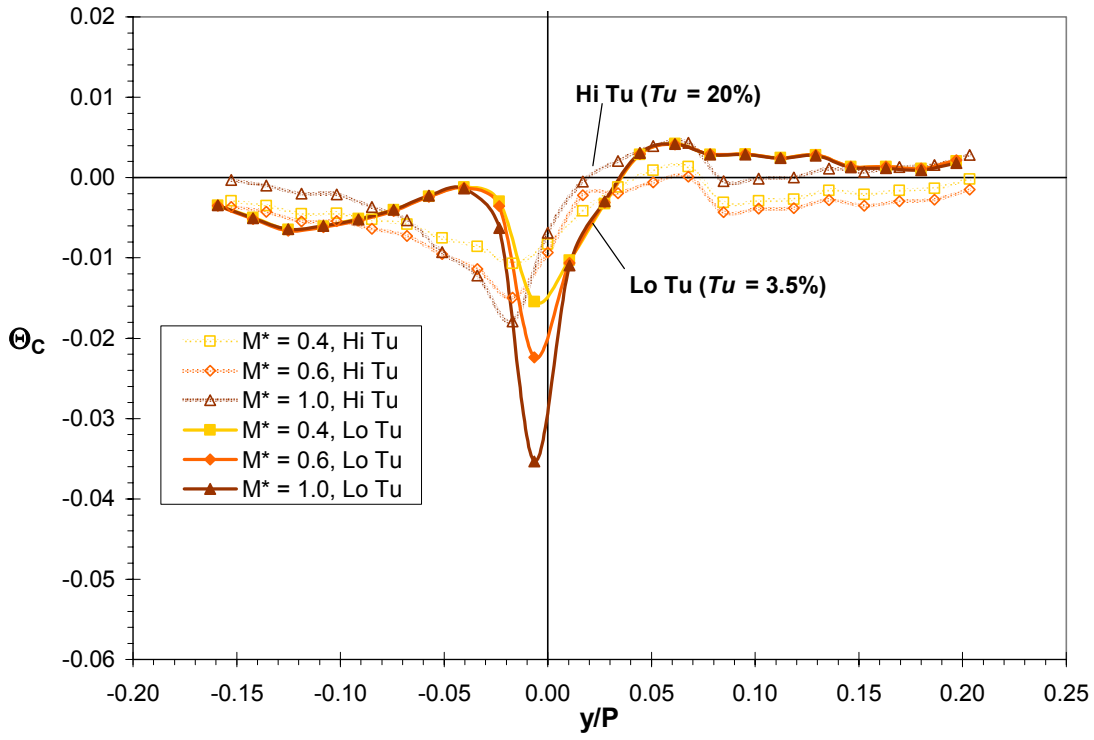

Figure 8.12: Normalized coolant temperature (Θ_C) profiles for at Position T at midspan (z/S = 0.50) for pressure side blowing at M_{avg} = 0.4, 0.6, and 1.0, for low turbulence (Tu = 3.5%) and high turbulence (Tu = 20%).

large with low mainstream turbulence than with high mainstream turbulence at the trailing edge. For the highest blowing ratio of M_{avg} = 1.0 at low mainstream turbulence, the peak coolant value was Θ_C = -0.035. This would be expected to have some effect on the hot streak peak, but not nearly as much as the suction side, where Θ_C values were more than twice as low at the lowest blowing ratio of M_{avg} = 0.5.

8.5 Effect of Turbulence Level on Full Coverage Coolant Dispersion

Immediately obvious in Figure 8.13 is the greater spread of the coolant under high mainstream turbulence conditions. Both tests were run with full coverage film cooling at high blowing ratios, which were M^* = 2.0 for the showerhead, M_{avg} = 1.0 for the suction side, and M_{avg} = 1.0 for the pressure side. In Figure 8.13a for the low turbulence condition, the coolant was tightly focused around the vane at the trailing edge with small portions of coolant extending beyond this core. A comparison between mainstream turbulence levels showed that the coolant peak value was about 30% lower under low turbulence conditions. This was due to mainstream turbulence spreading coolant further from the vane surface under high mainstream turbulence.

At midspan, in Figure 8.14, the low turbulence profile was even more different, at about 75% lower. The much narrower low mainstream turbulence coolant profile peaked just to the suction side of the trailing edge and did not spread away at its base like the high mainstream turbulence profile. Its 20% width was about twice as narrow as well.

In Figure 8.15, coolant profiles for individual regions are plotted along with the full coverage profile for low mainstream turbulence. As discussed in §7.5 with reference to high mainstream turbulence, the profiles were roughly additive, but with some showerhead/suction side coolant interaction which limited the spreading of suction side coolant to some extent. This was most evident away from the wall beyond y/P = 0.05 where the full coverage profile was stronger than the combination of individual profiles would suggest, but was less of an effect than at high mainstream turbulence levels (see Figure 7.14 and discussion in §7.5 for more details).

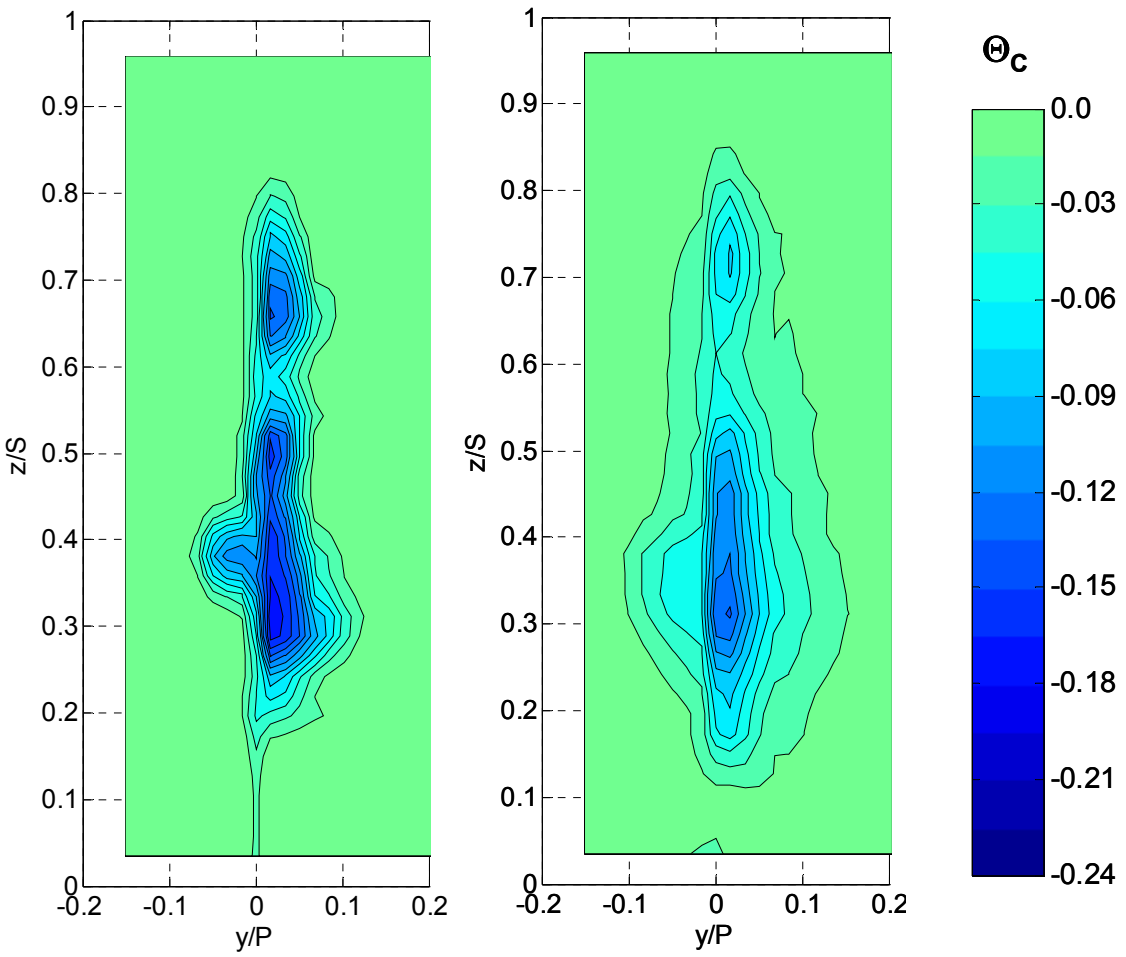

a. **b.**

Figure 8.13: Normalized coolant temperature (Θ_C) contours at Position T for full coverage blowing at $M^*_{showerhead}$ = 2.0, $M_{avg,suction}$ = 1.0, and $M_{avg,pressure}$ = 1.0, DR = 1.6 for:

a. Low mainstream turbulence (Tu = 3.5%)

b. High mainstream turbulence (Tu = 20%)

The effect of the sharply focused coolant profile on the hot streak was enormous, completely eliminating the hot streak to the suction side as seen in Figure 8.16. The remaining hot streak was centered just above midspan and to the pressure side with a peak of Θ_R = 0.46. Excess coolant remained both at positions well below midspan and just to the suction side above midspan. Unfortunately, the full potential benefit of full coverage film cooling on hot streak reduction could not be realized without repositioning

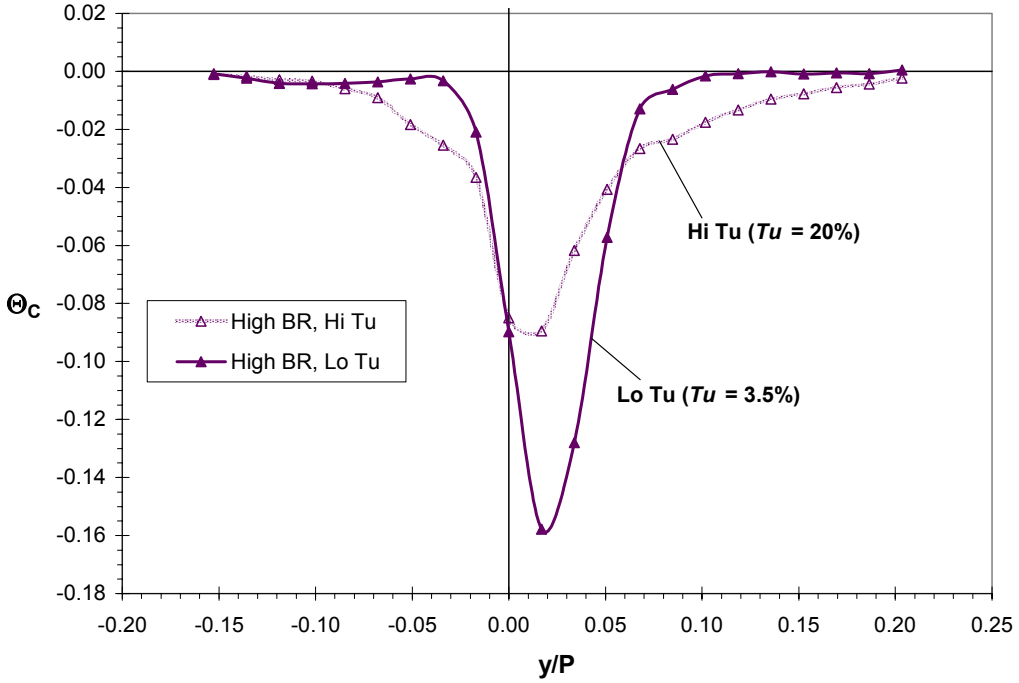

Figure 8.14: Normalized coolant temperature (Θ_C) profiles for at Position T at midspan (z/S = 0.50) for full coverage blowing at $M^*_{showerhead}$ = 2.0, $M_{avg,suction}$ = 1.0, and $M_{avg,pressure}$ = 1.0, for low turbulence (Tu = 3.5%) and high turbulence (Tu = 20%).

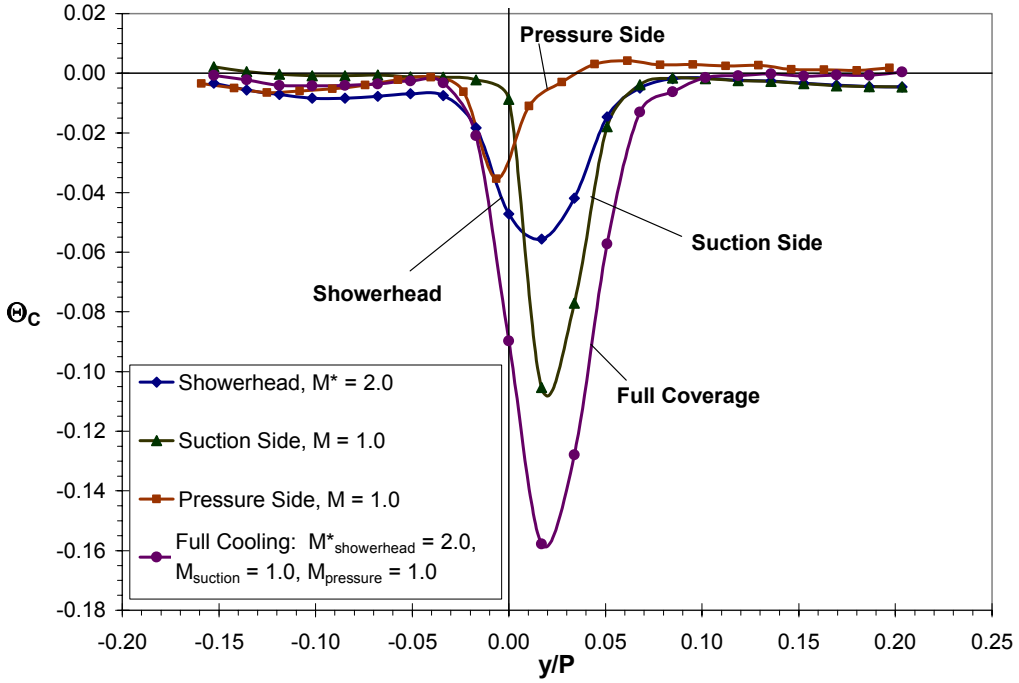

Figure 8.15: Normalized temperature ratio (Θ_R) coolant profiles at Position T comparing showerhead blowing (M^* = 2.0), suction side blowing (M_{avg} = 1.0), pressure side blowing (M_{avg} = 1.0), and full coverage blowing ($M^*_{showerhead}$ = 2.0, $M_{avg,\ suction}$ = 1.0, and $M_{avg,\ pressure}$ = 1.0), low mainstream turbulence (Tu = 3.5%).

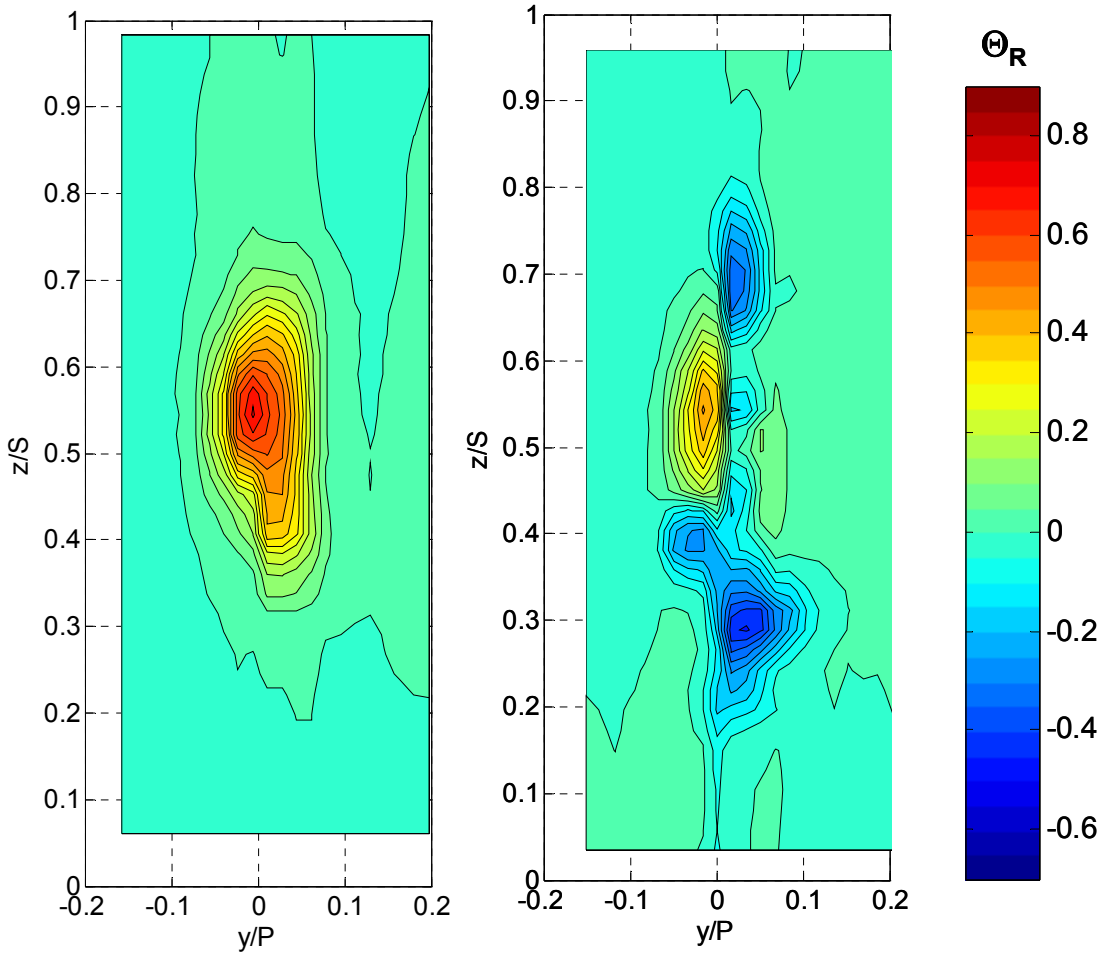

Figure **8.16: Normalized temperature ratio (Θ_R) contours at Position T with the hot streak at the stagnation line, low mainstream turbulence (Tu = 3.5%):**

a. No coolant

b. Full coverage blowing at $M^*_{showerhead}$ = 2.0, $M_{avg,\ suction}$ = 1.0, and $M_{avg,\ pressure}$ = 1.0

the hot streak relative to the vane since there was little coolant to the pressure side of the vane. This resulted in a hot streak that remained fairly strong even with full coverage cooling at high blowing ratios.

At midspan it was even clearer how full coverage blowing reduced the hot streak on the suction side, as shown in Figure 8.17. On the pressure side, full coverage film cooling at high blowing ratios of $M^*_{showerhead}$ = 2.0, $M_{avg,\ suction}$ = 1.0, and $M_{avg,\ pressure}$ = 1.0 reduced the peak by about 40%. At these blowing ratios on the suction side, where the peak of the uncooled hot streak was Θ_R = 0.60, the hot streak was reduced to below the mainstream temperature in some places, while for standard blowing ratios, the hot streak

just to the suction side of the trailing edge was reduced by about 75%. Slightly higher values were observed farther from the trailing edge, beyond the range of the suction side coolant with both sets of blowing ratios. All told, full coverage film cooling was effective at reducing the hot streak at low turbulence, especially on the suction side, although the hot streak remained moderately strong on the pressure side of the trailing edge.

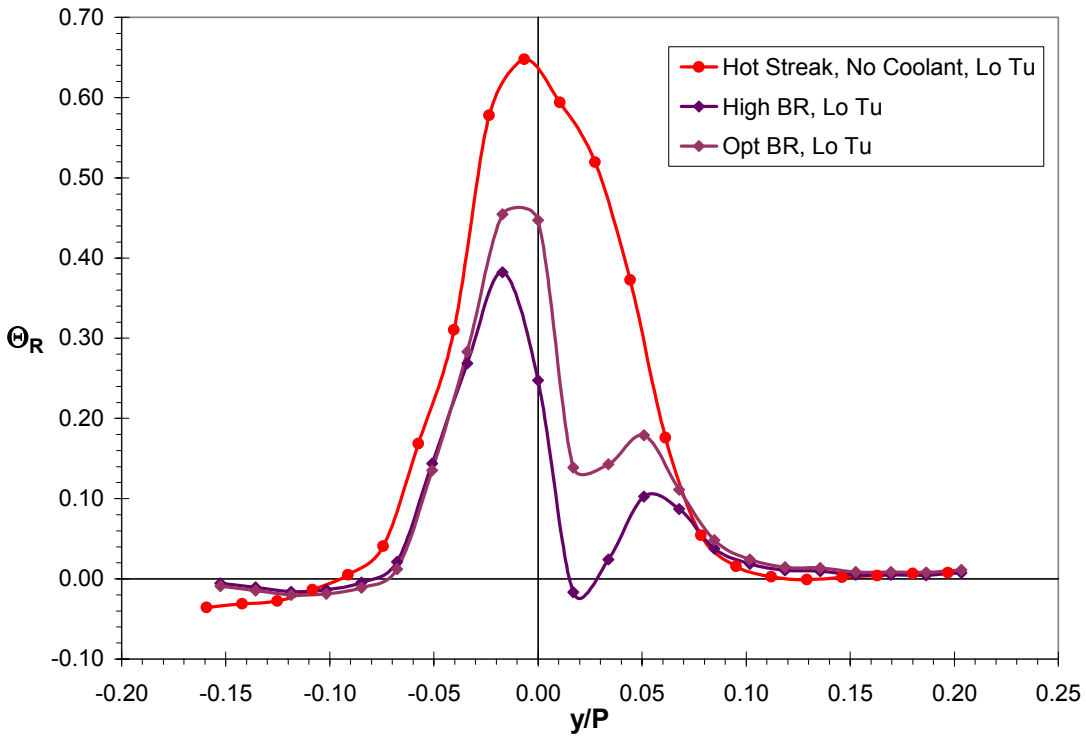

Figure **8.17: Normalized temperature ratio (Θ_R) profiles at Position T for the hot streak impacting the stagnation line without coolant and with full coverage blowing at $M^*_{showerhead}$ = 2.0, $M_{avg,\ suction}$ = 1.0, and $M_{avg,\ pressure}$ = 1.0, low mainstream turbulence (Tu = 3.5%).**

Chapter 9: Effects of Density Ratio on Hot Streak Reduction/Aero-Engine Hot Streak Scaling

9.1 Introduction

The density ratio of the coolant for the experiments in Chapters 4-8 was set to DR = 1.6 with a hot streak temperature ratio of T/T_∞ = 1.09, representative of ground-based engine conditions. A separate study involved varying the density ratio to assess the effect of coolant temperature on the fluid temperatures downstream at the trailing edge. Previous studies investigating adiabatic effectiveness at differing density ratios found that adiabatic effectiveness testing could be performed at a lower density ratio provided that the appropriate scaling of results was used. Conversely, lower density ratios for hot streak reduction would not be expected to result in the same reduction of the hot streak since the fixed temperature ratio hot streak would be interacting with coolant much closer to the mainstream temperature. Even though lower density ratios were not expected to reduce the hot streak as greatly, exactly how the hot streak reduction scaled with coolant density ratio was not known. The effect of lower density ratios on coolant profiles was investigated for individual regions and in combination for a fully film-cooled vane. Since the hot streak temperature ratio was fixed, appropriate scaling of the coolant temperature permitted the simulation of a higher hot streak temperature ratio. In this way, the higher hot streak temperature ratios found in aero-specific engines could be simulated.

9.2 Aero-Engine Scaled Hot Streak Reduction

Aero-specific engines tend to have higher hot streak temperature ratios, as well as higher coolant density ratios. Although the hot streak could not be adjusted in the facility, the effect of a higher hot streak temperature ratio may be simulated by adjusting the coolant density ratio and thereby the coolant temperature, while leaving the hot streak unchanged. Since hot streak/coolant mixing is dominated by temperature differences, scaling the coolant-to-mainstream and hot streak peak-to-mainstream temperature differences by the same factor should simulate aero-specific conditions as shown in Equations 9.1 and 9.2:

$$\left(T_{\infty} - T_{C,0}\right)_{actual} \cdot F = \left(T_{\infty} - T_{C,0}\right)_{simulated} \tag{9.1}$$

$$\left(T_{HS,0} - T_{\infty}\right)_{actual} \cdot F = \left(T_{HS,0} - T_{\infty}\right)_{simulated} \tag{9.2}$$

where F was the common multiplicative factor. It was shown in Chapter 2, Equations 2.5 and 2.6 that the hot streak ΔT should scale with the coolant ΔT through an energy balance at a point in the flow. The mainstream temperatures were T_{∞} = 300 K, the experimentally measured hot streak peak temperature was $T_{HS,0}$ = 327 K for the hot streak temperature ratio of T/T_{∞} = 1.09, and the coolant hole exit temperature was $T_{C,0}$ = 250 K, based on the density ratio of DR = 1.2. The conditions to be simulated were $T_{C,0}$ = 150 K for a scaled density ratio of DR = 2.0 and $T_{HS,0}$ = 381 K for a scaled hot streak temperature ratio of T/T_{∞} = 1.27, using a scaling factor of F = 3. In an actual aero-engine, the peak temperature may be as high as 2000 K [1], so it is instructive to see that the simulated conditions correspond to actual engine conditions. For a mainstream temperature of T_{∞} = 1600 K, a hot streak temperature ratio of T/T_{∞} = 1.27 would have a peak temperature of 2032 K. For a coolant density ratio of DR = 2.0, the coolant temperature would be $T_{C,0}$ = 800 K. Using Equations 9.1 and 9.2 and working in reverse, an "actual" density ratio of DR = 1.2 and an "actual" hot streak temperature ratio of T/T_{∞} = 1.09 is recovered. This demonstrates that the conditions may be translated between the engine condition and laboratory experiment by means of the hot streak temperature ratio and coolant density ratio. Although hot streak temperature ratios have been reported as high as T/T_{∞} = 1.5 in an aero-specific engine, the lower hot streak temperature ratio simulated should provide a good indication of how hot streak/coolant interaction may differ for aero-specific and ground-based engines. As such, the results in the following sections may be viewed as results for an aero-specific engine, while results previously presented at a density ratio of DR = 1.6 with the same hot streak temperature ratio represent ground-based engines.

9.3 Effect of Density Ratio on Coolant Profiles

Coolant profiles were measured for individual regions and for full coverage film cooling at low density ratios of DR = 1.2 and compared with results at high density ratio

(*DR* = 1.6) to evaluate the effect of density ratio on cooling potential. Coolant results for the showerhead demonstrate how large an effect density ratio has on coolant profiles. As shown in Figure 9.1, the normalized temperature contours were much closer to the mainstream at a density ratio of *DR* = 1.2 that at *DR* = 1.6. At the lower density ratio, the coolant had a peak value of Θ_R = -0.09 compared with Θ_R = -0.22 at the high density ratio, or roughly about half the coolant strength at the peak. The effect of the crossover region was still apparent at low density ratio, but it was only due to that large concentration of coolant that coolant was possible to distinguish from the mainstream.

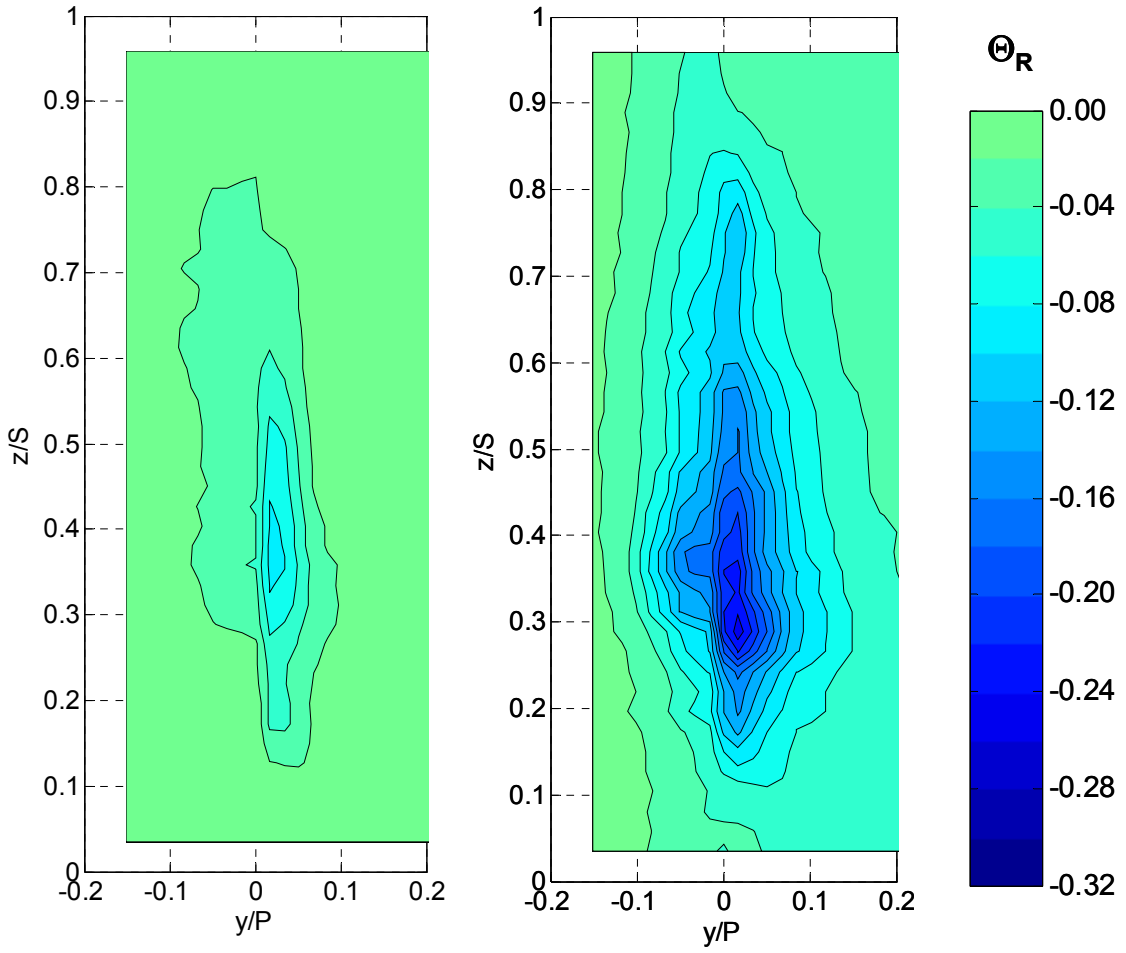

Figure 9.1: Normalized temperature ratio (Θ_R) contours for showerhead blowing at *M = 1.6 for:**

a. Low density ratio (*DR* = 1.2)

b. High density ratio (*DR* = 1.6)

A look at midspan profiles comparing low and high density ratio in Figure 9.2 shows again that the showerhead coolant peaks were roughly half as low for a density ratio of DR = 1.2 than DR = 1.6. As discussed in Chapter 1, the density ratio is defined as the ratio of coolant to mainstream density, and is the equivalent to the ratio of mainstream to coolant temperature using the ideal gas law. Given the same mainstream temperature for experiments at both density ratios, a ratio of coolant-to-mainstream temperature differences may be made resulting in $\Delta T_{Hi\ DR}/\Delta T_{Lo\ DR}$ = 2.25. This indicates that the cooling capacity is a little more than twice as large for high density ratio coolant at DR = 1.6 than low density ratio coolant at DR = 1.2 at the coolant hole exit. Since the normalized coolant temperature ratio, Θ_C, takes into account the difference in coolant temperature at the coolant hole exit, the data should collapse using this parameter. In Figure 9.3, the peaks were fairly similar for both sets of curves. Overall the data

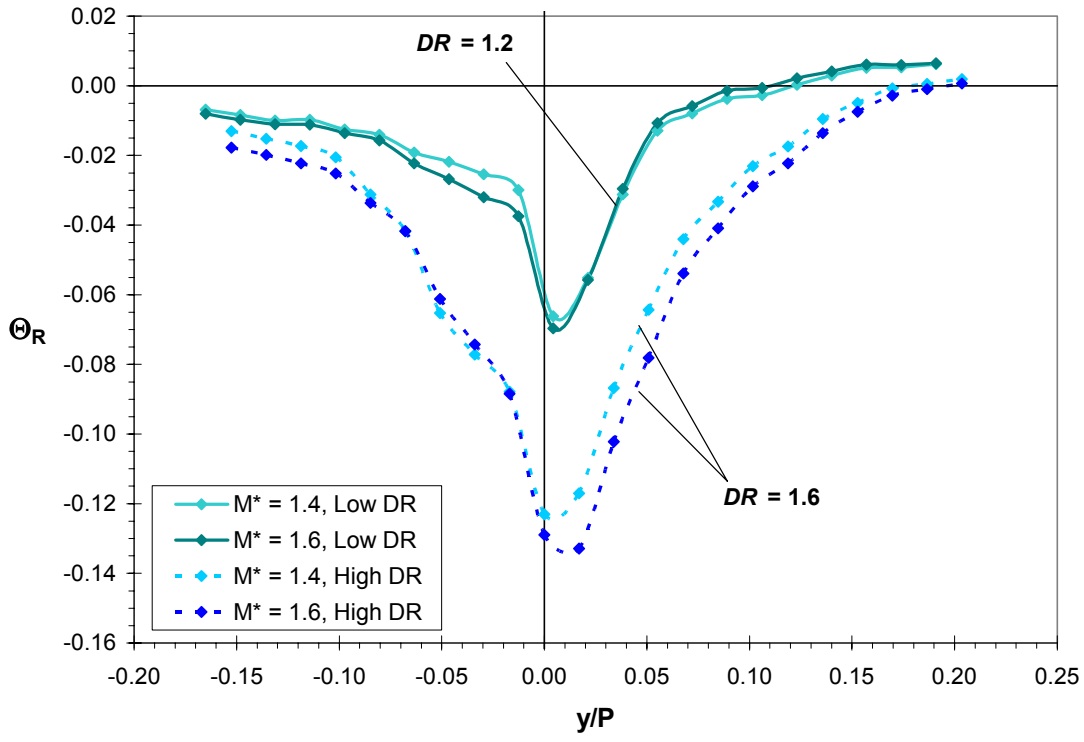

Figure 9.2: Comparison of normalized temperature ratio (Θ_R) profiles at Position T at midspan (z/S = 0.50) for showerhead blowing at M^* = 1.4 and 1.6, at low density ratio (DR = 1.2) and high density ratio (DR = 1.6), high mainstream turbulence (Tu = 20%).

collapsed fairly well, with some differences on the suction side, which were emphasized by the scaling method. This suggests that coolant profiles may be scaled using the normalized coolant temperature ratio, or additionally, that coolant profiles for other density ratios may be predicted from measured values using the definition of Θ_C.

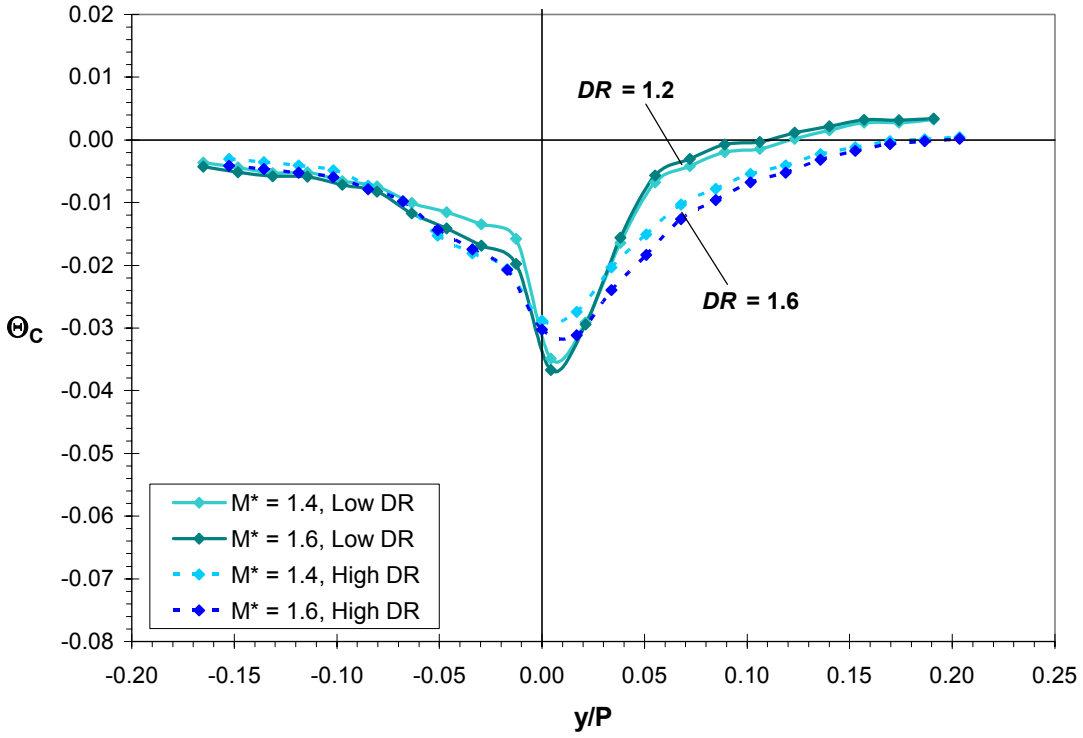

Figure 9.3: Comparison of normalized coolant temperature (Θ_C) profiles at Position T at midspan (z/S = 0.50) for showerhead blowing at M^* = 1.4 and 1.6, at low density ratio (DR = 1.2) and high density ratio (DR = 1.6), high mainstream turbulence (Tu = 20%).

Contours of suction side coolant in Figure 9.4 offer an even clearer picture of the effect of density ratio. Since suction side coolant did not spread into the mainstream as quickly as showerhead coolant, remaining much closer to the vane surface, the differences due to density ratio were easier to see. At both density ratios, the three regions of coolant were distinct, with contour levels about twice as low at the higher density ratio. These distinct regions were a result of coolant hole blockage by the suction side coolant hatch as described in §5.2. Low temperatures farther away from the vane were not observed at the lower density ratio (DR = 1.2), since the overall coolant temperature was much closer to the mainstream at the hole exit.

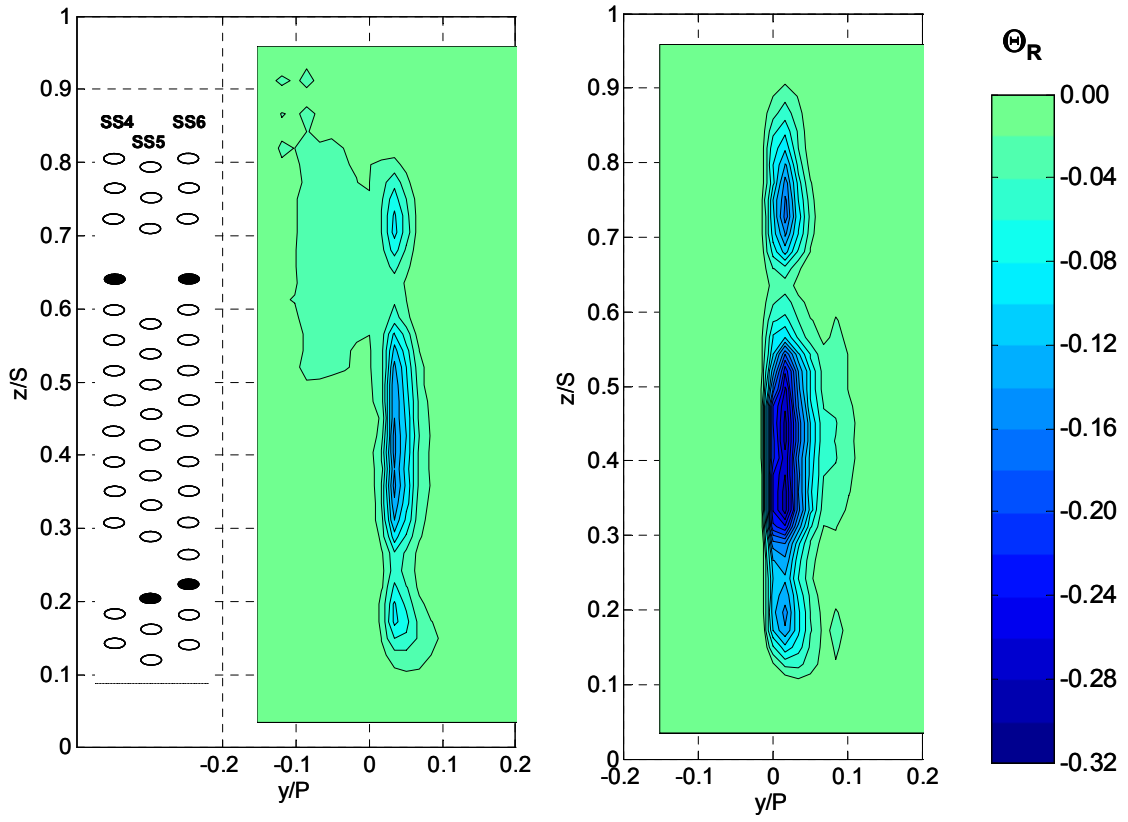

Figure 9.4: Normalized temperature ratio (Θ_R) contours for suction side blowing at M_{avg} = 0.7 for:

a. Low density ratio (*DR* = 1.2)

b. High density ratio (*DR* = 1.6)

This effect is more obvious in the midspan profiles presented in Figure 9.5. For the suction side, comparison of the peak coolant values showed almost exactly a factor of two in Θ_R between low and high density ratio results. As with the showerhead, the shapes of the coolant profiles were similar, indicating that the mixing process was essentially unaffected by the coolant temperature at the hole exit. Scaling the results using the normalized coolant temperature, Θ_C, again produced good results, with similar peaks and similar gradients away from the wall as shown in Figure 9.6.

Given the marginal performance of pressure side film cooling at high density ratio, it was not expected that coolant would be discernible from the mainstream

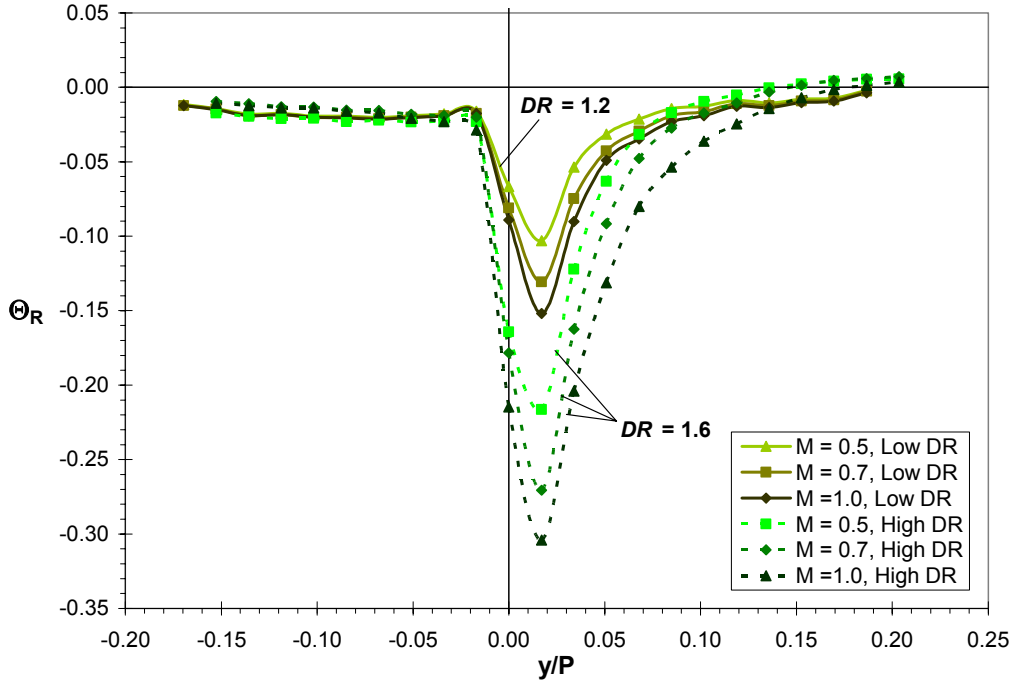

Figure 9.5: Comparison of normalized temperature ratio (Θ_R) profiles at Position T at midspan (z/S = 0.50) for suction side blowing at M_{avg} = 0.5, 0.7, and 1.0, at low density ratio (DR = 1.2) and high density ratio (DR = 1.6), high mainstream turbulence (Tu = 20%).

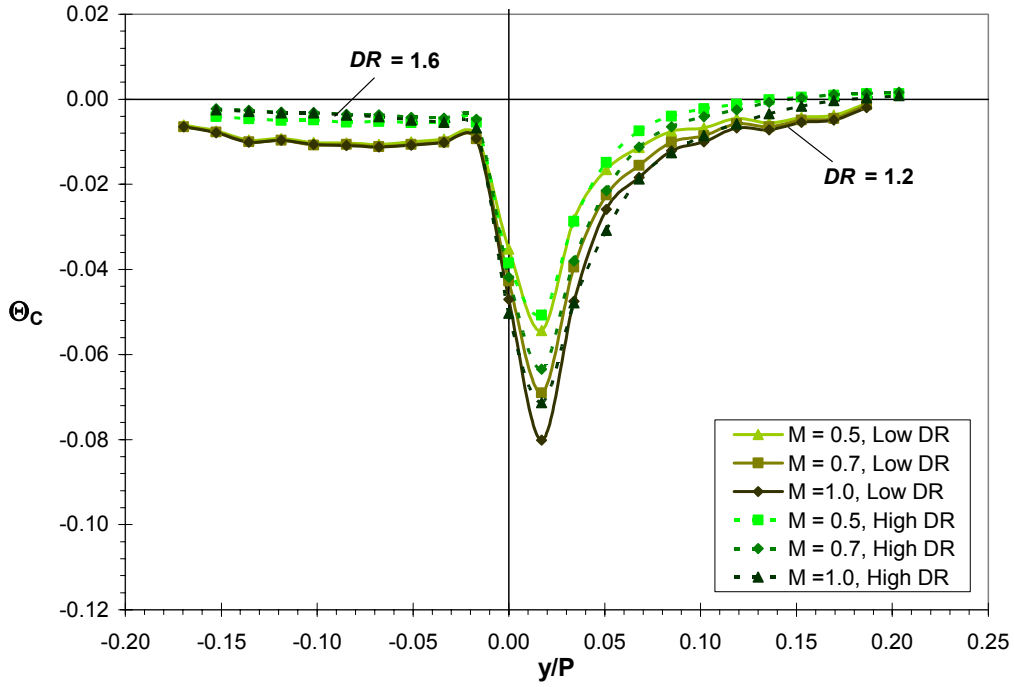

Figure 9.6: Comparison of normalized coolant temperature ratio (Θ_C) profiles at Position T at midspan (z/S = 0.50) for suction side blowing at M_{avg} = 0.5, 0.7, and 1.0, at low density ratio (DR = 1.2) and high density ratio (DR = 1.6), high mainstream turbulence (Tu = 20%).

temperatures at the trailing edge at low density ratios, especially considering the effect of density ratio on the showerhead and suction side. For this reason, the pressure side was not tested individually at low density ratio.

For full coverage film cooling at low density ratios, the high set of blowing ratios were used, i.e. $M^*_{showerhead} = 2.0$, $M_{avg,\ suction} = 1.0$, and $M_{avg,\ pressure} = 1.0$, since they were expected to have the largest effect on the hot streak. In Figure 9.7, the same effect of density ratio on coolant levels was observed as for individual regions. Once again, the

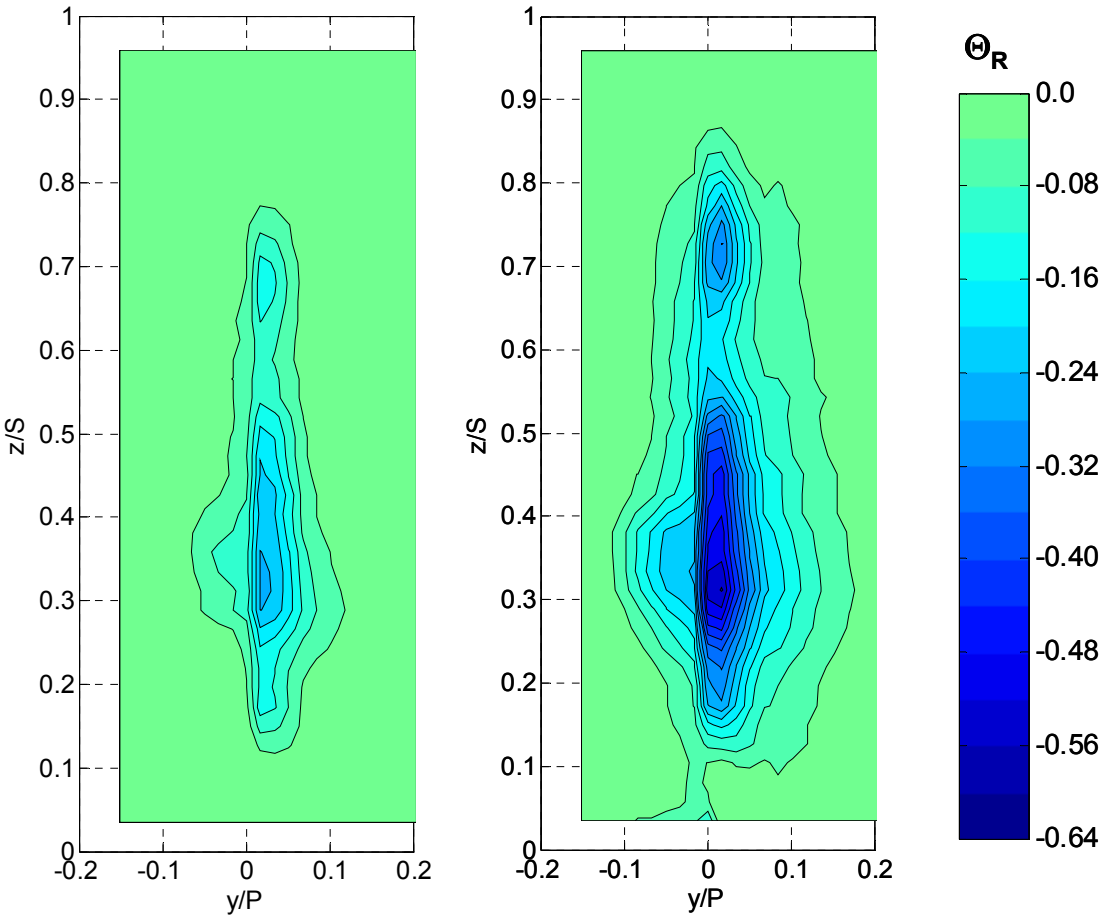

a. b.

Figure 9.7: Normalized temperature ratio (Θ_R) contours at Position T for full coverage blowing at $M^*_{showerhead} = 2.0$, $M_{avg,suction} = 1.0$, and $M_{avg,pressure} = 1.0$ for:

a. Low density ratio ($DR = 1.2$)

b. High density ratio ($DR = 1.6$)

coolant levels were roughly half as low for low density ratios as high density ratios, but the shape of the coolant regions was the same. In particular, the peak at low density ratio was Θ_R = -0.26, with the peak at high density ratio about 2.2 times higher. The shapes of midspan profiles in Figure 9.8 were also similar between density ratios at both midspan and at z/S = 0.31 where the coolant peak occurred for both density ratios suggesting that scaling would work well at both locations.

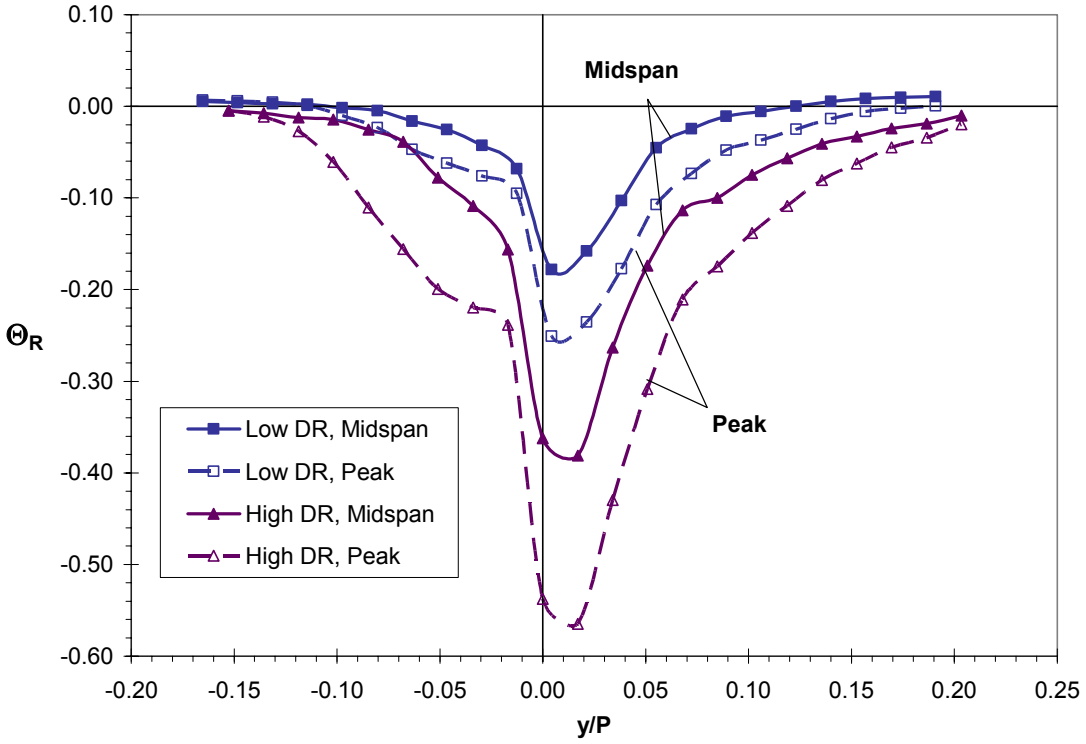

Figure 9.8: Comparison of normalized temperature ratio (Θ_R) profiles at Position T at midspan (z/S = 0.50) and the position of peak coolant (z/S = 0.31) for full coverage blowing at $M^*_{showerhead}$ = 2.0, $M_{avg,suction}$ = 1.0, and $M_{avg,pressure}$ = 1.0, at low density ratio (DR = 1.2) and high density ratio (DR = 1.6), high mainstream turbulence (Tu = 20%).

These results are shown scaled by Θ_C in the contour plots of Figure 9.9. It is immediately obvious that the range and shape of the contour levels were very similar for the two density ratios using Θ_C scaling. This indicates that the spreading rate of the coolant and resulting distributions of initial coolant were relatively independent of the density ratio within the range tested. Since the values of the coolant temperature at a given point were dependent on the coolant hole exit-to-mainstream temperature

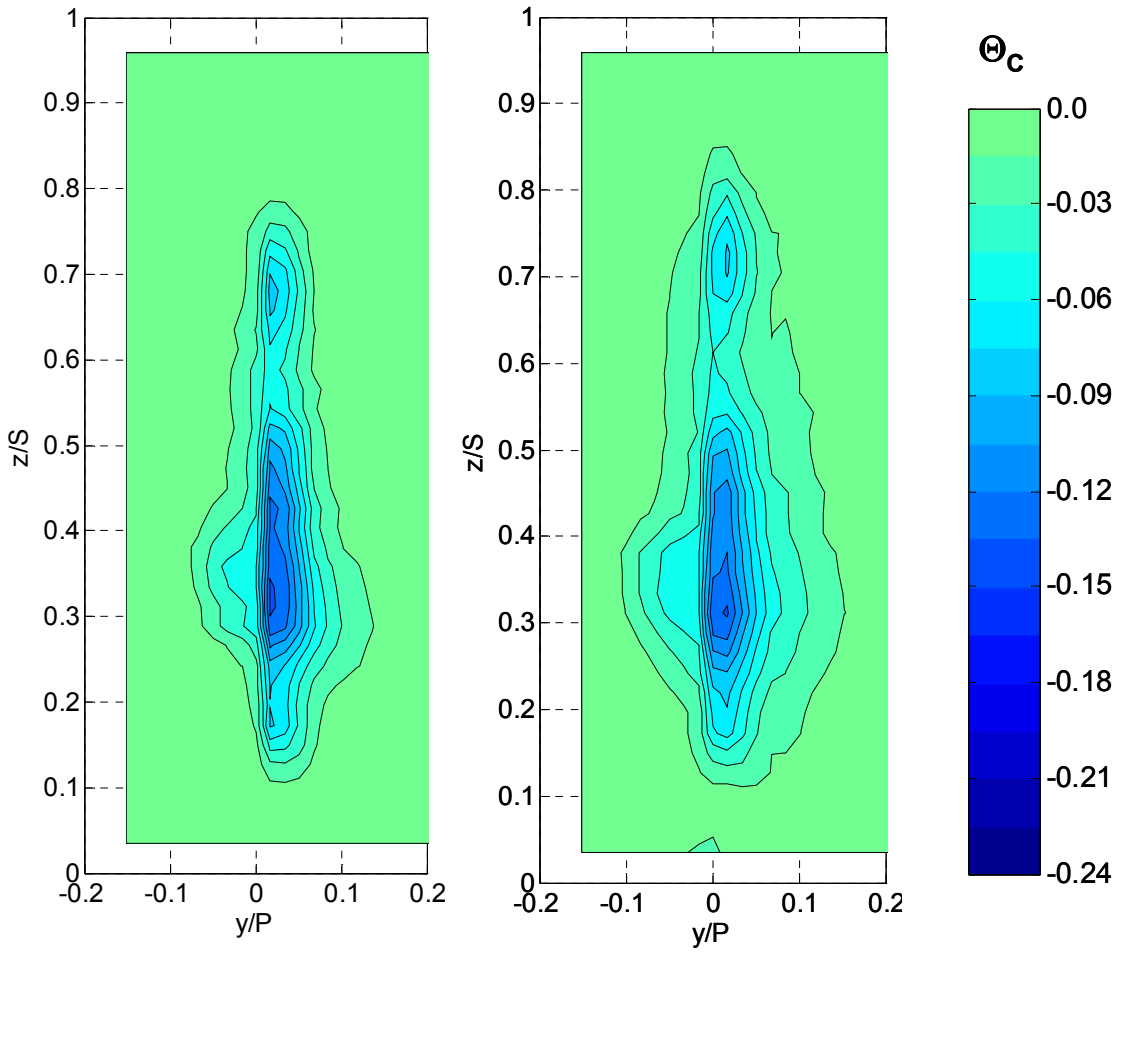

a. **b.**

Figure 9.9: Normalized coolant temperature (Θ_C) contours at Position T for full coverage blowing at $M^*_{showerhead}$ = 2.0, $M_{avg,suction}$ = 1.0, and $M_{avg,pressure}$ = 1.0 for:

a. Low density ratio (*DR* = 1.2)

b. High density ratio (*DR* = 1.6)

difference, as suggested before this could be used to extrapolate to other density ratios. Figure 9.10 shows midspan and 0.31*S* profiles using Θ_C scaling. The agreement was very good at the peaks of the profiles with some deviations on the pressure side for the 0.31*S* coolant profile and to the suction side away from the peak for all profiles.

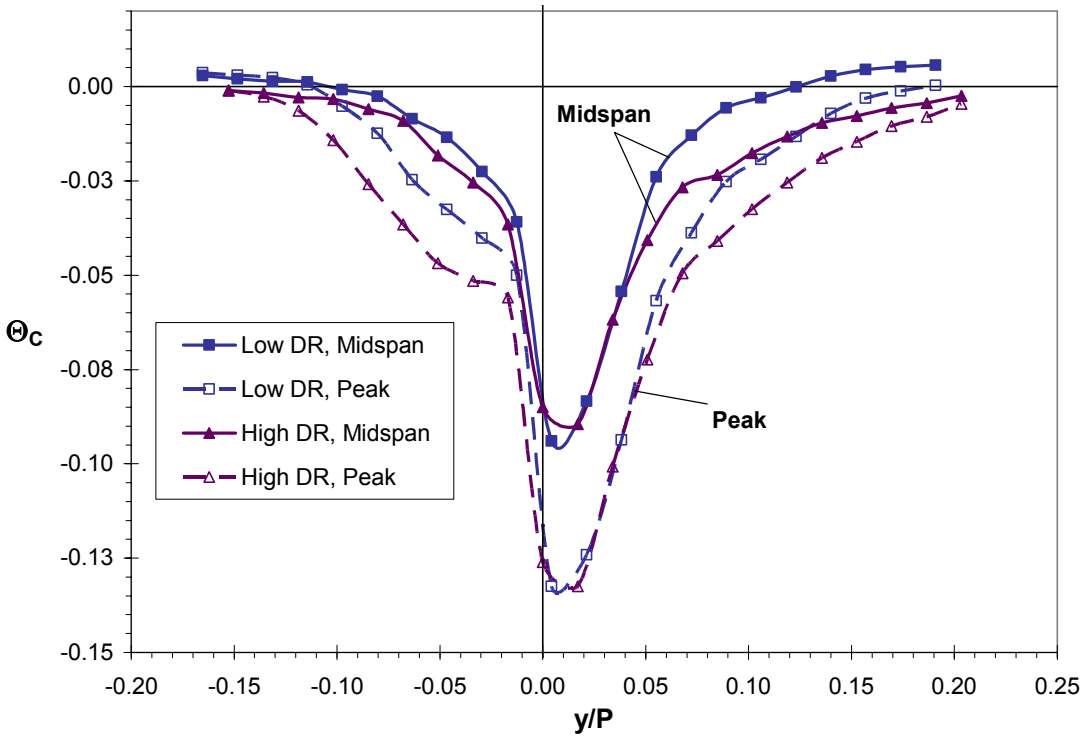

Figure 9.10: Comparison of normalized coolant temperature (Θ_C) profiles at Position T at midspan (z/S = 0.50) and the position of peak coolant (z/S = 0.31) for full coverage blowing at $M^*_{showerhead}$ = 2.0, $M_{avg,suction}$ = 1.0, and $M_{avg,pressure}$ = 1.0, at low density ratio (DR = 1.2) and high density ratio (DR = 1.6), high mainstream turbulence (Tu = 20%).

9.4 Effect of Density Ratio on Hot Streak Reduction

Overall, scaling of coolant profiles would suggest that low density ratio coolant at DR = 1.2 would be about half as effective at reducing the hot streak as high density ratio coolant at DR = 1.6. Measurements were made using showerhead, suction side, and full coverage blowing at a density ratio of DR = 1.2 with the hot streak activated. Due to expectations of the performance of the pressure side, it was not tested alone with the hot streak.

Figure 9.11 shows that showerhead film cooling at a low density ratio did reduce the hot streak somewhat as compared with no film cooling. The peak hot streak temperature with film cooling was Θ_R = 0.45, a drop of about 10% compared with no film cooling. Referring back to the coolant profiles in Figure 9.2 and corresponding discussions, the peak coolant at high density ratio was about two times as low as the low

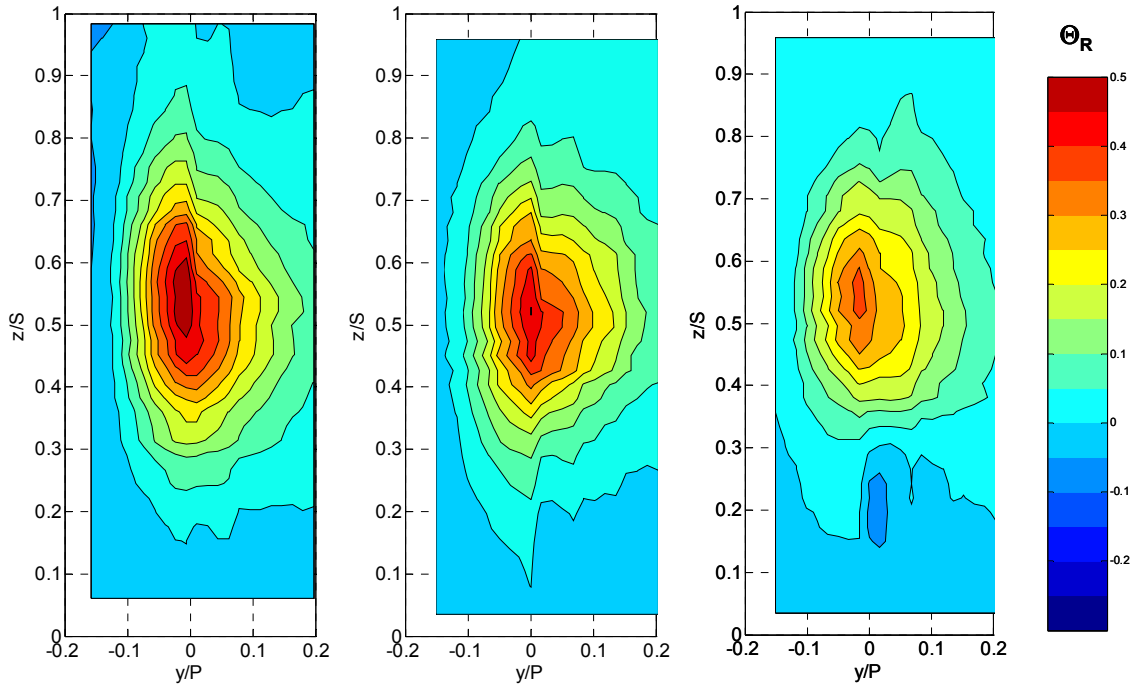

Figure 9.11: Normalized temperature ratio (Θ_R) contours at Position T with the hot streak at the stagnation line, high mainstream turbulence (Tu = 20%) with:

a. No coolant

b. Showerhead blowing at M^* = 1.6, low density ratio (DR = 1.2)

c. Showerhead blowing at M^* = 1.6, high density ratio (DR = 1.6)

density ratio peak. The reduction in hot streak peak due to film cooling was also about two times as large for high density ratio as for low density ratio. Low density ratio coolant (Figure 9.11b) did not noticeably reduce the lower portion of the hot streak, whereas high density ratio coolant (Figure 9.11c) had removed a substantial portion due to the effect of the crossover region. Midspan profiles in Figure 9.12 show how the low density ratio coolant reduced only the central pitchwise portion of the hot streak. This was because coolant mixing well away from the vane had less of a temperature driving potential at low density ratio and therefore was less effective than the high density ratio coolant as evidenced by coolant profiles in Figure 9.2.

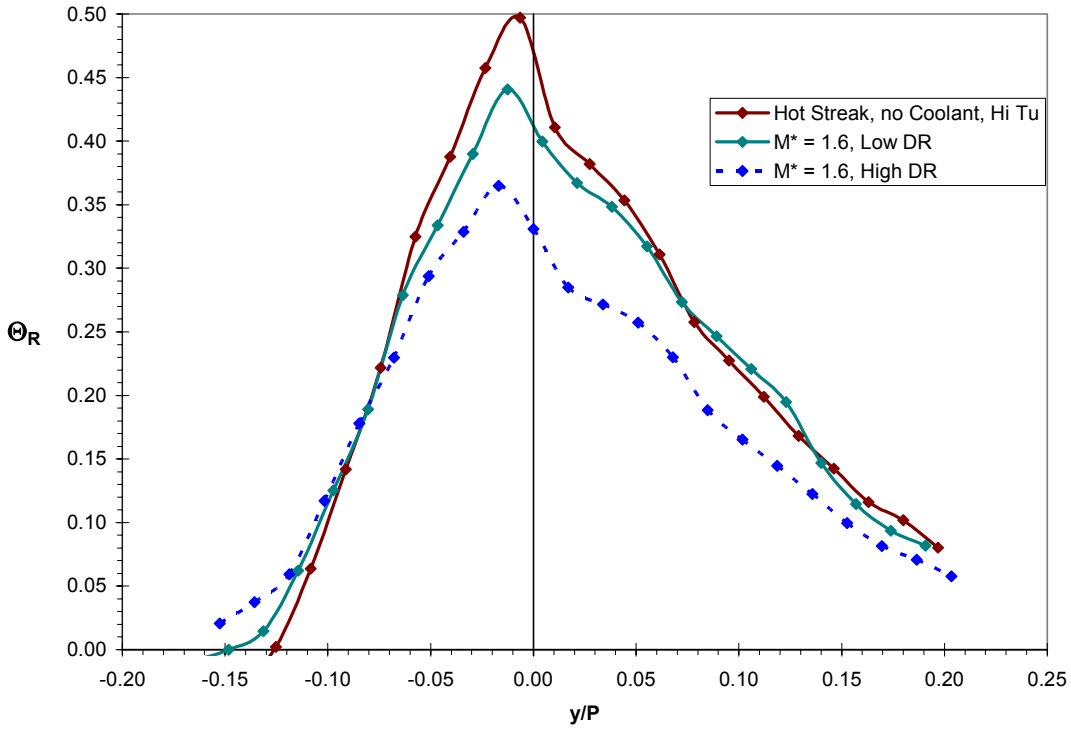

Figure 9.12: Normalized temperature ratio (Θ_R) profiles at Position T for the hot streak impacting the stagnation line without coolant and with showerhead blowing at M^* = 1.6 with density ratios of DR = 1.2 and 1.6, high mainstream turbulence (Tu = 20%).

Suction side film cooling had a more visible effect on the hot streak than showerhead film cooling at low density ratios as shown in Figure 9.13, but the effect was highly localized on the suction side of the trailing edge. On the suction side very near the trailing edge, the hot streak was reduced about one contour level. A small portion of coolant appeared well below the extent of the hot streak, while at high density ratio (Figure 9.13c) a great deal of excess coolant was observed above and below the remaining hot streak. The overall hot streak peak was very similar for both density ratios since the pressure side was unaffected, leaving a strong peak on that side. However, as discussed in §5.2, a fair comparison is only possible to the suction side of the trailing edge. For this region, the hot streak peak was Θ_R = 0.37 compared with Θ_R = 0.25 at high density ratio. The hot streak profile at midspan with suction side film cooling at low density ratio was flattened out on the suction side as illustrated in Figure 9.14, as

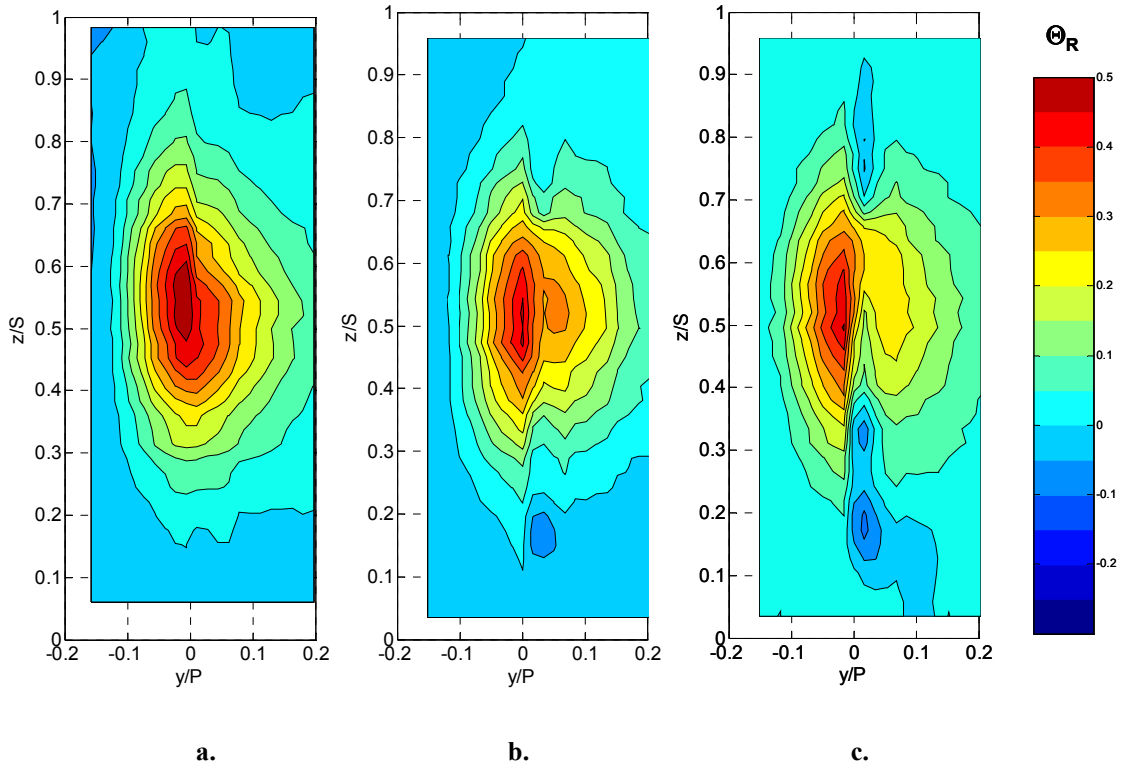

Figure 9.13: Normalized temperature ratio (Θ_R) contours at Position T with the hot streak at the stagnation line, high mainstream turbulence (Tu = 20%) with:

a. No coolant

b. Suction side blowing at M_{avg} = 0.7, low density ratio (DR = 1.2)

c. Suction side blowing at M_{avg} = 0.7, high density ratio (DR = 1.6)

opposed to the strong drop observed with high density ratio suction side coolant. Just away from the trailing edge to the suction side, the hot streak was reduced by more than 2.5 times the amount with high density ratio coolant that it was by low density coolant.

With full coverage film cooling at high blowing ratios and low density ratio coolant at DR = 1.2, the hot streak was reduced to under Θ_R = 0.25 on the suction side with extra coolant above and below the remaining hot streak as shown in Figure 9.15b. The pressure side was reduced less, with the peak hot streak temperature at about midspan just to the pressure side of the trailing edge. Overall the hot streak peak was reduced almost 20% to Θ_R = 0.41 compared with almost 40% with high density ratio coolant. Proportionally, the drop in hot streak peak with film cooling was just over two times greater with high density ratio than low density ratio.

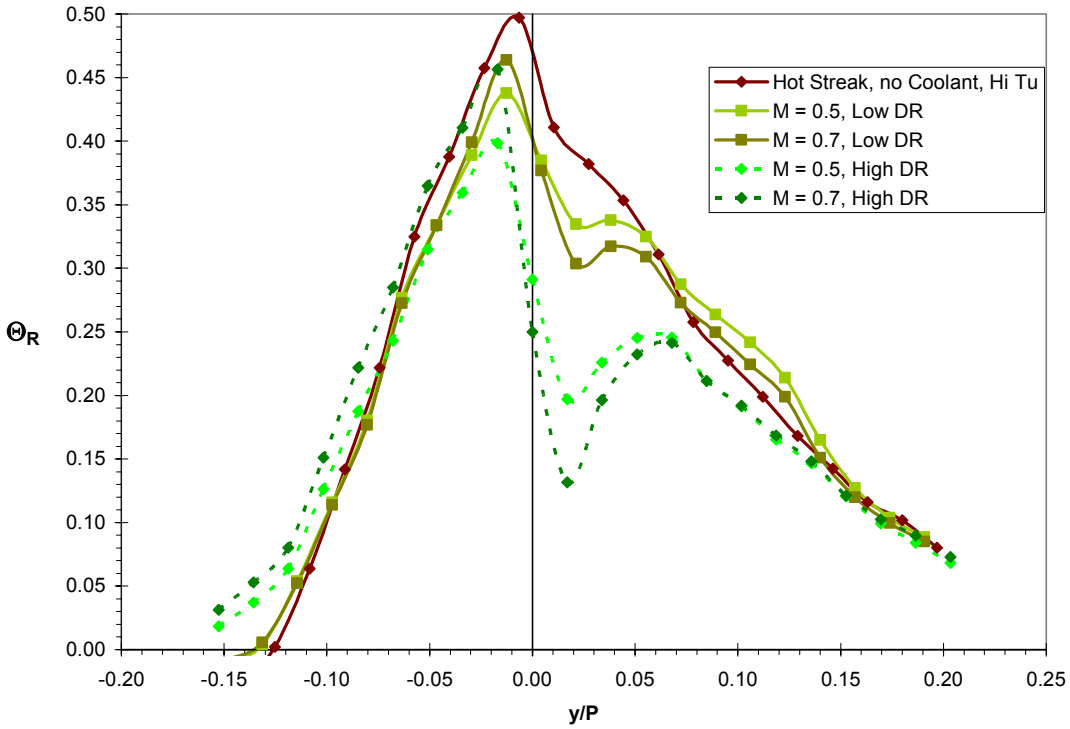

Figure 9.14: Normalized temperature ratio (Θ_R) profiles at Position T for the hot streak impacting the stagnation line without coolant and with suction side blowing at M_{avg} = 0.5 and 0.7, with density ratios of DR = 1.2 and 1.6, high mainstream turbulence (Tu = 20%).

Profiles at midspan in Figure 9.16 show how showerhead coolant augmented suction side coolant to the suction side of the trailing edge to reduce the hot streak much more than the suction side alone (compare to Figure 9.14). This reduced the hot streak to a fairly flat profile from the trailing edge up to about 6d from the vane (0.05P), while a significant dip in the profile occurred much closer with high density ratio coolant. The overall benefit of hot streak reduction due to full coverage film cooling at low density ratios was not large, with reductions of the peak at midspan of about 15% and 20% for optimum and high blowing ratios respectively. Comparing the drop in hot streak peak, high density ratio coolant provided about 2.5 times the reduction as low density ratio coolant, a bit higher than the proportion suggested by the ratio of coolant-to-mainstream temperature differences.

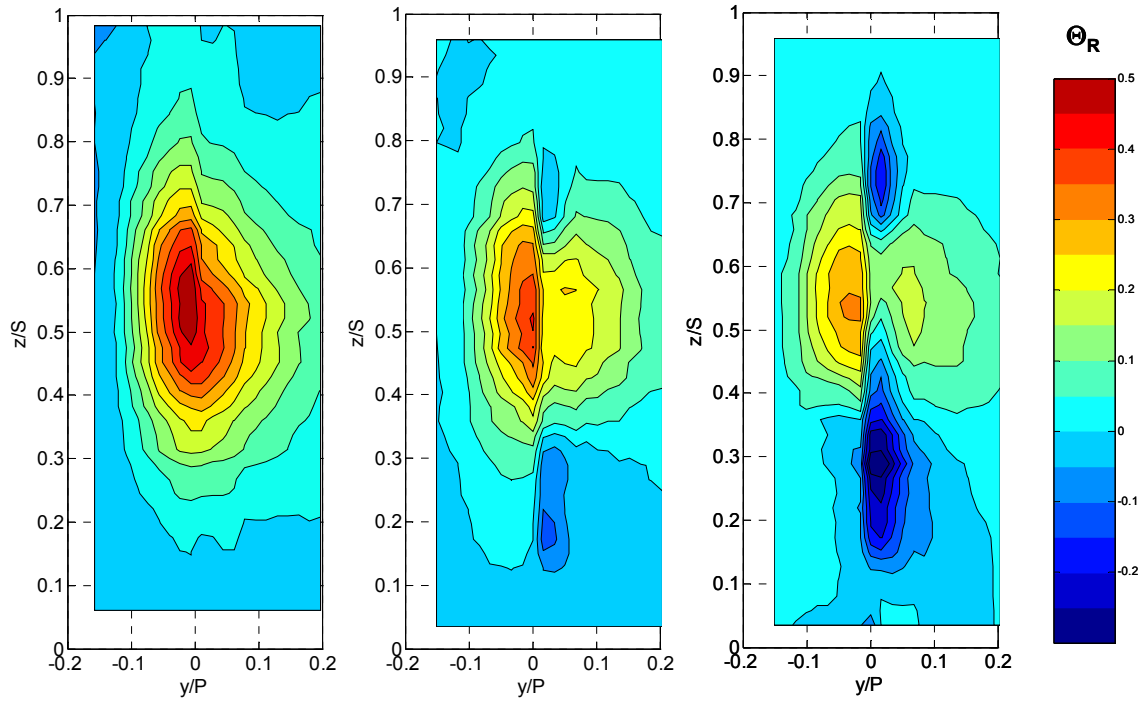

a. **b.** **c.**

Figure **9.15: Normalized temperature ratio (Θ_R) contours at Position T with the hot streak at the stagnation line, high mainstream turbulence (Tu = 20%) with:**

a. No coolant

b. Full coverage blowing at $M^*_{showerhead}$ = 2.0, $M_{avg,suction}$ = 1.0, and $M_{avg,pressure}$ = 1.0, low density ratio (DR = 1.2)

c. Full coverage blowing at $M^*_{showerhead}$ = 2.0, $M_{avg,suction}$ = 1.0, and $M_{avg,pressure}$ = 1.0, high density ratio (DR = 1.6)

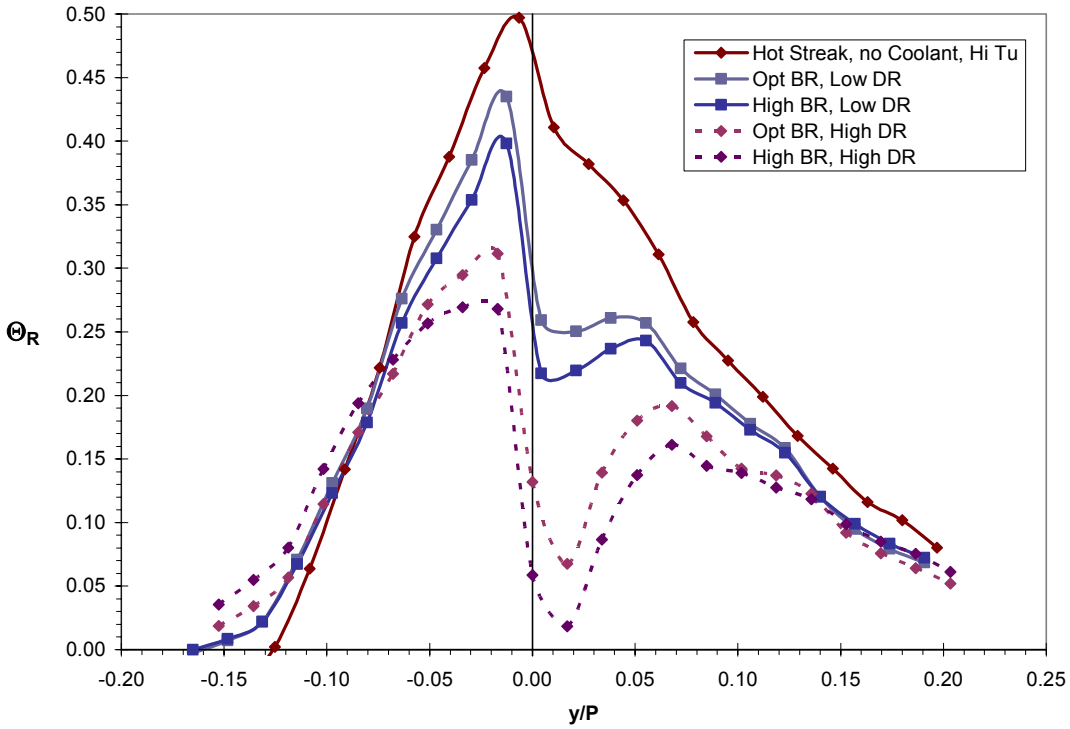

Figure **9.16: Normalized temperature ratio (Θ_R) profiles at Position T for the hot streak impacting the stagnation line without coolant and with full coverage blowing at adiabatic effectiveness optimum blowing ratios ($M^*_{showerhead}$ = 1.6, $M_{avg,\ suction}$ = 0.7, and $M_{avg,\ pressure}$ = 0.6) and above optimum blowing ratios ($M^*_{showerhead}$ = 2.0, $M_{avg,\ suction}$ = 1.0, and $M_{avg,\ pressure}$ = 1.0), with density ratios of DR = 1.2 and 1.6, high mainstream turbulence (Tu = 20%).**

Chapter 10: Superposition Analysis and Predictions

10.1 Introduction

The goal of superposition analysis was to predict the effect of coolant on the hot streak by adding coolant profiles to hot streak profiles. First, the capability of superposition was evaluated by comparing these predictions with measured data. Given sufficient agreement between predicted and measured data, the method was used to estimate the effect of coolant on the hot streak at different pitch positions and determine the ideal hot streak pitch position based on these predictions. Since results in Chapter 9 indicated that the coolant profiles could be scaled by the normalized coolant temperature, Θ_C, coolant profiles with a different density ratio were estimated as well. Superposition of these coolant profiles with measured hot streak profiles should extend the predictive range to conditions found in military aircraft and aero-specific engines.

Since the coolant temperature difference at a point in the flow should additively counteract a hot streak temperature difference of the same magnitude, a superposition equation was developed in Chapter 2, repeated here in Equation 10.1:

$$\Theta_{R,SP} = \Theta_{R,C,\exp} + \Theta_{R,HS,\exp} \tag{10.1}$$

where the subscripts *HS* and *C* refer to coolant only and hot streak only experimental results.

10.2 Superposition of Midspan Profiles at the Trailing Edge

The simplest application of superposition in predicting hot streak/coolant interaction is the prediction of midspan profiles. Since the hot streak was strongest at midspan, this was also the most relevant position for comparing experimental results with predictions using superposition. Since the measurement positions of the hot streak and coolant profiles were not precisely matched, some interpolation was needed to carry out a point-by-point additive superposition calculation. As shown in Chapter 2, Figure 2.17, interpolation of the hot streak profile was validated and should not result in any significant additional error for these calculations.

In Figure 10.1, measured profiles for the hot streak alone and showerhead coolant alone at $M^* = 1.6$ are shown along with the experimentally measured profile for the

showerhead coolant effect on the hot streak Addition of the hot streak only and coolant only profiles resulted in the superposition profile, shown with a fine dotted line. This prediction matched the overall shape of the experimental profile fairly well, but overestimated the peak temperature ratio by about 15%. As a result, for the showerhead cooled hot streak peak, superposition underpredicted the hot streak reduction at 21% compared with the 33% peak hot streak reduction measured. At blowing ratios of M^* = 1.4 and 2.0, not shown in the figure, superposition also underpredicted the benefit of showerhead coolant by similar amounts.

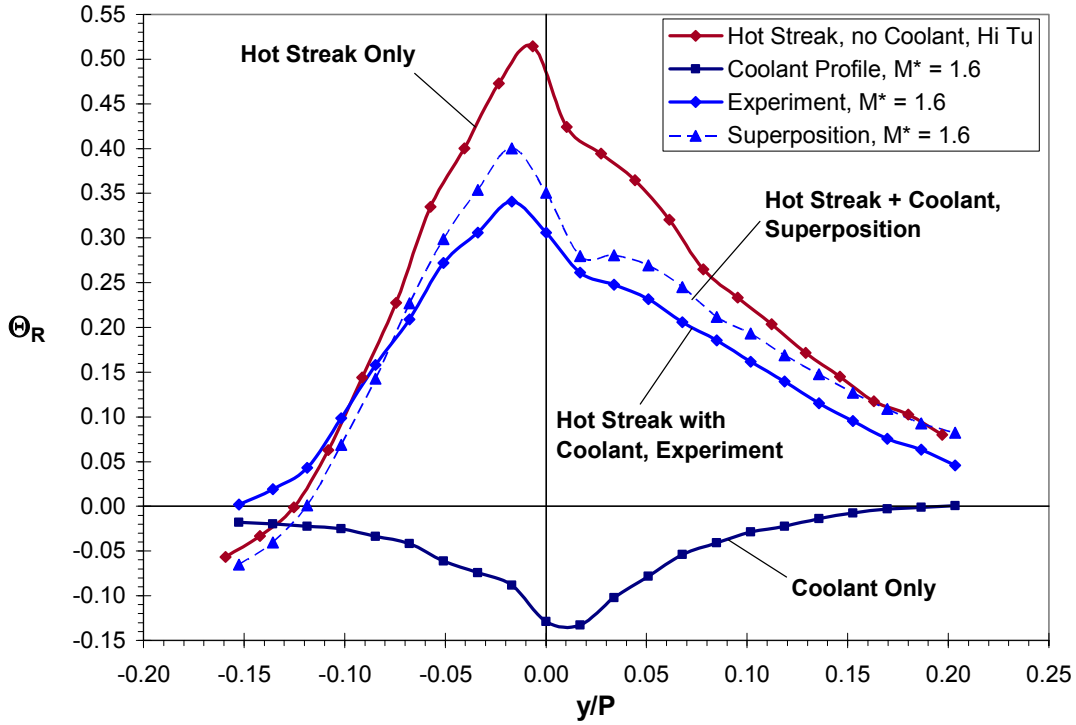

Figure 10.1: Comparison of experimental and superposition normalized temperature ratio (Θ_R) profiles at Position T at midspan (z/S = 0.50), for the hot streak at the stagnation line with showerhead blowing at M^* = 1.6, high mainstream turbulence (Tu = 20%).

On the suction side, prediction of the overall peak hot streak reduction was less of an issue given that the peak region was largely unaffected by suction side film cooling. Superposition, for a blowing ratio of M_{avg} = 0.7, shown in Figure 10.2, predicted the near wall dip in hot streak temperature well, and did a reasonable job of capturing the shape of the rise in hot streak temperature farther away, but the peak hot streak temperature on the

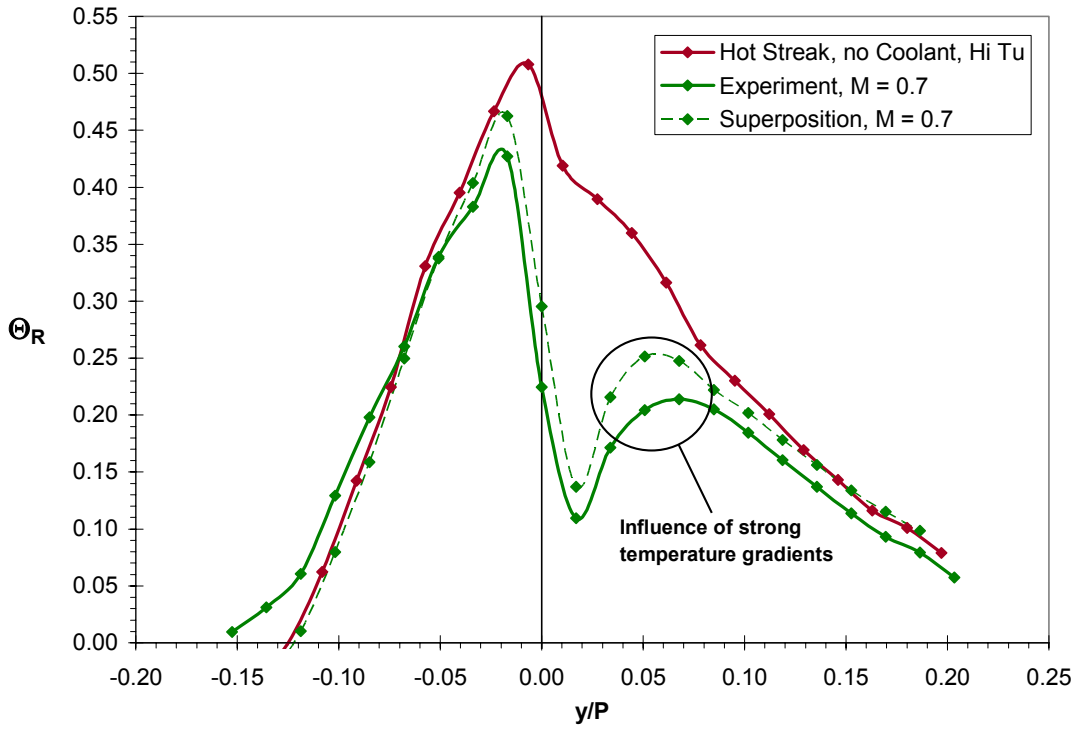

Figure 10.2: Comparison of experimental and superposition normalized temperature ratio (Θ_R) profiles at Position T at midspan (z/S = 0.50), for the hot streak at the stagnation line with suction side blowing at M_{avg} = 0.7, high mainstream turbulence (Tu = 20%).

suction side was slightly overpredicted. Essentially, superposition does not account for the effects of creating larger temperature gradients by mixing coolant directly with hot streak fluid. For this reason, coolant only profiles remained somewhat less diffused into the mainstream, while measurements of hot streak/coolant interaction showed the influence of coolant farther from the wall, a result of the strong temperature gradients created when coolant entered the hot streak. This effect was most noticeable for the suction side between 0.03P and 0.07P as indicated in Figure 10.2. In general, superposition overpredicted the hot streak temperatures by less than about Θ_R = 0.03 to the suction side of the trailing edge, and trends were similar for other blowing ratios not shown.

Pressure side predictions were somewhat less successful as shown in Figure 10.3. Near the wall, coolant reduced the hot streak much more than superposition predicted.

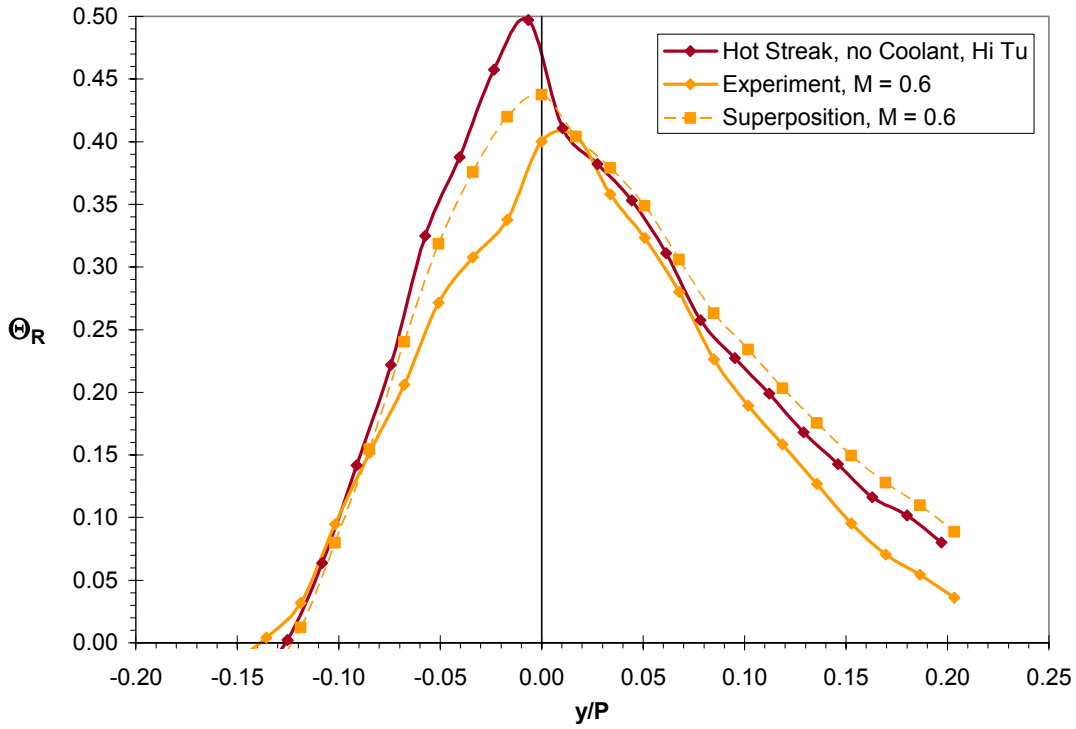

Figure 10.3: Comparison of experimental and superposition normalized temperature ratio (Θ_R) profiles at Position T at midspan (z/S = 0.50), for the hot streak at the stagnation line with pressure side blowing at M_{avg} = 0.6, high mainstream turbulence (Tu = 20%).

Superposition predictions with full coverage film cooling were subject to the same shortcomings as the individual coolant regions. Summarizing the results for individual regions, the superposition of showerhead coolant overpredicted the peak near the trailing edge while superposition of suction side coolant underpredicted the effect of coolant farther away from the wall. Superposition for pressure side coolant overpredicted temperatures for nearly all areas where the coolant had an effect. Therefore, it is not surprising that superposition of full coverage cooling profiles with the hot streak also overpredicted the temperatures for nearly the entire width of the hot streak, as shown in Figure 10.4a for standard blowing ratios. On the other hand, prediction of the shape of the cooled hot streak profile was very good with the superposition profile at a nearly constant offset from the measured profile. Prediction of the overall peak, positioned to the pressure side of the trailing edge, was a little more than 20% high with a similar amount of error in the suction side local maximum. While the measured hot streak

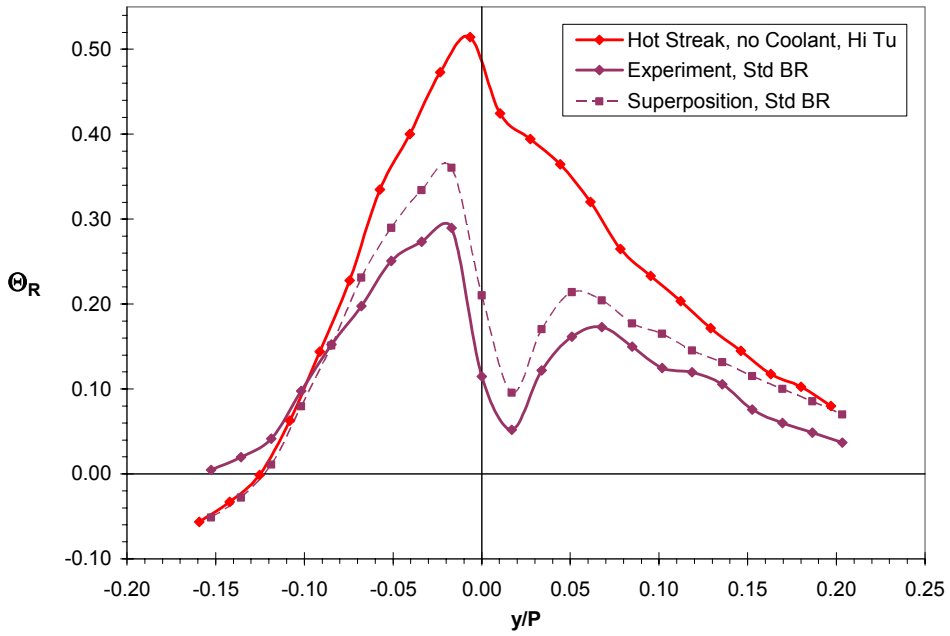

Figure **10.4a: Comparison of experimental and superposition normalized temperature ratio (Θ_R) profiles at Position T at midspan (z/S = 0.50), for the hot streak at the stagnation line with full coverage blowing at ($M^*_{showerhead}$ = 1.6, $M_{avg,\ suction}$ = 0.7, and $M_{avg,\ pressure}$ = 0.6), high mainstream turbulence (Tu = 20%).**

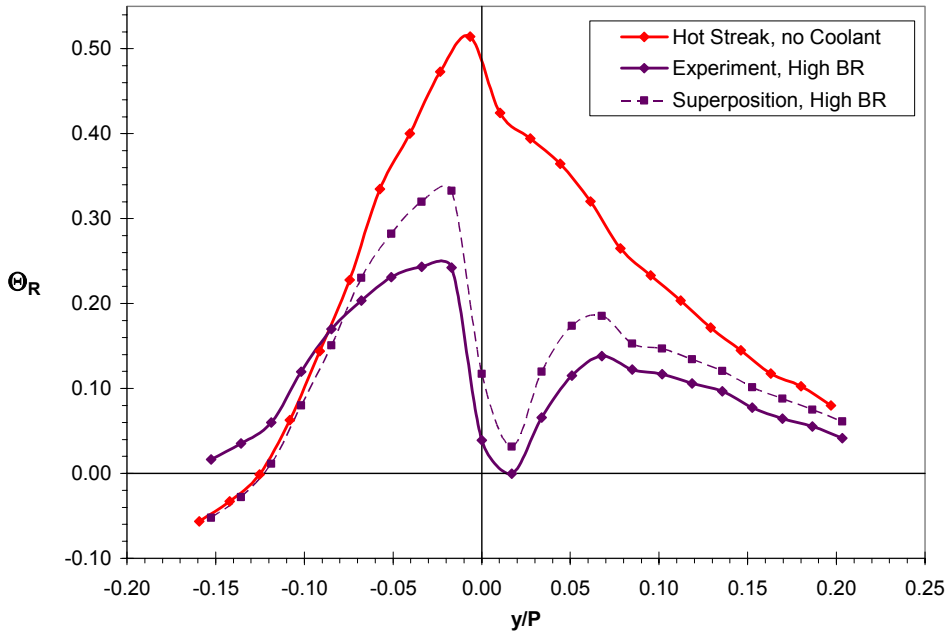

Figure 10.4b: Comparison of experimental and superposition normalized temperature ratio (Θ_R) profiles at Position T at midspan (z/S = 0.50), for the hot streak at the stagnation line with full coverage blowing at ($M^*_{showerhead}$ = 2.0, $M_{avg,\ suction}$ = 1.0, and $M_{avg,\ pressure}$ = 1.0), high mainstream turbulence (Tu = 20%).

reduction was over 40% compared with no film cooling, superposition predicted it would be a little less than 30%. At higher full coverage blowing ratios ($M^*_{showerhead}$ = 2.0, $M_{avg,\ suction}$ = 1.0, and $M_{avg,\ pressure}$ = 1.0), estimation of the shape of the cooled hot streak profile was a little less successful near the peak as seen in Figure 10.4b, but overall agreement was good. On the pressure side, the value of the hot streak peak was overestimated by just over 20%.

Theoretically it should be possible to estimate the full coverage coolant profile by superposition of individual region coolant profiles as well. However, as discussed in Chapter 7, interactions between coolant from the showerhead and suction side (and less so between the showerhead and pressure side) makes this a rough estimate around the peak of the coolant profile. As shown in Figure 10.5a, superposition estimated a lower coolant profile peak that was more than 20% colder than the measured profile. Figure 10.5b shows that this occurred with high blowing ratios also, where the coolant peak was overestimated by about the same amount. The difference in the total coolant contained in the profiles (area between the curves and Θ_R = 0.0) may be explained by again considering the role of strong temperature gradients. For individual coolant regions, the temperature gradients were not nearly as strong as with full coverage film cooling. This means that coolant spread more slowly into the mainstream for individual regions, maintaining more coherent profiles. For full coverage film cooling, the strong temperature gradients were dissolved more quickly by mainstream turbulence.

Superposition of these profiles with measured hot streak profiles produced varied results. Shown in Figures 10.6a and 10.6b, prediction of the cooled hot streak peak was fairly good for both sets of blowing ratios, where it was overestimated by about 15% and 20% for optimum and above optimum blowing ratios respectively. This was similar to the 20% errors from superposition using measured full coverage coolant profiles. Agreement along a majority of the profile varied, but temperatures were not consistently higher than the measured profile, especially at the dip in the cooled hot streak profile just to the suction side of the trailing edge. At this position, superposition using individual region coolant profiles greatly exaggerated the reduction due to film cooling with values well below the measured profile. As discussed before, this was likely due to neglecting showerhead/suction side interactions by combining individual region coolant profiles.

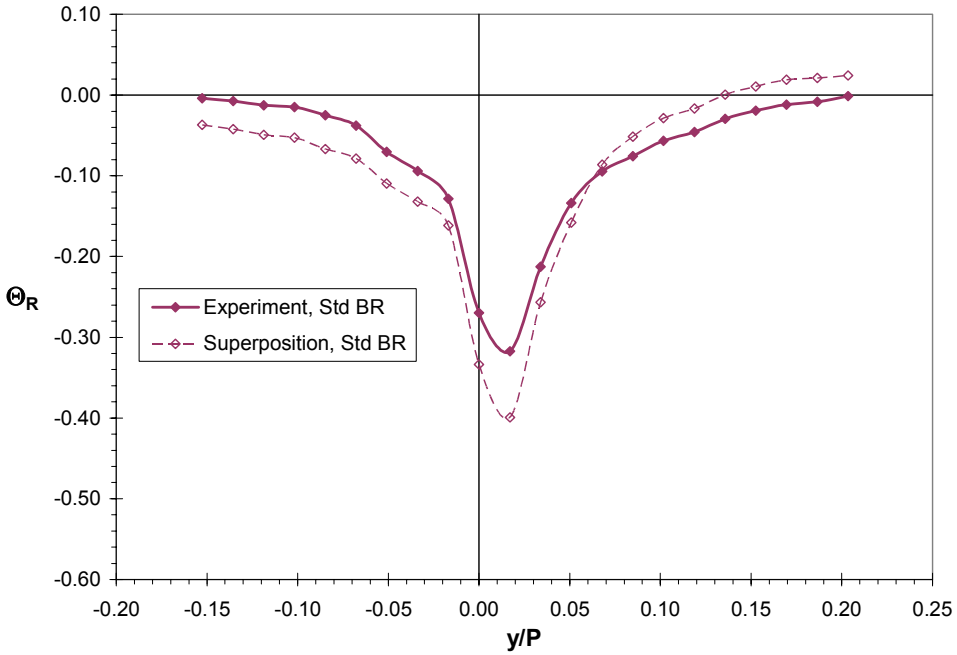

Figure **10.5a: Comparison of measured coolant temperature (Θ_R) profiles at Position T at midspan (z/S = 0.50), for full coverage film cooling at ($M^*_{showerhead}$ = 1.6, $M_{avg,\ suction}$ = 0.7, and $M_{avg,\ pressure}$ = 0.6) and superposition of individual region coolant temperature (Θ_R) profiles at the same blowing ratios, high mainstream turbulence (Tu = 20%).**

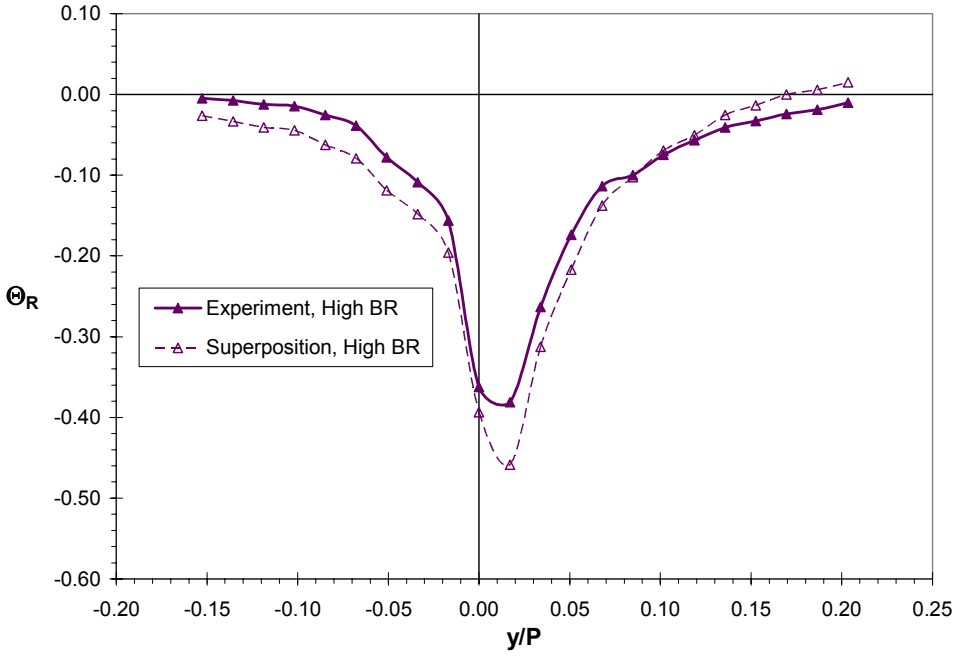

Figure 10.5b: Comparison of measured coolant temperature (Θ_R) profiles at Position T at midspan (z/S = 0.50), for full coverage film cooling at ($M^*_{showerhead}$ = 2.0, $M_{avg,\ suction}$ = 1.0, and $M_{avg,\ pressure}$ = 1.0) and superposition of individual region coolant temperature (Θ_R) profiles at the same blowing ratios, high mainstream turbulence (Tu = 20%).

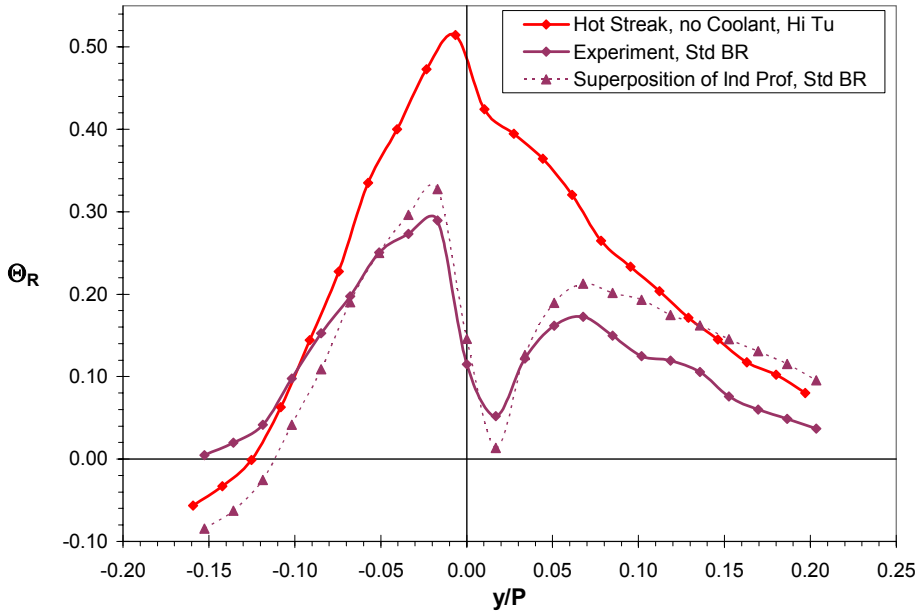

Figure **10.6a: Comparison of experimental normalized temperature ratio (Θ_R) profiles at Position T at midspan (z/S = 0.50), for the hot streak at the stagnation line with full coverage blowing at ($M^*_{showerhead}$ = 1.6, $M_{avg,\ suction}$ = 0.7, and $M_{avg,\ pressure}$ = 0.6) and superposition of individual region coolant temperature (Θ_R) profiles with the hot streak at the same blowing ratios, high mainstream turbulence (Tu = 20%).**

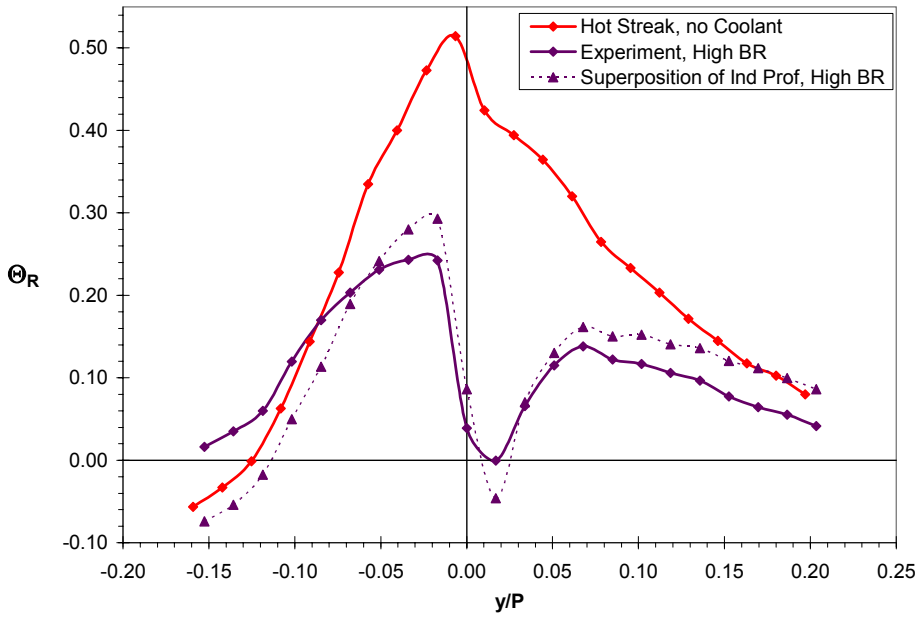

Figure 10.6b: Comparison of experimental normalized temperature ratio (Θ_R) profiles at Position T at midspan (z/S = 0.50), for the hot streak at the stagnation line with full coverage blowing at ($M^*_{showerhead}$ = 2.0, $M_{avg,\ suction}$ = 1.0, and $M_{avg,\ pressure}$ = 1.0) and superposition of individual region coolant temperature (Θ_R) profiles with the hot streak at the same blowing ratios, high mainstream turbulence (Tu = 20%).

It is important to note that this facility contained only one film cooled vane. In the actual engine, the coolant from vanes to either side would overlap the coolant profile shown, thus adding to the reduction of a hot streak in the passage. Since the coolant profile should be periodic with the vane, and coolant mixing may be estimated as roughly additive, a combined coolant profile may look like the one shown in Figure 10.7a. This combined coolant profile was computed using the high blowing ratios of $M^*_{showerhead}$ = 2.0, $M_{avg,\ suction}$ = 1.0, and $M_{avg,\ pressure}$ = 1.0 and overlapping coolant profiles from the vanes to each side of the test vane. As shown in Figure 10.7b, the benefit of this additional coolant was minimal with the hot streak impinging on the stagnation line. Near the peaks, the errors associated with superposition were similar to those shown in Figure 10.4b, except that slightly more coolant was computed at these locations due to the overlap, which makes the error appear smaller than in the previous figure. Well away from the vane, the hot streak was predicted to be reduced much more, but this did not affect the positions where the hot streak was the strongest.

For the hot streak passing through the mid-passage at 0.4P, blowing ratios were somewhat different as discussed in Chapter 7, but the benefit of overlap from adjacent vanes was much higher since the hot streak was stronger well away from the vane. The blowing ratios used for measurements of passage hot streak reduction were $M^*_{showerhead}$ = 1.4, $M_{avg,\ suction}$ = 1.0, and $M_{avg,\ pressure}$ = 1.0. In Figure 10.8, the predicted coolant profile including overlap from the adjacent vanes is shown. The predicted hot streak profile shown is much lower for the portion of the profile well away from the vane (y/P > 0.10) where coolant from the vane to the suction side would overlap and reduce that region as well. Nearer to the vane, at a position of about 0.075P, the superposition prediction suggests that the value of the overall peak with overlapping coolant would not be that great, however direct measurements show the peak in this region to be about Θ_R = 0.20. Due to the error inherent in the superposition calculation, it is expected that the peak would be close to this value, resulting in a hot streak peak about 25% lower with coolant from the adjacent vane. This suggests that the hot streak would have about the same peak value impinging on the leading edge as passing through the mid-passage due to the action of coolant from adjacent vanes.

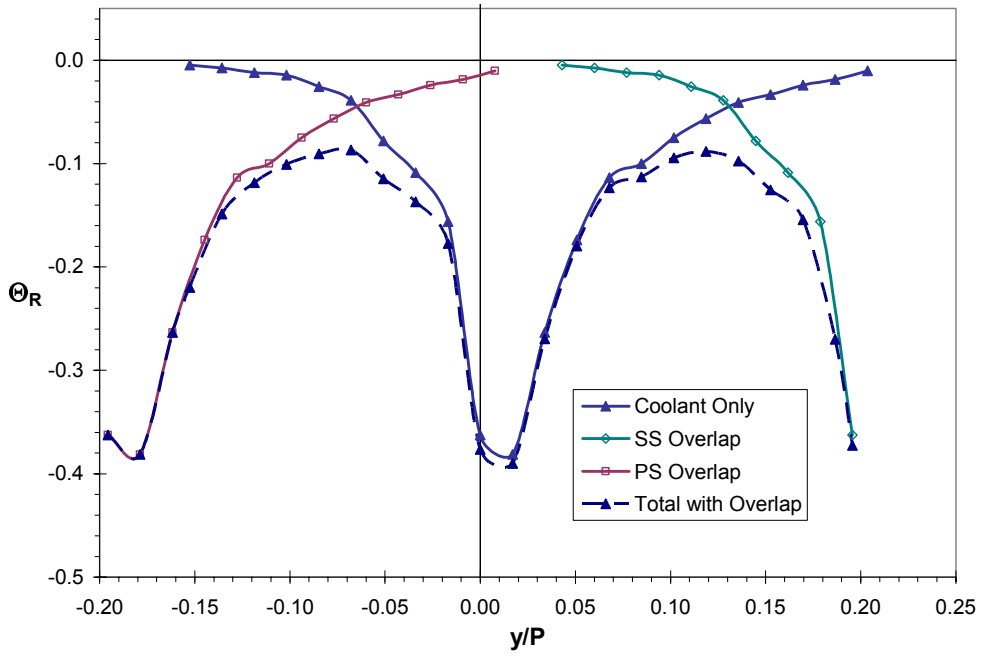

Figure **10.7a: Normalized temperature ratio (Θ_R) profiles at Position T showing the estimated coolant profile with overlapping coolant from the vanes to the suction side and pressure side of the test vane.**

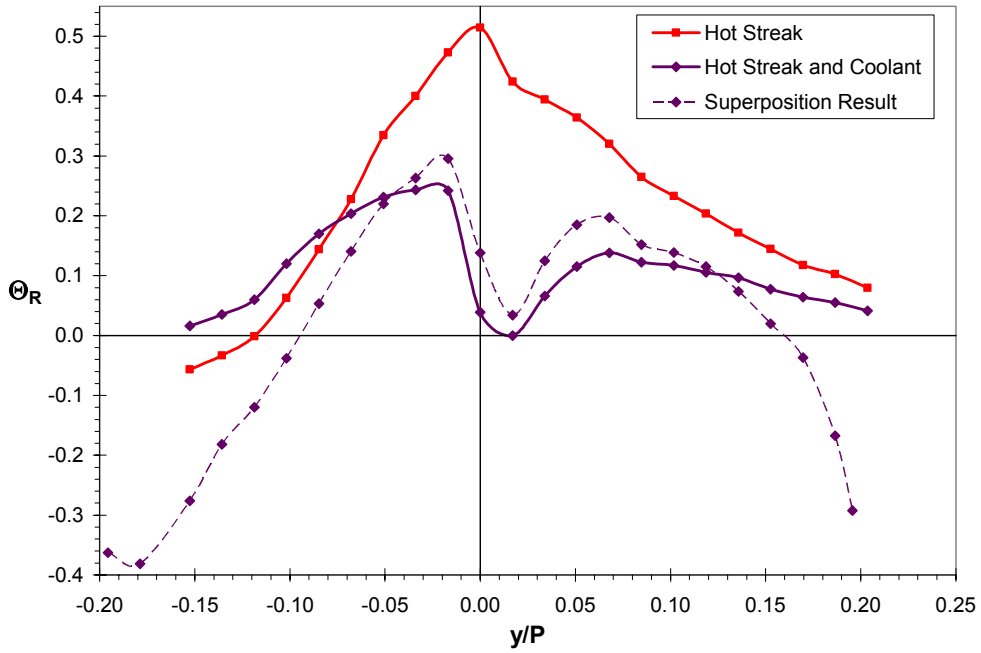

Figure 10.7b: Comparison of experimental and superposition normalized temperature ratio (Θ_R) profiles at Position T at midspan (z/S = 0.50), for the hot streak at the stagnation line with full coverage blowing at ($M^*_{showerhead}$ = 2.0, $M_{avg,\ suction}$ = 1.0, and $M_{avg,\ pressure}$ = 1.0) including the overlap from vanes to the suction side and pressure side of the test vane, high mainstream turbulence (Tu = 20%).

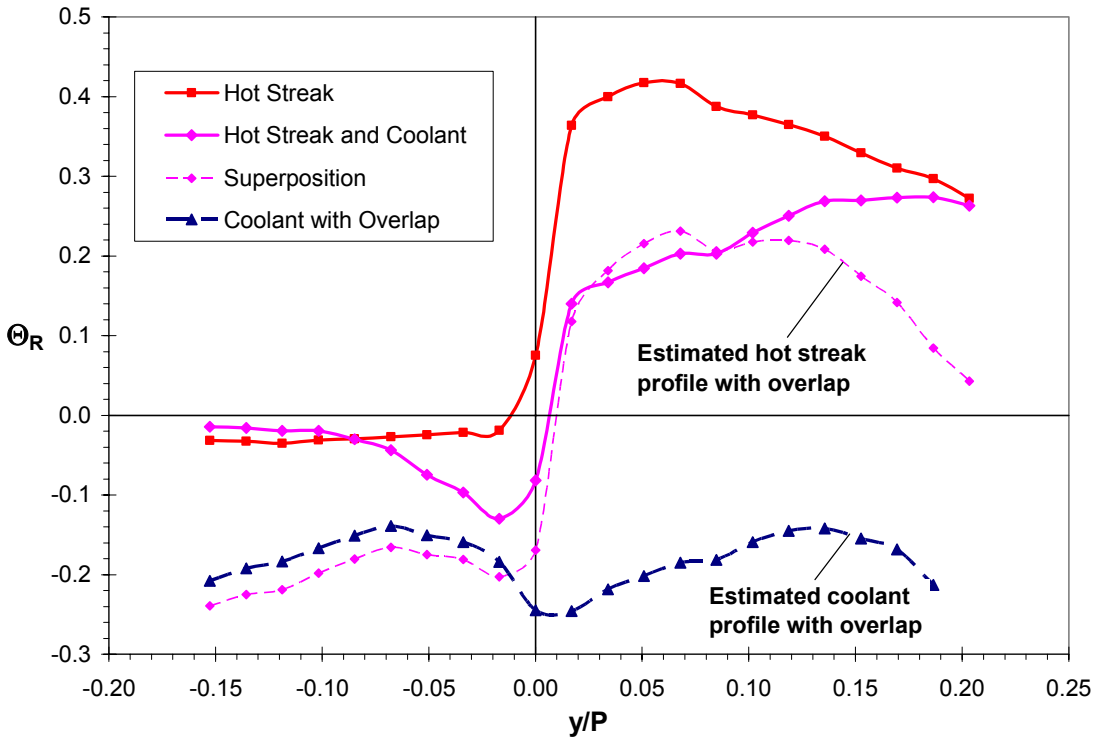

Figure 10.8: Normalized temperature ratio (Θ_R) profiles at Position T for the hot streak at 0.4*P* to the suction side showing the predicted hot streak profile and predicted coolant profile with overlapping coolant from vanes to the suction side and pressure side of the test vane.

For coolant at low density ratio (*DR* = 1.2), superposition predicted higher values over the width of the hot streak with full coverage blowing at high blowing ratios (Figure 10.9). The peak of the hot streak was predicted to be $\Theta_R = 0.43$, while the measured peak was $\Theta_R = 0.40$ (from $\Theta_R = 0.51$ for no film cooling). Therefore, the measured reduction of the peak ($\Delta\Theta_R$ = -0.11) was about 30% greater than predicted ($\Delta\Theta_R$ = -0.08). Compared with high density ratio (*DR* = 1.6), the proportional reduction predicted was about the same, e.g. $\Delta\Theta_R = -0.27$ measured versus $\Delta\Theta_R = -0.18$ predicted (Figure 10.4b). To the suction side of the trailing edge at low density ratio, the predicted values were offset upwards by about the same amount as observed with high density ratio coolant.

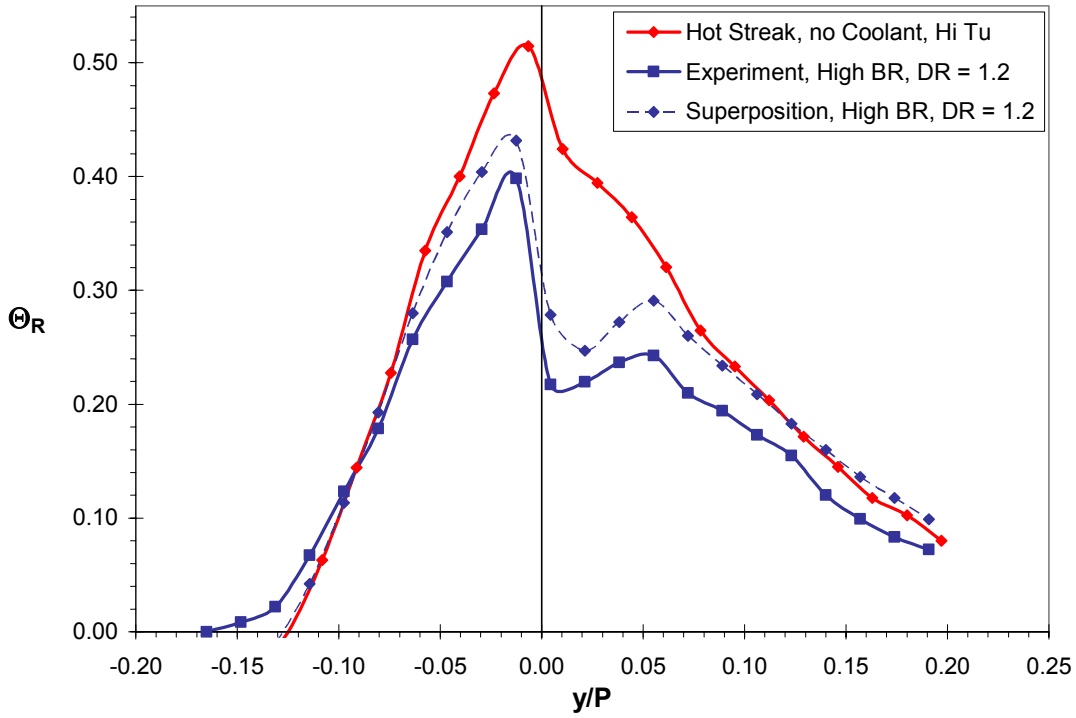

Figure 10.9: Comparison of experimental and superposition normalized temperature ratio (Θ_R) profiles at Position T at midspan (z/S = 0.50), for the hot streak at the stagnation line with full coverage blowing at ($M^*_{showerhead}$ = 2.0, $M_{avg,\ suction}$ = 1.0, and $M_{avg,\ pressure}$ = 1.0) at a density ratio of DR = 1.2, high mainstream turbulence (Tu = 20%).

10.3 Superposition of Midspan Profiles Downstream of the Vane at Position B

At Position B, results of predictions at high mainstream turbulence (Tu = 20%) for showerhead cooling only in Figure 10.10 were fairly similar to those at Position T at a blowing ratio of M^* = 2.0. The shape of the profile was predicted well, but the reduction in the hot streak peak was underpredicted.

For suction side cooling at M_{avg} = 1.0, superposition predicted more dispersion of the temperature gradient at 0.0P, while the experimental profile showed a steeper gradient (Figure 10.11). This resulted in a lower predicted peak, but higher values to the suction side of 0.0P.

Superposition comparisons of the pressure side alone in the wake were not made since differences in the hot streak due to pressure side film cooling were expected to be well within measurement uncertainty.

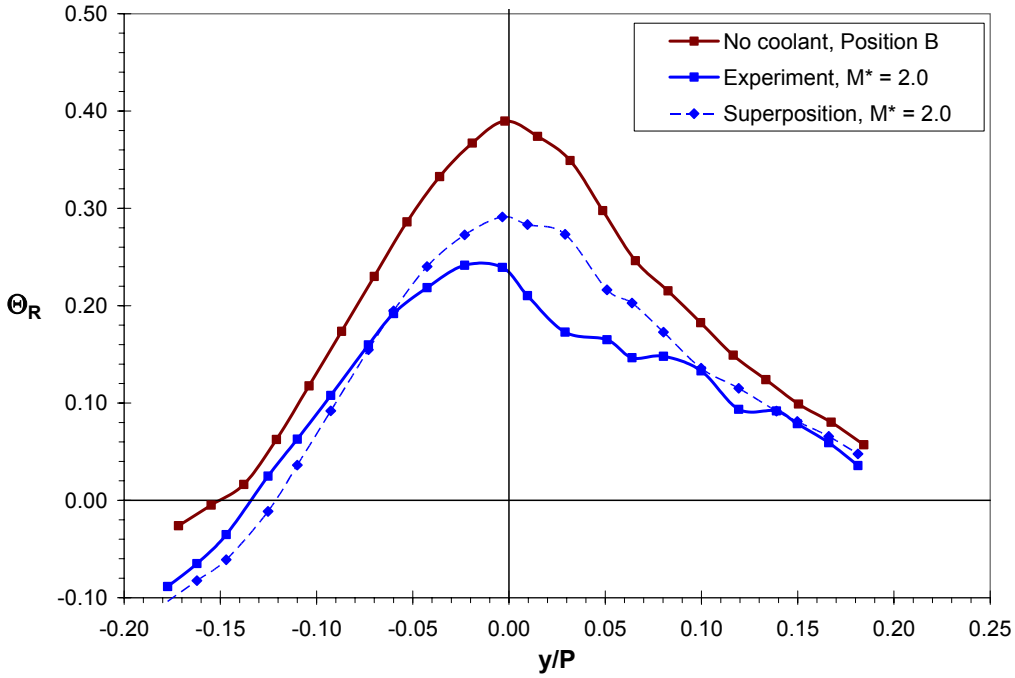

Figure 10.10: Comparison of experimental and superposition normalized temperature ratio (Θ_R) profiles in the wake at Position B at midspan (z/S = 0.50), for the hot streak at the stagnation line with showerhead blowing at M^* = 2.0, high mainstream turbulence (Tu = 20%).

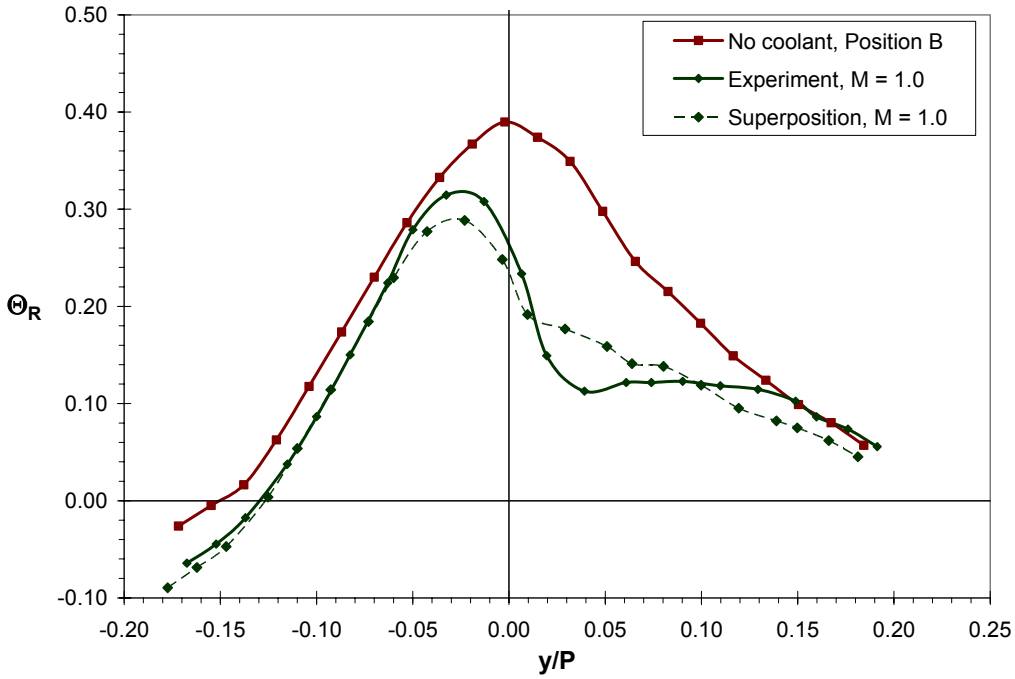

Figure 10.11: Comparison of experimental and superposition normalized temperature ratio (Θ_R) profiles in the wake at Position B at midspan (z/S = 0.50), for the hot streak at the stagnation line with suction side blowing at M_{avg} = 0.7, high mainstream turbulence (Tu = 20%).

For full coverage film cooling at Position B, superposition predictions gave better estimates of the reduction in peak strength of the hot streak compared to the trailing edge. As shown in Figure 10.12, prediction of the hot streak peak was fairly accurate. Superposition predicted a reduction of about 45% compared to 55% measured. The improved predictions at position B relative to predictions at the trailing edge may be due to the dispersion that occurs between the trailing edge and position B.

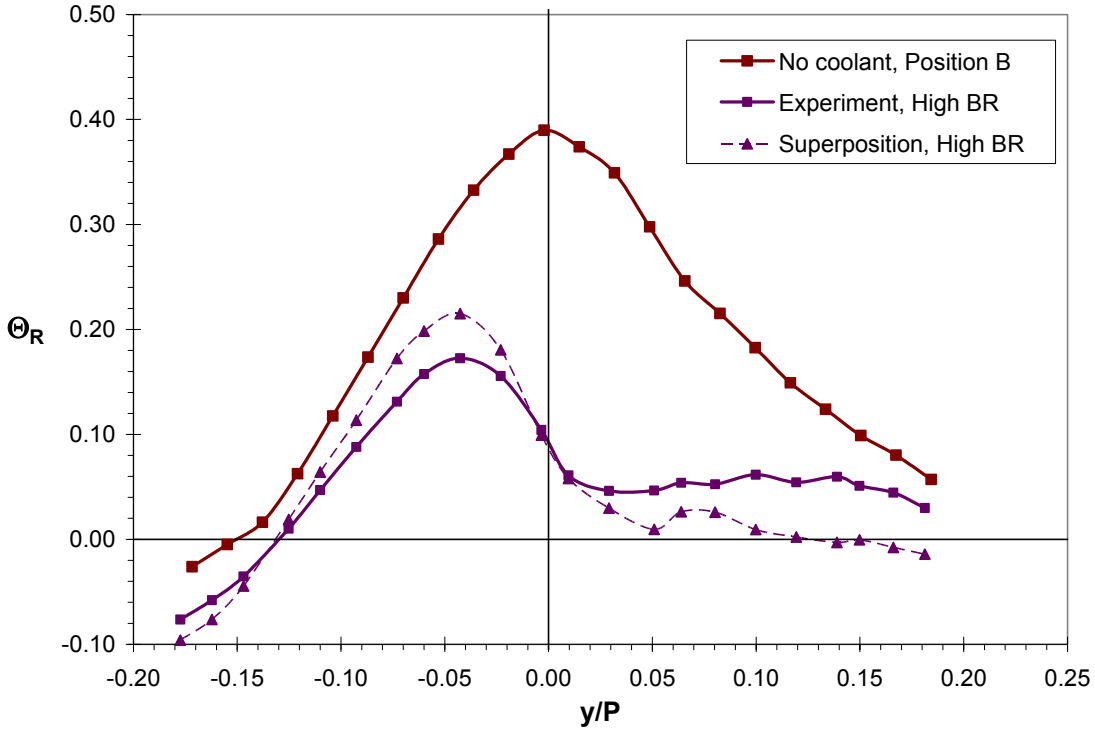

Figure 10.12: Comparison of experimental and superposition normalized temperature ratio (Θ_R) profiles in the wake at Position B at midspan (z/S = 0.50), for the hot streak at the stagnation line with full coverage blowing at $M^*_{showerhead}$ = 2.0, $M_{avg,\ suction}$ = 1.0, and $M_{avg,\ pressure}$ = 1.0, high mainstream turbulence (Tu = 20%).

10.4 Superposition of Midspan Profiles at Low Mainstream Turbulence

Predictions of cooled hot streak profiles under conditions of low mainstream turbulence were generally expected to be better than those at high mainstream turbulence since the additional turbulent transport would be minimized. For showerhead blowing at M^* = 1.6 (Figure 10.13), the overall shape of the predicted profile was fairly similar to the measured profile, except for differences on the suction side of the trailing edge where

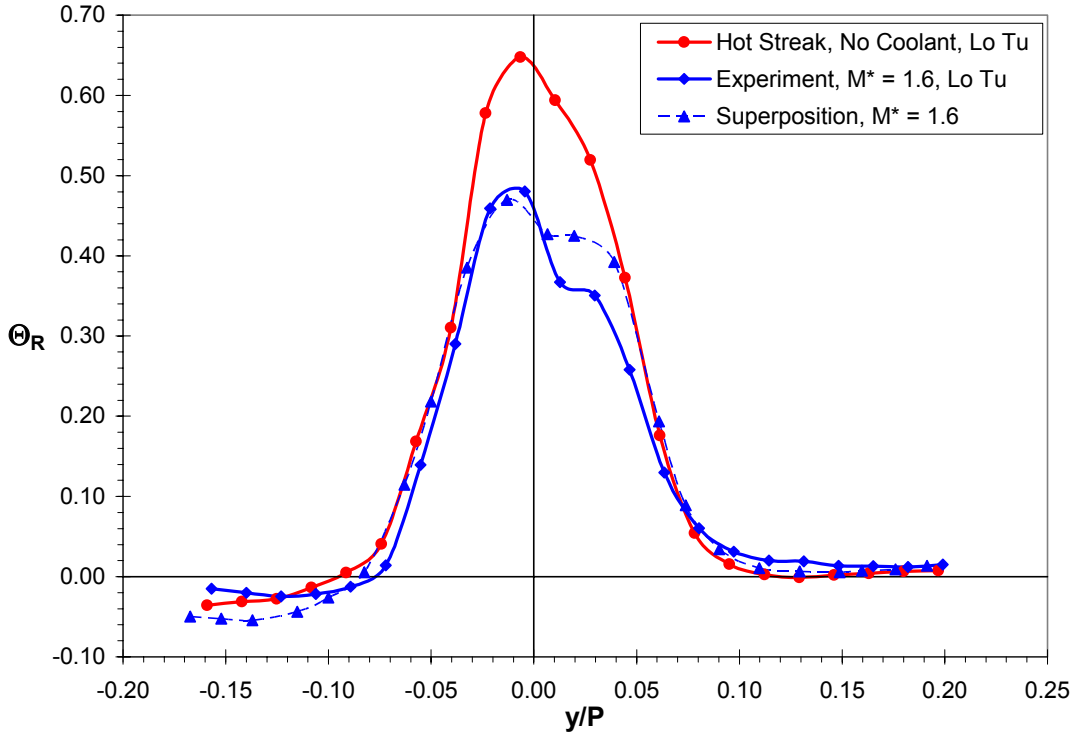

Figure 10.13: Comparison of experimental and superposition normalized temperature ratio (Θ_R) profiles at Position T at midspan (z/S = 0.50), for the hot streak at the stagnation line with showerhead blowing at M^* = 1.6, low mainstream turbulence (Tu = 3.5%).

it underpredicted the benefit of coolant on the suction side. Again, this was likely due to very steep temperature gradients near the wall on the suction side since coolant was injected into the hottest parts of the hot streak. Under conditions of low turbulence, both coolant and hot streak profiles were more tightly focused, resulting in stronger temperature gradients than with high mainstream turbulence levels. Prediction of the hot streak peak, on the other hand, was very good, at nearly the same value as the measured one and just to the pressure side of the trailing edge.

Predictions for suction side blowing at M_{avg} = 0.7, in Figure 10.14, were a bit better on the suction side, but still underpredicted the benefit due to film cooling. Whereas the predicted profile showed a rise at the outside edge of the hot streak (y/P = 0.05), the measured profile indicated this was not the case. An inversion in the temperature profile actually was eroded by the time it reached the trailing edge, as evidenced by measured results. Profiles for blowing ratios of M_{avg} = 0.5 and 1.0, showed

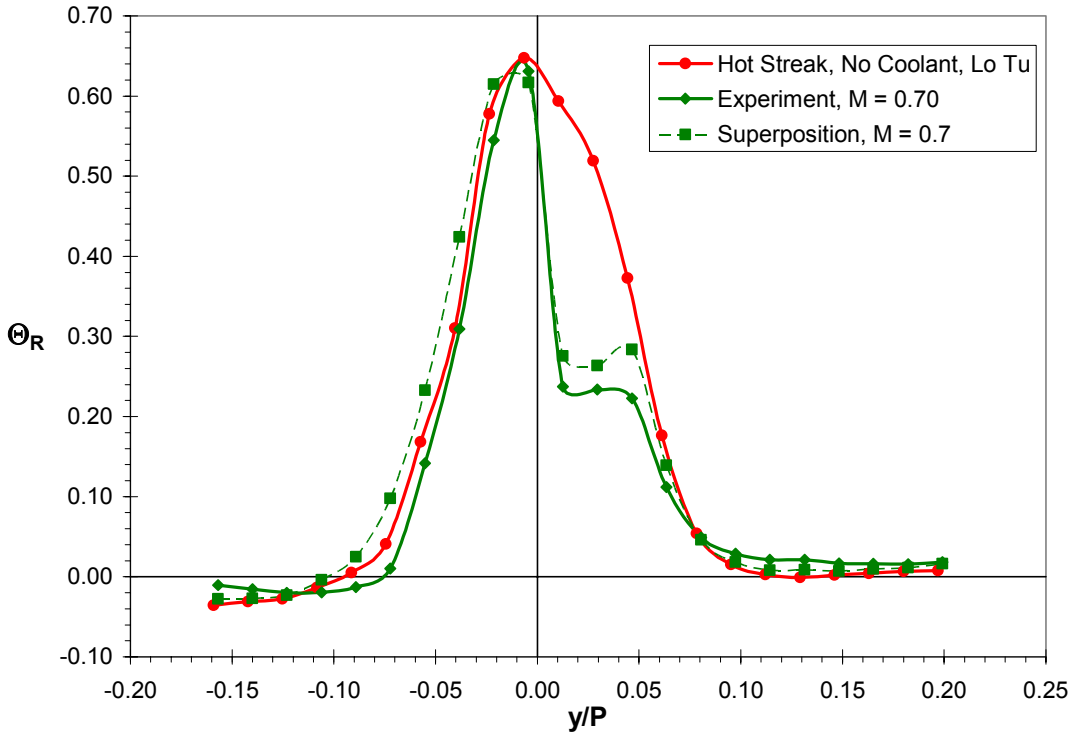

Figure 10.14: Comparison of experimental and superposition normalized temperature ratio (Θ_R) profiles at Position T at midspan (z/S = 0.50), for the hot streak at the stagnation line with suction side blowing at M_{avg} = 0.7, low mainstream turbulence (Tu = 3.5%).

the same tendency. Comparing this with results under high mainstream turbulence in Figure 10.2, a stronger temperature inversion than measured was also predicted, but in this case there was a drop in the temperature profile measured which disappeared quickly in the vane wake (Figure 10.11).

Predictions of the hot streak peak with full coverage film cooling were much worse. The predicted peak at Θ_R = 0.53 in Figure 10.15 was much higher than the measured peak at Θ_R = 0.38 and suggested that the remaining hot streak would be wider on the pressure side of the trailing edge. On the suction side, the prediction was better, especially away from the wall.

In general, predictions using superposition with conditions of low mainstream turbulence were less successful than with high mainstream turbulence. For the fully film cooled vane, the peak was overestimated by nearly 40% compared with the measured

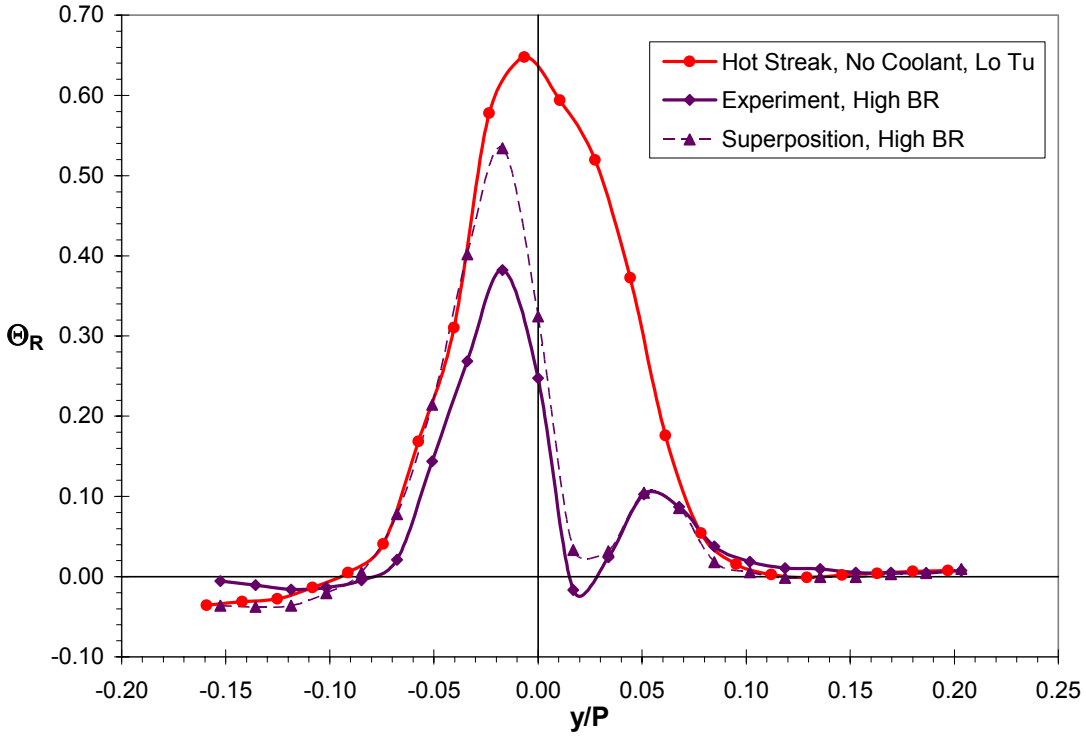

Figure 10.15: Comparison of experimental and superposition normalized temperature ratio (Θ_R) profiles at Position T at midspan (z/S = 0.50), for the hot streak at the stagnation line with full coverage blowing at $M^*_{showerhead}$ = 2.0, $M_{avg,\ suction}$ = 1.0, and $M_{avg,\ pressure}$ = 1.0, low mainstream turbulence (Tu = 3.5%).

results. For both the showerhead and suction side, strong temperature gradients in the film cooled hot streak were likely the cause of large errors in predicting the results of the coolant/hot streak mixing process on the suction side.

10.5 Superposition of Full Field Measurements

In general, comparisons of midspan profiles between measured results and superposition predictions showed both the strengths and weaknesses of the method. For a select group of conditions, superposition analysis was carried out for the full measurement plane at the trailing edge to determine how well superposition could capture the overall behavior of hot streak/coolant interaction.

Predictions for showerhead film cooling at a blowing ratio of M^* = 1.6, shown in Figure 10.16 were reasonably good, capturing the enhanced reduction of the lower

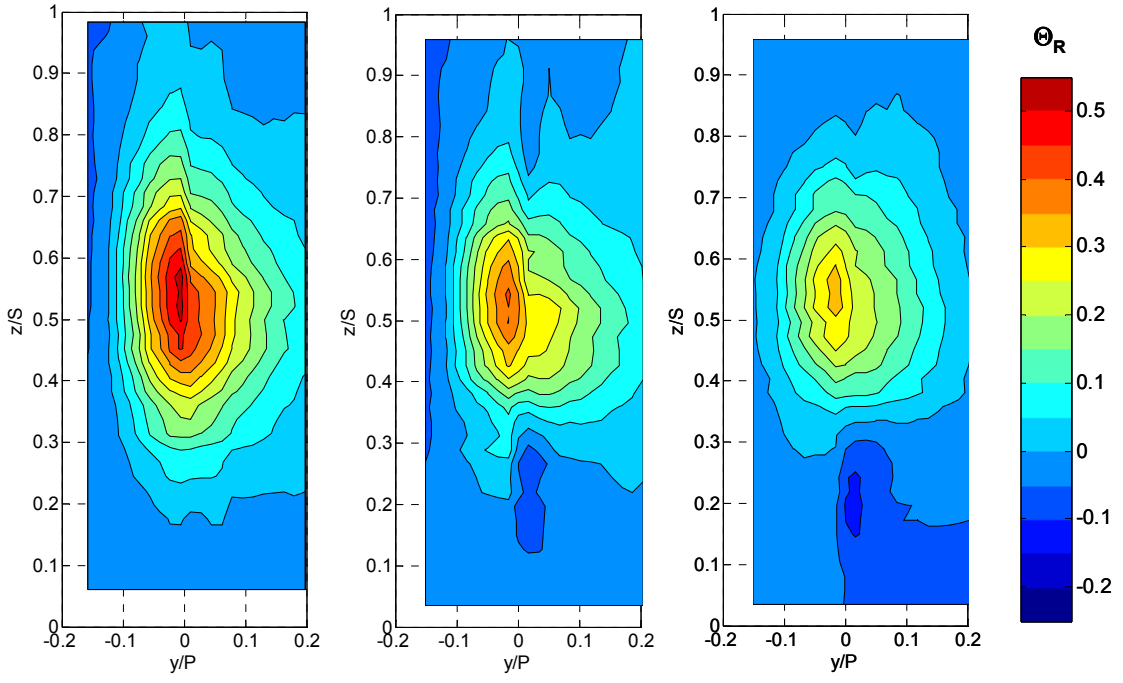

Figure 10.16: Normalized temperature ratio (Θ_R) contours at Position T with the hot streak at the stagnation line, high mainstream turbulence (Tu = 20%) with:

a. No coolant

b. Superposition prediction of showerhead blowing at M^* = 1.6

c. Measured values for showerhead blowing at M^* = 1.6

portion of the hot streak and excess coolant below it. On the other hand, Θ_R values near the center of the hot streak were overestimated as they had been at midspan in Figure 10.1. For showerhead blowing, the hot streak peak was predicted at Θ_R = 0.41 compared with Θ_R = 0.35 measured.

For suction side film cooling at M_{avg} = 0.7 (Figure 10.17), the patterns of hot streak reduction and excess coolant were also fairly well predicted, especially the irregular shape of the remaining hot streak to the suction side of the trailing edge. Predictions for pressure side film cooling indicated little change from the uncooled hot streak both in shape and magnitude as seen in Figure 10.18. Although pressure side blowing had relatively little effect on hot streak reduction, superposition predicted about half that measured.

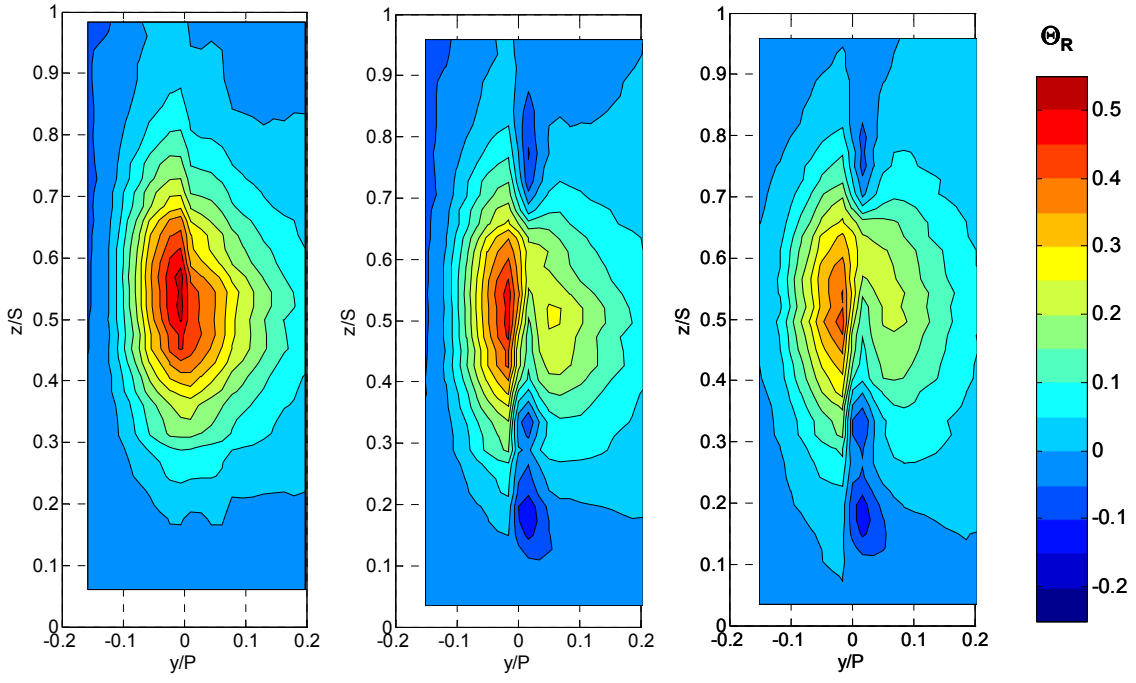

Figure 10.17: Normalized temperature ratio (Θ_R) contours at Position T with the hot streak at the stagnation line, high mainstream turbulence (Tu = 20%) with:

a. No coolant

b. Superposition prediction of suction side blowing at M_{avg} = 0.7

c. Measured values for suction side blowing at M_{avg} = 0.7

The overall trends of higher predicted hot streak peak values and lower predicted excess coolant temperatures continued with full coverage film cooling. Qualitatively, the predictions were successful in estimating the locations and shapes of features such as the excess coolant regions above and below midspan as shown in Figures 10.19 and 10.20 for standard and high blowing ratios respectively. Predicted peak values were estimated higher than measured by about 15% and 25% for the two sets of blowing ratios respectively, but correctly located the positions of the peaks just to the pressure side at about midspan.

At Position B in the wake, with full coverage blowing at above optimum blowing ratios, superposition predictions were not as good. As shown in Figure 10.21, superposition predicted a larger hot streak with higher values for the pressure side (y/P <

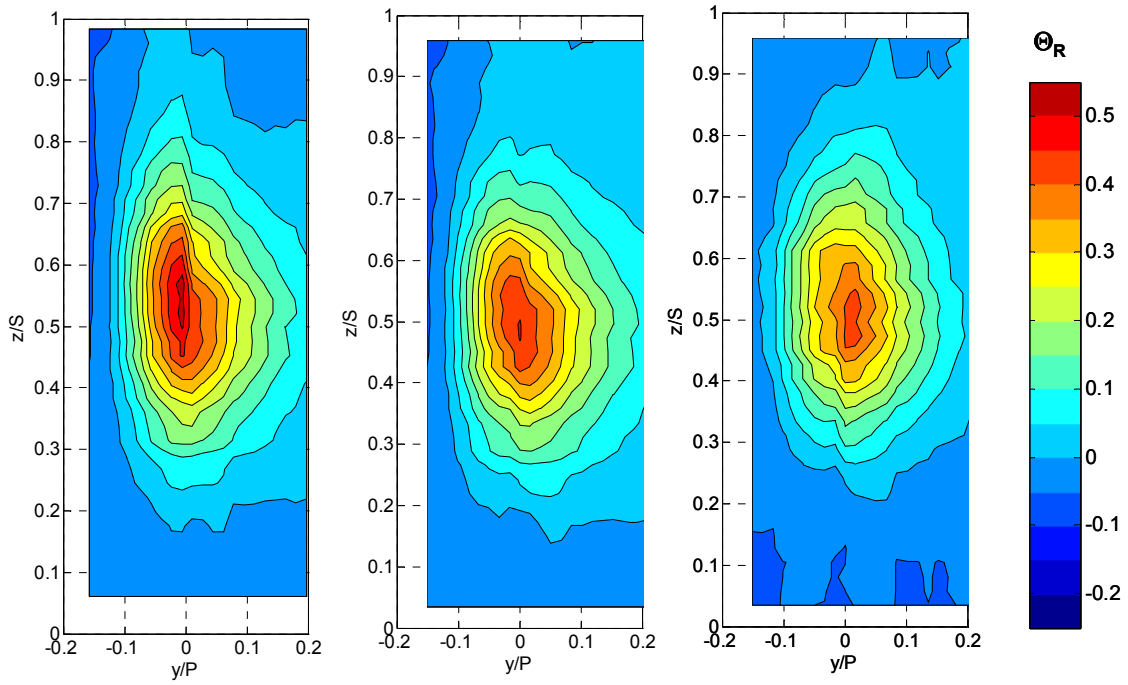

a. **b.** **c.**

Figure 10.18: Normalized temperature ratio (Θ_R) contours at Position T with the hot streak at the stagnation line, high mainstream turbulence (Tu = 20%) with:

a. No coolant

b. Superposition prediction of pressure side blowing at M_{avg} = 0.6

c. Measured values for pressure side blowing at M_{avg} = 0.6

0.0), and a more reduced hot streak for the suction side ($y/P > 0.0$) than those measured.

Overall, prediction of full field hot streak reduction was successful in describing the qualitative aspects of the reduced hot streak, and predictions of the peak hot streak value were good to within about 20% in general. As shown with midspan profiles, superposition estimated a higher peak value for all cases.

10.6 Prediction of the Ideal Hot Streak Pitch Position with Film Cooling

Armed with the knowledge of the predictive capabilities of superposition, this tool were used to estimate the ideal hot streak pitch position with film cooling. Analysis was performed using the hot streak pitch position data presented in Chapter 3 along with

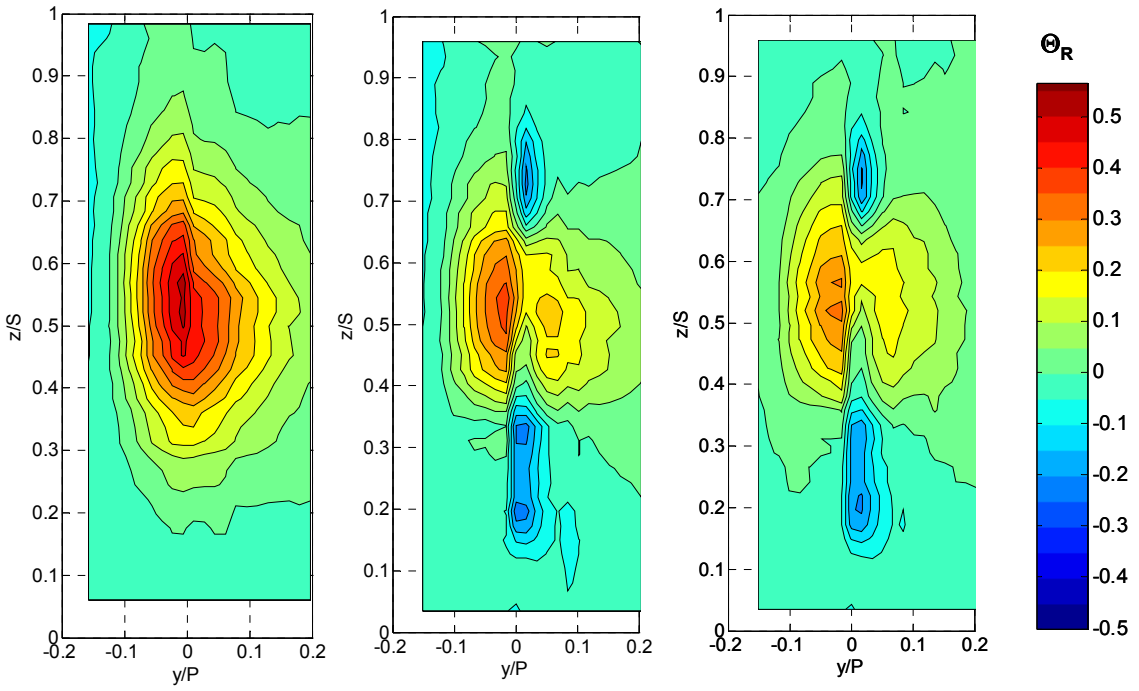

Figure 10.19: Normalized temperature ratio (Θ_R) contours at Position T with the hot streak at the stagnation line, high mainstream turbulence (Tu = 20%) with:

a. No coolant

b. Superposition prediction of full coverage blowing at $M^*_{showerhead}$ = 1.6, $M_{avg,\ suction}$ = 0.7, and $M_{avg,\ pressure}$ = 0.6

c. Measured values for full coverage blowing at $M^*_{showerhead}$ = 1.6, $M_{avg,\ suction}$ = 0.7, and $M_{avg,\ pressure}$ = 0.6

coolant profiles under conditions of high mainstream turbulence at the trailing edge. A minimum hot streak peak was identified for blowing from each coolant region at each blowing ratio tested and for full coverage film cooling at standard and high blowing ratios.

Results for the showerhead indicated an improvement in hot streak reduction for the hot streak positioned slightly to the suction side of the vane. For a showerhead blowing ratio of M^* = 1.6, superposition predicted an additional 6% reduction for the hot streak positioned at +0.043P to the suction side, compared with the hot streak positioned at the stagnation line. Uncooled and cooled profiles for the hot streak positioned at the stagnation line (0.0P) and the ideal pitch position are shown in Figure 10.22. Measured

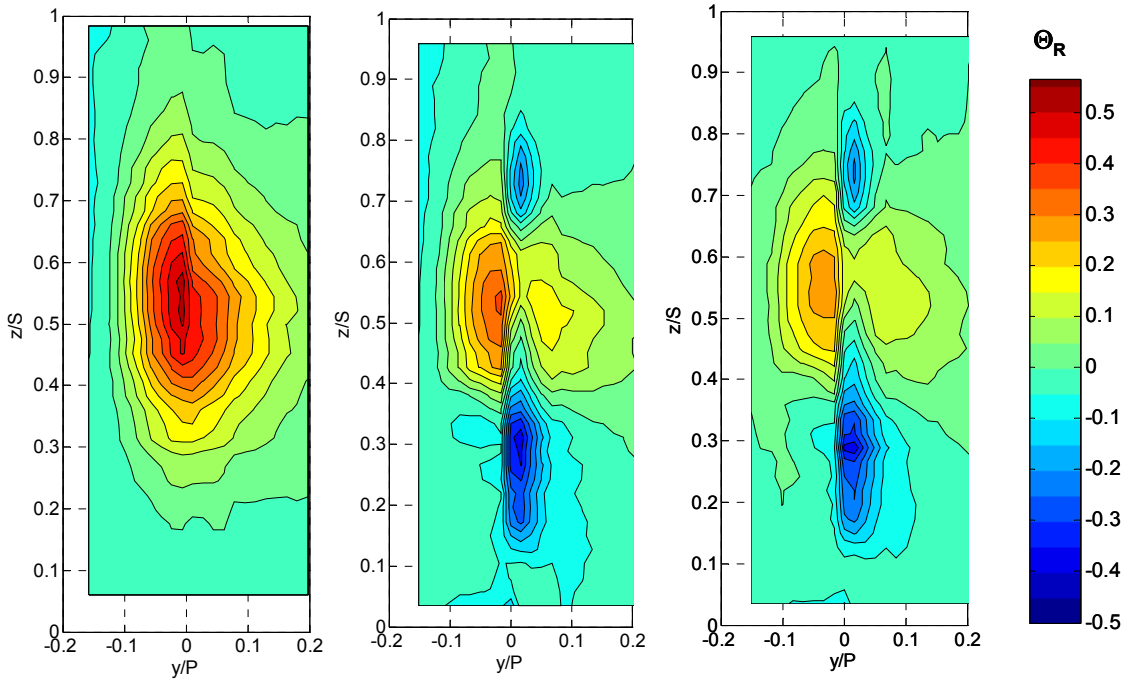

a. **b.** **c.**

Figure 10.20: Normalized temperature ratio (Θ_R) contours at Position T with the hot streak at the stagnation line, high mainstream turbulence (Tu = 20%) with:

a. No coolant

b. Superposition prediction of full coverage blowing at $M^*_{showerhead}$ = 2.0, $M_{avg,\ suction}$ = 1.0, and $M_{avg,\ pressure}$ = 1.0

c. Measured values for full coverage blowing at $M^*_{showerhead}$ = 2.0, $M_{avg,\ suction}$ = 1.0, and $M_{avg,\ pressure}$ = 1.0

hot streak profiles without film cooling are shown in dotted lines, while predicted film cooled profiles are shown with solid lines, indicating the distinct drop in hot streak strength with film cooling. Predictions at the other blowing ratios were similar and predicted the same ideal hot streak pitch position.

For the suction side, the ideal position was predicted to be slightly farther to the suction side than with showerhead film cooling. At all blowing ratios, the ideal position was predicted to be +0.065P to the suction side with a predicted additional 22% reduction in the hot streak with a blowing ratio of M_{avg} = 0.7. This large improvement makes sense for suction side film cooling since the hot streak could not be cooled effectively with the

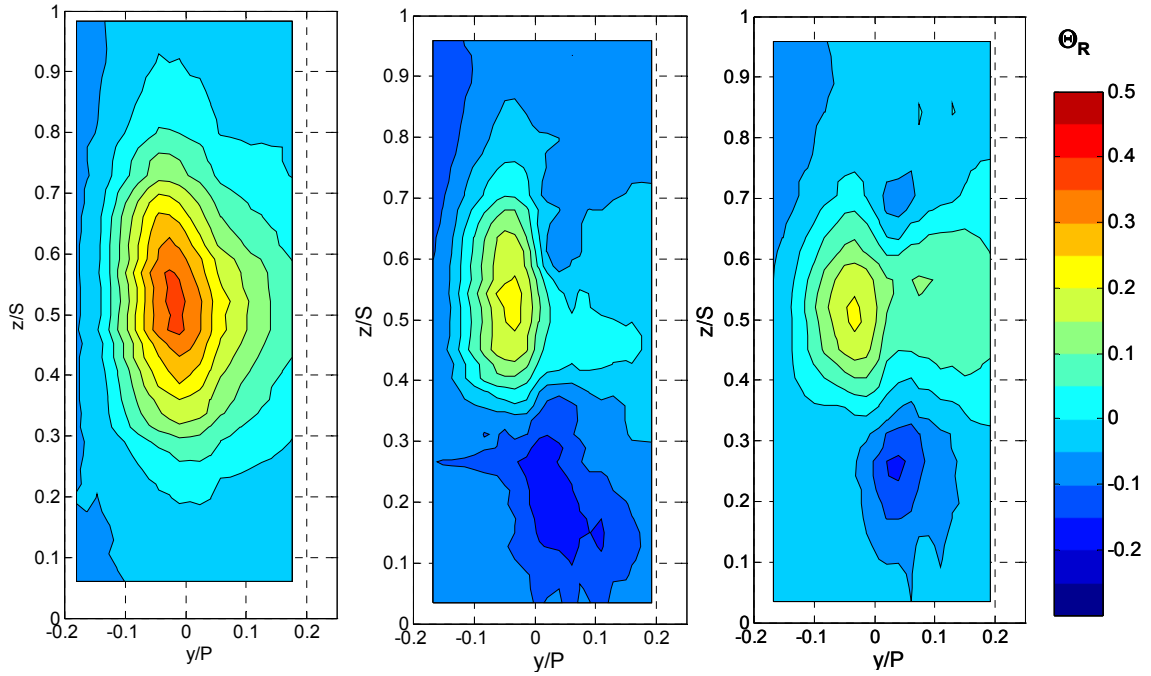

Figure 10.21: Normalized temperature ratio (Θ_R) contours in the wake at Position B with the hot streak at the stagnation line, high mainstream turbulence (*Tu* = 20%) with:

a. No coolant

b. Superposition prediction of full coverage blowing at $M^*_{showerhead}$ = 2.0, $M_{avg,\ suction}$ = 1.0, and $M_{avg,\ pressure}$ = 1.0

c. Measured values for full coverage blowing at $M^*_{showerhead}$ = 2.0, $M_{avg,\ suction}$ = 1.0, and $M_{avg,\ pressure}$ = 1.0

peak to the pressure side of the stagnation line. Figure 10.23 clearly shows the predicted improvement where on the stagnation line (0.0*P*) the hot streak would be reduced only to the suction side, while a hot streak positioned at +0.065*P* would have the peak reduced to a crater-like shape, the remaining highest point well away from the wall where suction side film cooling reduction dropped off. Suction side film cooling for hot streak pitch positions to either side of +0.065*P* left higher peaks to either the suction or pressure side of the trailing edge.

For pressure side film cooling, the ideal hot streak pitch position was on the stagnation line (0.0*P*) since the hot streak with no film cooling peaked just to the pressure side of the trailing edge for this hot streak pitch position. In Figure 10.24, a comparison is made between positions at the stagnation line and just to the pressure side at -0.022*P*,

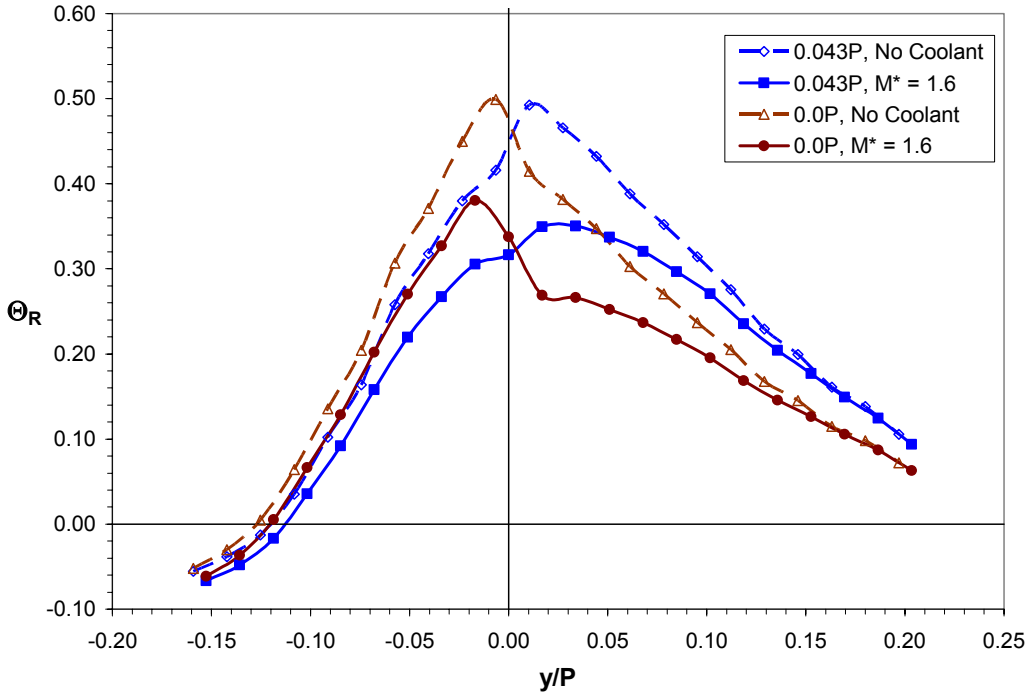

Figure 10.22: Comparison of normalized temperature ratio (Θ_R) profiles at Position T for pitch positions of 0.0*P* (baseline) and +0.043*P* (ideal) without coolant (measured) and with showerhead film cooling at M^* = 1.6 (predicted).

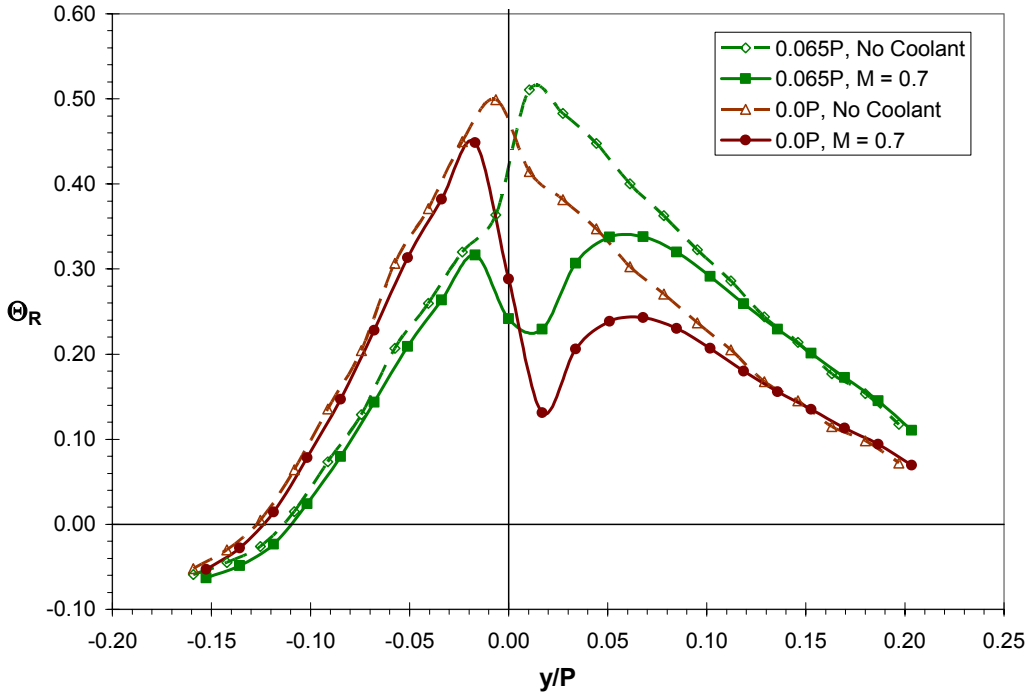

Figure 10.23: Comparison of normalized temperature ratio (Θ_R) profiles at Position T for pitch positions of 0.0*P* (baseline) and +0.065*P* (ideal) without coolant (measured) and with suction side film cooling at M_{avg} = 0.7 (predicted).

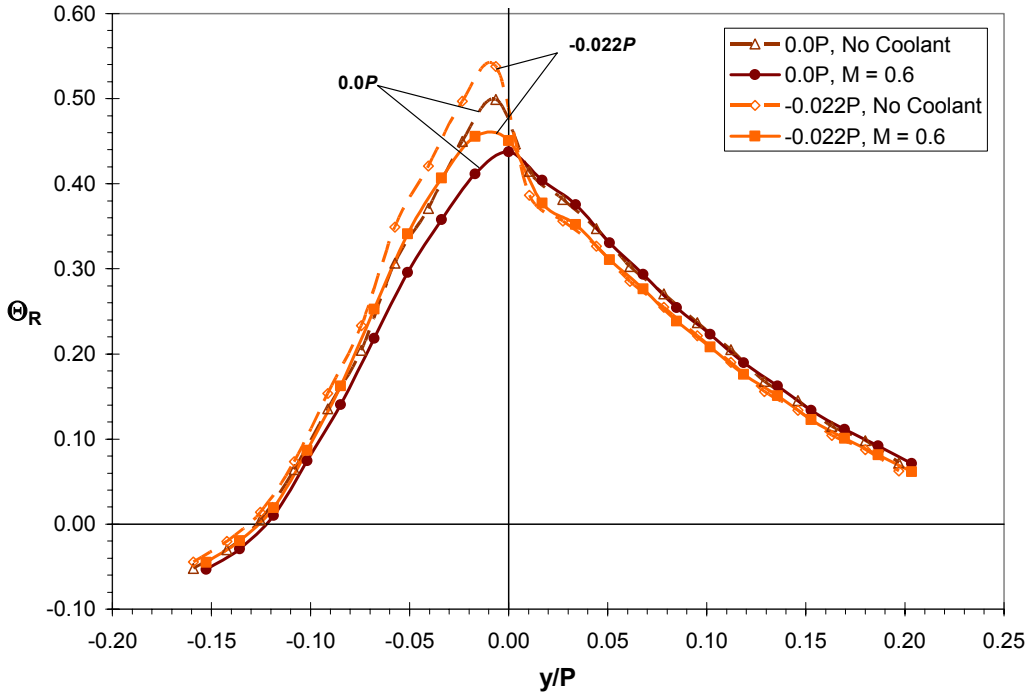

Figure 10.24: Comparison of normalized temperature ratio (Θ_R) profiles at Position T for pitch positions of 0.0*P*and -0.022*P* without coolant (measured) and with pressure side film cooling at M_{avg} = 0.6 (predicted).

with pressure side blowing at M_{avg} = 0.6. It is apparent in this figure that hot streak positions to the pressure side decreased the possible benefit of pressure side film cooling. Results for higher and lower blowing ratios were consistent with this conclusion.

Given the predictions for the individual regions, superposition was expected to predict an ideal hot streak position for reduction by full coverage film cooling to the suction side of the stagnation line. For both sets of blowing ratios, this ideal hot streak position was at +0.043*P*, the same location as for showerhead film cooling. With full coverage film cooling at standard blowing ratios, superposition predicted an additional reduction of the hot streak peak to the pressure side of 15% as shown in Figure 10.25a. However, the peak to the suction side was predicted to rise about 40% compared with the hot streak positioned on the stagnation line. Overall, superposition predicted the hot streak peak to be an additional 10% lower, where the highest point in the profile moved from the pressure side to the suction side of the trailing edge. The drop in hot streak strength from Θ_R = 0.34 to Θ_R = 0.28 represents a fairly large projected improvement in

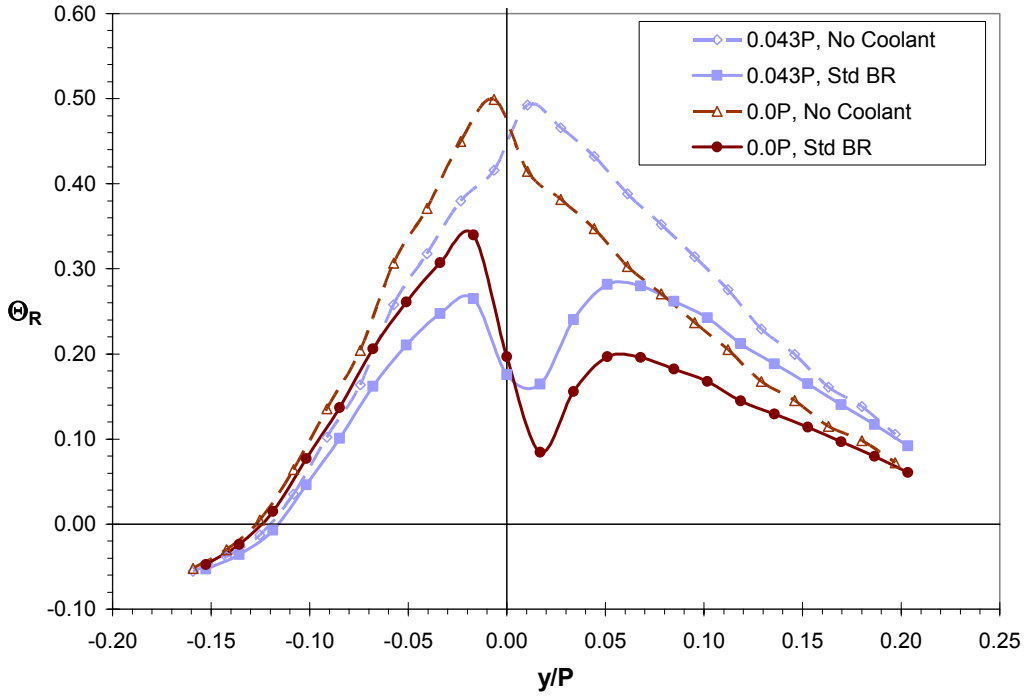

Figure **10.25a: Comparison of normalized temperature ratio (Θ_R) profiles at Position T for pitch positions of 0.0*P* (baseline) and +0.043*P* (ideal) without coolant (measured) and with full coverage blowing at $M^*_{showerhead}$ = 1.6, $M_{avg,\ suction}$ = 0.7, and $M_{avg,\ pressure}$ = 0.6 (predicted).**

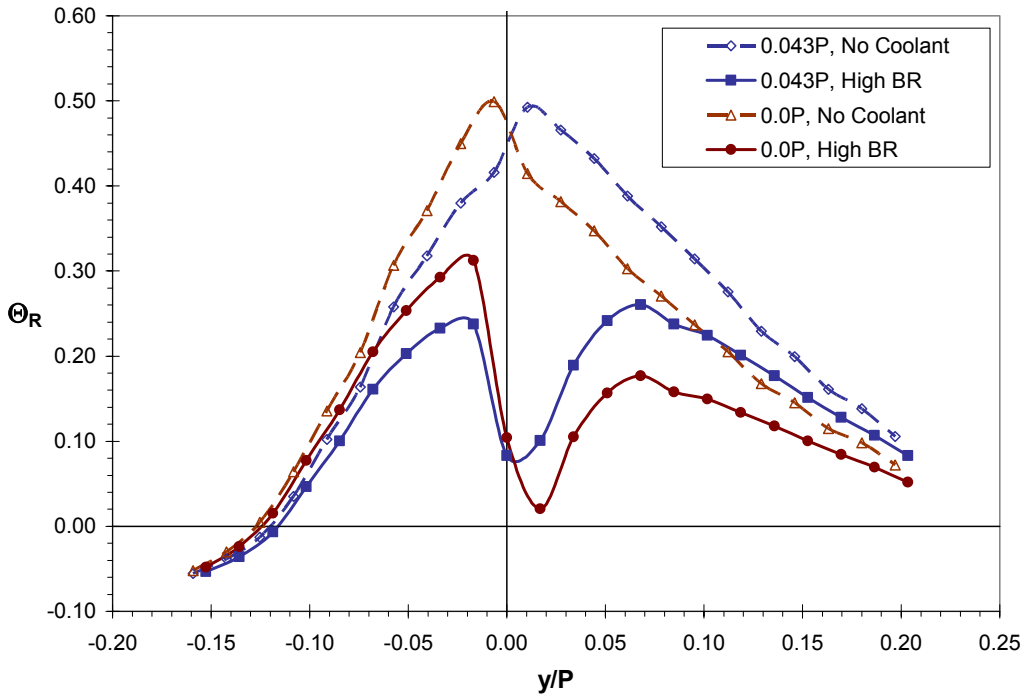

Figure 10.25b: Comparison of normalized temperature ratio (Θ_R) profiles at Position T for pitch positions of 0.0*P* (baseline) and +0.043*P* (ideal) without coolant (measured) and with full coverage blowing at $M^*_{showerhead}$ = 2.0, $M_{avg,\ suction}$ = 1.0, and $M_{avg,\ pressure}$ = 1.0 (predicted).

hot streak reduction. At high blowing ratios, the improvement was similar, projecting an additional 10% decrease in the hot streak peak, dropping from $\Theta_R = 0.31$ to $\Theta_R = 0.26$ for a hot streak pitch position of $+0.043P$. The additional hot streak reduction is illustrated in Figure 10.25b, indicating that trends were consistent between sets of blowing ratios.

An analysis was performed to determine how sensitive the hot streak reduction was to the hot streak pitch position, shown in Figure 10.26 for high blowing ratios. This figure also shows the effect of hot streak pitch position without film cooling as presented in Chapter 3. With film cooling, there was a distinctly lower hot streak peak at $+0.043P$ compared to all other hot streak pitch positions even though the total predicted reduction due to film cooling was similar for other hot streak locations. Moving the hot streak to the pressure side away from the ideal position resulted in a nearly linear trend up to a pitch position of $-0.065P$ with a predicted peak nearly 60% higher at $\Theta_R = 0.42$. From this point farther to the pressure side, the increase in predicted peak was less steep, reaching $\Theta_R = 0.52$ at a hot streak pitch position of $-0.50P$ where there was virtually no

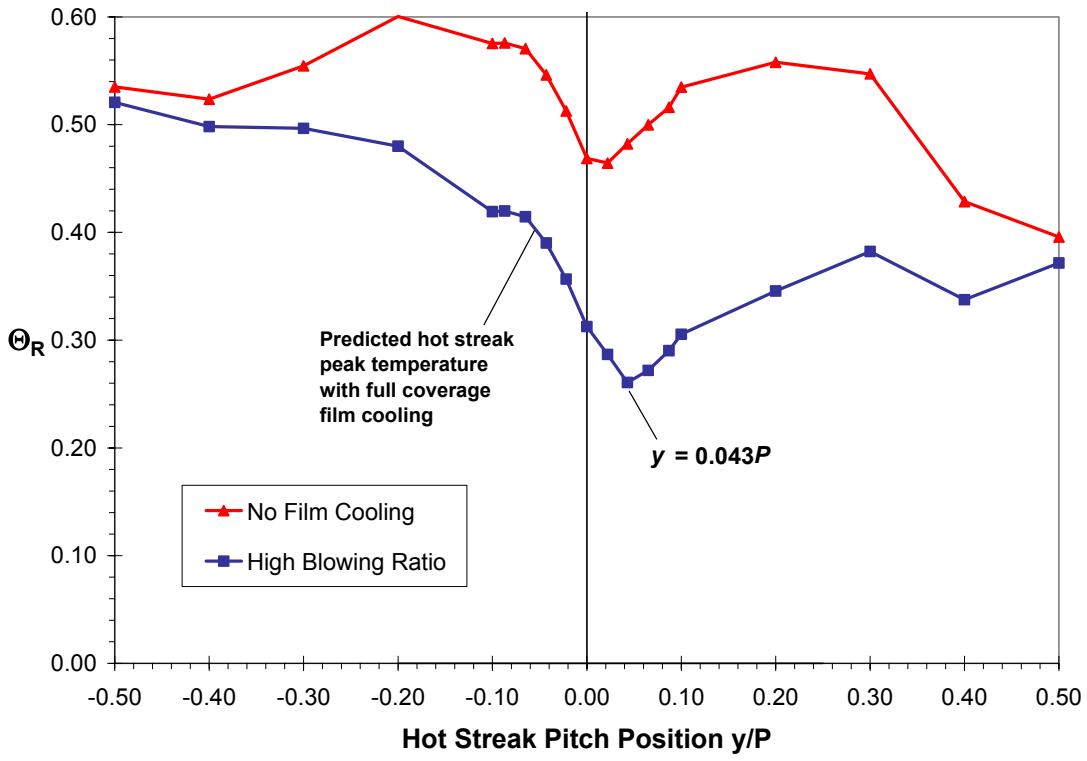

Figure 10.26: Peak hot streak temperature ratio (Θ_R) predictions versus hot streak pitch position at Position T for full coverage film cooling at $M^*_{showerhead} = 2.0$, $M_{avg,\ suction} = 1.0$, and $M_{avg,\ pressure} = 1.0$.

reduction of the peak due to film cooling. Moving the hot streak to the suction side resulted in a sharp increase in hot streak temperature as well, but not as great as to the pressure side. To the suction side the increase was roughly linear up to a pitch position of +0.30*P* with an increase of about 45% in peak hot streak temperature. As with the pressure side, moving the hot streak far from the vane to mid-passage at +0.50*P* resulted in a hot streak peak virtually unchanged due to film cooling. For a range between 0.00*P* to 0.10*P* surrounding the ideal predicted pitch position the predictions suggested that the hot streak peak temperature would rise about 20% up to about $\Theta_R = 0.31$ to either side of the range.

Comparing predicted profiles with full coverage film cooling to the measured profiles in Figure 10.27 leads to several observations. As discussed in §10.2, superposition predicted much higher values to the pressure side of the trailing edge than measured with the hot streak at the stagnation line (0.0*P*) and full coverage blowing at

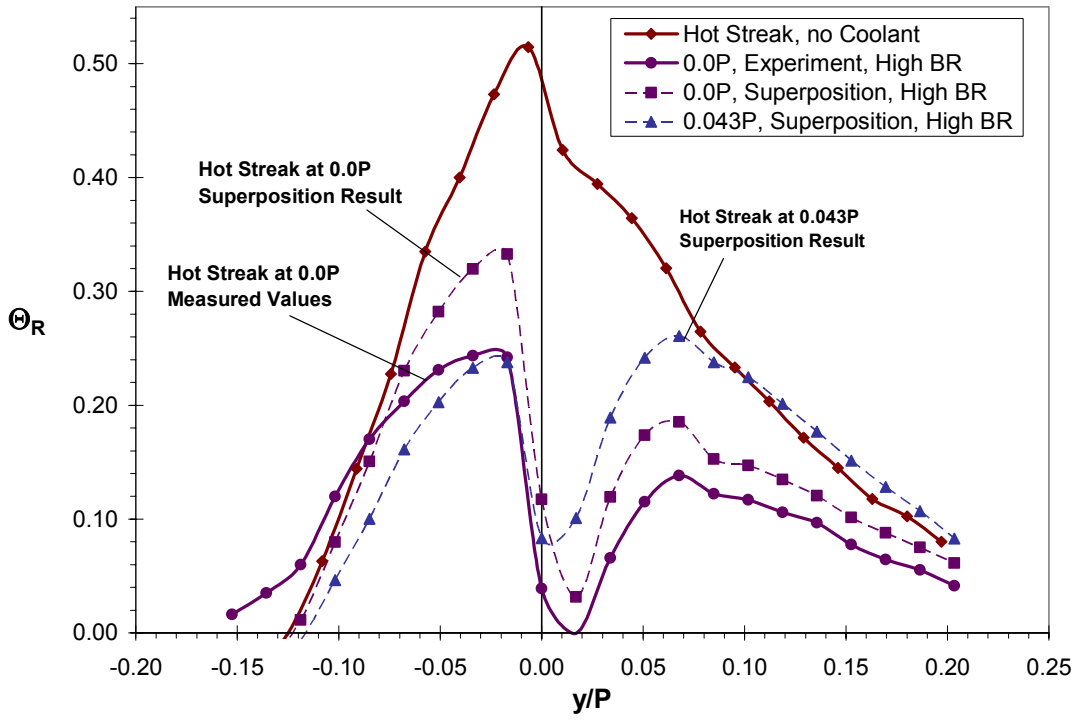

Figure 10.27: Comparison of normalized temperature ratio (Θ_R) profiles at Position T for pitch positions of 0.0*P* without coolant (measured), with full coverage blowing at $M^*_{showerhead} = 2.0$, $M_{avg,\ suction} = 1.0$, and $M_{avg,\ pressure} = 1.0$ (measured and predicted), and at +0.043*P* with full coverage blowing at $M^*_{showerhead} = 2.0$, $M_{avg,\ suction} = 1.0$, and $M_{avg,\ pressure} = 1.0$ (predicted).

above optimum levels. Therefore, measurements on the pressure side for the hot streak at +0.043*P* are expected to be somewhat lower than predicted as well. On the suction side, superposition predicted the peak with a tad more accuracy, although it is expected that the measured profile would also be slightly lower based on the trends observed in Figures 10.4a and 10.4b. Finally, the predicted peak on the suction side for the hot streak at +0.043*P* at a value of Θ_R = 0.26 was about the same as the measured peak for the hot streak at 0.0*P*, which was found on the pressure side of the trailing edge with a value of Θ_R = 0.24. Although superposition predictions suggest a large possible improvement moving the hot streak to the suction side, given the above observations, it is unlikely that a significant improvement in the reduction of the overall peak would be realized. On the other hand, it is highly likely that the peak to the pressure side could be reduced using a pitch position of +0.043*P*. This is further supported in Figure 10.28 by the predicted hot

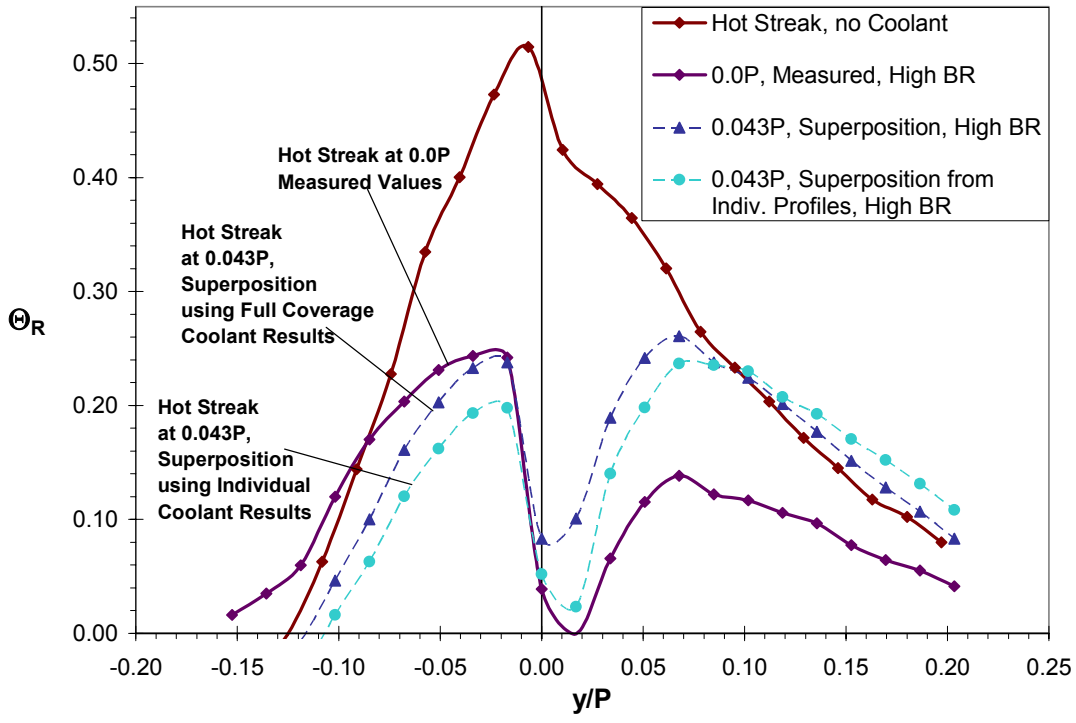

Figure 10.28: Comparison of normalized temperature ratio (Θ_R) profiles at Position T for pitch positions of 0.0*P* without coolant (measured), with full coverage blowing at $M^*_{showerhead}$ = 2.0, $M_{avg,\ suction}$ = 1.0, and $M_{avg,\ pressure}$ = 1.0 (measured), and at +0.043*P* with full coverage blowing at $M^*_{showerhead}$ = 2.0, $M_{avg,\ suction}$ = 1.0, and $M_{avg,\ pressure}$ = 1.0 (predicted using measured full coverage coolant profiles and using measured individual region coolant profiles).

streak profile generated by using superposition of individual coolant profiles from Figure 10.5b to produce a prediction of the ideal pitch position. Recall that this artificially generated full coverage coolant profile yielded somewhat better predictions of pressure side peaks as shown in Figure 10.6b than using the measured full coverage coolant profile as in Figure 10.4b. In Figure 10.28, a comparison between the alternate methods of superposition demonstrates the potential for a lower hot streak peak, possibly lower than the Θ_R = 0.20 shown on the pressure side given the assumption of better accuracy with superposition using individual region coolant measurements.

At Position B in the wake, an ideal hot streak pitch position to the suction side was also predicted, as shown in Figure 10.29. This pitch position was also at +0.043*P*, which is compared to the nominal hot streak pitch position of 0.0*P* in the figure. At Position B, superposition predicted a improvement of about a 10% additional reduction in hot streak strength for this pitch position from Θ_R = 0.18 to Θ_R = 0.14. However, it is

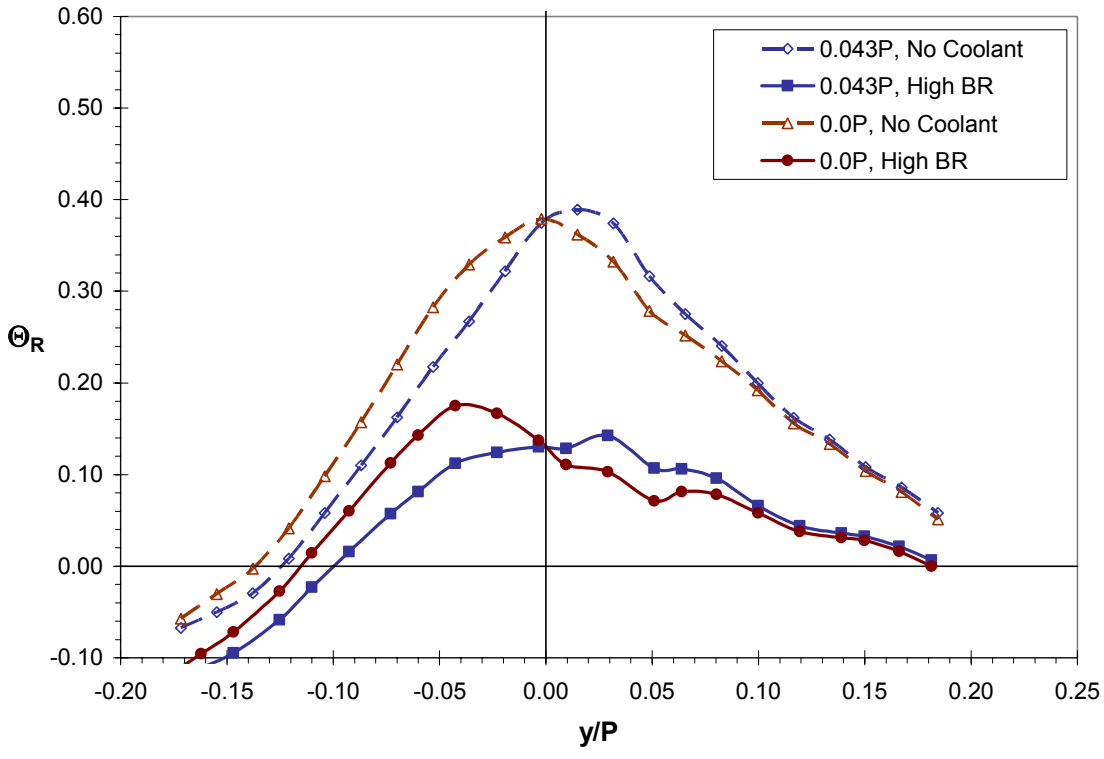

Figure 10.29: Comparison of normalized temperature ratio (Θ_R) profiles at Position B in the wake for pitch positions of 0.0*P* (baseline) and +0.043*P* (ideal) without coolant (measured) and with full coverage blowing at high blowing ratios ($M^*_{showerhead}$ = 2.0, $M_{avg,\ suction}$ = 1.0, and $M_{avg,\ pressure}$ = 1.0) (predicted).

important to note that the peak for the ideal pitch position was to the suction side where predictions involved the most error as shown in Figure 10.12. Particularly, predictions for the hot streak at the stagnation line predicted $\Theta_R = 0.12$ at $0.03P$ where the measured values were much lower at $\Theta_R = 0.05$. Based on these observations, it is likely that the hot streak positioned at $+0.043P$ would result in lower values than predicted to the suction side, perhaps well below $\Theta_R = 0.14$. On the other hand, predictions made at Position B were better on the pressure side for full coverage film cooling, referring again to Figure 10.12. Presuming this trend to be consistent with pitchwise movement of the hot streak, the ideal pitch position suggested would likely have its peak to the pressure side, where reduction of $\Theta_R = 0.18$ to $\Theta_R = 0.12$ might be realized.

At Position B downstream of the trailing edge, a sensitivity analysis for pitch position was also done, as shown in Figure 10.30. Towards the pressure side of the ideal pitch position, the hot streak reduction was a little less sensitive to hot streak pitch

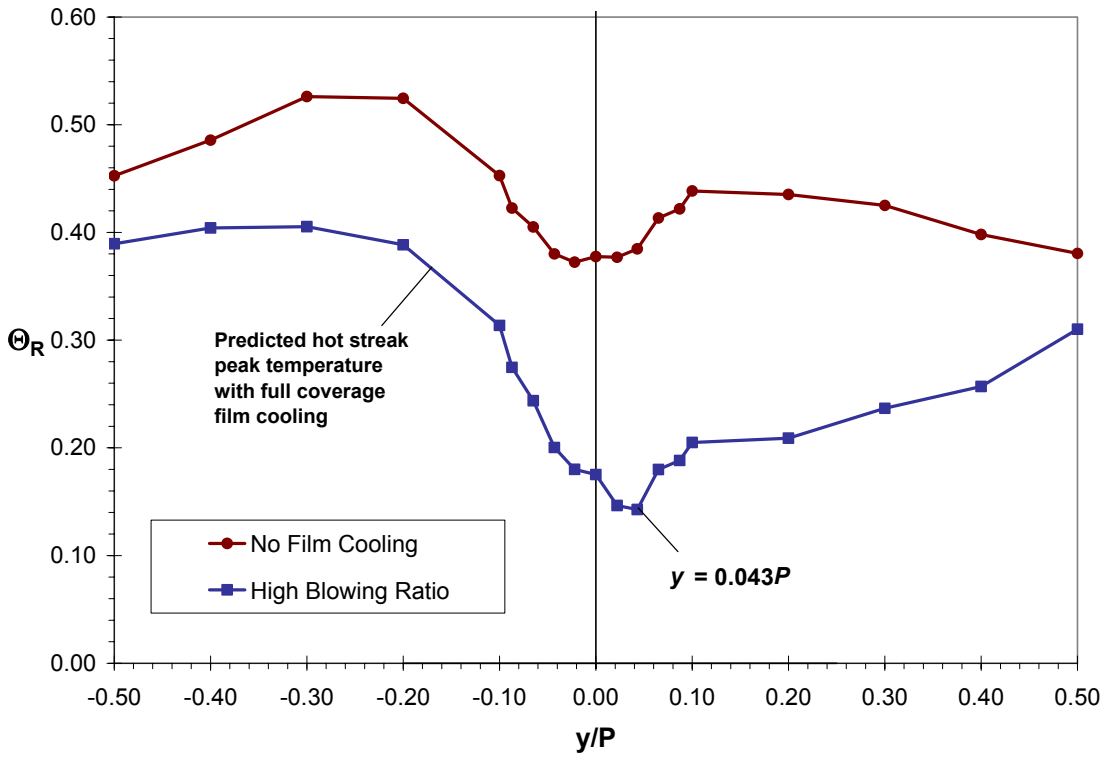

Figure 10.30: Peak hot streak temperature ratio (Θ_R) predictions versus hot streak pitch position at Position B for full coverage film cooling at $M^*_{showerhead} = 2.0$, $M_{avg,\ suction} = 1.0$, and $M_{avg,\ pressure} = 1.0$.

position than at Position T. However, the figure clearly shows that a hot streak pitch position of $+0.043P$ was distinctly better than surrounding pitch positions.

10.7 Predictions of Aero-Engine Scaled Hot Streak Reduction

In Chapter 9, effects of variations in the coolant density ratio were shown to scale well using the normalized coolant temperature, Θ_C. This, along with superposition, allowed for predictions of combinations of coolant density ratio and hot streak temperature ratio unattainable in the current facility. It was also noted that aero-specific engines may have hot streak temperature ratios as high as $T/T_\infty = 1.5$.

Predictions for a higher peak hot streak temperature ratio of $T/T_\infty = 1.5$ and coolant density ratio of $DR = 1.6$ are shown in Figure 10.31 for full coverage film cooling at high blowing ratios. An appropriate hot streak profile at the trailing edge was calculated by scaling measured values by the ratio of temperature differences on a point-by-point basis, as shown by Equation 10.2:

$$\left(T_{p,ij} - T_\infty\right) = \frac{T_{0,p} - T_\infty}{T_{0,m} - T_\infty} \cdot \left(T_{m,ij} - T_\infty\right) \qquad (10.2)$$

where the subscripts m and p refer to the measured and predicted values and $T_{0,m}$ and $T_{0,p}$ are the hot streak peak temperatures for the measured and predicted hot streaks respectively. The hot streak peak temperatures were obtained by knowledge of the measured or predicted mainstream temperatures and the temperature ratios $T_{0,m}/T_\infty = 1.09$ measured and $T_{0,p}/T_\infty = 1.5$ to be simulated. As such, the shape of the hot streak at the trailing edge was assumed to be invariant with upstream temperature ratio. Using numerical simulation, Dorney et al. [13] investigated the effect of the hot streak temperature ratio for a range of $T/T_\infty = 1.5$ to 2.5. Increasing the temperature ratio from $T/T_\infty = 1.5$ to 2.0 was found to have very little effect on the predicted kinematics of the hot streak, so it is unlikely that the hot streak shape would be significantly different between hot streak temperature ratios of $T/T_\infty = 1.09$ and 1.5. Superposition predicted a drop in peak temperature ratio due to film cooling from $\Theta_R = 0.51$ down to $\Theta_R = 0.47$ for

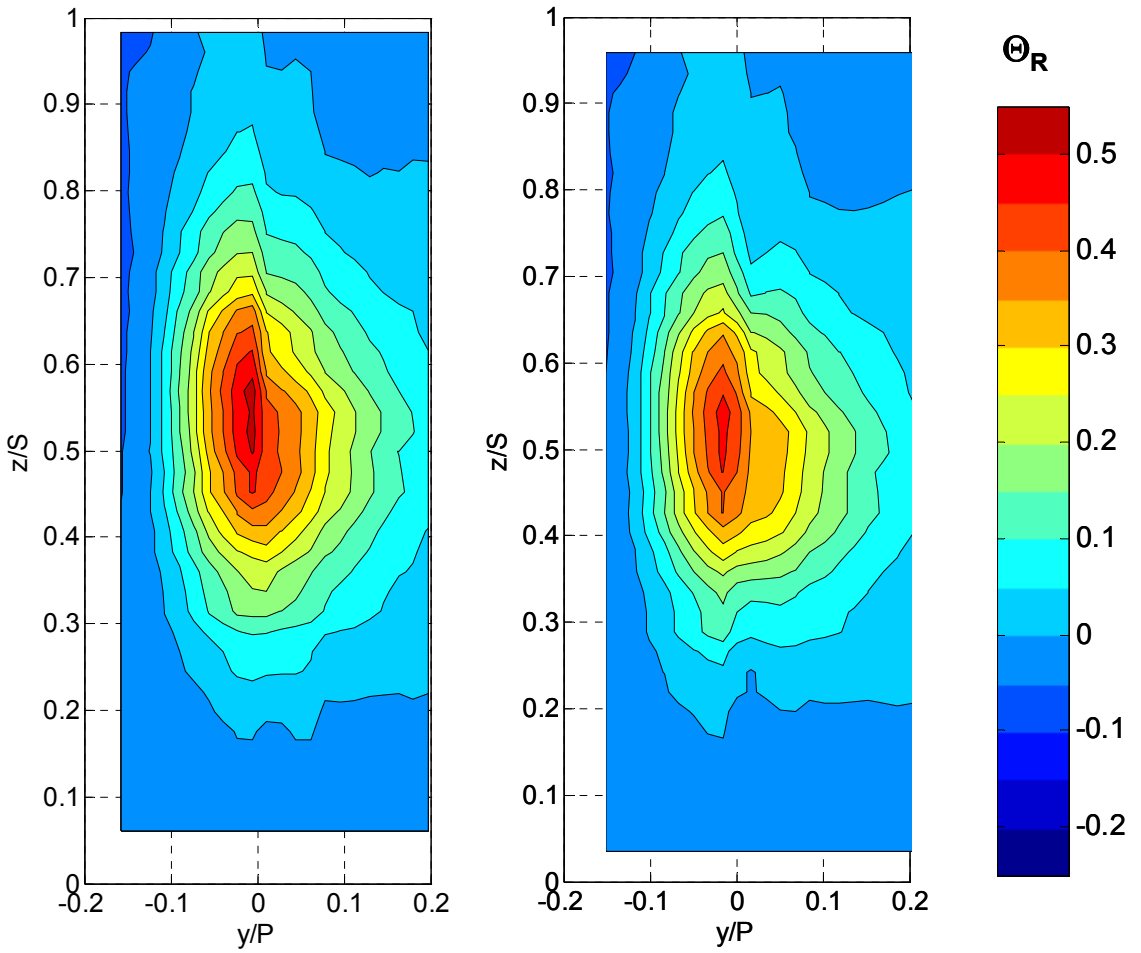

Figure 10.31: Normalized temperature ratio (Θ_R) contours at Position T with a simulated hot streak temperature ratio of $T/T_\infty = 1.5$ at the stagnation line, high mainstream turbulence ($Tu = 20\%$) with:

a. No coolant

b. Superposition prediction of full coverage blowing at $M^*_{showerhead} = 2.0$, $M_{avg,\ suction} = 1.0$, and $M_{avg,\ pressure} = 1.0$

this higher hot streak temperature ratio. Profiles at midspan in Figure 10.32 indicate that full coverage film cooling is predicted to have little effect on a much stronger hot streak at the hot streak temperature ratio simulated.

Aero-engine scaling discussed in §9.2 would require a density ratio of $DR = 1.1$ to simulate scaled conditions of a hot streak temperature ratio of $T/T_\infty = 1.5$ and a density ratio of $DR = 2.0$. However, testing with a density ratio this low was impractical due to limitations of measurement accuracy. Predicted coolant temperatures were estimated by scaling measured results with the ratio of coolant-to-mainstream temperature difference used and to be simulated as in Equation 10.3:

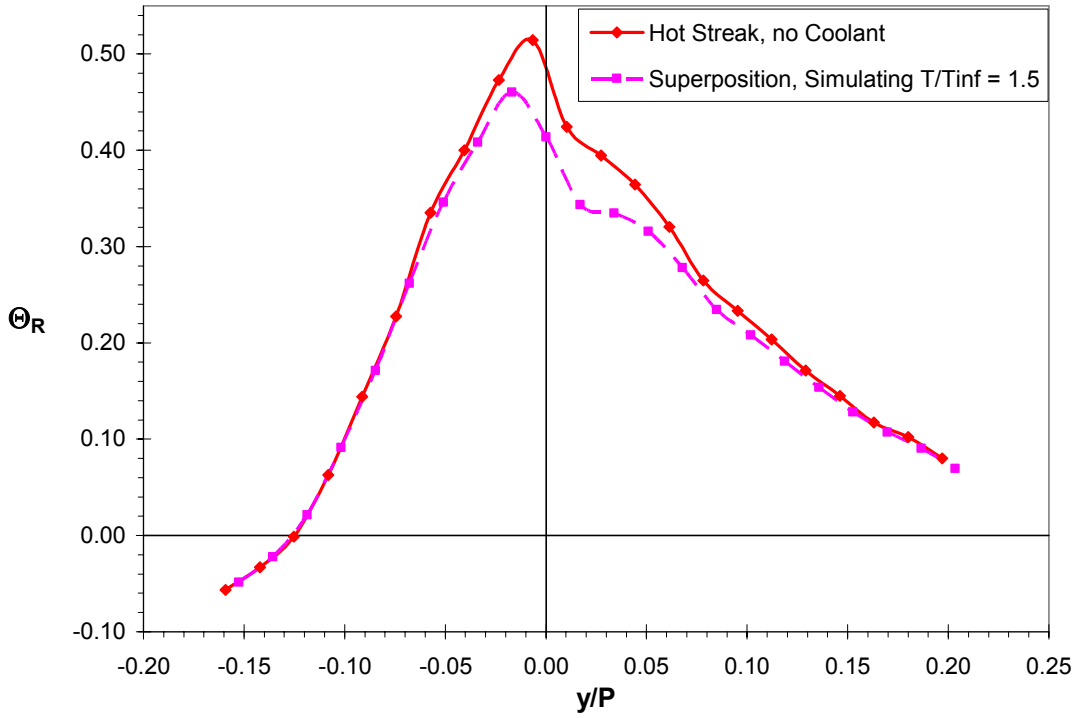

Figure 10.32: Comparison of normalized temperature ratio (Θ_R) profiles at Position T at midspan (z/S = 0.50), for the hot streak at a simulated temperature ratio of T/T_∞ = 1.5 at the stagnation line without cooling and with full coverage blowing at above optimum levels ($M^*_{showerhead}$ = 2.0, $M_{avg,\ suction}$ = 1.0, and $M_{avg,\ pressure}$ = 1.0), density ratio of DR = 1.6, high mainstream turbulence (Tu = 20%).

$$\left(T_\infty - T_{p,ij}\right) = \frac{T_\infty - T_{c,p}}{T_\infty - T_{c,m}} \cdot \left(T_\infty - T_{m,ij}\right) \qquad (10.3)$$

which is the same as scaling using the normalized coolant temperature, Θ_C. Equation 10.3 is essentially the same as Equation 10.2, except that mainstream-to-coolant temperature differences are used in place of peak hot streak-to-mainstream temperature differences. This equation allowed the calculation of a simulated coolant profile on a point-by-point basis at a different density ratio, where the simulated coolant hole exit temperature was calculated using the density ratio to be simulated. Superposition of these results with the hot streak estimated the probable effect of full coverage film cooling at above optimum blowing ratios for aero-engine specific conditions of T/T_∞ = 1.5 and a density ratio of DR = 2.0, using coolant results scaled to DR = 1.1 and a measured hot streak profile at T/T_∞ = 1.09. In Figure 10.33, it is clear that the hot streak

would be reduced much less for aero-specific engine conditions than ground-based engine conditions discussed in previous Chapters 4-8. Figure 10.34, showing the comparison of midspan profiles, indicates the simulated higher density ratio coolant of $DR = 2.0$ would have a larger effect on the hot streak than coolant at a density ratio of $DR = 1.6$ as shown in Figure 10.32. These predictions suggest that the hot streak peak would be reduced by about 10% compared with no film cooling. This is much less than the nearly 40% reduction with ground-based engine representative conditions, but indicates that film cooling still could assist in hot streak reduction for aero applications.

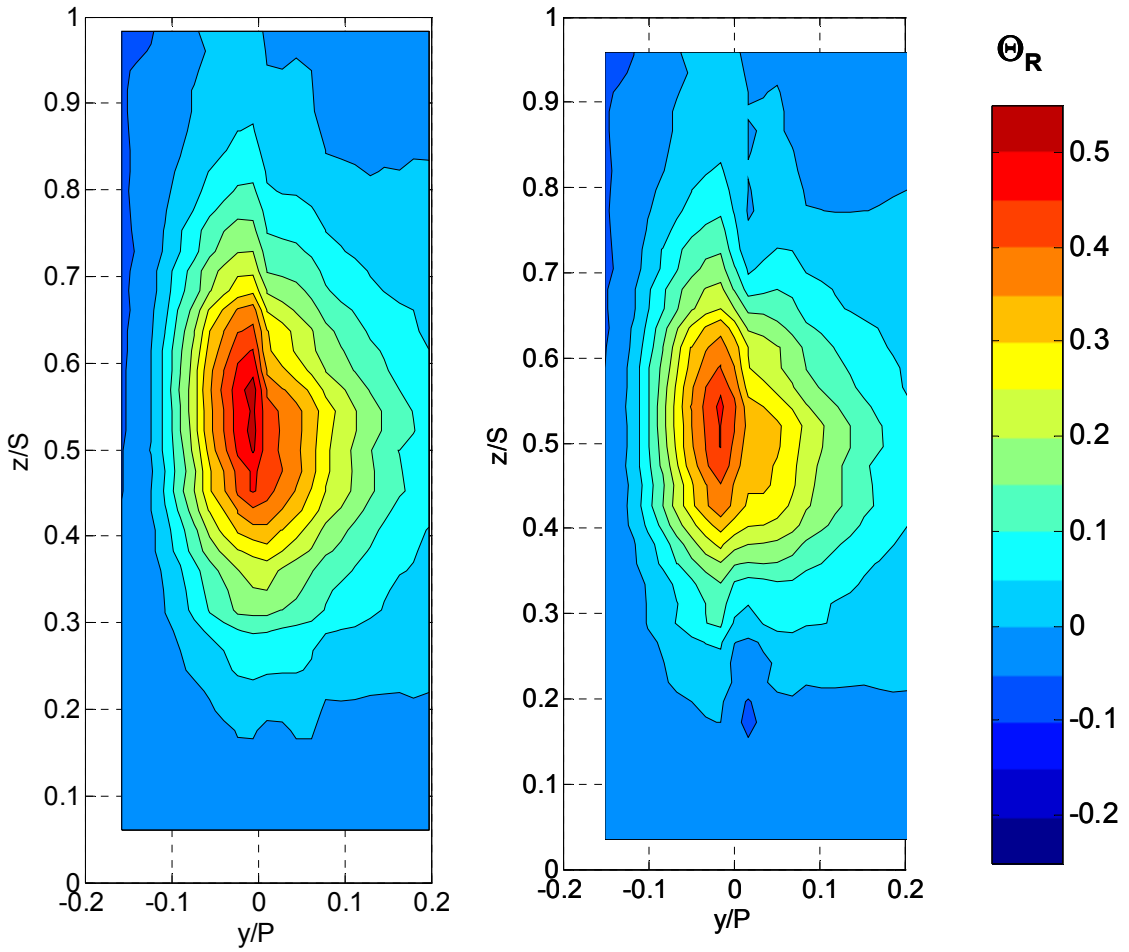

Figure **10.33: Normalized temperature ratio (Θ_R) contours at Position T with a simulated hot streak temperature ratio of $T/T_\infty = 1.5$ at the stagnation line, high mainstream turbulence ($Tu = 20\%$) with:**

a. No coolant

b. Superposition prediction of full coverage blowing at $M^*_{showerhead} = 2.0$, $M_{avg,\ suction} = 1.0$, and $M_{avg,\ pressure} = 1.0$ at a simulated density ratio of $DR = 2.0$

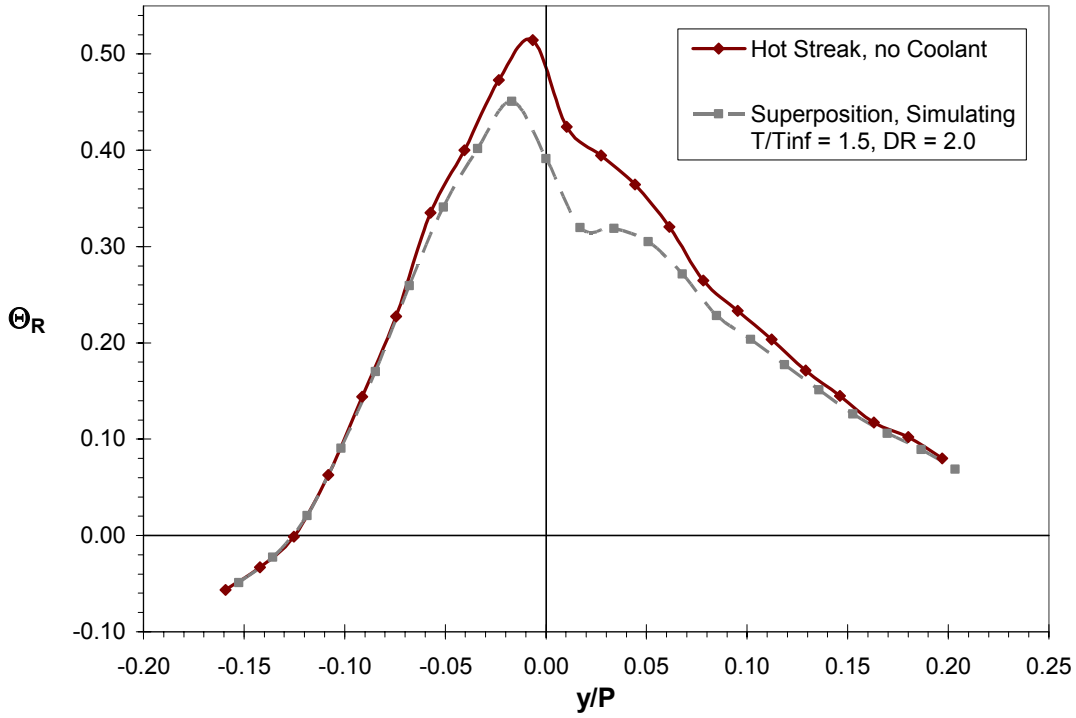

Figure **10.34: Comparison of normalized temperature ratio (Θ_R) profiles at Position T at midspan (z/S = 0.50), for the hot streak at a simulated temperature ratio of T/T_∞ = 1.5 at the stagnation line without cooling and with full coverage blowing at a simulated coolant density ratio of DR = 2.0 at $M^*_{showerhead}$ = 2.0, $M_{avg,\ suction}$ = 1.0, and $M_{avg,\ pressure}$ = 1.0, high mainstream turbulence (Tu = 20%).**

Chapter 11: Conclusions

11.1 Conclusions from the Present Study

Experiments were carried out to investigate the effects of mainstream turbulence and vane effects on a simulated hot streak for an uncooled 1st stage turbine vane. The effect of film cooling on the reduction of a simulated hot streak was determined by operating three distinct coolant regions individually and in combination to simulate a fully film cooled vane. Additionally, the effects of mainstream turbulence level and coolant density ratio on coolant profiles were investigated, as well as the resultant effect on hot streak reduction. Finally, superposition of coolant profiles and hot streak profiles was compared with measured data to evaluate the capability of additive superposition in predicting hot streak reduction due to film cooling. This method was used to predict other combinations of hot streak temperatures and coolant density ratios not attainable in the current facility.

The effects of mainstream turbulence on the attenuation of a hot streak were found to be significant. The hot streak spread about 10% in the spanwise direction at high mainstream turbulence passing through the mid-passage, while at low mainstream turbulence the height was essentially unchange. It was found that high turbulence levels were responsible for the higher level of attenuation seen downstream of an uncooled vane, where the peak at high mainstream turbulence was nearly 25% lower than at low mainstream turbulence. Moreover, under conditions of low turbulence the hot streak remained much more compact, with higher temperature gradients than for high turbulence.

Depending on the position of the hot streak relative to the stagnation line of the vane, interaction with the vane either increased or decreased the attenuation of the hot streak. Furthermore, parts of the hot streak that passed along the suction side of the vane were attenuated more than parts of the hot streak passing around the pressure side. This appeared to be due to the longer distance traveled along the suction side of the vane, and due to the higher compression of streamlines around the suction side of the vane, which caused higher temperature gradients on that side. The effects of the vane on the hot

streak were investigated for low and high mainstream turbulence levels, and trends were found to be similar.

Comparisons between the hot streak impacting the vane at the stagnation line and passing through the mid-passage showed that the peak hot streak temperature was the same for an impinging and non-impinging hot streak. This was true for both low and high turbulence, although for the high turbulence condition, the impinging hot streak had a strong temperature gradient at the trailing edge, making the comparison more difficult.

A major factor in the vane influence on the hot streak attenuation was the interruption of the hot streak dispersion caused when a hot streak impacted the vane and was split into two parts. This effect was most pronounced when the peak of the hot streak passed to either side of the vane so that a lower temperature outer edge, or "tail," of the hot streak was split from the core. The core of the hot streak was then attenuated less because dispersion of heat from the core was blocked on one side by the vane. However, the outer edge of the hot streak that was split from the core was attenuated more because it was isolated from the peak. This interaction with the adiabatic vane caused very sharp temperature gradients in the hot streak at the trailing edge of the vane, resulting in an increase or decrease in hot streak peak strength depending on pitch position. Additional attenuation of the hot streak occurred in the stator/rotor axial gap, and was also dependent on the hot streak pitch position, while the reduction due to the independent action of the vane wake was confirmed for high mainstream turbulence.

The showerhead reduced the hot streak in a broad fashion, reducing hot streak values over nearly the entire hot streak width. A change in blowing ratio, had the expected result, with lower blowing ratios reducing the hot streak less, and higher blowing ratios reducing it more. For all blowing ratios, a great deal of additional coolant was observed well below the hot streak due to the crossover region in the showerhead coolant hole configuration. This coolant did not have any significant effect on the hot streak due to its position, however, the potential for additional reduction of the hot streak was demonstrated by comparison of the hot streak peak normalized temperature values with peak coolant temperature values. Spreading of the coolant profile occurred in the stator/rotor axial gap due to turbulence effects and the vane wake, but was also transported towards the pressure side by the passage vortex. Ultimately, the hot streak

was reduced by almost 75% with showerhead film cooling compared with the hot streak strength upstream of the vane.

The effect of suction side film cooling on hot streak reduction was distinctly different from showerhead film cooling. While the showerhead reduced the hot streak temperature over a broad area, the suction side coolant was tightly focused near the vane surface. At the trailing edge, coolant from the suction side did not affect the pressure side of the hot streak, but reduced the suction side of the hot streak considerably. However, between the trailing edge (Position T) and Position B in the wake, the large temperature gradient at the trailing edge was eroded reducing the hot streak much further. As a result, effects of the two coolant regions were comparable downstream of the vane at Position B.

Hot streak reduction for film cooling from the pressure side was much lower than for the showerhead or suction side regions. In part, this was due to a large disparity in mass flow rates, but also due to differences in the hot streak on the pressure side. For optimum adiabatic effectiveness blowing ratios, the mass flow rate from the pressure side was much lower than from the showerhead or suction side. It was only 16% of the flow rate from the showerhead at $M^* = 1.6$ and 21% of the mass flow rate from the suction side at $M_{avg} = 0.7$. Since reduction of the hot streak by coolant was primarily due to the mixing process between coolant and hot streak fluid, and the coolant temperature was fixed by the density ratio, a greater mass flow of coolant would mix out the hot streak more. This explains why the pressure side coolant had only a slight effect on the hot streak. The hot streak was also much wider on the pressure side, resulting in pressure side coolant interacting with only a small portion of the hot streak to that side of the vane. Although this implies that the pressure side coolant would interact with the hottest portion of the profile, the reduction was not as significant as for suction side film cooling which produced a large dip in the hot streak profile measured at the trailing edge.

Experiments using all three film cooling regions were conducted at standard and high blowing ratios, simulating a fully film-cooled vane. Hot streak profiles at the trailing edge showed a significant reduction in peak temperature due to film cooling at standard blowing ratios with reductions of about 35% compared with no film cooling. Coolant only profiles at the trailing edge showed a large region of coolant well below midspan which did not interact with the hot streak. Peak coolant levels were comparable

to the hot streak peak, indicating that the coolant had the potential to completely eliminate the hot streak if the peaks were positioned to coincide. As expected, an increase in the blowing ratios resulted in lower temperatures and larger regions of coolant in the coolant profiles, especially below midspan. As a result, increased blowing ratios did not decrease the hot streak by a comparable amount since a majority of the additional coolant was below midspan due to the increased momentum of showerhead coolant driving fluid below the position of the hot streak. The large temperature gradients at the trailing edge produced by the mixture of coolant and hot streak fluid were mixed out in the stator/rotor axial gap, resulting in significant decreases in the hot streak peak strength at Position B. At this location with high blowing ratios, the hot streak peak was reduced by 83% compared with the peak value upstream of the vane at Position A. Compared with no film cooling for the same measurement position, the peak hot streak value was 55% lower, demonstrating the considerable benefit possible with full coverage film cooling.

The mainstream turbulence level had a strong effect on the spreading of coolant from all coolant regions with high mainstream turbulence levels attenuating the coolant peaks by nearly half in some cases compared with low mainstream turbulence. Under low mainstream turbulence conditions, the tightly focused suction side coolant profile peaked close the vane trailing edge, while higher mainstream turbulence levels quickly pulled coolant away from the vane wall. This effect was strong for pressure side film cooling, where the peak under high mainstream turbulence was much lower. For the showerhead, areas of coolant below midspan coming from the crossover region were distinct in contour plots at the trailing edge under low turbulence conditions, but spread quickly with high turbulence levels into a thicker, less distinct region of relatively high coolant strength. Generally, the showerhead affected most of the hot streak, with a greater effect on the suction side, while suction side film cooling reduced the near wall hot streak on that side substantially. At both turbulence levels, the pressure side had little effect on hot streak reduction, due to the much lower mass flow rates and wide hot streak along the pressure surface. The combined effects of the coolant regions under full coverage blowing greatly reduced the hot streak on the suction side, while leaving a reasonably strong hot streak to the pressure side. Nonetheless, full coverage film cooling

reduced the hot streak by about 35% at the trailing edge under both turbulence levels compared with no film cooling. The overall reduction measured at the trailing edge with full coverage film cooling at standard blowing ratios with respect to the upstream reference position was about 55%, lower than that with high mainstream turbulence at just over 60%. This was due to the role of high mainstream turbulence levels in reducing the hot streak without the aid of film cooling.

Density ratio had a large effect on the capacity of coolant to reduce the hot streak. Low density ratio coolant at DR = 1.2 reduced the hot streak by roughly half the amount that it was reduced by high density ratio coolant at DR = 1.6. It was discovered that coolant profiles for the showerhead, suction side, and full coverage film cooling at the trailing edge could be scaled using the normalized coolant temperature, Θ_C, suggesting that coolant profiles for other density ratios could be estimated. Reduction of the hot streak was less for film cooling at low density ratio, as would be expected. For the showerhead, low density ratio coolant was less than half as effective at reducing the hot streak, while the tightly focused coolant from suction side film cooling holes reduced the hot streak a fair amount on the suction side only. For suction side film cooling a fair comparison was difficult to make, since both density ratios resulted in the same overall peak hot streak temperature to the unaffected pressure side. However, to the suction side of the trailing edge, high density ratio coolant resulted in about twice as large a reduction in the hot streak as low density ratio coolant In general, these results show that film cooling in an aero-specific engine would have much less of an effect in reducing the hot streak. With an even higher hot streak temperature ratio than that simulated in these experiments, the effect of film cooling would be still less.

Superposition proved to be fairly capable of predicting film cooled hot streak profiles. Errors in predicting the peak of the cooled hot streak were generally below 20%, with some much lower. Under conditions of high mainstream turbulence, predictions were much better than with low mainstream turbulence due to the effects of strong temperature gradients. The predictive capacity of the superposition method was used to determine the ideal pitch position of the hot streak relative to the stagnation line of the vane as well. This predicted position was just to the suction side with full coverage film cooling at high blowing ratios. An in-depth analysis of the predicted profiles using

measured profiles suggested that the hot streak peak value would actually be similar for both hot streak positions. While the overall hot streak peak was predicted to be similar, this peak would be positioned on the suction side as opposed to the pressure side of the trailing edge. The same ideal hot streak pitch position was predicted at Position B for full coverage film cooling and additional reductions due to the pitch position were predicted to be on the order of about 10%. However, due to the nature of errors in using superposition at Position B shown earlier, it is unclear how much improvement would be realized. Superposition was also used to predict the effect of higher hot streak temperature ratios and aero-specific engine conditions. These predictions indicated that film cooling would reduce the hot streak by about 10% compared with no film cooling. As such, the coolant would be less effective at reducing the hot streak under these conditions, but could still provide some cooling benefit.

11.2 Recommendations for Future Work

As discussed in Chapters 4 and 7, a great deal of additional coolant was available for hot streak reduction below midspan. It is this author's understanding that newer designs of 1st stage nozzle guide vanes do not include a crossover region in the showerhead region, however the inclusion of such a crossover region would provide the potential for significant reduction of the hot streak if the hot streak were positioned appropriately in the spanwise direction. In the current facility, modifications of the hot streak generator section to provide adjustment in the spanwise direction would be easier than replacement of the test vane to allow the hot streak and crossover coolant to coincide. In addition, there has been interest in spanwise positioning of the hot streak in the literature, as evidenced by the computational study by Gundy-Burlet and Dorney [12]. They suggest that the spanwise position of the hot streak may have an effect on the heat load on the rotor and components further downstream. While their study was a computational study, presumably with very low inlet turbulence levels, and the current facility cannot directly determine the effect of positioning on a rotor, the effects of spanwise position noted in the paper can be investigated. Additionally, as mentioned above, the benefit of a crossover region in the showerhead could be investigated, potentially reducing the hot streak much more than shown in the current project.

Surface temperature measurements, given the limited access of the current facility for infrared measurements, were less than satisfying. Since the facility was constructed from plexiglass, the infrared measurement technique is unlikely to provide good coverage for surface temperature measurements even with extensive modifications. However, wide-band liquid crystals could provide good coverage and with current digital video technology, surface temperatures for nearly the entire vane surface could be measured with some interference from multiple layers of plexiglass. If surface temperature measurements using thermocouples were used to corroborate the surface image data, the resulting data could be very high quality. Surface temperatures for various pitch and spanwise positions could fill in a large gap in data available in the literature.

Bibliography

[1] Han, J. C., Dutta, S., Ekkad, S., *Gas Turbine Heat Transfer and Cooling Technology*, Taylor & Francis Group, New York, NY, 2000.

[2] Ames, F. E., Barbot, P. A., Wang, C., 2003, "Measurement and prediction of the influence of catalytic and dry low NOx combustion turbulence on vane surface heat transfer," *Journal of Turbomachinery*, v 125, n 2, April, 2003, p 221-231.

[3] Dorney, D. J., Gundy-Burlet, K. L., Sondak, D. L., 1999, "Survey of Hot Streak Experiments and Simulations," *International Journal of Turbo and Jet Engines*, vol. 16, no. 1, pp. 1-15.

[4] Schwab, J. R., Stabe, R. G., and Whitney, W. J., 1983, "Analytical and Experimental Study of Flow Through an Axial Turbine Stage with Nonuniform Inlet Radial Temperature Profiles," NASA Technical Memorandum 83431, AIAA 83-1175.

[5] Stabe, R. G., Whitney, W. J., and Moffitt, T. P., 1984, "Performance of a High-Work Low Aspect Ratio Turbine Tested with a Realistic Inlet Radial Temperature Profile," NASA Technical Memorandum 83655, AIAA Paper No. 84-1161.

[6] Butler, T. L., Sharma, O. P., Joslyn, H. D., and Dring, R. P., 1989, "Redistribution of an Inlet Temperature Distortion in an Axial Flow Turbine Stage," *Journal of Propulsion and Power*, vol. 5, no. 1, pp. 64-71.

[7] Joslyn, D. and Dring, R., "Three Dimensional Flow in an Axial Turbine: Part 2-Profile Attenuation," *Journal of Turbomachinery*, vol. 114, no. 1, pp. 71-78.

[8] Roback, R. J. and Dring, R. P., 1993, "Hot Streaks and Phantom Cooling in a Turbine Rotor Passage: Part 1 – Separate Effects," *Journal of Turbomachinery*, vol. 115, no. 4, pp. 657-666.

[9] Shang, T., Guenette, G. R., Epstein, A. H., Saxer, A. P., 1995, "The Influence of an Inlet Temperature Distortion on Rotor Heat Transfer in a Transonic Turbine," AIAA Paper 95-3042.

[10] Shang, T. and Epstein, A. H., 1996, "Analysis of Hot Streak Effects on Turbine Rotor Heat Load," ASME Paper No. 96-GT-118.

[11] Gundy-Burlet, K. L. and Dorney, D. J., 1997, "Three-Dimensional Simulations of Hot Streak Clocking in a 1-1/2 Stage Turbine," *International Journal of Turbo and Jet Engines*, vol. 14, no. 3, pp. 123-132.

[12] Gundy-Burlet, K. L. and Dorney, D. J., 2000, "Effects of Radial Location on the Migration of Hot Streaks in a Turbine," *Journal of Propulsion and Power*, vol. 16, no. 3, pp. 377-387.

[13] Dorney, D. J., 1997, "Investigation of Hot Streak Temperature Ratio Scaling Effects," *International J. of Turbo and Jet Engines*, vol. 14, pp. 217-227.

[14] Varadarajan, K., 2003, A Study of the Effects of a Hot Streak on Film Cooling Effectiveness on a Turbine Vane, Masters Thesis, The University of Texas at Austin.

[15] Polanka, M.D., 1999, "Detailed Film Cooling Effectiveness and Three Component Velocity Field Measurements on a First Stage Turbine Vane Subject to High Freestream Turbulence," Ph.D. Dissertation, The University of Texas at Austin.

[16] Cutbirth, J. M. and Bogard, D. G., 2002, "Evaluation of Pressure Side Film Cooling with Flow and Thermal Field Measurements, Part I: Showerhead Effects," ASME Paper No. GT-2002-30174.

[17] Cutbirth, J. M., 2000, "Turbulence and Three-Dimensional Effects on the Film Cooling of a Turbine Vane," Ph.D. Dissertation, The University of Texas at Austin.

[18] Robertson, D., 2004, “Roughness Impact on Turbine Vane Suction Side Film Cooling Effectiveness,” Masters Thesis, The University of Texas at Austin.

[19] Goldstein, R., *Fluid Mechanics Measurement*, Taylor & Francis Group, Philadelphia, PA, 1996.

[20] Burd, S. W. and Simon, T. W., 1999, “Measurements of discharge coefficients in film cooling,” *Journal of Turbomachinery*, vol. 121, no. 2, pp. 243-248

[21] Kline, S. J., and McClintock, F. A., 1953, “Describing Uncertainties in Single Sample Experiments,” *Mechanical Engineering* vol. 75.

[22] R. J. Moffat. “Uncertainty analysis” K. Azar, editor, *Thermal Measurements in Electronic Cooling*, pp. 45–80, CRC Press, Boca Raton, FL, 1997.

[23] Thole, K. A., 2003, personal communication.

[24] Bogard, D.G., Schmidt, D.L., and Tabbita, M., 1998, "Characterization and Laboratory Simulation of Turbine Airfoil Surface Roughness and Associated Heat Transfer," *Journal of Turbomachinery*, vol. 120, pp. 337-342.

[25] Bons, J. P., McClain, S. T., Taylor, R. P., and Rivir, R. B., 2001, “The Many Faces of Turbine Surface Roughness,” ASME Paper 2001-GT-0163.

[26] Rutledge, J., 2004, “Suction Side Roughness Effects on Film Cooling Heat Transfer on a Turbine Vane,” Masters Thesis, The University of Texas at Austin.

[27] Cutbirth, J. and Bogard, D., 2002, “Evaluation of pressure side film cooling with flow and thermal field measurements-Part I: Showerhead effects,” *Journal of Turbomachinery*, vol. 124, no. 4, pp. 670-677.

[28] Reinmöller, U. and Gallus, H. E., 1999, “An Experimental Investigation of the Flow in a 1½ Stage Axial Turbine With Regard to a High Level of Cooling-Air Injection,” ASME Paper 99-GT-41.

[29] Sauer, H., Muller, R., Vogeler, K., 2001, "Reduction of Secondary Flow Losses in Turbine Cascades by Leading Edge Modifications at the Endwall," *Journal of Turbomachinery*, vol. 123, pp. 207-213.

VITA

Sean Craig Jenkins was born in Austin, Texas on August 13, 1970, the son of Dr. J. Craig Jenkins and Mary Ellen Jenkins. After completing his work at Upper Arlington High School in Columbus, Ohio, he entered The Ohio State University in Columbus, Ohio. He received the degree of Bachelor of Fine Arts in March 1994. He spent two years serving as a Peace Corps volunteer in the country of Panama with his wife, Elizabeth Ann Heading Jenkins. In January 1997, he entered The Graduate School at The University of Texas at Austin. He received the degree of Master of Science in May 2001.

Permanent Address: 7200 Thomas Springs Rd.
Austin, TX 78736

This thesis was typed by the author.